

ON THE PATH TO ELUCIDATING THE SPECIATION OF MERCURY
IN THE FLUE GASES OF COAL COMBUSTION

by

Jennifer Wilcox

=====

A Dissertation Submitted to the Faculty of the
DEPARTMENT OF CHEMICAL AND ENVIRONMENTAL ENGINEERING

In Partial Fulfillment of the Requirements
For the Degree of

DOCTOR OF PHILOSOPHY
WITH A MAJOR IN CHEMICAL ENGINEERING

In the Graduate College

THE UNIVERSITY OF ARIZONA

2004

STATEMENT BY AUTHOR

This dissertation has been submitted in partial fulfillment of requirements for an advanced degree at The University of Arizona and is deposited in the University Library to be made available to borrowers under rules of the Library.

Brief quotations from this dissertation are allowable without special permission, provided that accurate acknowledgment of source is made. Requests for permission for extended quotation from or reproduction of this manuscript in whole or in part may be granted by the head of the major department or the Dean of the Graduate College when in his or her judgment the proposed use of the material is in the interests of scholarship. In all other instances, however, permission must be obtained from the author.

SIGNED: _____

TABLE OF CONTENTS

LIST OF TABLES.....	8
LIST OF FIGURES	9
ABSTRACT.....	11
CHAPTER 1. INTRODUCTION	13
CHAPTER 2. BACKGROUND	21
2.1. Literature Review of Current Experimental Data.....	21
2.2. Literature Review on Current Models and their Predictions.....	32
2.3. Quantum Mechanics and Basis Sets.....	42
2.4. Chemical Kinetics Tools	53
CHAPTER 3. OVERVIEW OF THEORETICAL RESULTS.....	58
3.1. Validation of Quantum Mechanical Methods and Basis Sets	58
3.2. First Stages of Oxidation	67
3.2.1. $\text{Hg} + \text{Cl} + \text{M} \rightarrow \text{HgCl} + \text{M}$ (3.1).....	67
3.2.2. $\text{Hg} + \text{Cl}_2 + \text{M} \rightarrow \text{HgCl}_2 + \text{M}$ (3.5).....	75
3.2.3. $\text{Hg} + \text{Cl}_2 \rightarrow \text{HgCl} + \text{Cl}$ (3.9).....	85
3.2.4. $\text{Hg} + \text{HCl} \rightarrow \text{HgCl} + \text{H}$ (3.11)	92
3.3. Second Stages of Oxidation.....	98
3.3.1. $\text{HgCl} + \text{Cl} + \text{M} \rightarrow \text{HgCl}_2 + \text{M}$ (3.12).....	98
3.3.2. $\text{HgCl} + \text{Cl}_2 \rightarrow \text{HgCl}_2 + \text{Cl}$ (3.16).....	104
3.3.3. $\text{HgCl} + \text{HCl} \rightarrow \text{HgCl}_2 + \text{H}$ (3.17)	113
3.4. Discrepancies with other Theoretical Results Published in the Literature	123
CHAPTER 4. EXPERIMENTAL RESULTS	130
4.1. Experimental Objectives.....	130
4.2. Experimental Background	134
4.3. Experimental Approach.....	137
4.3.1. Reactor and Plumbing	137
4.3.2. Sample Probe Calculations	150
4.3.3. Quadrupole Mass Spectrometry.....	157

TABLE OF CONTENTS-*Continued*

4.4. Experimental Results	163
4.4.1. Preliminary Results.....	163
4.4.2. Final Results.....	171
4.5. Modeling Results	179
4.5.1. Thermodynamic and Kinetic Analysis.....	180
4.5.2. Global model.....	186
CHAPTER 5. CONCLUSIONS	191
CHAPTER 6. FUTURE WORK.....	196
6.1. On the Theoretical Front.....	196
6.2. On the Experimental Front	199
APPENDIX A. BASIS SETS	202
A.1. Mercury: Stuttgart, Stevens and Krauss, LANL2DZ, and SDD.....	203
A.2. Chlorine: Pople, Dunning, LANL2DZ, and SDD	207
A.3. Hydrogen: Pople, Dunning, LANL2DZ, and SDD	210
A.4. Oxygen: Pople, Dunning, LANL2DZ, and SDD.....	212
APPENDIX B. PES DATA	215
B.1. $\text{Hg} + \text{Cl}_2 \rightarrow \text{HgCl} + \text{Cl}$	216
B.2. $\text{Hg} + \text{HCl} \rightarrow \text{HgCl} + \text{H}$	218
APPENDIX C. TRANSITION STATE THEORY RATE CONSTANT DATA.....	227
C.1. $\text{HgCl} + \text{HCl} \rightarrow \text{HgCl}_2 + \text{Cl}$	228
APPENDIX D. VARIATIONAL TST RATE CONSTANT DATA	230
D.1. $\text{Hg} + \text{Cl}_2 \rightarrow \text{HgCl} + \text{Cl}$	231
D.2. $\text{Hg} + \text{HCl} \rightarrow \text{HgCl} + \text{H}$	233
D.3. $\text{HgCl} + \text{Cl}_2 \rightarrow \text{HgCl} + \text{Cl}$	235

TABLE OF CONTENTS-*Continued*

APPENDIX E. VARIATIONAL RRKM THEORY RATE CONSTANT DATA	237
E.1. $\text{Cl} + \text{Cl} + \text{M} \rightarrow \text{Cl}_2 + \text{M}$	238
E.2. $\text{Hg} + \text{Cl} + \text{M} \rightarrow \text{HgCl} + \text{M}$	240
E.3. $\text{Hg} + \text{Cl}_2 + \text{M} \rightarrow \text{HgCl}_2 + \text{M}$	248
E.4. $\text{HgCl} + \text{Cl} + \text{M} \rightarrow \text{HgCl}_2 + \text{M}$	264
APPENDIX F. EQUILIBRIUM CONSTANT DATA.....	280
F.1. $\text{Cl} + \text{Cl} + \text{M} \rightarrow \text{Cl}_2 + \text{M}$	281
F.1.1. forward	281
F.1.2. reverse	283
F.2. $\text{HCl} + \text{OH} \rightarrow \text{Cl} + \text{H}_2\text{O}$	284
F.3. $\text{Hg} + \text{Cl} + \text{M} \rightarrow \text{HgCl} + \text{M}$	285
F.4. $\text{Hg} + \text{Cl}_2 + \text{M} \rightarrow \text{HgCl}_2 + \text{M}$	286
F.5. $\text{HgCl} + \text{Cl} + \text{M} \rightarrow \text{HgCl}_2 + \text{M}$	287
F.6. $\text{Hg} + \text{HCl} \rightarrow \text{HgCl} + \text{H}$	288
F.7. $\text{HgCl} + \text{HCl} \rightarrow \text{HgCl}_2 + \text{H}$	289
APPENDIX G. MODELING PARAMETERS	290
G.1. Mechanism.dat File	291
G.2. Thermo.dat File.....	292
APPENDIX H. DATA FROM MASS SPECTROMETRY RESULTS.....	293
APPENDIX I. CONTACT INFORMATION.....	304
APPENDIX J. STEPS FOR PUMPING DOWN THE VACUUM ASSEMBLY.....	306
APPENDIX K. STEPS ON OBTAINING DATA FROM MERLIN.....	309
APPENDIX L. TROUBLESHOOTING ON THE EXPERIMENTAL FRONT	315
APPENDIX M. DIRECTORY OF RESEARCH DATA	326
APPENDIX N. CURRICULUM VITAE	329
REFERENCES	333

LIST OF TABLES

Table 2-1. Chemical Environments of Hg ⁰ Oxidation via HCl.....	24
Table 2-2. Literature Review of Homogeneous Mercury Oxidation Gas Phase Reactions	26
Table 2-3. Experimental Rate Constants, Hg + Cl ₂ + M → HgCl ₂ + M.....	30
Table 2-4. Equilibrium Calculations for Selected Mercury Oxidation Reactions	35
Table 2-5. Widmer et al. Kinetic Parameters for Mercury Oxidation Model.....	39
Table 3-1. Bond Lengths (Å) of Mercury Species.....	62
Table 3-2. Heats of Reaction (kcal/mol) For Mercury Oxidation Reactions.....	63
Table 3-3. Theoretical Heats of Reaction (kcal/mol) with 1992 Extensions	64
Table 3-4. Theoretical Heats of Reaction (kcal/mol) with 1997 Extensions	65
Table 3-5. Thermodynamic and Kinetic Data, HgCl + M → Hg + Cl + M	71
Table 3-6. Thermodynamic and Energetics Data, Hg + Cl ₂ + M → HgCl ₂ + M.....	76
Table 3-7. Rate Constant Data, Hg + Cl ₂ + M → HgCl ₂ + M	79
Table 3-8. Energetics Data, HgCl ₂ + M → HgCl + Cl + M	103
Table 3-9. Energetics Data, HgCl + Cl ₂ → HgCl ₂ + Cl.....	109
Table 3-10. Thermodynamic and Kinetic Parameters, HgCl + Cl ₂ → HgCl ₂ + Cl	111
Table 3-11. Energetics Data, HgCl + HCl → HgCl ₂ + H	115
Table 3-12. Thermodynamic and Kinetic Data, HgCl + HCl → HgCl ₂ + H	116
Table 4-1. Mercury Concentrations Studied with Mass Spectrometry.....	132
Table 4-2. Physical Properties of Mercury	133
Table 4-3. Reactor Residence Times	141
Table 4-4. Dissociation Energies and Ionization Potentials of Mercury Species	160
Table 4-5. Vapor Pressure of Common Pump Oils	163
Table 4-6. Mass Ranges for Mercury and Chlorine Species	168
Table 4-7. Stable Mercury Isotopes and their Relative Abundances.....	169
Table 4-8. Stable Mercury Isotopes and their Relative Abundances.....	170
Table 4-9. Mercury Speciation of Hg + Cl ₂ For the Uncoated Reactor.....	172
Table 4-10. Mercury Speciation of Hg + Cl ₂ For the Coated Reactor.....	176
Table 4-11. Hard Sphere Collision Model Predictions.....	182
Table 4-12. Hard Sphere Collision Model Rate Expressions	182
Table 4-13. Comparison of Rate and Equilibrium Constants at Various Temperatures	184
Table 4-14. Theoretical Combustion Model parameters	187
Table 4-15. Complete List of Theoretical Combustion Model parameters	189

LIST OF FIGURES

Figure 2-1. Experimental Results of Full Oxidation of Hg ⁰ by HCl	25
Figure 2-2. Possible Mercury Oxidation Pathway Hypotheses	41
Figure 2-3. Molecular Orbital Diagram of HgCl	46
Figure 2-4. Schematic of Energy Level Splittings for HgCl	47
Figure 2-5. RRKM Energy Description	56
Figure 3-1. Comparison of Rate Constants, Cl ₂ + M → 2Cl + M	68
Figure 3-2. Rate Constants Varying β _c , HgCl + M → Hg + Cl + M	73
Figure 3-3. Comparison of Rate Constants, HgCl + M → Hg + Cl + M	74
Figure 3-4. Comparison of Rate Constants, HgCl ₂ + M → Hg + Cl ₂ + M	77
Figure 3-5. Transition Structures, Hg + Cl ₂ + M → HgCl ₂ + M	81
Figure 3-6. Potential Energy Surface (1992 BS), Hg + Cl ₂ → HgCl + Cl	86
Figure 3-7. Potential Energy Surface (1997 BS), Hg + Cl ₂ → HgCl + Cl	87
Figure 3-8. Example of a Crossing Potential Energy Surface	89
Figure 3-9. Potential Energy Surface (QCISD/1992 BS), Hg + HCl → HgCl + H	93
Figure 3-10. Potential Energy Surface (QCISD/1997 BS), Hg + HCl → HgCl + H	94
Figure 3-11. Potential Energy Surface (B3LYP/1992 BS), Hg + HCl → HgCl + H	95
Figure 3-12. Potential Energy Surface (B3LYP/1997 BS), Hg + HCl → HgCl + H	96
Figure 3-13. Comparison of Rate Constants, HgCl ₂ + M → HgCl + Cl + M	101
Figure 3-14. Potential Energy Surface (1997 BS), HgCl + Cl ₂ → HgCl ₂ + Cl	106
Figure 3-15. Potential Energy Surface (1992 BS), HgCl + Cl ₂ → HgCl ₂ + Cl	107
Figure 3-16. Comparison of Rate Constants, HgCl + HCl → HgCl ₂ + H	117
Figure 3-17. Comparison of Rate Constants, H + HgCl ₂ → HgCl + HCl	118
Figure 3-18. Rate Comparison of B3LYP with QCISD, HgCl + HCl → HgCl ₂ + H	121
Figure 4-1. Schematic of the Reactor	138
Figure 4-2. Schematic of the Mercury and Chlorine Flow System	142
Figure 4-3. Flow Through Deflected Jets to Obtain Optimum Mixing	144
Figure 4-4. Schematic of Control Panel Wiring	148
Figure 4-5. Photograph of Control Panel	149
Figure 4-6. Parameters for the Sample Probe Orifice in the Reactor	150
Figure 4-7. Schematic of the Experimental Set-up	155
Figure 4-8. Photograph of Vacuum Assembly	156
Figure 4-9. Mass Spectrum of Oil Backstreaming from DC 704	164
Figure 4-10. Mass Spectrum of Oil Backstreaming from Santovac 5	165
Figure 4-11. Mass Spectrum of HCl, 300 ppm	167

LIST OF FIGURES-*Continued*

Figure 4-12. Possible Homogeneous Reaction Pathways, Hg + Cl ₂	174
Figure 4-13. Possible Homogeneous Reaction Pathways, Hg + HCl	178
Figure 4-14. Graphical Results of the Large-Scale Modeling of Mercury	187
Figure 4-15. Proposed Mercury Oxidation Model via Chlorine Species.....	194
Figure L-1. Schematic of the 10-Pin Connector to Vacuum Flange.....	323

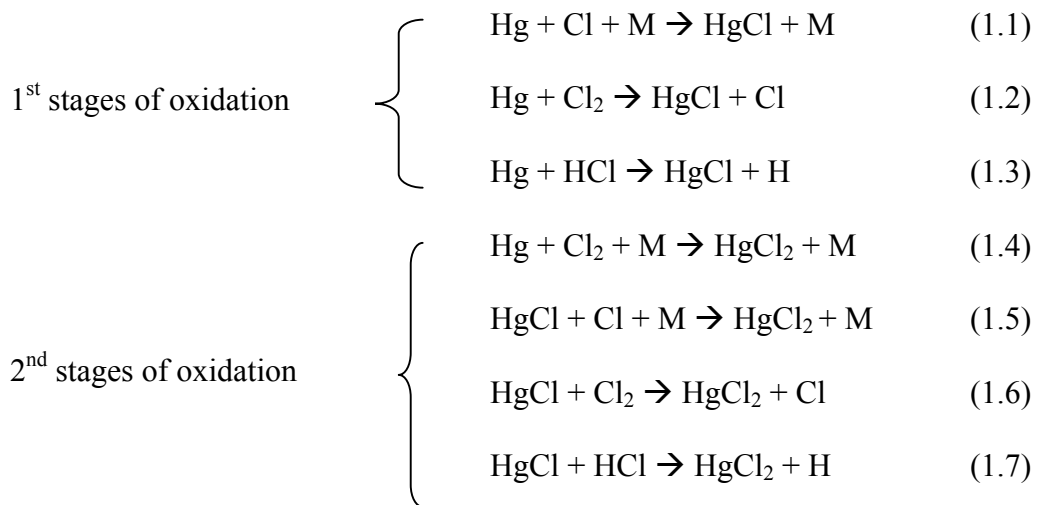
ABSTRACT

The goal of this research is to understand the speciation of mercury in the flue gases of coal combustion. As the flue gas cools, thermochemical equilibrium calculations indicate that elemental mercury, Hg^0 , is converted to oxidized mercury, Hg^{2+} , in the form of HgO or HgCl_2 . Hg^0 is insoluble in water, HgO has low solubility in water and HgCl_2 is highly soluble in water. Since HgCl_2 is water-soluble, it can be captured in wet chemical scrubbers to prevent its release to the atmosphere. Therefore, the understanding of the mechanisms of mercury's oxidation in flue gases is paramount when considering mercury capture. This research attempts to elucidate the mechanisms of oxidation through a detailed kinetic and thermodynamic analysis. The current research focuses specifically on the oxidation of mercury via chlorine-containing compounds. Future research will involve the oxidation via oxygen-containing compounds and the effect of SO_2 and NO_x compounds on mercury's oxidation. Quantum chemistry is used to determine accurate transition structures, which are required for the calculation of activation energies and rate constants from theory. Simultaneous to the theoretical work, an experimental apparatus has been designed and fabricated with the inclusion of a quadrupole mass spectrometer. The mass spectrometer is used in conjunction with a laminar flow reactor to simulate the oxidation of mercury via chlorine-containing compounds in flue gases. The ultimate goal of this research is to obtain a potential mercury oxidation mechanism based upon theoretically predicted kinetic parameters, which are then validated through concentration profiles obtained from experimental measurements. In addition, results from the

experimental work indicate that at ambient conditions, the oxidation of mercury via chlorine may result as a consequence of heterogeneous reactions involving the Pyrex reactor surface. This work not only allows for a more thorough understanding of mercury's speciation in the flue gas environment, but also questions current sampling devices and their potential interference with reactivity measurements involving mercury-chlorine species.

CHAPTER 1. INTRODUCTION

The oxidized forms of mercury, HgCl_2 is water-soluble, allowing this form of mercury to be captured in wet chemical scrubbers to prevent its release to the atmosphere. The current research focuses specifically on the oxidation of mercury via chlorine-containing compounds. This research attempts to elucidate the mechanism of oxidation through a detailed kinetic and thermodynamic analysis. Quantum chemistry is used to determine accurate transition structures, which are required for calculating activation energies and rate constants that are used in both the kinetic analysis and in the incorporation of a global combustion model. The following reactions are ones that have been studied in this work in an attempt to elucidate the speciation of mercury amongst various chlorine species.



Simultaneous to the theoretical work, an experimental apparatus has been designed and fabricated with the inclusion of a quadrupole mass spectrometer. The mass spectrometer will be used in conjunction with a laminar flow reactor to examine mercury oxidation reactions involving chlorine species. The mass spectrometer has been used to directly examine the speciation of mercury for reactions (1.2) and (1.3) above. Future work will involve using the vacuum assembly and mass spectrometer that was developed in this work to further understanding mercury reactions in flue gas environments. In the literature there is a great deal of mercury speciation research aimed at understanding these oxidation mechanisms, but the measurements have involved difference techniques that often have difficulty accurately distinguishing between the different oxidation states of mercury. The difference in the current work is that the mass spectrometer allows for the direct measurement of the differing mercury species through a separation process involving their mass to charge ratio. In addition to this unique experimental work, the combustion model involves theoretical mercury kinetic data derived from high level quantum mechanical techniques. This approach is much different than those used in the current models available in the literature, which include kinetic data that is based upon rough approximations such as the hard sphere collision model. In fact, in many of the models, kinetic parameters are included for mercury that involve reactions with other metals with properties different from mercury. The ultimate goal of this research is to obtain a realistic mercury oxidation pathway involving chlorine species. The determination of the oxidation pathway is based upon a detailed kinetic and

thermodynamic analysis. The kinetics of reactions (1.1) through (1.7) are analyzed through the theoretical prediction of rate constants. The thermodynamic analysis is based upon equilibrium constant calculations derived from experimental data available from the National Institute of Standards and Technology (NIST). In addition, the theoretical predictions are validated through concentration profiles obtained from direct mercury speciation measurements.

Whether the source of release is anthropogenic or natural, mercury is released through the combustion of organic matter due to the existence of more than 25 mercury-containing minerals in the Earth's mantle. (Schroeder and Munthe, 1998) In the United States, power generation is responsible for 37% of the mercury released into the environment from human activity. Specifically, coal burning is the primary source of anthropogenic release of mercury, with about 48 tons per year being released in the U.S. alone. (U.S. EPA, 2003) Once in the atmosphere, elemental mercury is relatively inert and has a residence time of the order of one year, which classifies mercury as a "global pollutant". (Slemr et al.; Lindqvist and Rodhe, 1985) In 1998, the EPA began discussion of mandatory mercury emission measurements from all coal burning plants to lay the groundwork for reducing these mercury emissions in the future. (Federal Register Notices, 1998) The Clear Skies Act initiated by the EPA is a mandatory program that will aim at reducing power plant emissions of SO₂, NO_x, and mercury by placing a national cap on each at an average of 70% below today's levels. This will be the first-ever national cap on mercury emissions. In addition, emissions would be cut from 2000

emissions of 48 tons to a cap of 26 tons in 2010 and to a cap of 15 tons in 2018. The EPA plans to issue final regulations on mercury emissions from coal- and oil-fired power plants by December 15, 2004, with full compliance by December 2007. (U.S. EPA, 2003) These steps are being taken because mercury can be found in many of the foods we eat, from fish (Boening, 2000; Qian et al., 2001), to other foods we generally do not expect to have mercury, like vegetables. (Patra and Sharma, 2000; Ristori and Bargigiani, 1994) Inorganic forms of mercury, such as that released from coal combustion flue gases, can be converted by natural biological processes to the highly toxic methyl mercury form. Methyl mercury has the ability to bio-accumulate more than a million fold in the aquatic food chain. (Schroeder and Munthe, 1998) This would not be of concern except research has repeatedly shown that mercury may have many toxic effects on organisms, from reproductive effects, to developmental problems in children, and psychological or intellectual damage. (Aschner, 2001; Karimi et al., 2002)

In order to effectively capture mercury from the exhaust of coal combustion, it is necessary to understand the speciation of mercury in the exhaust environment. Mercury is in its elemental state when it is released from the coal combustion process, which makes it very difficult to capture. Elemental mercury is not soluble in water, the primary liquid media used for emissions control, and does not adsorb readily on most solid substrates with capture rates between 10 and 80%. (Ghorishi, 1998) Fortunately, elemental mercury reacts with oxidizing species that exist naturally in the coal exhaust and can be transformed into an oxidized form, HgCl_2 , that can be captured more easily.

However, the amount of oxidation is dependent on the concentration of oxidizing species available in the coal exhaust.

The major ways of determining possible mechanisms of oxidation are through:

- extraction of kinetic data from simplifications of experimental flue gas oxidation conditions,
- calculation of kinetic and thermodynamic data for oxidation reactions using quantum mechanics, and
- kinetic modeling based upon partial data that is available through a combination of the above techniques.

There are many difficulties associated with experimentally determining mercury speciation kinetics. Current EPA Methods 29 and 101A that are being used to measure mercury can only differentiate between Hg^0 and Hg^{2+} , leaving Hg^{1+} unmeasured; this form of oxidized mercury cannot be experimentally determined. (Senior et al., 2000) Another difficulty with experimental measurements is due to the inability to measure mercury at low concentrations and high temperatures. Mercury is normally only present in quantities around 10 ppbv in flue gases, and simulated flue gases often use mercury concentrations that are orders of magnitude higher. (Hall et al., 1991) In addition, temperatures below that of real flue gas conditions are used in many kinetic experiments so the reactions will be slower and can be measured. (Sliger et al., 2000)

The current research is unique in that it involves both experimental and theoretical mercury kinetic predictions. In fact, this work is the first that uses quantum mechanics to predict high quality rate constants for reactions (1.1) through (1.7). Quantum chemical methods are capable of estimating reaction rates and kinetic parameters for mercury reactions and do not suffer from the difficulties in speciating mercury that the experimental methods do. However, few computational studies have been performed thus far for understanding mercury reactions using quantum chemistry. (Sliger et al., 2000; Xu et al., 2003) Within the current research, a series of basis sets along with various quantum mechanical methods will be compared in order to determine which combination provides the most accurate results for the oxidation of mercury via chlorine containing species.

The applications of this research to the capture of mercury from the flue gases of coal combustion are abound. In the flue gases of coal combustion systems, mercury is typically in the vapor form at the flue gas cleaning temperatures, and the control of mercury is directly related to the speciation of mercury and the type of capture devices employed. In dry scrubbing systems, the control of mercury is dependent upon the adsorption of mercury on particulate matter that can then be captured via a particulate matter control device. In wet scrubbing systems, the principal mechanism of control is through the oxidized water-soluble form of mercury. At combustion temperatures, however, it is believed that mercury is dominantly in the elemental form (Hg^0). As the

flue gas cools, thermochemical equilibrium calculations conclude that the elemental form is oxidized to the ionic form, Hg^{2+} in the form of mercuric chloride (HgCl_2) or mercuric oxide (HgO). The elemental form, Hg^0 is insoluble in water while HgO is slightly soluble and HgCl_2 is highly soluble. Understanding the reaction mechanisms and more specifically the overall speciation of mercury in the flue gases will allow for the development of more effective control strategies. Characteristics of coal-fired power plants that affect mercury emissions are (i) the mercury content of the coal, (ii) the design and operation of any particulate control devices, and (iii) the design and operation of any flue gas treatment systems.

The mercury concentrations of various coal types are available through the U.S. Geological Survey's (USGS) COALQUAL database. (Toole-O'Neil et al., 1999) In general, the amount of oxidized mercury formed in the flue gases is dependent upon the type of coal. For instance, burning lignite coal produces less oxidized mercury than burning bituminous coal. Sulfur dioxide scrubbers allow for mercury removals between 37 to 65 percent for bituminous coals with only about 5 percent removal for lignite coals. (Brown et al., 2000)

Predicting the chemical form of mercury in the stack gases is difficult since the transformations of elemental mercury in the post-combustion regime are unknown. However, the pathways may include heterogeneous reactions, where fly ash surfaces serve as a catalyst, as well as homogeneous gas phase reactions. The major reaction

pathways for mercury oxidation in combustion flue gases are still in question and are the current focus within this work. Specifically, the homogeneous gas phase oxidation reactions of mercury via chlorine species will be examined throughout this research.

CHAPTER 2. BACKGROUND

2.1. Literature Review of Current Experimental Data

One of the benefits of pursuing theoretical results for the study of mercury speciation is due to some of the limitations of the methodology of the experimental mercury measurements. Mercury is released in 1-30 ppbw concentrations ($1 - 30 \mu\text{g}/\text{m}^3$), making accurate measurements extremely difficult. Accurate measurements of mercury are paramount when estimating the anthropogenic flux of mercury into the atmosphere, identifying mercury transport and transformation processes, determining the deposition and methylation mechanisms in ecosystems, assessing mercury bioaccumulation, determining the speciation from fossil fuel combustion systems, and ensuring the compliance of sources with emission regulations. (Laudal et al., 2000)

One major aspect of the current research is to directly measure mercury concentrations from oxidation reactions using a quadrupole mass spectrometer. A limitation in much of the research involving the speciation of mercury is the inability to directly measure mercury speciation. Rather, the methods that have been used traditionally for measuring mercury speciation are difference techniques, which are unable to distinguish between the two different oxidation states of mercury, Hg^+ and Hg^{2+} . Therefore, the published measuring techniques involve coupling these two distinct mercury species. One of the benefits of mass spectrometry is that it allows one to distinguish between these two forms through a separation based upon a mass to charge ratio. Since the two distinct oxidation

states have different charges, mass spectrometry will allow for the direct measurement of each.

Aside from the difficulty of distinguishing between the two different oxidized forms, current methods are consistently poor at distinguishing between the elemental and combined oxidized forms. Current measurement methods simply cannot distinguish between the specific oxidized forms of mercury. (Senior et al., 2000) A mercury speciation study consisting of data from fourteen different coal combustion systems obtained very inconsistent mercury speciation results. The study reported numbers ranging anywhere from 30 to 95% of oxidized mercury upstream of the air pollution device. (Prestbo and Bloom, 1995) In addition, the analysis of mercury speciation in the flue gases is often performed by passing the mercury sample through a series of impingers that contain solutions capable of capturing and separating the oxidized (Hg^{2+}) form from the elemental mercury form (Hg^0). The Ontario Hydro and Alkaline Mercury Speciation are two of these methods. Research has shown that concentrations of Cl_2 as low as 1 ppm can misrepresent Hg^0 as Hg^{2+} by as much as 10 – 20 %. (Linak et al., 2001) This lack of consistency in the current methods for distinguishing between these different oxidation states of mercury allows further appreciation for mass spectrometry measurements.

The overall reaction mechanisms of mercury's oxidation in the flue gases of coal combustion systems is still in question and has been pursued aggressively through

experimental research since the early nineties. Heterogeneous reaction mechanisms have been studied in which fly ash was composed of oxides of silicon, aluminum, calcium, iron and copper, which may serve as catalytic surfaces for mercury's oxidation. In addition, homogeneous gas-phase mercury oxidation reactions have been experimentally studied through the presence of chemical species such as Cl_2 , HCl , HOCl , H_2O , NO_x and SO_x , among others.

The question that remains to be answered is, "what is the overall oxidation process by which mercury becomes oxidized in the flue gases of coal combustion processes?" Both HCl and Cl_2 are present in the flue gases and are therefore the major players in mercury oxidation. Although, HCl is present in much greater concentrations in typical coal combustion flue gases than Cl_2 , from experimental results, mechanisms involving Cl_2 are more likely to be the reactions resulting in the oxidation of mercury. (Sliger et al., 2000; Mamani-Paco and Helble, 2001) To gain more perspective on this hypothesis, an examination of all the currently available experimental results must be performed.

From Table 2-1, the chemical environments of the simulated flue gases are shown for each experimental set-up available in the literature for the oxidation of mercury via HCl . Since HCl is present in the flue gases at higher concentrations than Cl_2 , this was naturally the first oxidation pathway considered, and for this reason there is more mercury speciation data in the literature for this potential mechanism.

Table 2-1. Chemical Environments of Hg⁰ Oxidation via HCl

(Hall et al, 1991)	(Widmer et al, 1998)
10% O ₂ in N ₂ Varying HCl (1-100µL/L) 100µg/m ³ of Hg ⁰ No H ₂ O or NO Residence time: 1 second Temperature Range: 20 – 900 °C	10% O ₂ , 10% CO ₂ , 8% H ₂ O Varying HCl (300, 3000 ppm) 370 ppb Hg ⁰ No NO Residence time: 1 second Temperature Range: 420 – 880 °C
(Sliger et al., 2000)	(Mamani-Paco et al., 2000)
7.43% O ₂ , 6.15% CO ₂ , 12.3% H ₂ O Varying HCl (50 - 3000 ppm) 53µg/m ³ Hg ⁰ No NO Residence time: 1.4 seconds Temperature Range: 860-1071 °C	26% H ₂ O, 25 ppm NO Varying HCl (up to 100 ppm) 50µg/m ³ Hg ⁰ No O ₂ or CO ₂ Residence time: 1-6 seconds Temperature Range: up to 1225 °C

Widmer et al. and Sliger et al. provide the most realistic flue gas environments with the inclusion of both water vapor and CO₂. Mamani-Paco et al. did not consider CO₂ or oxygen, but considered the presence of NO and consequently found that NO acts as an inhibitor of mercury oxidation. In flue gases where the HCl concentrations are low, Hall et al. found that oxidized mercury in the HgO form is additionally present. Therefore NO can act as an inhibitor by reacting with HgO to form NO₂ and reduce mercury back to its non-water-soluble elemental form. From Figure 2-1, it is clear that the results of Hall et al. are very different than the other researchers for the mercury oxidation via HCl. This

may be due to the inclusion of inhibition and promotion that other chemical species play in the flue gases. More details of the experimental results are listed in Table 2-2.

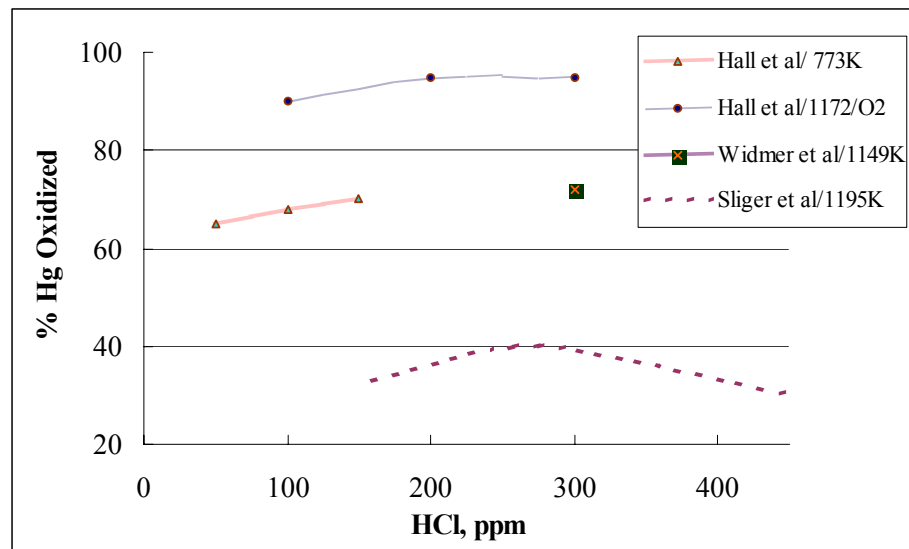


Figure 2-1. Experimental Results of Full Oxidation of Hg⁰ by HCl

Table 2-2. Literature Review of Homogeneous Mercury Oxidation Gas Phase Reactions

	Reaction Studied	Temperature (°C)	Possible Reaction Schemes	Conclusions
Hall et al.	$\text{Hg} + \text{HCl} \rightarrow \dots$ *50 – 150 ppm of HCl/ 13 ppm of Hg^0	500 w/ $\tau = 1.5$ s	$\text{Hg} + 2\text{HCl} \rightarrow \text{HgCl}_2 + \text{H}_2$	*formation of HgCl_2
Hall et al.	$\text{Hg} + \text{HCl} \rightarrow \dots$ w/ 10% O_2 /90% N_2 *100 – 300 ppm HCl/ 13 ppm of Hg^0	900 w/ $\tau = 0.7$ s 20 w/ $\tau = 2.8$ s	$2\text{Hg} + 4\text{HCl} + \text{O}_2 \rightarrow 2\text{HgCl}_2 + 2\text{H}_2\text{O}$ $4\text{Hg} + 4\text{HCl} + \text{O}_2 \rightarrow 2\text{Hg}_2\text{Cl}_2 + 2\text{H}_2\text{O}$	*obtained 90% oxidation in less than 1 second
Hall et al.	$\text{Hg} + \text{Cl}_2 \rightarrow \dots$ *50 – 150 ppm of Cl_2 / 13 ppm of Hg^0	20 w/ $\tau = 2.8$ s 500 w/ $\tau = 1.5$ s 700 w/ $\tau = 0.8$ s	$\text{Hg} + \text{Cl}_2 \rightarrow \text{HgCl}_2$ $2\text{Hg} + \text{Cl}_2 \rightarrow \text{Hg}_2\text{Cl}_2$	* Hg^0 reacts with Cl_2 at 20 °C *70% oxidized at 500 °C
Widmer et al.	$\text{Hg} + \text{HCl} \rightarrow \dots$ w/ 10% O_2 /10% CO_2 /8% H_2O /72% N_2 *370 ppb of Hg^0 / 300/3000 ppm HCl	Ranging from 420 – 880 w/ $\tau \sim 1$ s	Elementary and/or global reactions were not reported	*oxidation increases with HCl increase
Sliger et al.	$\text{Hg} + \text{Cl} \rightarrow \dots$ w/ 7.4% O_2 /6.2% CO_2 / 12.3% H_2O / N_2 balance *53 – 1390 $\mu\text{g}/\text{m}^3$ / 100 – 600 ppm HCl/ 25 ppm NO	540 w/ $\tau \sim 1.4$ s	(1) $\text{HCl} + \text{OH} \rightarrow \text{Cl} + \text{H}_2\text{O}$ (2) $\text{Hg} + \text{Cl} \rightarrow \text{HgCl}$ (3) $\text{HgCl} + \text{HCl} \rightarrow \text{HgCl}_2 + \text{H}$	*NO acts as an inhibitor to Hg^0 oxidation * Hg^0 oxidation occurs during the quenching stage
Mamani-Paco and Helble	$\text{Hg} + \text{HCl} \rightarrow \dots$ w/ 26% H_2O / N_2 balance *50 $\mu\text{g}/\text{m}^3$ / 100 ppm HCl	290, 350, and 520 residence time not reported	Elementary and/or global reactions were not reported	*at most 2% Hg^0 oxidation
Mamani-Paco and Helble	$\text{Hg} + \text{Cl}_2 \rightarrow \dots$ w/ 26% H_2O / N_2 balance *50 $\mu\text{g}/\text{m}^3$ / 50,100,300 and 500 ppm Cl_2	270, 300, and 500 residence time not reported	$\text{Hg} + \text{Cl}_2 \rightarrow \text{HgCl}_2$	*despite lower temperatures, obtained 93% Hg^0 oxidized

Table 2-2 shows the overall results from a literature review on all the currently available experimental mercury speciation data.

Hall et al. have studied mercury speciation through oxidation via both HCl and Cl₂. Hall found that HCl will not oxidize Hg⁰ at room temperature without the presence of oxygen. Hall also predicts an increase in mercury oxidation with an increase in temperature, resulting in either HgCl₂ and/or Hg₂Cl₂. The second form, also known as calomel has not been considered as a possible product in other experimental flue gas observations.

However, calomel decomposes at 382 °C, implying it will exist only at low temperatures. In the current experimental research, reactions are considered at ambient conditions. Since calomel is stable at these low temperature conditions, it is not unusual that it plays a large role as a product formed in the oxidation of mercury via Cl₂. In fact, there have been other similar studies, which have considered the oxidation of mercury via Cl₂ at room temperature and similarly found that calomel is in fact a major product species.
(Horne et al., 1991; P'yankov, 1949; Hall et al., 1991)

Hall et al. found that Hg⁰ reacts readily with Cl₂ even at temperatures as low as 20 °C. Similar to the conclusions reached from the study of mercury oxidation via HCl, Hall et al. propose that both HgCl₂ and Hg₂Cl₂ are both possible product species through the oxidation via Cl₂. Hall additionally reports that the oxidation of Hg⁰ by Cl₂ can occur heterogeneously at ambient conditions. There has been a great deal of other research, which also supports this hypothesis. (Medhekar, 1979; Hall et al., 1991; Menke and

Wallis, 1980; Ariya et al., 2002) It has been unanimously concluded in this past work that surfaces such as Pyrex and quartz are reactive and can facilitate the oxidation of mercury via Cl_2 . The theoretical predictions of the current work also support this claim. The homogeneous oxidation of Hg via Cl_2 is both kinetically and thermodynamically limited at low temperatures. This will be examined in greater detail throughout the discussion of the current research.

Widmer et al. studied the oxidation of Hg^0 via HCl and found the reaction to be kinetically limited at temperatures less than 800 °C and thermodynamically limited without high concentrations of HCl. They concluded that the HCl concentration has as large of an impact as temperature on the mercury conversion. Mamani-Paco and Helble also studied the oxidation of mercury via HCl and found similar results to that of Widmer et al. They examined the addition of HCl to elemental mercury at temperatures ranging from 563 to 793 K and found a 2% oxidation rate with HCl concentrations in the 100 ppm range. In fact, comparing all experimental mercury oxidation data involving HCl, most tend to agree with each other, aside from the results of Galbreath et al. The possible reason for why Galbreath et al. obtained higher mercury oxidation levels is that their reactions were not strictly homogeneous. Galbreath et al. observed 70 – 80% oxidation of mercury with HCl concentrations at 100 ppm and the presence of particles, which may serve as catalysts to facilitate in mercury's oxidation.

Sliger et al. proposed a mechanism involving the oxidation of mercury via chlorine atoms for the first stage, and HCl for the second stage of mercury's oxidation. Sliger et al. also introduced quenching rates so that the flue gas is cooled. As the flue gas cools, it has been found that the rate of oxidation is increased. Sliger et al. concluded in their work that the chemical environment of the simulated flue gases is important in obtaining reliable mercury speciation results. One reason that the data between Hall et al., Widmer et al. and Sliger et al. data disagrees is due to the fact that Widmer et al. and Sliger et al. have more realistic flue gas environments, involving species that Hall et al. neglect, such as CO₂ and H₂O.

Mechanisms have been studied (Lee et al., 1998) that predict very slow oxidation of Hg⁰ via HCl below 700°C, and only at temperatures above 700°C and HCl concentrations greater than 200 ppm do these reactions proceed at measurable rates. They also found that SO₂ and water vapor in the simulated flue gas inhibits the gas-phase oxidation of Hg⁰. On the other hand, they found the reaction of elemental mercury with molecular chlorine, Cl₂, to be fast, with 100% oxidation to HgCl₂ in the presence of 50 ppm Cl₂ at 40°C in less than two seconds. Lee et al. also studied heterogeneous reactions involving simulated fly ash consisting of mixtures of some major components found in the fly ash from coal. They propose that the surface acts to catalyze the reaction of HCl to form molecular chlorine, which then reacts to form HgCl₂. With the fly ash present, the addition of HCl to Hg⁰ caused a 95% oxidation of elemental mercury in the temperature range from 150 to 250°C.

Table 2-3. Experimental Rate Constants, $\text{Hg} + \text{Cl}_2 + \text{M} \rightarrow \text{HgCl}_2 + \text{M}$

	Rate Constant (298K)
Seigneur et al.	$2.47 * 10^{10} \text{ cm}^3/\text{mol*s}$
Mamani-Paco et al.	$\sim 2.38 * 10^{10} \text{ cm}^3/\text{mol*s}$
Schroeder et al.	$2.41 * 10^{10} \text{ cm}^3/\text{mol*s}$
Hall et al.	$7.8 \pm 0.4 * 10^8 \text{ cm}^3/\text{mol*s}$

Table 2-3 above lists agreeing experimental rate constants that have been calculated for the oxidation of Hg^0 via Cl_2 . This implies that, kinetically, this reaction is likely to occur at ambient conditions. Hall et al. reported a rate constant two orders of magnitude smaller than the one listed above, which accounts for potential surface reactions with the reaction vessel at ambient conditions. Hence, when studying this reaction at room temperature the possibility of surface reactions should be considered and may result in errors if neglected. Schroeder et al. report that their value is an overestimate of the actual rate constant for this reaction, questioning whether the product species are indeed HgCl_2 . The original data of the paper published by Schroeder et al. (P'yankov, 1949) report that the dominant product formed by this reaction is Hg_2Cl_2 .

Although there has been much experimental mercury speciation research performed, very little is directly applicable to obtaining rate constants for all possible conditions for the entire list of possible mercury oxidation reactions. Many of the researchers use the

limited kinetic data that has been measured and then create combustion models involving mercury oxidation. (Niksa et al., 2001; Widmer et al., 2000) Recall, the overall goal is to accurately determine which pathway is dominant in the flue gas environment at oxidizing elemental mercury to the water-soluble form, HgCl_2 . Answering this question involves a combination of close examination of both thermodynamic and kinetic calculations.

2.2. Literature Review on Current Models and their Predictions

Several thermodynamic and kinetic models have been developed to elucidate mercury's speciation in the coal combustion flue gases. The calculation of Gibbs free energy (ΔG°_T) allows one to determine the propensity that a given reaction will occur at a given temperature, T. The equilibrium constant is dependent upon ΔG°_T , and its calculation can determine whether or not a given reaction should be studied in detail. However, it is important to note that the equilibrium calculation does not lend any information on the kinetics or time scale for the reaction to proceed. Does the reaction take a fraction of a second or perhaps months to reach equilibrium? Therefore, a complete picture of these possible mercury oxidation reactions will involve the knowledge of both thermodynamics and kinetics so the overall reaction mechanism for oxidation can be determined. The following equation represents the temperature and Gibbs free energy relationship:

$$\Delta G^\circ_T = \Delta H^\circ_T - T * \Delta S^\circ_T \quad (2.1)$$

Using thermodynamic tables such as those available through the NIST webbook (Afeefy et al., 2003) or JANAF (Chase, 1998), one can determine the Gibbs free energy of a given reaction using the following relationship involving the stoichiometric coefficients, v_i , of the reactant and product species:

$$\Delta G^\circ_T = \sum v_i \Delta G^\circ_f \quad (2.2)$$

One more step allows for the calculation of the equilibrium constant, K_{eq} using equation (2.3) below:

$$K_{eq} = \exp[-\Delta G^\circ / RT] \quad (2.3)$$

Given a general gas phase reaction, K_{eq} is defined as,

$$K_{eq} = \prod_i \left(\frac{p_i}{p^0} \right)^{v_i} \quad (2.4)$$

such that p_i = partial pressure and p^0 = standard pressure (for the ideal gas phase, 1atm).

These equations allow for the calculation of the equilibrium constant over a range of temperatures. Examination of K_{eq} for a series of mercury oxidation reactions will allow one to see the importance behind these thermodynamic calculations. Recall from the experimental results in the previous chapter that some researchers proposed mechanisms involving Cl atoms, Cl_2 molecules, and/or HCl molecules. Some straightforward equilibrium calculations can provide insight on the likelihood of such reaction mechanisms. Keep in mind, however, that by purely examining the thermodynamics of these reactions, the kinetics are being neglected, which implies only half the story is being told at this point.

Table 2-4 below provides a list of equilibrium constants for reactions from possible mercury oxidation mechanisms that have been proposed by experimentalists. It is clear that any reactions involving the oxidation of HCl at high temperatures is not

thermodynamically favorable. It is interesting to note that the oxidation of Hg^0 in the presence of oxygen at temperatures less than 1200 K is thermodynamically probable, agreeing with the experimental results obtained by Hall et al. Examining reaction (3) at 298 K, the reaction is far from thermodynamically impossible. Recall that the equilibrium constant is proportional to the ratio of the product concentrations over the reactant concentrations. Therefore, examining the equilibrium constant for the oxidation of Hg^0 without oxygen, there would have to be a high concentration of the HCl reactant species.

Table 2-4. Equilibrium Calculations for Selected Mercury Oxidation Reactions

(1)	$Hg + Cl_2 \rightarrow HgCl_2$			
T(K)	298	600	1000	1200
K_{eq}	9.7×10^{-30}	5.2×10^{-12}	3.5×10^{-5}	5.9×10^{-3}
(2)	$2Hg + 4HCl + O_2 \rightarrow 2HgCl_2 + 2H_2O$			
T(K)	298	600	1000	1200
K_{eq}	2.0×10^{75}	3.7×10^{28}	1.4×10^1	3.7×10^{-5}
(3)	$Hg + 2HCl \rightarrow HgCl_2 + H_2$			
T(K)	298	600	1000	1200
K_{eq}	3.6×10^{-3}	4.4×10^{-5}	1.0×10^{-5}	3.7×10^{-6}
(4)	$HgCl + HCl \rightarrow HgCl_2 + H$			
T(K)	298	600	1000	1200
K_{eq}	1.1×10^{-17}	3.3×10^{-10}	4.2×10^{-7}	2.6×10^{-6}
(5)	$Hg + Cl \rightarrow HgCl$			
T(K)	298	600	1000	1200
K_{eq}	1.2×10^{14}	6.7×10^4	1.2×10^1	8.3×10^{-2}
(6)	$Hg + HCl \rightarrow HgCl + H$			
T(K)	298	600	1000	1200
K_{eq}	1.9×10^{-57}	1.1×10^{-28}	2.7×10^{-17}	2.0×10^{-14}
(7)	$HCl + OH \rightarrow Cl + H_2O$			
T(K)	298	600	1000	1200
K_{eq}	8.2×10^{10}	5.9×10^4	4.3×10^2	1.1×10^2
(8)	$Cl + Cl \rightarrow Cl_2$			
T(K)	298	600	1000	1200
K_{eq}	8.3×10^{36}	5.4×10^{15}	1.8×10^7	2.5×10^4
(9)	$Cl_2 \rightarrow 2Cl$			
T(K)	298	600	1000	1200
K_{eq}	1.2×10^{-37}	1.8×10^{-16}	5.4×10^{-8}	3.9×10^{-5}

Examining the equilibrium constant for reaction (7) from Table 2-4, one can conclude that this reaction is possible over a wide range of temperatures. Sliger et al. proposed that reaction (7) is the mechanism by which chlorine atoms are produced in the flue gases. Once the chlorine atoms are produced, they can readily react to oxidize elemental mercury. Atomic chlorine can react with elemental mercury via reaction (5) and appears thermodynamically favorable at temperatures below 1200 K. However, reaction (8) is a

very probable reaction over a wide temperature range, which also allows for the oxidation of mercury via molecular chlorine. The equilibrium calculation for reaction (1) exhibits that this reaction pathway of oxidation is also thermodynamically favorable. Again, it is important to emphasize that this current discussion is based solely upon thermodynamics and has not yet considered the kinetics of these reactions.

Equilibrium calculations performed by Senior et al. predicted that below 725 K all the mercury will be in the HgCl_2 form. Above 975 K, 99% of the mercury is predicted to be in the elemental form, Hg^0 , with the remaining 1% existing as HgO . In addition, they propose that between these two temperature limits, the relative concentrations of HgCl_2 and Hg^0 are dependent upon the chlorine concentration of the coal itself. (Senior et al., 2000) Since the flue gas is cooled prior to air pollution control devices, it is expected that all mercury should exist as the water-soluble HgCl_2 form. However, this is only the case if equilibrium conditions were dominant in the flue gas. In fact, other minor species such as CO and SO_2 do not have time to establish equilibrium as the flue gas cools. (Flagan and Seinfeld, 1988) Similarly, mercury also may not have time to equilibrate after the flue gas quenches. Senior et al. conclude in their study that the mercury oxidation is frozen in the flue gas at about 800 K.

Besides thermodynamic analysis, in an attempt to gain insight to the entire problem, a great amount of kinetic analysis and modeling has been performed. Sliger et al. suggested that the direct oxidation of Hg^0 via HCl has a high energy barrier through a

comparison to a similar reaction performed with cadmium. (Hranisavljevic et al., 1997) From this observation, they conclude that the oxidation occurs via an intermediate derived from HCl, with the intermediate being atomic chlorine. They report a fast rate at room temperature for the reaction of Hg^0 and Cl (Horne et al., 1968) of $1.95 \pm 1.05 * 10^{13}$ $\text{cm}^3/\text{mol*s}$. They propose a second step via HCl to the fully oxidized, HgCl_2 water-soluble form. The model that they developed required kinetic parameters including activation energies and rate constants. For the proposed first stage, they used the 1968 data from Horne et al. For the proposed second stage, they employed purely theoretical techniques. Sliger et al. used quantum mechanics and transition state theory to predict an activation energy and rate constant for the step involving the full oxidation of mercury via HCl. At room temperature their rate prediction is $6.88 * 10^2 \text{ cm}^3/\text{mol*s}$. Details of this calculation and its validity are discussed in great detail later in chapter 3.3.3.

A kinetic model was developed (Widmer et al., 2000) using SENKIN software and an adapted general combustion chemistry mechanism. (Glarborg et al., 1986) Required for their model were activation energies and rate constants for a series of mercury oxidation reactions. The data for the model which are listed below in Table 2-5, came from many different sources. Just as for the Sliger et al. proposed mechanism, Widmer et al. used the experimental data by Horne et al. for reaction (1). It is important to note that this research was performed in ideal conditions with just elemental mercury and chlorine atoms. There were no flue gas components such as water vapor, oxygen or carbon dioxide that the experimental results that much of the current literature include. Also, the

data from Horne et al. consists only of one data point at 393K. For reactions (2) and (4) Widmer et al. use analogous kinetic parameters taken from reactions that do not involve mercury, but rather, involve lead. Reactions (5), (6) and (8) were assigned the same values that were given to reactions (2), (4) and (3) without reasoning or validation. They found that their model underpredicts mercury oxidation at high temperatures. They propose, based upon research by Sliger et al., that the formation of chlorine atoms at these high temperatures is thermodynamically limited, which is evident through reaction (9) of Table 2-4. Overall, the kinetic model developed by Widmer et al. concludes that at high temperatures, free radicals such as chlorine exist, but the thermodynamics favor the decomposition of HgCl_2 . At the same time, at low temperatures where thermodynamics favors complete conversion of mercury, the oxidation process is too slow. Widmer et al. admit in their work, that required critical rate constants, and in some cases, even reliable thermodynamic data are currently lacking.

Table 2-5. Widmer et al. Kinetic Parameters for Mercury Oxidation Model

	A [cm ³ /mol*s]	B	E _a [kcal/mol]	ΔH _{rxn} [kcal/mol]
(1) Hg + Cl + M → HgCl + M	2.40*10 ⁸	-1.4	-14.4	-23.6
(2) Hg + Cl ₂ → HgCl + Cl	1.39*10 ¹⁴	0	34.0	34.0
(3) Hg + HOCl → HgCl + OH	4.27*10 ¹³	0	19.0	33.6
(4) Hg + HCl + → HgCl + H	4.94*10 ¹⁴	0	79.3	79.3
(5) HgCl + Cl ₂ → HgCl ₂ + Cl	1.39*10 ¹⁴	0	1.0	-26.0
(6) HgCl + HCl → HgCl ₂ + H	4.94*10 ¹⁴	0	21.5	19.1
(7) HgCl + Cl + M → HgCl ₂ + M	2.19*10 ¹⁸	0	3.1	-84.1
(8) HgCl + HOCl → HgCl ₂ + OH	4.27*10 ¹³	0	1.0	-26.9

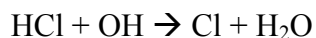
Kinetic modeling was also performed by Niksa et al. for homogeneous mercury oxidation, and their models included the influence of NO and H₂O in the simulated flue gases. They began the modeling with the kinetic framework provided by Widmer et al. as presented in Table 2-5 above. However, for reaction (7) from Table 2-5, the theoretical rate constant calculated by Sliger et al. was used. The model includes submechanisms accounting for a broad range of Cl and NO_x chemistry. (Roesler et al., 1992; Roesler et al., 1995) In addition, they use an updated moist CO oxidation submechanism (Roesler et al., 1992; Mueller et al., 1999a; Mueller et al., 1999b) at low to moderate temperatures, allowing for perturbations from NO_x conversion (Mueller et al., 1999b) and interactions between NO_x and SO_x (Mueller et al., 2000) conversion chemistry. The model also includes an H/N/O submechanism (Mueller et al., 1999b; Mueller et al., 2000; Allen et al., 1997), which describes the kinetics of NO_x conversion

at low to moderate temperatures. In total, the model developed by Niksa et al. includes 102 elementary chemical reactions. Just as Widmer et al., they used Senkin for the differential equation solving. They concluded that the only channel that oxidized mercury at appreciable rates is the oxidation of Hg^0 via atomic chlorine, while the decomposition of HgCl via OH radical was an inhibitor of mercury's oxidation. They found the primary production channel for the oxidation to the water-soluble form, HgCl_2 to be the oxidation of HgCl via Cl_2 . Niksa et al. found large inhibition effects from NO, which will react readily with OH radical to form HONO. One may question this initially since scavenging OH may mean promoting the formation of HgCl as previously mentioned. However, it turns out that the major role of OH is to produce Cl atoms and water through reactions with HCl . Therefore, if these OH radicals are scavenged via NO, then they are unavailable to create atomic chlorine which could react directly to oxidize Hg^0 .

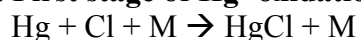
Overall, from reviewing the literature, it appears unanimous among the modelers that side reactions involving chlorine species play a key role in the mercury oxidation process. This implies that the recombination reaction involving chlorine atoms to produce molecular chlorine, Cl_2 , is as important to consider as the direct oxidation reactions involving mercury. This makes sense when one considers a mechanism involving the oxidation of mercury involving both atomic chlorine and molecular chlorine.

In addition, from both the thermodynamic and kinetic models, which have primarily been based on experimental mercury speciation data, one or a combination of the following channels appear to be the pathways of mercury's oxidation in the flue gases of coal combustion processes:

I. Formation of chlorine atoms:



II. First stage of Hg^0 oxidation:



III. Possible Second Stages of Hg^0 oxidation:

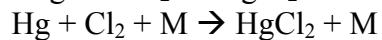
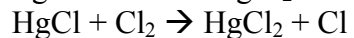
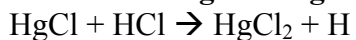


Figure 2-2. Possible Mercury Oxidation Pathway Hypotheses

The current work focuses on a slightly larger pool of potential mercury oxidation reactions and the results will be compared in future chapters through a combination of theoretical, experimental, and modeling results.

2.3. Quantum Mechanics and Basis Sets

Ab initio methods of quantum chemistry have in recent years proven to be effective in predicting the structure and thermodynamic properties of chemical systems. (Steinfeld et al., 1998; Pople, 1999; Gao and Truhlar, 2002; Alcami et al., 2001) All such methods seek to derive a solution of the Schrödinger Wave Equation (SWE) for the molecular system, formulated as a stationary configuration of nuclei with an accompanying set of interacting electrons.

The nuclei can be considered stationary as, being approximately three orders of magnitude heavier than the electrons, their motion occurs on a much slower timescale than that of the electrons, and thus the nuclear and electronic motions are effectively decoupled. Therefore, the SWE can be separated for the two. This is commonly known as the Born-Oppenheimer approximation, and has the consequence that one need only seek solutions for the electronic SWE (stated here in the usual atomic system of units):

$$\hat{H}_{el}\psi_{el} = E_{el}\psi_{el} \quad (2.5)$$

such that, $\hat{H}_{el} = -\frac{\hbar^2}{2m_e} \sum_i \nabla_i^2 - \sum_{\alpha} \sum_i \frac{Z_{\alpha} e'^2}{r_{i\alpha}} + \sum_j \sum_{i \neq j} \frac{e'^2}{r_{ij}}$ (2.6)

In equation (2.5), ψ_{el} is the wave function describing a particular electron, E_{el} are the electronic energies that lead one to predict such things as heats of reaction and activation energies, and the purely electronic Hamiltonian operator is defined in equation (2.6). (Levine, 2000) The first term in equation (2.6) is the operator for the kinetic energy of the electrons. The second term is the potential energy of the attractions between the electrons and the nuclei, r_{ia} , where α is the distance between electron i and nucleus. The third term is the potential energy of the repulsions between electrons i and j . It is important to note that this Hamiltonian operator neglects relativistic interactions such as the spin-orbit coupling of the electrons. The spin-orbit interaction would add another term to the Hamiltonian, and typically the influence of the addition of this term to the Hamiltonian increases with an increase in the atomic number. From the frame of reference of the electron, the nucleus appears to be moving around the electron, which induces a magnetic field on the electron. The spin-orbit coupling is the coupling of the magnetic field induced by the nucleus and its relationship to the intrinsic spin (magnetic moment) of the electron. The strength of the magnetic field is proportional to the orbital angular momentum while the magnitude of the electronic magnetic moment is proportional to the intrinsic spin of the electron. In general, the spin-orbit coupling equation is of the following form:

$$\hat{H}_{SO} = \xi(r) \hat{\mathbf{l}} \cdot \hat{\mathbf{s}} \quad (2.7)$$

$$\text{such that, } \xi(r) = \frac{1}{2\mu^2 c^2} \frac{1}{r} \frac{\partial V}{\partial r} = \frac{1}{2\mu^2 c^2} \left(\frac{Ze^2}{4\pi\epsilon_0 r} \right) \quad (2.8)$$

The wave equation becomes,

$$[\hat{H}_{el} + \hat{H}_{SO}] \psi_{el} = [\hat{H}_{el} + \xi(r) \hat{\mathbf{l}} \cdot \hat{\mathbf{s}}] \psi_{el} = E_{el} \psi_{el} \quad (2.9)$$

Perturbation theory can be used if the spin-orbit coupling is relatively small. If this method is applied, the spin-orbit Hamiltonian is treated as the perturbation. (Bernath, 1995; Berning et al., 2000) In addition, for lighter atomic species, L-S or Russell-Saunders is the coupling scheme used. Larger atoms on the other hand experience greater spin-orbit coupling and so configuration interaction has been the method used to obtain the zero-order wave functions. (Berning et al., 2000) Also, for larger atoms such as mercury, j-j coupling is required rather than L-S coupling. (Dicke and Wittke, 1960) The details of each coupling scheme are difficult and are omitted here.

Recalling that the focus of this research is on mercury-chlorine species, consider the molecule HgCl with a total of 115 electrons. For this molecule, spin-orbit coupling could potentially be a factor for energy computations. In order to examine the effect of spin-orbit coupling on HgCl, a review on how to obtain its term symbol is necessary.

For an atom, the term symbol is represented by,

$$^{2s+1}L_J \quad (2.10)$$

such that, $\hat{L} = \sum_i \hat{l}_i$, $\hat{S} = \sum_i \hat{s}_i$, and $\hat{J} = \hat{l} + \hat{s}$. (2.11)

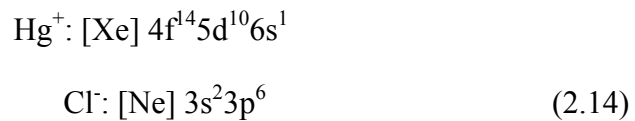
On the other hand, for a molecule, the term symbol is represented by,

$$^{2s+1}\Lambda_{\Omega} \quad (2.12)$$

such that Λ is the orbital angular momentum projection along the internuclear axis (z), Σ is the spin projection along the z-axis and

$$\hat{\Lambda} + \hat{\Sigma} = \hat{\Omega}. \quad (2.13)$$

Consider the electron configuration of Hg^+ and Cl^- separately,



As can be seen in Figure 2-3, when a mercury ion bonds with a chlorine ion, one valence electron goes into an antibonding orbital, σ^* in the ground state. Four of the p electrons, specifically two each from the p_x and p_y orbitals go into the two nonbonding π orbitals. The remaining two electrons go into the σ bonding orbital. The ground state term symbol for HgCl is $X^2\Sigma^+$. In general, the ground state is always represented with an X, the first excited state an A, the second excited state a B and so forth. In the case of HgCl , as seen in Figure 2-3, there is only one unpaired electron, yielding a spin multiplicity of two (i.e. $2S+1$), (where $S = \frac{1}{2}$). The plus in the exponent of the term symbol arises from the symmetry of the molecule with respect to a σ_v plane.

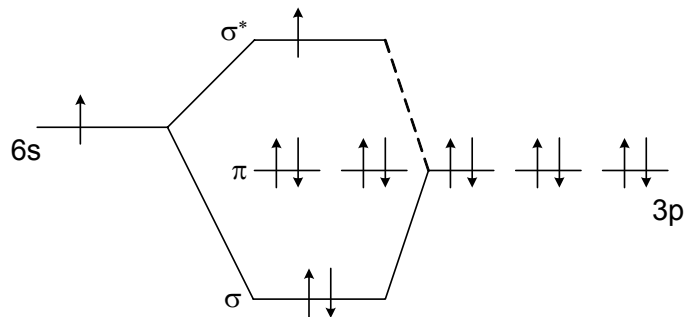


Figure 2-3. Molecular Orbital Diagram of HgCl

Examination of excited states of HgCl results in two different scenarios. Either an electron can be excited from σ to σ^* , or from π to σ^* . The first scenario results in a similar term symbol to that above, but since this corresponds to the second excited state, results in $B^2\Sigma^+$. The first excited state is not as straightforward since, in this case, the electron is being excited from a π nonbonding orbital. The π orbital corresponds to orbital angular momentum quantum numbers, Λ , of ± 1 . Also, the one unpaired electron can exist with Σ as either plus or minus $\frac{1}{2}$. From equation (2.14) above, this corresponds to Ω values of $1/2$ and $3/2$, yielding term symbols $A^2\Pi_{1/2}$ and $A^2\Pi_{3/2}$. Below in Figure 2-4 these different energy levels with possible transitions are presented. Spectroscopic techniques can be applied so that these excited states can be investigated. The two different Ω values correspond to different relative orientations of \hat{L} and \hat{S} , resulting in different amounts of spin-orbit interaction.

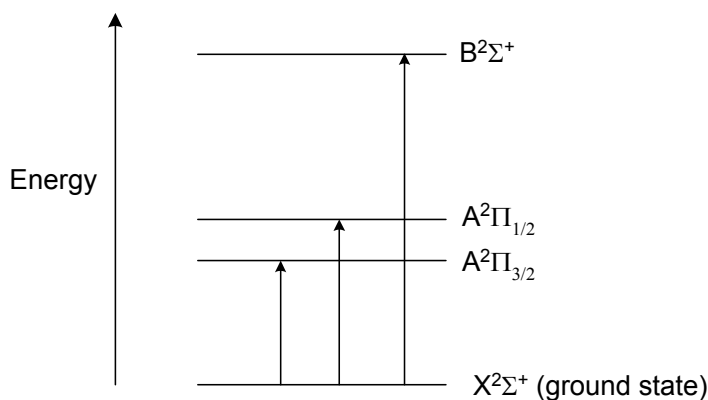


Figure 2-4. Schematic of Energy Level Splittings for HgCl

The Ω -splitting levels shown in Figure 2-4 is a representation of what is termed, “fine structure” in molecular spectroscopy. This current discussion offers a starting point to considering spin-orbit effects in future mercury calculations. Much work would still need to be done in terms of understanding how to apply some of the complex methods referenced here. Therefore, within the current work, spin-orbit coupling was not included in the Hamiltonian for the energy calculations. The concept of spin-orbit interaction will appear again later when nonadiabatic reactions are considered in chapters 3.2.3 and 3.2.4.

The wave equation (2.5) may only be solved analytically for the single-electron problem, and so for larger systems of interest, an approximate method must be employed. First it should be observed that the wave equation has an infinite dimensional solution space, and thus for computational purposes this must be approximated by a finite dimensional subspace spanned by a chosen set of basis functions which hopefully offer a reasonable representation of the electronic motion. In the usual ab initio molecular orbital (MO)

approach, one considers the molecular orbitals to be linear combinations of the atomic orbitals:

$$\Psi_i = \sum c_{\mu i} \phi_{\mu} \quad (2.15)$$

Ψ_i is the i -th molecular orbital, $c_{\mu i}$ are the coefficients of the linear combination, ϕ_{μ} is the μ -th atomic orbital, and n is the number of atomic orbitals. (Szabo and Ostlund, 1989) In the software used in this research, Gaussian 98 (Ref. 37), Gaussian-type orbitals are used in the calculations. A Gaussian-type orbital has the following form:

$$\chi_{a,b,c}(r, \theta, \phi) = N'_{a,b,c,\alpha} x^a y^b z^c e^{-\alpha r^2} \quad (2.16)$$

such that a , b , and c are quantum numbers which describe the angular shape and direction of the orbital, and exponents α which apply to the radial size of the electron. (Simons, 2003) In general, a basis set is a linear combination of these Gaussian Type Orbitals (GTOs). The explicit basis sets of each of the atoms studied in this work are presented in Appendix A.

The atomic orbitals are themselves expressable as linear combinations of the atomic basis functions. In general, the larger the basis set, the closer to the "exact" solution one gets. However, larger basis sets require more computational resources so there are practical limits to the accuracy one can obtain.

In addition, it is important to note that both polarization and diffuse functions were added to the basis sets of hydrogen, chlorine, oxygen and nitrogen when they were used in the calculations. Polarization functions are functions of one higher orbital angular momentum than an atom actually has in its valence orbital space. The orbital exponent of the basis function, however, cause their radial sizes to be similar to the actual sizes of the true valence orbital. The goal of the addition of polarization functions is to provide additional angular flexibility to the linear combination of atomic orbitals in forming bonding orbitals. (Simons, 2003) The addition of diffuse functions to a basis set can also improve the accuracy of the calculations. Typically diffuse functions are added for anions or compounds with lone pairs of electrons; in general, these species have significant density at large distances from the nucleus. A diffuse basis function is one with a small orbital exponent in the range of 0.01 to 0.1. (Levine, 2000)

Calculation methods can be divided into two categories; ab initio methods, which base themselves on the aforementioned MO statement, and density functional methods. The simplest ab initio method in common usage yielding at least semi-qualitative results is the Hartree-Fock Self Consistent Field (HF-SCF) approach. (Hehre et al., 1986) In this method, (2.5) is reduced to a one-electron problem for each electron, coupled so that each electron interacts with the averaged field of the other electrons. These are the so-called Fock equations, and are solved iteratively until self-consistency is obtained. HF-SCF has the advantage of being a variational method - the energy obtained is an upper bound of the exact energy, and is also reasonably cheap in terms of computational requirements.

However, the "averaged field" assumption in the scheme means that short-range correlations between electrons are ignored, and this can be particularly important when heavy elements are part of the system under study.

Thus for the present reaction systems of interest, a post-SHF correlated method is greatly desirable. Møller-Plesset (MP) perturbation theory is the next step in sophistication beyond HF, taking the HF wavefunction and energy as the zeroth-order components and applying the standard ansatz of Rayleigh-Schrodinger (RS) perturbation theory. (Møller and Plesset, 1934) Most commonly one takes the perturbation expansion to second order (MP2) or fourth order (MP4) depending on the computational resources available. (Bartlett and Shavitt, 1977; Purvis and Bartlett, 1978) MP methods generally do well at including the correlation energy (the difference between the "exact" HF energy and the energy from the exact solution), however it has been shown that the MP series expansion yields poor results for many heavy element systems. (Schwerdtfeger et al., 1989)

Thus for systems such as the mercury reactions of present interest, an "infinite order" method such as Coupled Cluster (CC) or Quadratic Configuration Interaction (QCI) is preferred. (Cizek, 1966; Cizek and Paldus, 1971; Chavitt and Schaefer, 1977; Pople et al., 1977) These methods use summation techniques to add certain terms in the MP expansion to infinite order, thus alleviating the problem of convergence. These approaches are also size-consistent - meaning that the method scales correctly with the number of particles in the system. This can be a problem when MP or truncated

Configuration-Interaction methods are applied to systems with a large number of electrons such as the species in this work.

A final matter of concern with these calculations is consideration of special relativistic effects, which can have a marked effect on systems including heavy elements. These are most evident in the inner core electrons of heavy atoms where electron velocities can be a considerable fraction of the speed of light. As previously mentioned, the relativistic effect of spin-orbit coupling will not be considered in the Hamiltonian. The time independent wave equation can only be solved exactly for the hydrogen atom and H_2^+ . The hydrogen atom being a two body problem and the hydrogen molecule ion being a three body problem, but solvable due to the nuclear distance being fixed while finding solutions for the electronic energies. In the current situation, mercury itself has eighty electrons. The Hamiltonian operator takes into account the kinetic energy of each electron, the attractive forces of each electron with the nucleus and each repulsive interaction experienced pairwise by the electrons. In order to simplify the calculations, the use of Effective Core Potentials (ECP) are essential. The ECP (also referred to as a pseudopotential) is an effective potential describing the inner core and at the same time semi-empirically accounts for relativistic effects. (Pettersson et al., 1983; Dyall, 2001)

The following relativistic effective core potentials are the most recent ones developed in the literature for mercury and are compared in this research: Stuttgart 1997 (Häussermann et al., 1993), Stevens and Krauss 1992 (Stevens et al., 1992), and Hay and Wadt 1985.

(Hay and Wadt, 1985). Further details of the methods and basis sets used are presented in chapter three where each reaction is studied in detail.

The Gaussian 98 (Pople et al., 1998) software package was used to calculate the relative energies of reactants, transition structures and product species for each reaction studied in this work. In addition, each energy in the work includes thermal corrections that include zero point energies. The frequency calculations were left unscaled due to the unavailability of proper scaling factors. (Pople et al., 1993) Tunneling corrections of the form below (Gonzalez-Lafont et al., 1991) were used in all of the rate constant calculations.

$$\kappa(T) = 1 + \left(\frac{1}{24} \right) \left(\frac{h v_{im} c}{k_b T} \right)^2 \quad (2.17)$$

such that h is Planck's constant, v_{im} is the imaginary frequency accounts for the vibrational motion along the reaction path, c is the speed of light, k_b is Boltzmann's constant, and T is the temperature. Tunneling is more of a factor for lighter atoms, but nevertheless was accounted for throughout the rate constant calculations in this work. This correction must be multiplied by the calculated rate constant in order to obtain the rate where tunneling is accounted for.

2.4. Chemical Kinetics Tools

A. Transition state theory

For bimolecular reactions, one traditionally uses transition state theory, which requires knowledge of an accurate transition structure so the activation energy is known. The following is a familiar equation for calculating the rate constant for a bimolecular reaction, originally derived from Eyring (1935):

$$k_{\text{bim}} = L^* \kappa \frac{Q^{\text{TS}}}{Q_A Q_B} \frac{k_B T}{h} e^{-\frac{E_a}{k_B T}} \quad (2.18)$$

such that κ is the tunneling correction; L^* is the statistical factor; Q^{TS} , Q_A , and Q_B are the partition functions of the transition structure and reactant species respectively; k_B is Boltzmann's constant; h is Planck's constant; and E_a is the activation energy.

The key to calculating the bimolecular rate constant is in finding an accurate activation energy, which requires knowledge of the location of the transition structure on the potential energy surface. In general, each of the $3n-6$ degrees of freedom of an n -atom non-linear molecule contributes one dimension to a potential energy surface ($3n-5$ for a linear molecule). In some cases, one may be fortunate if some of these degrees of freedom are constant along the reaction coordinate such that a three dimensional potential energy surface can be generated. However, in general, there are often more than just

three degrees of freedom that are involved during a reaction so the potential energy surface cannot be constructed except in a hyperspace, making the energetic analysis difficult. The transition structure is defined as the saddle point on the adiabatic potential energy surface. The following is a more mathematical definition (Steinfeld et al., 1999):

$$\begin{aligned}\frac{\partial U}{\partial s} &= 0, & \frac{\partial^2 U}{\partial s^2} &< 0 \\ \frac{\partial U}{\partial \xi} &= 0, & \frac{\partial^2 U}{\partial \xi^2} &> 0,\end{aligned}\tag{2.19}$$

such that U is the electronic potential energy, s is defined as the coordinate along the reaction path in which the energy is a maximum and ξ is defined as the coordinate perpendicular to the reaction path in which the energy represents a minimum. It is important to note that the second partial derivative with respect to the reaction coordinate, s , is negative which implies the vibrational frequency for motion along the reaction path is imaginary. Hence, when using quantum mechanical packages such as Gaussian 98, the criteria for a transition state search is that a stationary point is found where one imaginary frequency exists. However, when using this software, one should not stop after this point has been found. Locating a structure with one imaginary frequency does not guarantee a “correct” transition structure has been detected for a given reaction. To validate that the structure found is indeed a transition structure, either the vibrational modes should be carefully analyzed to ensure the negative frequency corresponds to the reaction coordinate or an intrinsic reaction coordinate (IRC) calculation should be performed.

One can obtain a summary of the IRC reaction path where the assumed transition structure geometry links the correct products to the correct reactants. Once an IRC calculation is performed, one can recognize with confidence that the transition structure is the true saddle point along the reaction path of interest.

B. Canonical variational transition state theory

Many of the reactions studied within this work appear to be barrierless reactions. For such reactions, the rate constants for each combination of method and basis set were calculated using canonical variational transition state theory (CVTST) given by:

$$k^{CVT/G}(T) = \kappa^G(T) k^{CVT}(T) \quad (2.20)$$

where T is the temperature, $\kappa^G(T)$ is a ground-state (G) transmission coefficient which primarily accounts for tunneling, and $k^{CVT}(T)$ is the hybrid canonical variational transition state theory (CVT) rate constant where the intrinsic reaction coordinate is treated classically and the bound vibrations are quantized. (Gonzalez-Lafont et al., 1991; Truhlar and Gordon, 1990) The hybrid CVT rate can be obtained by variationally minimizing the universal RRKM-theory rate constant, $k_{uni}(T)$ with respect to the position x of the generalized transition state along the reaction coordinate,

$$k^{CVT}(T) = \min_x k_{uni}(T, x) \quad (2.21)$$

where $k_{\text{uni}}(T, x)$ is expressed in equation (2.20).

C. RRKM theory

Transition state theory is traditionally used to calculate rate constants for bimolecular reactions. However, many of the reactions within this work are unimolecular, making RRKM (Rice-Ramsperger-Kassel-Marcus) theory a necessary tool. The overall unimolecular reaction is written in terms of two energies; E^+ and E^* as shown below in Figure 2-5. E^* is the energy of the reactant once it acquires the energy needed to react. The energy, E^+ , is the activation energy, E_0 , subtracted from the energy of the energized reactant (i.e. $E^+ = E^* - E_0$). (Holbrook et al., 1996)

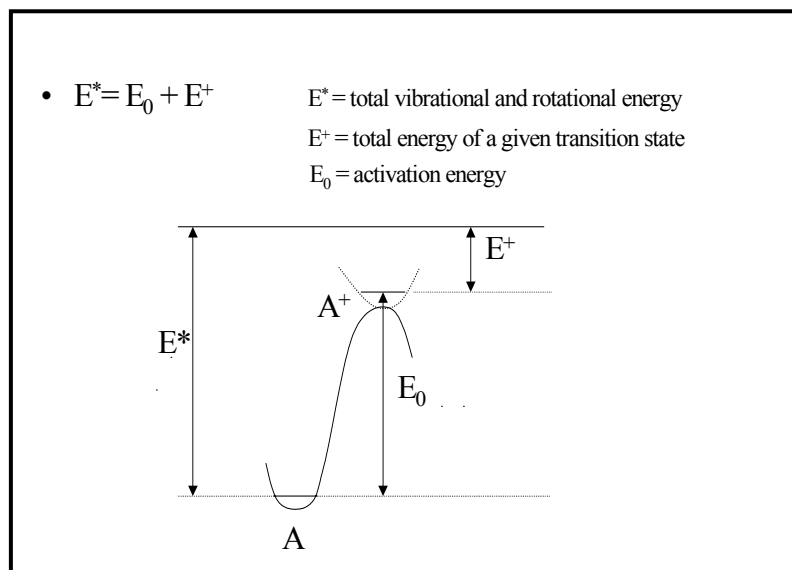


Figure 2-5. RRKM Energy Description

The density of states, $\rho(E^*)$, and the sum of states, $W(E^+)$, were calculated using the Beyer-Swinehart algorithm. (Beyer and Swinehart, 1973) The universal rate constant for a unimolecular reaction can then be calculated from:

$$k_{uni} = \frac{LQ_1^+ \exp(-E_0 / kT)}{hQ_1Q_2} \int_{E^+=0}^{\infty} \frac{W(E^+) \exp(-E^+ / kT) dE^+}{1 + k_a(E^*)/\beta_c Z_{LJ}[M]} \\ k_a(E^*) = \frac{LQ_1^+}{hQ_1\rho(E^*)} W(E^+) \quad (2.22)$$

E^* = total vibrational and rotational energy	L = statistical factor
E^+ = total energy of a given transition state	k = Boltzmann's constant
E_0 = activation energy	β_c = collisional efficiency
Q_1^+ = partition function for the rotation of A ⁺	$W(E^+)$ = sum of states
Q_1 = partition function for the rotation of A	$\rho(E^*)$ = density of states
Z_{LJ} = Lennard-Jones collision frequency	h = Plank's constant
Q_2 = partition function for non-rotational modes	[M] = concentration of bath gas

All of the parameters listed above can be obtained from theory with the exception of the collisional deactivation efficiency, β_c . This collisional efficiency is an empirical value that can be obtained through experimental knowledge of the reaction. (Troe, 1977) Many models have been determined for calculating the collisional efficiency, but again experimental data is necessary. (Keck and Carrier, 1965; Tardy and Rabinovitch, 1966) Due to the lack of experimental data for the reactions studied in this work, β_c is used as a fitting parameter that ranges between zero and one.

CHAPTER 3. OVERVIEW OF THEORETICAL RESULTS

3.1. Validation of Quantum Mechanical Methods and Basis Sets

Due to mercury having 80 electrons, relativistic effects are crucial to the calculations. Therefore each of the basis sets examined in this work include relativistic pseudopotentials. The following relativistic effective core potentials are the most recent developed in the literature for mercury and are the ones compared in this research: Stuttgart 1997 (Küchle et al., 1991; Häussermann et al., 1993; Dolg et al., 1991) and Stevens et al. 1992 (Stevens et al., 1992), and will be referred to as the 1997 and 1992 basis sets respectively throughout this work. However, in the early stages of the research a basis set developed by Hay and Wadt (Hay and Wadt, 1985) was also considered. Due to its disagreement with experiment it was disregarded in further calculations. The basis set used for chlorine is a standard Pople basis set including both diffuse and polarization functions: 6-311++G(3df, 3pd).

The LANL2DZ and SDD basis sets include relativistic pseudopotentials and are easy to use since they are built in to the Gaussian 98 software package. For this reason, these basis sets have been readily used by other researchers to perform the quantum mechanical calculations necessary for obtaining rate constant data. (Sliger et al., 2000; Li L.C. et al., 2003; Xu M. et al., 2003) Typically, the smaller the number of electrons accounted for in the effective core of the pseudopotential, the more accurate the energy predictions will

be. Both the LANL2DZ and SDD basis sets use a Dunning and Hay (1976) full double zeta basis set for first row elements. The LANL2DZ basis set includes the Los Alamos National Labs Double Zeta Effective Core Potential (ECP) for the sodium through bismuth elements, which was developed by Hay and Wadt in 1985. The SDD basis set includes a Stuttgart/Dresden ECP for the remainder of the elements after the first row. (Wedig et al., 1985; Schwerdtfeger et al., 1989; Häussermann et al., 1993) The current research, however, has focused on the use of relativistic pseudopotentials that have been developed more recently in literature and in fact include fewer electrons in the effective core in comparison to the built-in Gaussian basis sets for mercury.

It is important to recall the environment of the mercury oxidation reactions of interest in this research; these are possible reactions that are taking place within the flue gases of coal combustion. There are many chemical species that make up combustion flue gases and, depending on the source of the coal, the concentrations of these species can vary (Hall et al., 1991). Within this research the focus is on the oxidation of mercury via chlorine-containing species. Many researchers have concluded that the majority of mercury is oxidized through chlorine (Sliger et al., 2000; Widmer et al., 1998; Lee et al., 1998). However, it is important to note that there are other species that can either promote or inhibit mercury oxidation in the flue gases. Within these quantum chemical rate constant derivations, the conditions are ideal and only mercury and chlorine are examined. The presence of NO₂, SO₂, etc. are neglected for the sake of providing a

starting point to these calculations. Many of the experimentalists consider the entire chemical environment when obtaining mercury oxidation data. However, the data obtained is based upon mercury speciation data rather than rate constant data, making comparison to experiment a difficult task.

Table 3-1 provides a list of optimized bond lengths for all basis set and method combinations, showing the QCISD/1992 combination to be the most accurate with an average absolute error of 0.03 Angstroms. In fact, the 1992 and 1997 basis sets give fairly low errors for all computational methods that have been examined. In contrast, the research performed by Lai-Cai Li, et al. was based upon the SDD basis set and yielded an overall average error of 0.119 angstroms with the QCISD(T) results and 0.103 angstroms with the MP2 optimizations carried out for this work. Inaccuracies in molecular geometries will lead to incorrect vibrational analyses, which will then shift the partition functions and give an incorrect reaction rate. Once one verifies that geometries are correct, one needs to compare energetic results to available experimental data too.

Heats of reaction predictions are compared to experimental results using a large set of reactions involving mercury, chlorine, oxygen, and hydrogen atoms below in Table 3-2 to further validate the choice of method and basis set.

Although the 1992 and 1997 basis sets, which are the focus of this work, are less user-friendly than the LANL2DZ and SDD basis sets, they yield the most accurate predictions to experiment, as is evident from the heats of reaction comparison in Table 3-2.

In fact, Table 3-2 shows that the higher level QCISD method used in conjunction with the 1992 basis set provides the smallest deviation from experiment with an overall average error of 4.37 kcal/mol. It is also important to note how well the lower level B3LYP method performs in conjunction with the 1997 basis set. The computational effort for the B3LYP method is a fraction of that for the QCISD method, and the overall absolute error for this combination is 4.93 kcal/mol. Hence, it appears that B3LYP may be a reasonable method when used with the 1997 basis set in predicting reaction parameters. The SDD basis set with the QCISD calculational method was also considered in Table 3-2 due to its use in recent mercury speciation work (Xu et al., 2003; Li et al., 2003). However, for the nine reactions in Table 3-2, the SDD basis set with the QCISD method provided the greatest errors with an average absolute error of 16.14 kcal/mol. The MP2 calculational method in combination with the built-in SDD Gaussian basis set provides the greatest deviation from experimental heats of reaction values with an overall average error of 26.64 kcal/mol. Unfortunately, there have recently been publications using this unsuccessful combination (Li, L.C. et al., 2003). Modelers that depend on these theoretical predictions for kinetic data need to be aware that although the 1992 and 1997 basis sets may be less user-friendly because they are not built-in basis sets, they clearly are providing more accurate results than the built-in basis sets that have been used in the past (Sliger et al., 2000; Li L.C. et al., 2003; Xu M. et al., 2003).

Table 3-1. Bond Lengths (\AA) of Mercury Species

Method: Basis Set:	MP2 SDD	QCISD(T) SDD	QCISD 1992*	QCISD 1997*	B3LYP 1992*	B3LYP 1997*	B3LYP LANL2DZ	Experiment
HOCl :	0.997	0.9965	0.961	0.961	0.9666	0.9666	0.9576	0.975 ^a
H-O :	1.856	1.889	1.6869	1.6869	1.6996	1.6996	1.7012	1.690
O-Cl :	$\angle 103.4^\circ$	$\angle 102.8^\circ$	$\angle 103.5^\circ$	$\angle 103.5^\circ$	$\angle 103.6^\circ$	$\angle 103.6^\circ$	$\angle 103.2^\circ$	$\angle 102.5^\circ$
OH	0.9973	1.0036	0.9684	0.9684	0.9739	0.9739	1.0017	0.9708
HCl	1.3144	1.3243	1.2833	1.2833	1.285	1.285	1.3149	1.2746 ^a
HgCl	4.4587	4.4267**	2.412	2.4085	2.4896	2.4648	2.6122	2.23 ^b
HgCl ₂	2.3489	2.3612**	2.3003	2.3116	2.3195	2.3211	2.4423	2.28 ^c
Cl ₂	2.2455	2.2858	1.997	1.997	2.0106	2.0106	2.2244	1.9878 ^a
H ₂	0.7384	0.7473	0.7422	0.7422	0.7427	0.7427	0.7434	0.7414 ^a
HgO	1.9075	2.0025	1.9413	1.9535	1.9497	1.9474	2.0444	---
Average Absolute Bond Distance Error	0.351	0.360	0.030	0.031	0.044	0.041	0.110	

* Pople: 6-311++G(3df,3pd) basis set used for atoms other than mercury

** due to convergence problems these were run only to double excitations

^aRef (CRC, 2003-04); ^bRef (Maxwell and Moseley, 1940); ^cRef (Braune and Knoke, 1933)

Table 3-2. Heats of Reaction (kcal/mol) For Mercury Oxidation Reactions

Method: Basis Set:	MP2 SDD	QCISD SDD	QCISD 1992*	QCISD 1997*	B3LYP 1992*	B3LYP 1997*	B3LYP SDD	B3LYP LANL2DZ	Experiment NIST
Hg + HOCl → HgCl + OH	-18.79	26.11	22.71	14.94	29.99	22.61	36.67	11.19	31.199
Hg + HCl → HgCl + H	70.6	73.47	77.06	69.28	85.65	78.27	86.91	62.53	78.243
HgCl + Cl ₂ → HgCl ₂ + Cl	-60.09	-54.43	-30.07	-33.35	-18.04	-24.32	-50.97	-29.83	-24.723
HgCl + HCl → HgCl ₂ + H	-9.48	-4.04	23.78	20.5	35.81	29.53	1.92	25.77	20.449
Hg + 2HCl → HgCl ₂ + H ₂	-25.96	-22.67	-3.67	-14.73	2.45	-11.21	-15.9	-16.42	-5.514
Hg + Cl ₂ → HgCl ₂	-60.47	-54.87	-55.34	-66.4	-40.77	-54.44	-51.29	-54.43	-49.634
Hg + Cl → HgCl	-0.3783	-0.4454	-25.27	-33.05	-22.73	-30.11	-0.32	-24.59	-24.911
Hg + Cl ₂ → HgCl + Cl	19.99	23.07	23.2	15.43	31.79	24.41	34.01	6.92	33.071
HgCl + Cl → HgCl ₂	-80.47	-77.95	-78.55	-81.84	-72.57	-78.85	-85.3	-61.35	-82.705
HgCl + HOCl → HgCl ₂ + OH	-98.89	-51.39	-30.56	-33.84	-19.84	-26.12	-48.31	-25.57	-26.595
Average Absolute Error	26.64	15.05	4.42	9.37	6.77	4.67	12.08	11.06	

* Pople: 6-311++G(3df,3pd) basis set used for atoms other than mercury

In an attempt to decrease the error of the theoretically calculated heats of reaction, the 1992 and 1997 basis sets were extended. In general, it is important for the basis sets of the atoms in a given reaction to be balanced in terms of polarization and diffuse functions (Martin et al., 1999).

An imbalance can possibly result in superposition errors which may account for the errors in the theoretically calculated heats of reaction data from Table 3-2. Results of some basis set extensions were analyzed on only four of the nine reactions in Table 3-2 due to the computational expense of calculating the energies for HgCl₂. The extensions included the addition of a d-type diffuse function of 0.0837 and 0.01 to the 1992 and 1997 mercury basis sets, respectively, along with the addition of two f-type polarization functions with exponents of 0.4 and 0.9. These extensions were added to each of the basis sets in an attempt to gain a better balance. The results of this modification can be seen in Tables 3-3 and 3-4 below.

Table 3-3. Theoretical Heats of Reaction (kcal/mol) with 1992 Extensions

Method	QCISD	QCISD	QCISD(T)	QCISD(T)	QCISD	
Basis set for mercury	1992*	1992*	1992*	1992*	1992	NIST
Basis set for all other atoms	Dunning	Pople	Dunning	Pople	Pople	Experiment
(1) Hg + Cl + M → HgCl + M	-22.01	-23.96	-30.54	-32.65	-25.27	-24.91
(2) Hg + HOCl → HgCl + OH	24.48	23.55	20.43	19.30	22.24	31.20
(3) Hg + HCl → HgCl + H	76.53	76.23	69.36	68.97	74.92	78.24
(4) Hg + Cl ₂ → HgCl + Cl	25.50	24.51	20.97	19.84	23.20	33.07
Average Absolute Error	4.73	4.79	9.35	10.54	5.63	

Dunning: cc-pVTZ

Pople: 6-311++G(3df,3pd)

*refers to the modified 1992 basis set

Table 3-4. Theoretical Heats of Reaction (kcal/mol) with 1997 Extensions

Method	QCISD	QCISD	QCISD(T)	QCISD(T)	QCISD	
Basis set for mercury	1997*	1997*	1997*	1997*	1997	NIST
Basis set for all other atoms	Dunning	Pople	Dunning	Pople	Pople	Experiment
(1) $\text{Hg} + \text{Cl} + \text{M} \rightarrow \text{HgCl} + \text{M}$	-27.51	-28.65	-28.84	-30.11	-33.05	-24.91
(2) $\text{Hg} + \text{HOCl} \rightarrow \text{HgCl} + \text{OH}$	18.98	18.87	22.14	21.84	14.46	31.20
(3) $\text{Hg} + \text{HCl} \rightarrow \text{HgCl} + \text{H}$	71.03	71.55	71.07	71.51	67.14	78.24
(4) $\text{Hg} + \text{Cl}_2 \rightarrow \text{HgCl} + \text{Cl}$	20.00	19.83	22.67	22.39	15.43	33.07
Average Absolute Error	8.78	9.00	7.64	7.99	13.41	

Dunning: cc-pVTZ

Pople: 6-311++G(3df,3pd)

*refers to the modified 1997 basis set

This modification decreased the overall absolute error for the 1992/QCISD combination by 0.834 kcal/mol.

Also, the use of the correlation-consistent basis sets of Dunning instead of the Pople basis set used in the previous calculations decreased the error by an additional 0.069 kcal/mol. In fact, careful observation of the results in Tables 3-3 and 3-4 show that the use of Dunning or Pople basis sets for all other atoms aside from mercury provide similar results and either is a reasonable basis set choice for this system. Comparing the results of Tables 3-3 and 3-4 for the given set of reactions, it is clear that the extended 1992 basis set with the QCISD method provides the most accurate results in terms of heats of reaction predictions.

To obtain further energetic accuracy compared to experiment, the Quadratic Configuration calculations were extended to include triple excitations. However, using the 1992/QCISD(T) combination, the triple excitations increased the overall absolute error for heats of reaction predictions. On the other hand, in the case of the 1997 basis set, the use of QCISD(T) decreased the error significantly. Based upon the results of Tables 3-3 and 3-4, the extended 1992 basis set for mercury with the QCISD method will be strongly considered for calculating transition structures for future rate constant calculations. When the 1997 basis set for mercury is used, QCISD(T) should be used in addition to the extensions to the basis sets.

It is important to emphasize that these thermodynamic results are based upon only four of the nine reactions studied in Table 3-2 due to the computational expense of computing the structure and frequencies of HgCl₂. In order to verify that the above mentioned combination is indeed the most accurate, calculations should be carried out on all nine of the reactions in future work.

3.2. First Stages of Oxidation



This is a reaction for which experimental data is available. Thus, with this relatively simple system, a comparison of the accuracy of various theoretical methods can be made. Given the discovery of a sufficiently accurate method, it may be employed to make theoretical predictions on related mercury - chlorine systems for which experimental data is currently absent.

The basis set for chlorine was chosen due to the agreement of the calculated theoretical rate constant with the experimental rate constant for the following reaction:



as shown by Figure 3-1 below. (Carabetta and Palmer, 1967) Comparing the theoretical results to experiment, the decomposition reaction of chlorine has a collisional efficiency in the range of 0.1 to 0.2 . Agreement between the theoretical and experimental rate constants showed that the Pople, 6-311++G(3df, 3pd) basis set was adequate for chlorine.

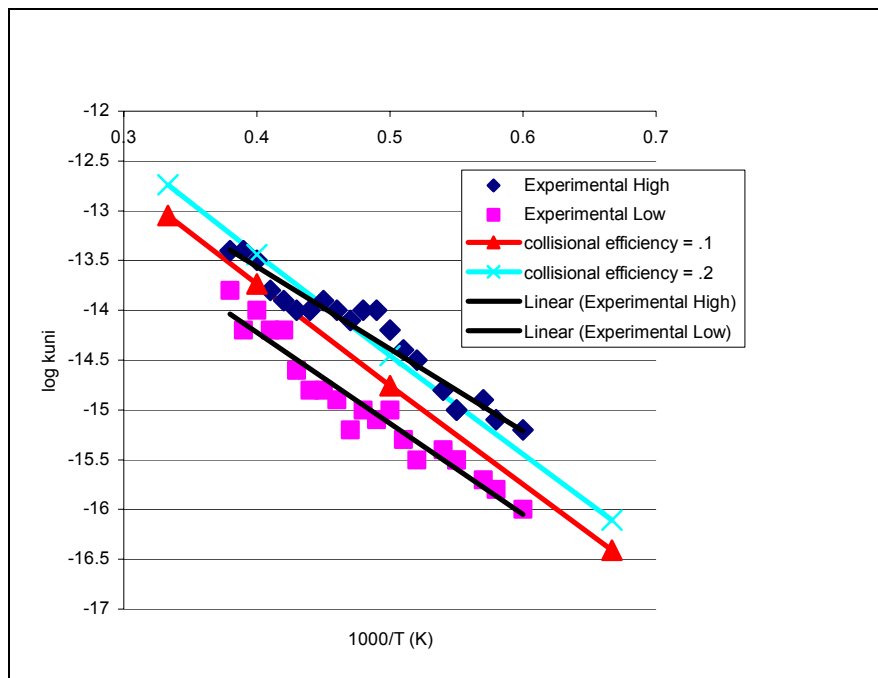


Figure 3-1. Comparison of Rate Constants, $\text{Cl}_2 + \text{M} \rightarrow 2\text{Cl} + \text{M}$

The experimental rate constant reported for the reverse of reaction (3.1) is $1.95 \times 10^{10} \text{ M}^{-1}\text{sec}^{-1}$. (Horne et al., 1968) RRKM theory allows for the calculation of unimolecular decompositions in the forward direction only. Thus, the equilibrium constant was found to be $K_{eq} = 2.21 * 10^{-10}$ with the Shomate Equation and data from the NIST webbook before the following relationship was used to calculate the equilibrium rate constant,

$$K_{eq} = \frac{k_1}{k_{-1}} \quad (3.3)$$

The experimental rate constant for the forward reaction is $4.309 \text{ M}^{-1}\text{sec}^{-1}$. In addition to the 1992 and 1997 basis sets, a third basis set developed in 1985 by Hay and Wadt was also examined. Within the present research, reaction (3.1) was the first studied and so a broader range of mercury basis sets was initially considered. As the research progressed, calculations were carried out using the 1992 and 1997 basis sets only. Each of the mercury basis sets (1985, 1992, 1997) were combined with two chosen methods (MP4SDQ, QCISD) forming six different combinations. Density functional theory using B3LYP with the LANL2DZ basis set was also studied giving seven theoretical combinations evaluated in this work. Experimental thermodynamic and kinetic data are compared to theory for each combination of method and basis set in Table 3-5.

The 1985 basis set was eliminated from consideration after comparing the calculated geometries with experiment with a minimum error of 25%. A reason for the inaccuracy of the 1985 basis set is due to the small number of basis functions outside the effective core. Recall that a basis function contains an exponent that is allowed to change throughout the calculation to provide orbital flexibility. Each basis function acts as a single electron orbital. In general, the smaller the number of electrons represented as functions on their own with the flexibility of the orbital exponent, the less accurate the results will be. Unfortunately in the case of the 1985 basis set, a majority of the electrons are held ‘fixed’ in an effective core. The explicit basis functions of the 1985 basis set is available in Appendix A.

Similarly, density functional theory using the B3LYP/LANL2DZ combination yielded an inaccurate geometry value with an error of 11.6%. However, it is important to note that the theoretical rate constant is within two orders of magnitude of the experimental value. Due to the large error of the estimated geometry by density functional theory, the accuracy of the rate constant calculation should be questioned and this method and basis set will not be considered further for this reaction. At this point there are four combinations left for comparison for reaction (3.1).

Table 3-5. Thermodynamic and Kinetic Data, $\text{HgCl} + \text{M} \rightarrow \text{Hg} + \text{Cl} + \text{M}$

	Experimental	LANL2DZ B3LYP	1985 MP4SQ	1985 QCISD	1992 MP4SQ	1992 QCISD	1997 MP4SDQ	1997 QCISD
Geometry (Å)	2.23 ^a	2.612	1.689	1.689	2.406	2.412	2.404	2.407
ΔH_{rxn} (kcal/mol)	24.91 ^b	24.95	-	-	26.00	25.89	32.98	33.02
Frequency (1/cm)	-	228	1583	1582	292	290	300	292
Activation Energy (kcal/mol) at 393K	-	82.15	-	-	71.60	67.52	87.01	84.34
Rate Constant ($\text{M}^{-1}\text{s}^{-1}$) at 393K	$k_1=4.309$ $k_{-1}=1.95*10^{10}$ [c]	$k_1=2.29*10^{-1}$	-	-	$k_1= 4.25$	$k_1= 14.6$	$2.98*10^{-2}$	$6.11*10^{-2}$

^aRef (Maxwell and Mosely, 1940), ^bRef (NIST), , ^cRef (Horne et al., 1968)

Experimental frequency values for mercuric chloride could not be found, but the four theoretical combinations remaining give frequencies that range between 290 and 300 wave numbers. Comparing each combination of method and basis set to the experimental geometries, the errors are relatively equal, with 1997/MP4sdq having the lowest error of 2.7% and 1992/QCISD having the greatest error of 3.0%. A comparison of the heats of reaction shows that the 1992 basis set has a maximum error of 3.9% compared to the 1997 basis set which has a minimum error of 32.3%. This implies the energies using the 1997 basis set will not be accurate, leading to incorrect activation energies.

Comparing the theoretical rate constants to experiment, the most accurate combinations are 1992/QCISD and 1992/MP4SDQ. Using Figure 3-2 below, with $\beta_c = 0.2$ for the decomposition reaction of mercuric chloride, both rate constant estimates are within an order of magnitude of the experimental rate constant value. These results lead to the conclusion that the 1992 basis set is the most accurate when compared to all available experimental data.

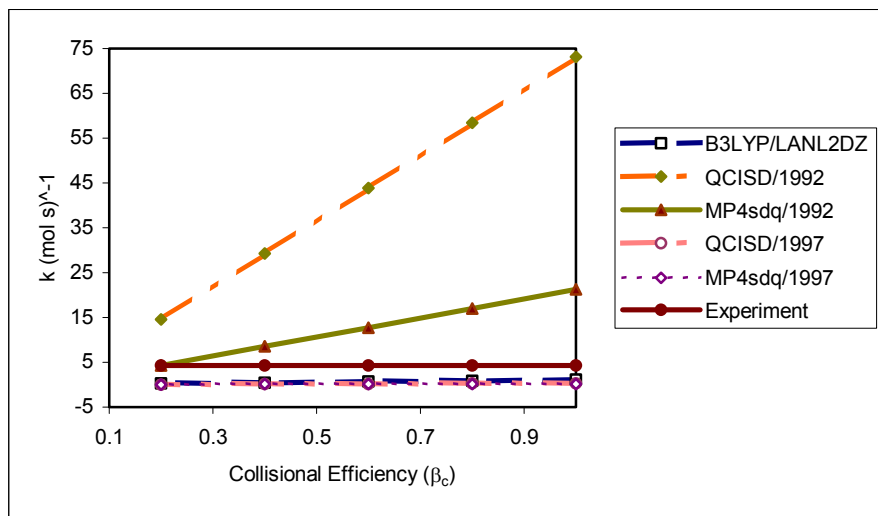


Figure 3-2. Rate Constants Varying β_c , $\text{HgCl} + \text{M} \rightarrow \text{Hg} + \text{Cl} + \text{M}$

This research strongly suggests that the 1992 basis set is a good basis set for representing mercury when calculating reaction phenomena. However, due to the lack of experimental data for reaction (3.1), it will be important to consider both the 1992 and 1997 basis sets for future oxidation reactions involving mercury and chlorine. Also, due to the convergence problems associated with large basis sets and Møller-Plesset perturbation theory, QCISD will be the method of choice.

From the calculations in this work and using Figure 3-3 below, it was found that a good estimation of the rate constant for the reverse of reaction (3.1) is:

$$k^{\text{CVT/G}} [\text{M}^{-1}\text{s}^{-1}] = 4.25 \times 10^{10} e^{-8588/T} \quad (3.4)$$

in the temperature range of 393 - 1500 K.

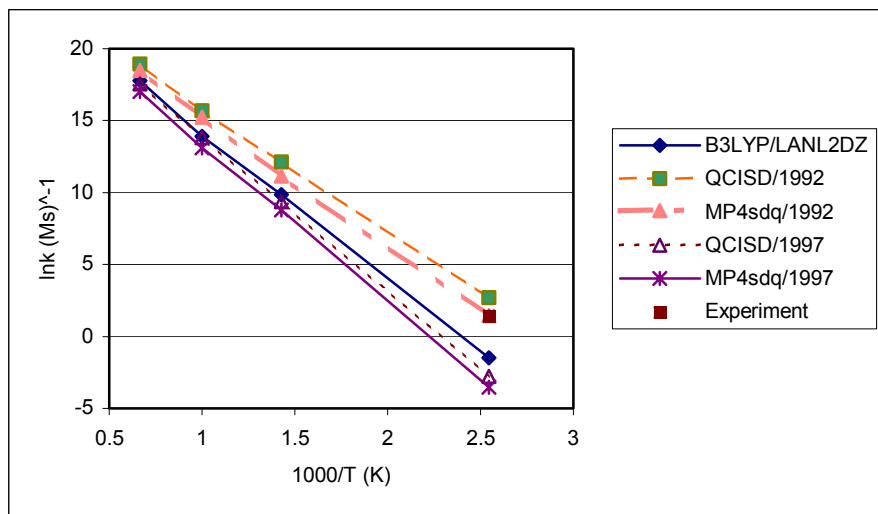


Figure 3-3. Comparison of Rate Constants, $\text{HgCl} + \text{M} \rightarrow \text{Hg} + \text{Cl} + \text{M}$

The rate constant expression is based upon the QCISD calculational method and the 1992 basis set for mercury. This expression will be used as a final expression for this reaction which will be incorporated later in the modeling section of this work.



Similar to reaction (3.1), the Stuttgart 1997 and Stevens et al. 1992 basis sets including relativistic effective core potentials are used for mercury in the study of reaction (3.5). The basis set used for chlorine and hydrogen is a standard Pople basis set including both diffuse and polarization functions; 6-311++G(3df, 3pd).

The B3LYP calculational method was used in the kinetic predictions of reaction (3.5). Recall from Table 3-2, the 1997 basis set in combination with the B3LYP method resulted in heats of reaction errors of less than 5 kcal/mol. Although QCISD has proven to be a more accurate method, B3LYP is computationally less expensive. The motivation behind the kinetic study of reaction (3.5) was to obtain fairly accurate energies, but with a reduction in the computational cost than results with the use of QCISD.

To the author's knowledge, this is the first time that reaction (3.5) has been examined theoretically through quantum mechanical techniques. The B3LYP density functional computational method, in combination with each of the 1992 and 1997 basis sets, was used to calculate rate constants and activation energies for reaction (3.5) from 298 – 2000 Kelvin.

Due to the lack of experimental kinetic data available for reactions (3.5) over a sufficient temperature range, it is imperative to compare to data that is experimentally available such as heats of reaction, geometries and frequencies. Table 3-6 below shows a comparison of varying calculational method and basis set combinations.

Table 3-6. Thermodynamic and Energetics Data, $\text{Hg} + \text{Cl}_2 + \text{M} \rightarrow \text{HgCl}_2 + \text{M}$

T=298K

	Experimental	1992 B3LYP	1997 B3LYP
Geometry (Å)			
HgCl	2.23 ^a	2.4896	2.4648
HCl	1.2746 ^b	1.2808	1.2808
HgCl ₂	2.28 ^c ∠180°	2.3195 ∠180°	2.3211 ∠180°
Frequencies (1/cm)			
HgCl ^d	292.61	244.40	260.97
HCl ^d	2989.74	2943.60	2943.60
HgCl ₂ ^e	75, 75, 363, 413	92,92,318,374	84,84,319,373
Transition Structure	no experimental data available	105, 222, -247	96, 227,-237
ΔH_{rxn} (kcal/mol)^f	-49.63	-55.34	-54.44
Activation Energy (kcal/mol)			
forward	no experimental data available	39.34	30.51
reverse	no experimental data available	80.12	84.95

^aRef (Maxwell and Mosely, 1940), ^bRef (CRC, 2004), ^cRef (Braune and Knoke, 1933), ^dRef (Herzberg,),

^eRef (Herzberg,), ^fRef (NIST)

Table 3-6 above also shows a comparison of experimental geometries and frequencies to the theoretical predictions regarding reaction (3.5). In terms of the optimized

geometries, both basis sets have similar predictions, with the 1997 basis set being just slightly more accurate. In terms of predicted frequencies, the 1997 basis set proves to be the most accurate with an overall absolute average error of 30.0 cm^{-1} compared to 35.4 cm^{-1} for the 1992 basis set. The 1997 basis set also performed better with the heat of reaction prediction being within 5 kcal/mol to experiment. The 1992 basis set in combination with B3LYP has an error of 5.71 kcal/mol when compared to the experimental heat of reaction value.

Transition state theory was used in combination with Figure 3-5 below to calculate the theoretical rate constant data for reaction (3.5).

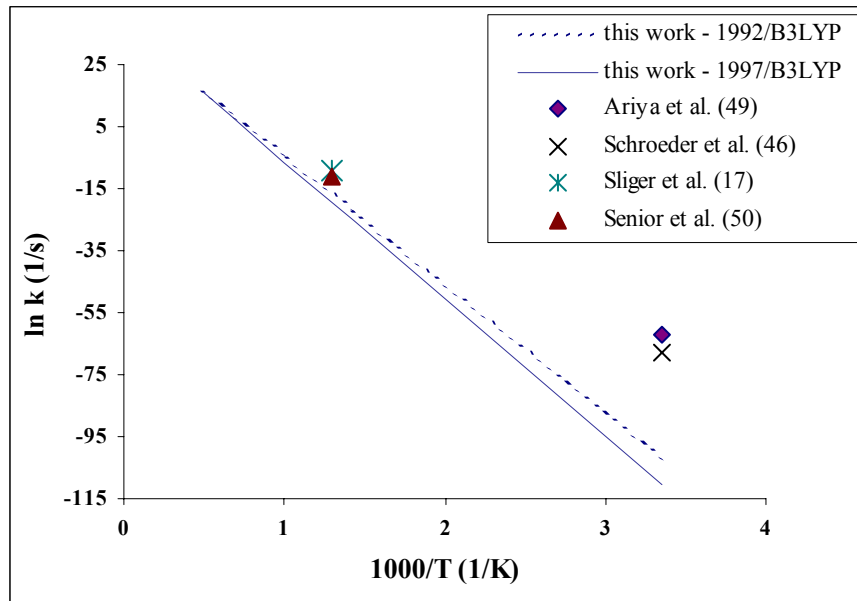


Figure 3-4. Comparison of Rate Constants, $\text{HgCl}_2 + \text{M} \rightarrow \text{Hg} + \text{Cl}_2 + \text{M}$
For the theoretical predictions, $\beta_c = 0.1$

In Figure 3-4 above, both experimental and model results are compared to the theoretical results predicted in the current research. Schroeder et al. performed a detailed analysis (1991) on the experimental findings of P'yankov (1949) and Menke and Wallis (1980). There has also been more recent experimental progress on this reaction by Ariya et al. (2002). It is important to note that these experimental kinetic findings are for ambient conditions at 1 atmosphere and 298 Kelvin. In addition, there have been both experimental (Sliger et al., 2000) and modeling work (Senior et al., 2000) performed for this reaction at 1 atmosphere and 773 Kelvin. Again, the limited experimental data available in the literature for a sufficient temperature range poses difficulty in comparing the theoretical predictions to experiment. This emphasizes the importance of quantum mechanical predictions of such data where experimental results are difficult to carry out. Table 3-7 below provides a comparison of the theoretical kinetic predictions to those found in the literature.

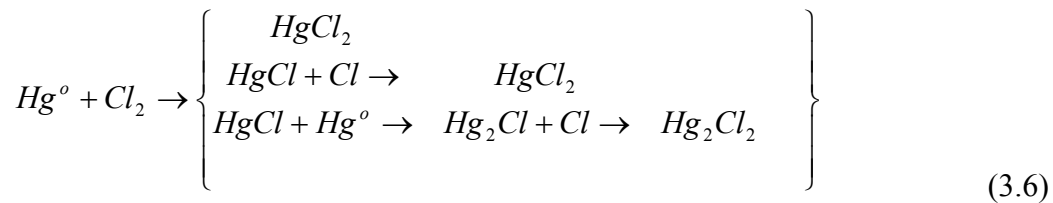
Table 3-7. Rate Constant Data, $\text{Hg} + \text{Cl}_2 + \text{M} \rightarrow \text{HgCl}_2 + \text{M}$

Temperature (K)	K_{eq}^{a}	$k_{\text{for}} (\text{cm}^3/\text{mol s})$	$k_{\text{rev}} (1/\text{s})$
298	1.018×10^{31}	Experimental 2.40×10^8 [b] 6.02×10^5 [c]	Theoretical 1992/B3LYP: 3.98×10^{-45} 1997/B3LYP: 1.06×10^{-48} Experimental 9.63×10^{-28} [b] 2.41×10^{-30} [c]
773	5.08×10^8	Experimental 3.4×10^9 [d] Model 6.44×10^8 [e]	Theoretical 1992/B3LYP: 7.79×10^{-8} 1997/B3LYP: 3.61×10^{-9} Experimental 1.05×10^{-4} [d] Model 1.99×10^{-5} [e]

^aRef (NIST), ^b(Schroeder et al., 1991), ^c(Ariya et al., 2002), ^d(Sliger et al., 2000), ^e(Senior et al., 2000)

The lack of agreement of the theoretical predictions to experimental and model findings requires some explanation. The experimental rate constant value calculated at ambient conditions from the analysis of Schroeder et al. is based heavily on the concentration of chlorine and water vapor in the reaction. It is important to note that the quantum mechanical predictions are based on ideal conditions, that is, without the presence of water vapor and other constituents that may exist in either the flue gases of coal combustion or the atmospheric environment of mercury oxidation. In fact, the experimental work described by Schroeder, et al. also considers the oxidation of mercury via molecular chlorine in the troposphere, which differs greatly from the chemical environment of the coal combustion exhaust. Therefore, using this experimental data for modeling the flue gases of coal combustion should be done carefully. Schroeder, et al.

claim that this value is an upper estimate for the rate constant of reaction (3.5). Another aspect to consider is the potential complexity of solely studying reaction (3.5) as an isolated system from an experimental perspective. In other words, one does not know if the experimental rate constant found is a global rate constant accounting for product species other than $HgCl_2$, like would happen in multichannel reactions. Below is a representation of the potential complexities that experimentalists may confront when reacting elemental mercury with molecular chlorine.



In fact, the work of P'yankov explicitly states that the principal formation was that of mercurous chloride (Hg_2Cl_2) not mercuric chloride ($HgCl_2$). Ariya, et al. also claim that their calculated rate constant for reaction (3.5) is an overestimate, but provide few details on why this is true. A third experimental data point for reaction (3.5) was reported by Sliger, et al. and although this experimental data also disagrees from the theoretical prediction, the difference is much less, within four orders of magnitude. When comparing this experimental rate constant data to the 1997/B3LYP combination that has performed very well thus far, there is a disagreement of five orders of magnitude. There are two comments to be made here. The first point is that there is a lack of experimental data at this temperature since we have only one data point for comparison. Second, the

purpose of this paper is to determine whether the lower level B3LYP method is suitable for kinetic predictions. At this point one should not rule out the use of B3LYP completely without more experimental data for reaction (3.5), which may be impossible to generate for an isolated system.

Figure 3-5 below shows the transition structure bond lengths and angles of reaction (3.5). The transition structure is a trigonal planar structure that proceeds via a very slow rate constant as can be seen from the theoretical predictions in Table 3-7.

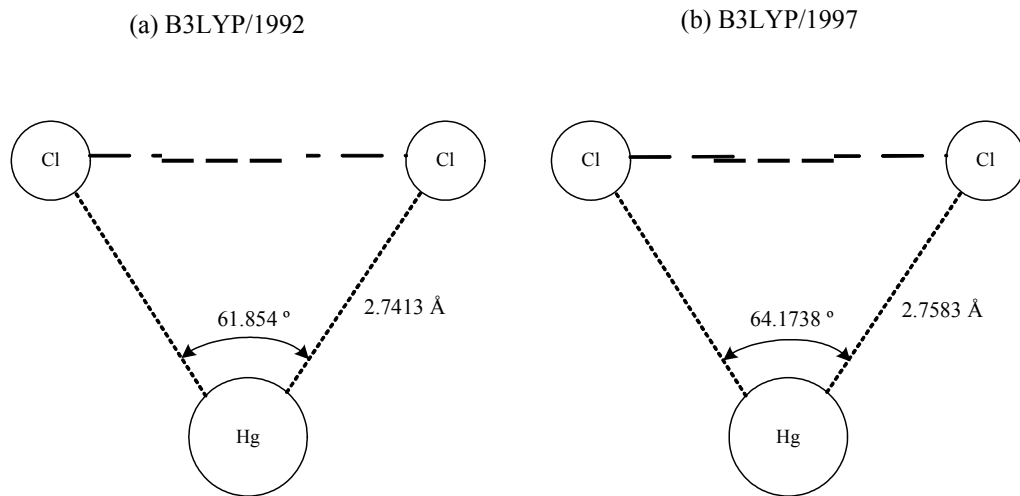


Figure 3-5. Transition Structures, $\text{Hg} + \text{Cl}_2 + \text{M} \rightarrow \text{HgCl}_2 + \text{M}$

Since RRKM theory allows for the calculation of unimolecular decompositions in the forward direction only, to compare to the experimental data, the equilibrium constant had

to be calculated at 298 and 773 K. The equilibrium constant at 298 K and 773 K was found to be 1.018×10^{31} and 5.08×10^8 , respectively, using the Shomate equation and data from the NIST webbook. Using the following equation for the equilibrium constant,

$$K_{eq} = \prod (a_i)^{\nu_i}, \quad (3.7)$$

and the forward and reverse rate expressions for equation (3.5), a relationship between K_{eq} and the forward and reverse rate coefficients using activity coefficients can be described with the following equation:

$$K_{eq} = \left(\frac{RT}{1bar} \right) \frac{k_1}{k_{-1}} \quad (3.8)$$

Substitution of K_{eq} and the experimental forward rate constants yield experimental rate constants for the reverse of reaction (3.5), which are listed in Table 3-7 for comparison to the theoretical predictions.

RRKM theory was used to calculate the theoretical rate constants in Figure 3-5. The collisional efficiency, β_c , for reaction (3.5) was assumed to be 0.1, which is typical for this type of decomposition reaction involving mercury and chlorine. (Wilcox et al., 2003)

Using Figure 3-4, the rate expressions calculated for the oxidation of mercury via molecular chlorine are:

$$k^{\text{UNI}} [1/\text{s}] = 1.94 \times 10^{16} e^{-41642/T}, \text{ using B3LYP/1992}$$

$$k^{\text{UNI}} [1/\text{s}] = 2.29 \times 10^{16} e^{-44144/T}, \text{ using B3LYP/1997}$$

in the temperature range of 298 - 2000 K. We see here that the very large activation barrier for direct insertion of mercury into Cl_2 will lead to a very slow reaction that probably will not contribute to the overall reaction mechanism of mercury oxidation by chlorine. However, this work is the first work to even demonstrate that this reaction is feasible and could contribute to the overall rate of mercury oxidation.

Finally, reaction (3.5) has been modeled in previous work (Edwards et al., by using the experimental rate constant for reaction (3.1), which was reported by Horne et al. using flash photolysis in 1968. (Horne et al., 1968) Due to the difference in the collisional diameters between HgCl (molecule colliding with chlorine in reaction (3.5)) and Hg , the overall reaction energetics and collisional frequency will be substantially different for these reactions. Also, Edwards et al. assumed an activation energy for reaction (3.5) of zero, however, from the theoretical estimates obtained in this work, the activation energy for reaction (3.5) is estimated to be a substantial 30.51 kcal/mol using the 1997/B3LYP basis set and quantum mechanical method. Hence, it is evident that the few modelers

who have identified this reaction as important were making severe extrapolations from the lack of available data for this reaction.

Future work could entail examining reaction (3.5) toward other product species like HgCl and Cl. It will be interesting to compare the upper limit experimental estimates to the combined rates obtained from the two different pathways in this work with the multichannel results from the entire mechanism when all of the data has been generated. The results reported for this reaction will allow the older models to now be updated to correctly reflect the kinetics of reaction (3.5).



When the computational time is available, the best method of obtaining a valid transition structure for a given reaction is to create a potential energy surface. The QCISD method with each of the 1992 and 1997 basis sets were used to create three dimensional potential energy surfaces for reaction (3.9). Due to the reaction only having three atoms, it was assumed that chlorine approached mercury linearly on the path to the transition state and this was verified to be the lowest energy configuration for many sample coordinates. Hence, in the potential energy surface calculations, one axis corresponds to the chlorine bond stretching, while the other corresponds to the mercury chlorine bond forming. The potential energy surfaces for the 1992 and 1997 basis sets are presented as Figures 3-7 and 3-8 respectively. These surfaces are representing a three dimensional energy plot with respect to sequential changes in the nuclear distance. Recall the basis of the Born-Oppenheimer approximation is that the motion of the electrons is decoupled from that of the nucleus so that the solution to the SWE is an electronic energy solution with a fixed nuclear distance. The reaction coordinate of reaction (3.9) is such that the Cl_2 bond is stretching as the HgCl bond is forming as it approaches a transition structure. The surfaces presented in Figures 3-6 and 3-7 represent the ground energy surfaces for reaction (3.9) with each the 1992 and 1997 basis sets. The triplet surface is the excited surface of the reactant species, while the singlet surface is the excited surface of the product species. These excited surfaces are not studied in this work and not presented in the potential energy surfaces in Figures 3-6 and 3-7.

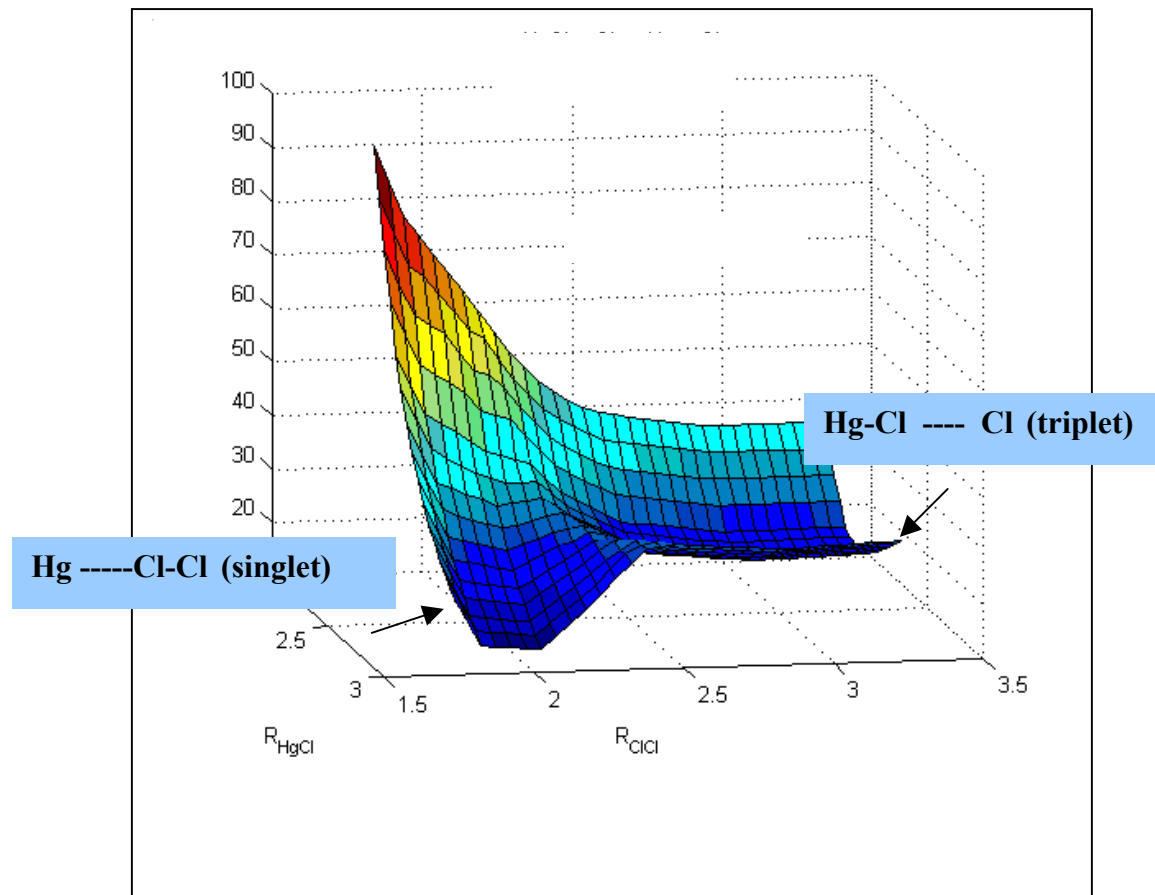


Figure 3-6. Potential Energy Surface (1992 BS), $\text{Hg} + \text{Cl}_2 \rightarrow \text{HgCl} + \text{Cl}$

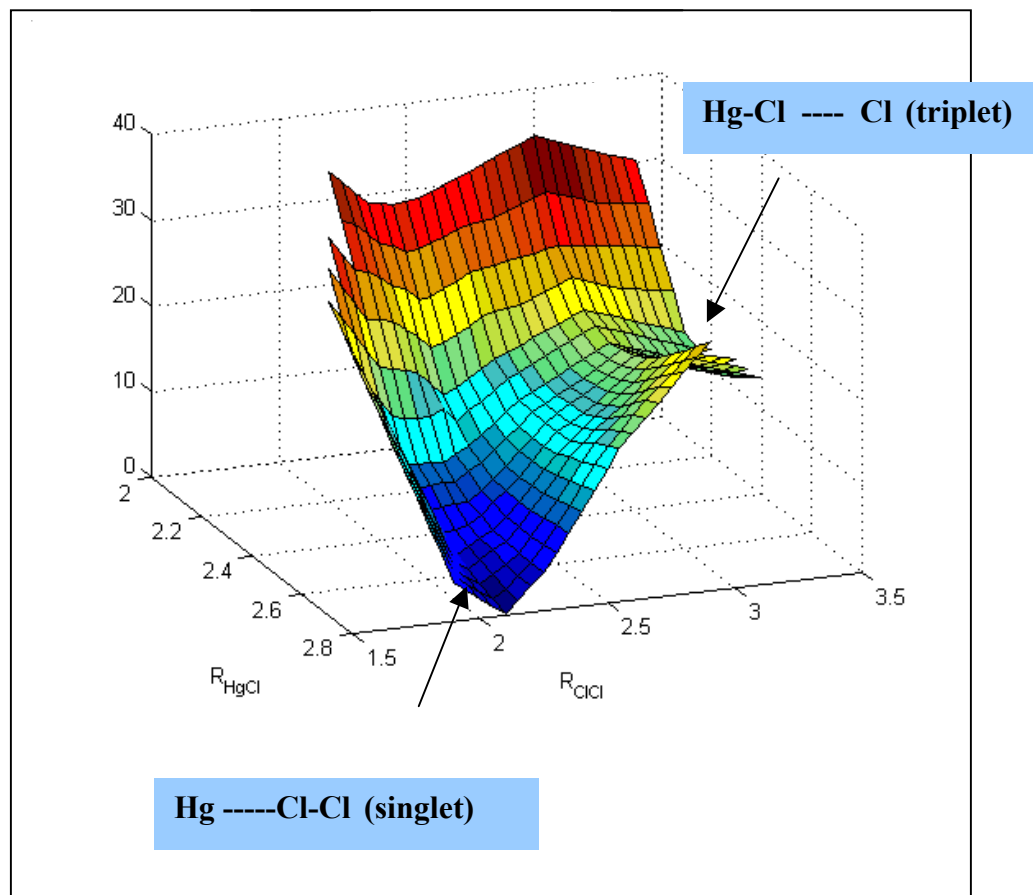


Figure 3-7. Potential Energy Surface (1997 BS), $\text{Hg} + \text{Cl}_2 \rightarrow \text{HgCl} + \text{Cl}$

To generate the potential energy surface, single point energies were calculated at approximately 100 different points corresponding to the Cl_2 molecule stretching and the HgCl molecule forming. After compiling a list of energies versus geometries, the potential energy surface was generated using three dimensional plotting software in Matlab. Ideally one would locate a saddle point on the three dimensional surface and with a frequency analysis in combination with an intrinsic reaction coordinate (IRC) calculation, determine the location of the transition structure. Within performing the single point energy calculations for the generation of a potential energy surface, one has to specify the spin multiplicity of the species of interest. Mercury as presented in equation (3.9) as a reactant has two valence electrons. These electrons can be paired in which case their spins must be opposite, corresponding to a singlet state. However, the electrons may also be unpaired, in which case, each would have a spin of $\frac{1}{2}$ corresponding to a triplet state. In the generation of the potential energy surface, both the ground state (singlet) and the excited state (triplet) were examined. Similarly, when the geometry structure approaches that of the product species, there exists both a singlet and triplet surface. In this case, the triplet is lower in energy, more specifically the ground state. Close examination of Figures 3-6 and 3-7 above reveals the crossing of the singlet surface where the geometries are close to the reactant species, with the triplet surface where the geometries are close to the product species. An extreme case of this example of surface crossing in a two dimensional picture is shown below in Figure 3-8. If the system “hops” from state A to A’, this is considered a nonadiabatic process, whereas, if the system stays on the lower level, this is termed an adiabatic process. In general, the

adiabatic assumption is based upon the high speed that the electrons move with respect to the “heavy” nucleus. In other words, the electronic wave function can instantaneously recover to their original state for every change in nuclear position.

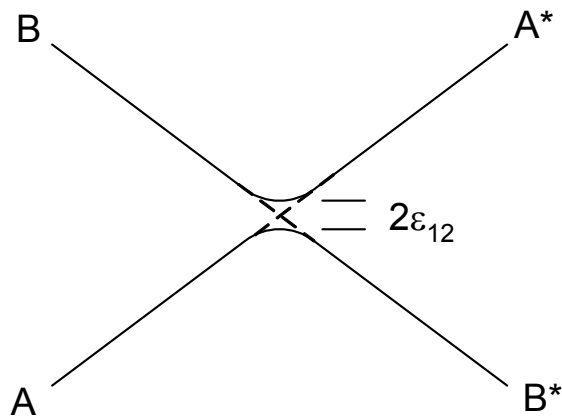


Figure 3-8. Example of a Crossing Potential Energy Surface

Traditionally a system that starts out on the ground-state surface should always remain on that surface, despite changes in the nuclear coordinates, such as reacting to form product species. (Moore and Pearson, 1981). Given that the distance between the two surfaces is small enough there will be some finite probability that the two surfaces will interact, resulting in an energy splitting, $2\epsilon_{12}$. This probability of surface hopping can be expressed by the Landau, Zener, and Stueckelberg equation below (Landau, 1932; Zener, 1932; Stuckelberg, 1932):

$$P = e^{-\left(\frac{4\pi^2\epsilon_{12}^2}{hv|s_1-s_2|}\right)} \quad (3.10)$$

such that v is the velocity along the reaction coordinate, s_1 and s_2 are the slopes of where each surface would cross if splitting did not exist. Notice that the probability of a nonadiabatic process occurring approaches one as the energy splitting, ε_{12} becomes small as the velocity becomes very large. Under a nonadiabatic process, the Born-Oppenheimer approximation breaks down and the vibrational and electronic motions can no longer be separated. In order to calculate an interaction energy between the two states, one has to consider both vibronic coupling and spin-orbit coupling. Due to the increasing complexity of this material, further details will not be presented in the current work. As mentioned in Chapter 2.3, future work should account for the spin-orbit coupling of these heavy mercury-chlorine species. Spin-orbit coupling would not only increase the accuracy of the energy solutions, but also in the present case, it would assist in determining the interaction energy between these two surfaces.

It should be noted that since the probability of surface hopping has been neglected here, the rate expression calculated below is a first approximation.

$$k [1/\text{M}^*\text{s}] = 3.59 \times 10^9 e^{-13564/T}, \text{ using QCISD/1997.}$$

A contour plot was generated for a series of points from both the singlet and triplet surfaces in order to locate the approximate saddle point on the total lower energy surface.

The transition structure at this seam crossing has a stretched Cl_2 bond of 2.8\AA and a forming HgCl bond of 2.5\AA .



Reaction (3.11) is very similar to (3.9) previously discussed. Similarly the 1992 and 1997 basis sets were used with the QCISD calculational method to generate two different three dimensional potential energy surfaces which are presented in Figures 3-9 and 3-10, respectively. In addition, potential energy surfaces have also been generated at the B3LYP level of theory using each of the two basis sets and these are presented in Figures 3-11 and 3-12.

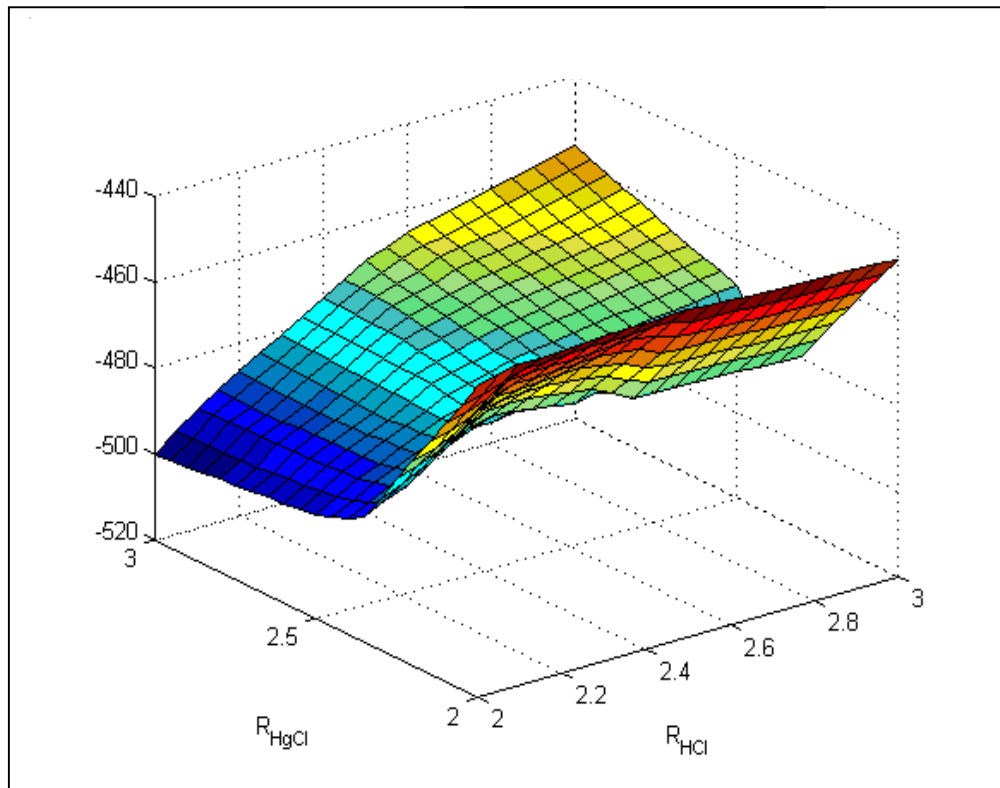


Figure 3-9. Potential Energy Surface (QCISD/1992 BS), $\text{Hg} + \text{HCl} \rightarrow \text{HgCl} + \text{H}$

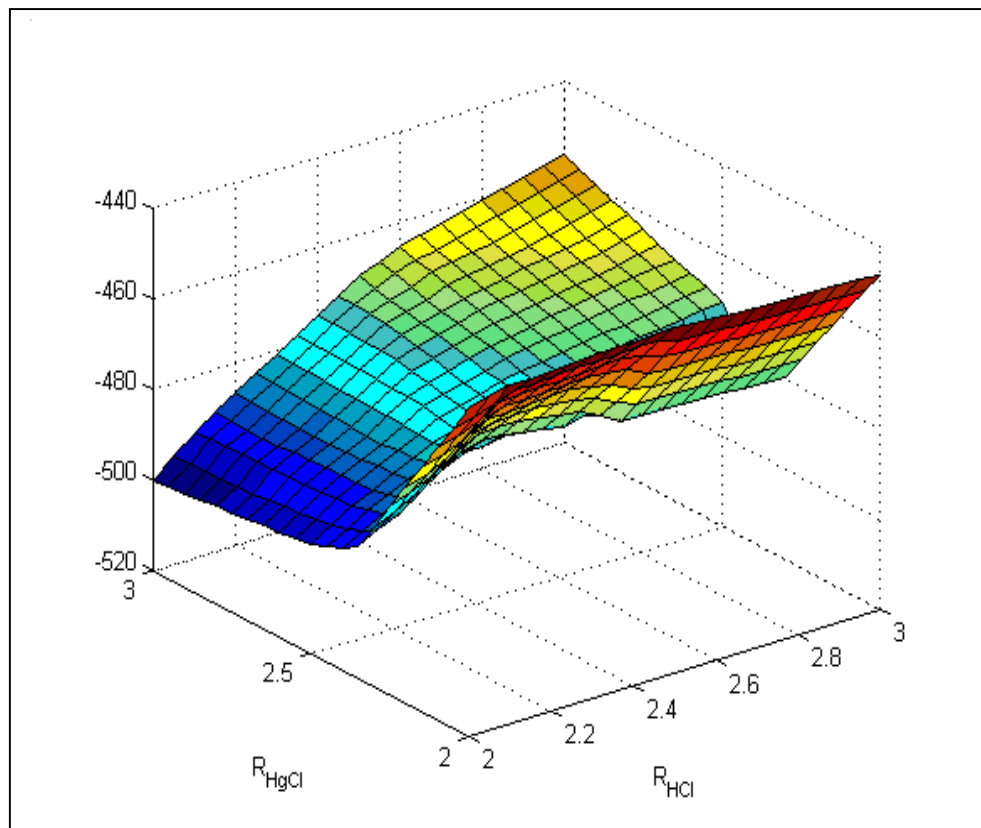


Figure 3-10. Potential Energy Surface (QCISD/1997 BS), $\text{Hg} + \text{HCl} \rightarrow \text{HgCl} + \text{H}$

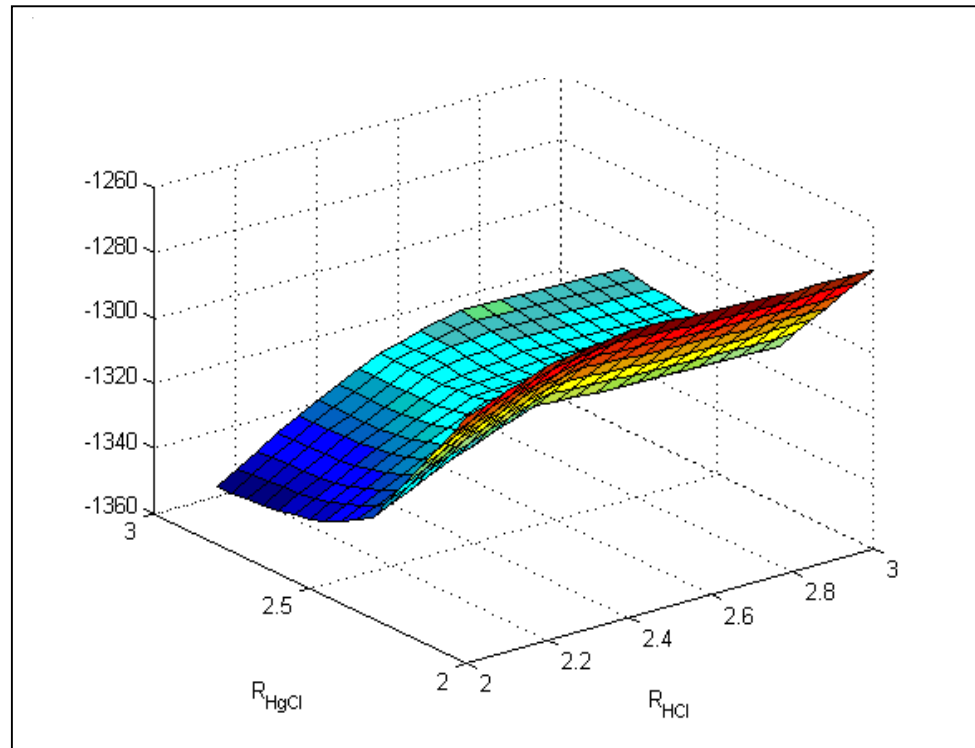


Figure 3-11. Potential Energy Surface (B3LYP/1992 BS), $\text{Hg} + \text{HCl} \rightarrow \text{HgCl} + \text{H}$

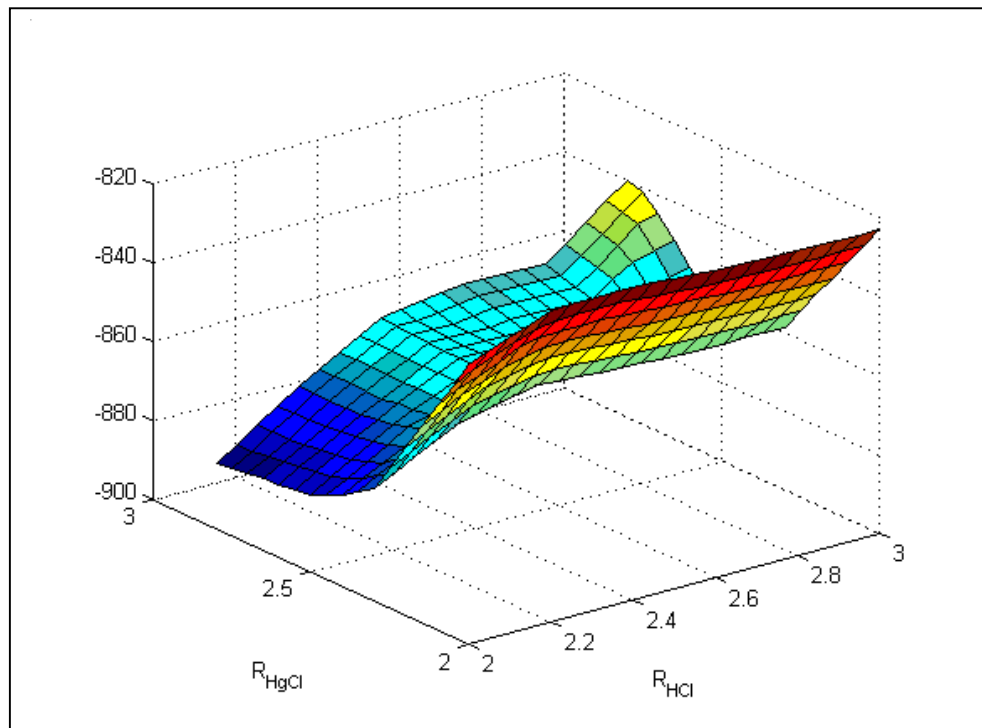


Figure 3-12. Potential Energy Surface (B3LYP/1997 BS), $\text{Hg} + \text{HCl} \rightarrow \text{HgCl} + \text{H}$

Just as before, for the present reaction, these surfaces present a crossing of ground and excited states. Also, the assumption will be made that the system in the product stage stays on the lower (triplet) surface since it began on the ground state (singlet) with respect to the geometry near the reactant species. Again, it should be noted that since the probability of surface hopping has been neglected here, the rate expression calculated below is a first approximation.

$$k [1/\text{M}^*\text{s}] = 7.66 \times 10^7 e^{-48278/T}, \text{ using QCISD/1992.}$$

The rate expression was calculated for only the one combination of basis set and method due to the excellent agreement with experimental geometries and heats of reaction, as exhibited back in Tables 3-1 and 3-2. A contour plot was generated for a series of points from both the singlet and triplet surfaces in order to locate the approximate saddle point on the total lower energy surface. The transition structure at this seam crossing has a stretched Cl₂ bond of 2.8 Å and a forming HgCl bond of 2.4 Å.

3.3. Second Stages of Oxidation



To the authors' knowledge, this is the first time that reaction (3.12) has been examined theoretically through quantum mechanical techniques. The B3LYP density functional computational method in combination with each of the 1992 and 1997 basis sets was used to calculate rate constants and activation energies in the range of 298 – 2000 Kelvin. Due to the ambient pressure conditions of the coal combustion flue gases, the unimolecular rate constant is calculated using RRKM theory. For more details on this methodology, see previous research which employs the same technique for rate constants of similar mercury-chlorine reactions. (Wilcox et al., 2004) All of the parameters required in RRKM theory can be obtained from theory with the exception of the collisional deactivation efficiency, β_c . This collisional efficiency is an empirical value that can be obtained through experimental knowledge of the reaction. (Troe, 1977) While many models have been determined for calculating the collision efficiency, experimental data is necessary. (Keck and Carrier, 1965; Tardy and Rabinovitch, 1966) Due to the lack of experimental data for the reaction studied in this paper, the collisional efficiency for reaction (3.11) is assumed to be 0.1, which is typical for this type of decomposition reaction involving mercury and chlorine. (Wilcox et al., 2004)

Because there is a shallow barrier on the potential energy surface for reaction (3.12), the rate constants for each combination of method and basis set were calculated using canonical variational transition state theory (CVTST). (Gonzalez-Lafont et al., 1991) The rate constant is obtained by variationally minimizing the universal RRKM-theory rate constant, $k_{\text{uni}}(T)$, with respect to the position of the generalized transition state along the reaction coordinate. In the remainder of this section, thermal corrections that include the zero point energy were included in all calculated results, and the frequency calculations were left unscaled due to the unavailability of proven scaling factors. (Pople et al., 1993)

There is a lack of experimental kinetic data available for reaction (3.12), making it imperative to compare to data that is experimentally available such as heats of reaction, geometries and frequencies. Previous work based upon these types of comparisons has repeatedly shown that both the 1992 and 1997 basis sets when used in conjunction with the density functional method, B3LYP, provide both accurate geometries and heats of reaction. Table 3-8 below examines these comparisons specifically for reaction (3.12). Comparing the 1992 and the 1997 basis sets, Table 3-8 shows that the 1997 basis set provides more accurate vibrational frequencies and heats of reaction, implying that the kinetic rates with this method will be more accurate. With confidence that the computational method and basis set are able to reproduce the species in this system, the rate constants can be calculated.

Since RRKM theory allows for the calculation of unimolecular decompositions in the forward direction only, to compare to the model data, the equilibrium constant must be calculated from 298 to 2000 K. The equilibrium constants throughout this range were found using the Shomate equation and data from the NIST webbook. Using the following equation for the equilibrium constant,

$$K_{eq} = \prod (a_i)^{\nu_i}, \quad (3.13)$$

and the forward and reverse rate expressions for equation (3.12), a relationship between K_{eq} and the forward and reverse rate coefficients using activity coefficients can be described with the following equation:

$$K_{eq} = \left(\frac{RT}{1bar} \right) \frac{k_1}{k_{-1}} \quad (3.14)$$

Use of K_{eq} and combustion-based model-derived forward rate constants (Widmer et al., 2000; Edwards et al., 2001) yields a prediction for the reverse of reaction (3.12), allowing for a comparison to the RRKM derived theoretical prediction as shown below in Figure 3-13. The models have been used in the past by other researchers to predict mercury speciation in flue gases (Niksa et al., 2001; Xu et al., 2003) and their accuracy is essential for developing more effective control strategies for preventing mercury's release into the atmosphere.

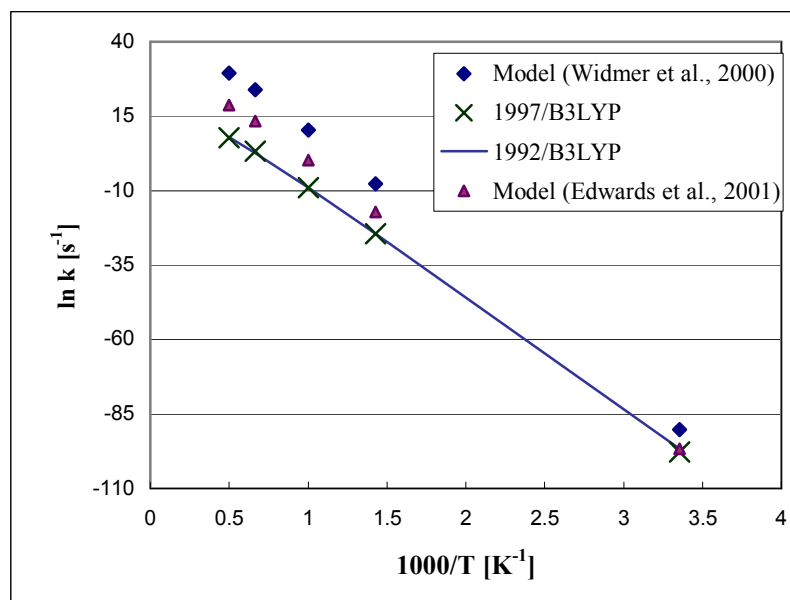
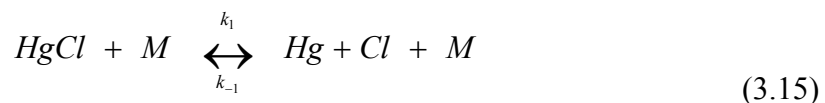


Figure 3-13. Comparison of Rate Constants, $HgCl_2 + M \rightarrow HgCl + Cl + M$ For Theoretical Predictions $\beta_c = 0.1$

The rate constant data for the reverse of reaction (3.12) from the model developed by Widmer, et al., differs from that of the model developed by Edwards, et al.. The model developed by Widmer, et al., predicts this rate constant through a complex non-linear fit to global experimental data, whereas the model developed by Edwards, et al., uses an experimental rate constant for the following mercury-chlorine reaction:



As it turns out, the approximation used by Edwards, et al., predicts rate constants that are more similar to the ones derived in this work through quantum mechanical techniques than the rate constant predicted through the Widmer, et al., model. Only at low temperatures do all the methods agree.

Using Figure 3-13, the rate expressions calculated for the decomposition of mercuric chloride are:

$$k^{\text{UNI}}(\text{s}^{-1}) = 7.43 \times 10^{11} e^{-36828/T}, \text{ using B3LYP/1992}$$

$$k^{\text{UNI}}(\text{s}^{-1}) = 1.16 \times 10^{12} e^{-37297/T}, \text{ using B3LYP/1997}$$

in the temperature range of 298 - 2000 K. These rate constant estimations are based on quantum chemical methods and should be more accurate than the model estimates currently in use. Despite the better agreement of the 1997 basis set results in Table 3-8 below, both methods are nearly identical and either rate expression above can be used in mercury speciation kinetic models.

Table 3-8. Energetics Data, $\text{HgCl}_2 + \text{M} \rightarrow \text{HgCl} + \text{Cl} + \text{M}$

Note: T = 298 K

	Experimental	1992 B3LYP	1997 B3LYP
Geometry (Å)			
HgCl	2.23 ^a	2.4896	2.4648
HgCl ₂	2.28 ^b $\angle 180^\circ$	2.3195 $\angle 180^\circ$	2.3211 $\angle 180^\circ$
Frequencies (1/cm)			
HgCl	292.61 ^c	244.40	260.97
HgCl ₂	75, 75, 363, 413 ^d	92,92,318,374	84,84,319,373
ΔH_{rxn} (kcal/mol)	82.70 ^e	72.57	78.85

^a(Maxwell and Mosley, 1939), ^b(Braune and Knoke, 1933), ^c(Herzberg, 1939), ^d(Herzberg, 1966),^eRef (NIST)



Currently there is no published theoretical data on this reaction so that this will be the first time that reaction (3.16) has been studied theoretically. Although other mercury oxidation reactions have been studied with the high level QCISD method, currently the goal is to determine if the less computationally expensive B3LYP density functional theory method can produce just as accurate results as QCISD, but with increased efficiency. The reasonable agreement of theoretical heats of reaction and geometries to experimental values are exhibited in Tables 3-1 and 3-2. This leads one to believe that the less computationally expensive B3LYP method is a contender for determining reasonably accurate rate constants. Two potential energy surfaces were generated for this work and are presented in Figures 3-14 and 3-15. It is important to note that within these potential energy surface, it was assumed that the transition structure for this reaction is linear and several calculations were done to show that the linear structure was the minimum energy structure. Each potential energy surface was generated using different basis sets, but produce similar surfaces confirming the consistency of the theoretical data. The surfaces were generating similarly to the surfaces in chapter 3.2.4. The Cl₂ bond length was stretched as the HgCl bond was formed. The second HgCl bond was held fixed. In Figures 3-14 and 3-15, it is important to notice the change in color of the surface as the reaction coordinate is followed. The dark blue colors on the surface correspond to low energies, whereas the yellow and red colors correspond to higher

energy values. The surface rises and continues to do so in the direction of the reaction path without moving through a saddle point or transition structure on the surface.

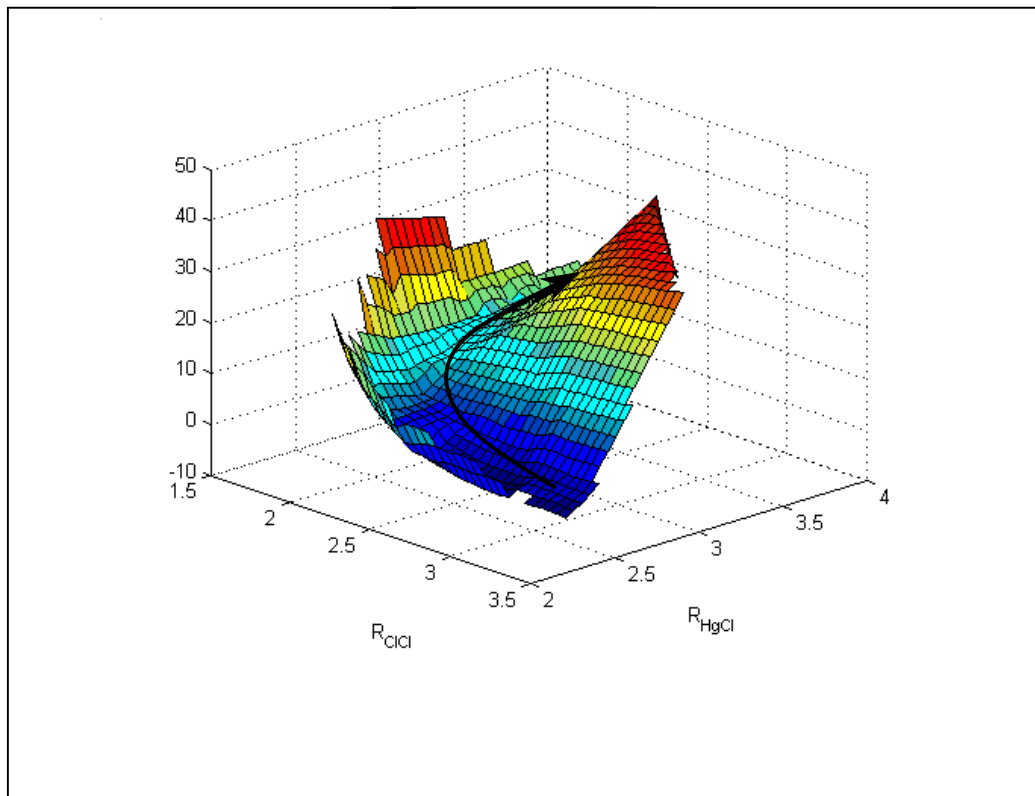


Figure 3-14. Potential Energy Surface (1997 BS), $\text{HgCl} + \text{Cl}_2 \rightarrow \text{HgCl}_2 + \text{Cl}$

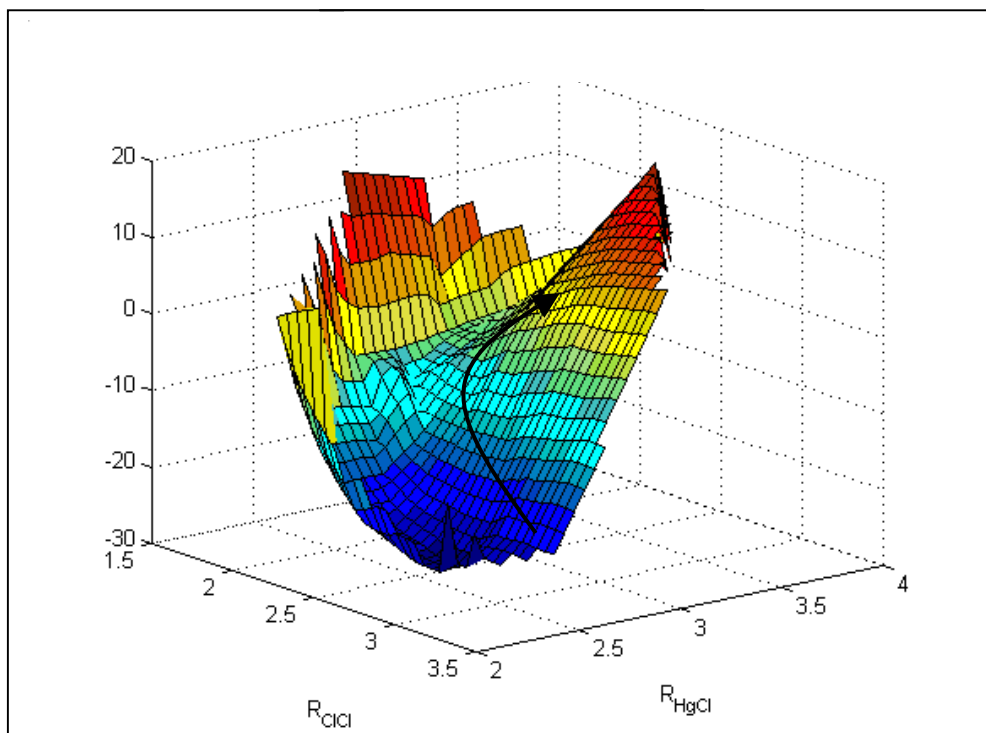


Figure 3-15. Potential Energy Surface (1992 BS), $\text{HgCl} + \text{Cl}_2 \rightarrow \text{HgCl}_2 + \text{Cl}$

For the current research, the goal is to obtain the transition structure, which is ideally located at the saddle point of the energy surface. However, reaction (3.16) appears to be barrierless and requires the use of canonical variational transition state theory (CVTST). CVTST involves determining a series of rate constants at a specific temperature, at varying geometries along the reaction coordinate, with the minimum rate constant along the reaction coordinate being the true rate. In order to obtain an Arrhenius expression, this procedure must be repeated at varying temperatures.

A comparison of reactant and product geometries and frequencies can be seen below in Table 3-9. Consistent with the conclusions of Table 3-1, the LANL2DZ basis set provides less accurate results than the more recently developed basis sets. Again, the 1992 basis set with QCISD provides the most accurate results.

Table 3-9. Energetics Data, $\text{HgCl} + \text{Cl}_2 \rightarrow \text{HgCl}_2 + \text{Cl}$

Note: T=298 K

Basis Set: Method:	LANL2DZ B3LYP	1992 B3LYP	1997 B3LYP	1992 QCISD	1997 QCISD	Experimental
Geometries (Å)						
HgCl	2.6122	2.4896	2.4648	2.4121	2.4084	2.23 ^a
Cl ₂	2.2244	2.0106	2.0106	1.997	1.997	1.9878 ^b
HgCl ₂	2.4417 ∠180°	2.3195 ∠180°	2.3211 ∠180°	2.3002 ∠180°	2.3116 ∠180°	2.28 ^c
Frequencies (1/cm)						
HgCl ^d	228.92	244.40	260.97	290.69	297.81	292.61
Cl ₂ ^d	467.99	540.50	540.50	562.82	562.82	564.9
HgCl ₂ ^e	66,66, 288,345	92,92, 318,374	84,84, 319,373	97,97, 340,394	89,89, 338,388	75, 75, 363, 413

Note: for chlorine is the following Pople basis set was used: 6-311++G(3df,3pd).

^a(Maxwell and Mosley, 1939), ^b(CRC, 2004), ^c(Braune and Knoke, 1933), ^d(Herzberg, 1939), ^e(Herzberg, 1966)

Unlike the heats of reaction results, in this case, both the 1992 and 1997 basis sets provide the most accurate results with the higher level QCISD method. The accuracy of the results in Table 3.9 above for B3LYP do not measure up to that of QCISD, but should not be ruled out as a possible contender for estimating accurate rate constants.

Canonical Variational Transition State Theory (CVTST) was carried out for the current reaction of focus due to the barrierless nature of the reaction. The minimum rate constant was found for each of the basis sets with the B3LYP method at the geometries listed below in Table 3-10. A closer look at this table shows the differing results between the 1992 and 1997 basis sets. Due to the 1997/B3LYP agreement obtained from the heats of reaction data, one may be inclined to favor the results of the 1997 calculated rate constants. The details of these rate constant calculations can be found in Appendix D.3.

Table 3-10. Thermodynamic and Kinetic Parameters, $\text{HgCl} + \text{Cl}_2 \rightarrow \text{HgCl}_2 + \text{Cl}$

Note: T= 298 K

	1992 B3LYP	1997 B3LYP
Geometries of Transition Structure (Å)	Cl-Cl: 2.3 Cl-Hg: 3.7 Hg-Cl: 2.44 $\angle \text{Cl-Cl-Hg}$: 180° $\angle \text{Cl-Hg-Cl}$: 180°	Cl-Cl: 2.3 Cl-Hg: 3.7 Hg-Cl: 2.42 $\angle \text{Cl-Cl-Hg}$: 180° $\angle \text{Cl-Hg-Cl}$: 180°
Frequencies of Transition Structure (cm⁻¹)	-87.91, 43.81, 44.13, 128.69, 128.70, 140.32, 267.99	-102.65, 42.31, 42.42, 127.14 127.15, 129.86, 283.39
Activation Energy: (kcal/mol)	7.45	6.92
Rate Constant: (M ⁻¹ s ⁻¹)	Forward: 1.70*10 ⁶	Forward: 1.27*10 ⁶

The following rate expressions were calculated for reaction (3.16),

$$k(\text{M}^{-1}\text{s}^{-1}) = 2.92 * 10^9 e^{-2220/T}, \text{ using B3LYP/1992}$$

$$k(\text{M}^{-1}\text{s}^{-1}) = 1.29 * 10^9 e^{-2063/T}, \text{ using B3LYP/1997}$$

from 298 to 1500 K.

In total, theoretical rate constants have been estimated for mercury oxidation reactions by molecular chlorine that may occur in the flue gases of coal combustion. Due to the lack of experimental kinetic data available for this reaction, the method and basis set choice has been validated by a comparison of heats of reaction for a series of potential mercury oxidation reactions occurring in the flue gases. Although these predicted rate constants are very similar to each other, recall that the 1997/B3LYP combination resulted in more

accurate heats of reaction. If one of the above expressions should be chosen over the other for a combustion model involving mercury, one should choose to use the predicted rate with the 1997/B3LYP combination.



Agreement between the theoretical and experimental rate constants from chapter 3.2.1, showed that the 6-311G++(3df, 3pd) Pople basis set is an adequate choice for chlorine. The basis set chosen for hydrogen was based upon the high accuracy of the theoretical heat of reaction compared to the experimental heat of reaction obtained from the NIST webbook. The theoretical heat of reaction for the decomposition of H₂ with the 1.37.1 basis set (Poirier et al., 1985) is 104.52 kcal/mol compared to the experimental value of 104.20 kcal/mol. It should be noted that reaction (3.17) was one of the first examined in the series of mercury oxidation reactions and that this hydrogen basis has since been replaced with the 6-311G++(3df, 3pd) Pople basis set for the theoretical heats of reaction predictions in Table 3-2. This rate constant calculation of this reaction is the only calculation which does not use the extended Pople basis set.

The experimental ΔH_{rxn} and the experimental geometries of the products and reactants for reaction (3.17) are compared to predictions from each combination of method and basis set in Table 3.2. For comparison, results from density functional theory using the LANL2DZ basis set are shown as this method was used in previous calculations for this reaction (Sliger et al., 2000). Overall, density functional theory with the B3LYP method and the standard double-zeta LANL2DZ basis set provided the greatest errors with respect to the geometries and the frequencies of the products and reactants. Also, for

reaction (3.17), density functional theory exhibited the greatest error in terms of ΔH_{rxn} with a 5.27 kcal/mol deviation from experiment.

Table 3-11. Energetics Data, $\text{HgCl} + \text{HCl} \rightarrow \text{HgCl}_2 + \text{H}$

Note: T=298 K

	Experimental	LANL2DZ B3LYP ^a	1992 QCISD	1997 QCISD	1992 B3LYP	1997 B3LYP
Geometry (Å)						
HgCl	2.23 ^b	2.6122	2.4121	2.4084	2.4896	2.4648
HCl	1.2746 ^c	1.3149	1.2833	1.2833	1.2808	1.2808
HgCl ₂	2.28 ^d $\angle 180^\circ$	2.4417 $\angle 180^\circ$	2.3002 $\angle 180^\circ$	2.3116 $\angle 180^\circ$	2.3195 $\angle 180^\circ$	2.3211 $\angle 180^\circ$
Transition Structure	no experimental data available	HCl: 2.3335 HgCl (1): 2.4634 HgCl (2): 2.4517 $\angle \text{HHgCl}$: 179.89° $\angle \text{ClHgCl}$: 179.5°	HCl: 1.7781 HgCl (1): 2.3697 HgCl (2): 2.3576 $\angle \text{HHgCl}$: 180° $\angle \text{ClHgCl}$: 180°	HCl: 1.7598 HgCl (1): 2.3799 HgCl (2): 2.3383 $\angle \text{HHgCl}$: 180° $\angle \text{ClHgCl}$: 180°	HCl: 2.1827 HgCl (1): 2.3462 HgCl (2): 2.3312 $\angle \text{HHgCl}$: 180° $\angle \text{ClHgCl}$: 180°	HCl: 2.0855 HgCl (1): 2.3588 HgCl (2): 2.3331 $\angle \text{HHgCl}$: 180° $\angle \text{ClHgCl}$: 180°
Frequencies (1/cm)						
HgCl ^e	292.61	228.92	290.69	297.81	244.40	260.97
HCl ^e	2989.74	2709.61	2947.12	2947.12	2943.60	2943.60
HgCl ₂ ^f	75, 363, 413	66,66,288,345	97,97,340,394	89,89,338,388	92,92,318,374	84,84,319,373
Transition Structure	no experimental data available	61,61,103,103, 283,335,-247	81,81,250,300, 508,508,-1647	81,81,260,305, 423,423,-1584	83,83,161,161, 311,360,-375	76,76,163,163, 315,357,-424

^a(Maxwell and Mosley, 1939), ^b(CRC, 2004), ^c(Braune and Knoke, 1933), ^d(Herzberg, 1939), ^e(Herzberg, 1966), ^f(NIST)

Table 3-12. Thermodynamic and Kinetic Data, $\text{HgCl} + \text{HCl} \rightarrow \text{HgCl}_2 + \text{H}$

Note: T=298 K

	Experimental	LANL2DZ B3LYP	1992 QCISD	1997 QCISD	1992 B3LYP	1997 B3LYP
ΔH_{rxn} (kcal/mol) ^a	20.50	25.77	24.42	20.50	29.17	22.89
Activation Energy (kcal/mol)						
forward	no experimental data available		25.89	30.27	27.11	37.30
reverse	no experimental data available		0.121	5.85	6.61	8.13
Rate Constant (cm ³ /mol s)						
forward	no experimental data available		3.57 * 10 ⁻⁵	3.91 * 10 ⁻¹²	8.86 * 10 ⁻¹⁰	4.07 * 10 ⁻¹⁷
reverse	no experimental data available		4.11 * 10 ¹²	1.62 * 10 ⁹	3.91 * 10 ⁸	4.19 * 10 ⁷
						1.65 * 10 ⁷

^aRef (NIST)

From Table 3-11, the QCISD method with either the 1992 or 1997 basis set provides reasonably accurate molecular geometries and frequencies. Due to the lack of experimental kinetic data, each method and basis set combination is considered in Figures 3-16 and 3-17.

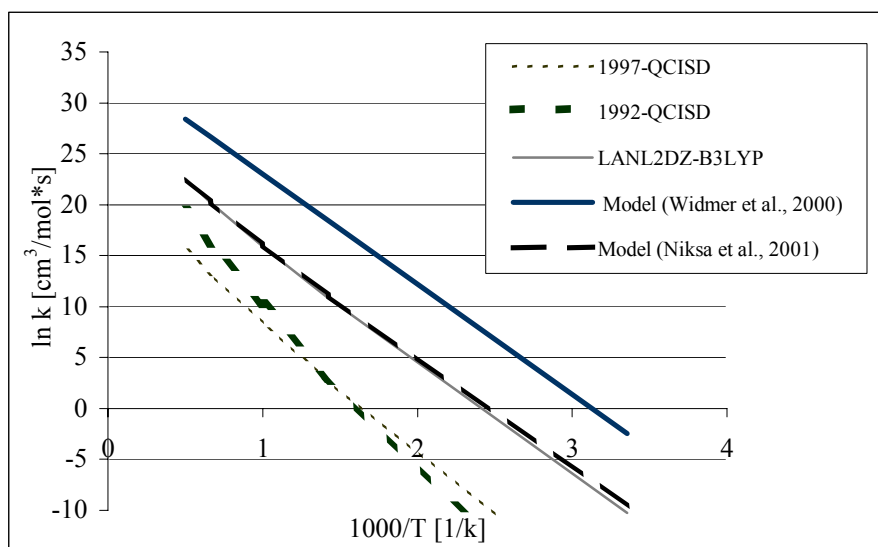


Figure 3-16. Comparison of Rate Constants, $HgCl + HCl \rightarrow HgCl_2 + H$

Using Figure 3-16 above, the rate expressions calculated for the oxidation of mercury chloride via hydrogen chloride are:

$$k^{TST} [cm^3/mol*s] = 3.11 \times 10^{11} e^{-15713/T}, \text{ using QCISD/1992}$$

$$k^{TST} [cm^3/mol*s] = 1.95 \times 10^9 e^{-12586/T}, \text{ using QCISD/1997}$$

in the temperature range of 298 - 2000 K.

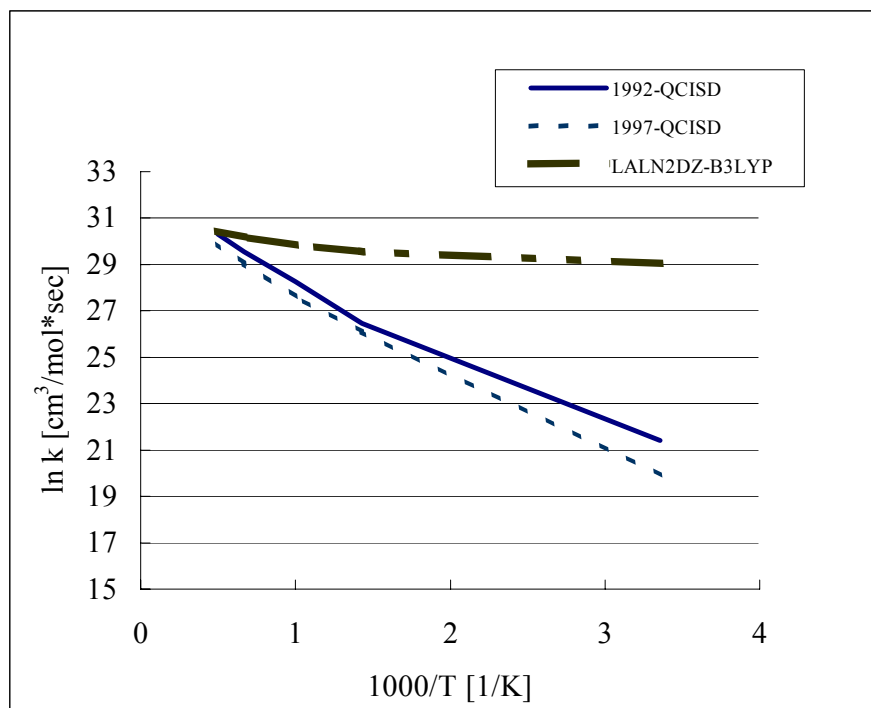


Figure 3-17. Comparison of Rate Constants, $H + HgCl_2 \rightarrow HgCl + HCl$

For the reverse of reaction (3.17), the calculated rate constant expressions are:

$$k^{\text{TST}} [\text{cm}^3/\text{mol*s}] = 4.5 \times 10^{13} e^{-3049.2/T}, \text{ using QCISD/1992}$$

$$k^{\text{TST}} [\text{cm}^3/\text{mol*s}] = 3.8 \times 10^{13} e^{-3420.3/T}, \text{ using QCISD/1997}$$

These values are compared directly at 298 K in Table 3-12.

Figure 3-18 shows a comparison of these theoretically determined rate constants compared to model-derived rate constants from previous work. Both models developed rate constants for reaction (3.17) of the form $k = A \cdot T^n \exp(-E/RT)$. The model developed

by Widmer et al. was developed using the SENKIN routine to solve the ODE's, which is part of Reaction Design's CHEMKIN III software. In addition, a general combustion chemistry mechanism adapted and used in their model. (Glarborg et al., 1986) and the preexponential factors for some of their reactions were taken from corresponding reactions involving lead. (Cosic and Fontijn, 1999) The model developed by Niksa et al. is in good agreement with the theoretical results of Sliger et al. because Niksa et al. used a 'frequency' factor in their model for reaction (3.17) in order to obtain this agreement. Niksa's original value was based upon the hard sphere collision model, which was an order of magnitude lower than their new scaled value. However, in general, the hard sphere collision number derived from elementary gas-kinetic theory is calculated at the gas-kinetic limit and should be an overestimate of the rate constant (Weston and Schwartz, 1972). This highlights that fact that one of the difficulties of modeling is that one has to fit limited available data, which can lead to results that disagree with basic kinetic theory like in the case just described here.

Previous calculations for the reaction investigated in this work used the B3LYP method with the LANL2DZ basis set (Sliger et al., 2000) to estimate the rate constant. However, the results from this work show that the reaction energetics using this basis set and density functional theory are highly inaccurate. The B3LYP method, even with larger basis sets, still does not lead to the same degree of accuracy that the QCISD results show with the 1992 basis set. In addition, the work here showed that use of the SDD basis sets even with high level methods leads to large errors.

In general, for mercury oxidation reactions involving chlorine, either the 1992 or 1997 basis set combined with the QCISD method will provide reasonably accurate thermodynamic and kinetic results. However, a careful review of Table 3-2 reveals that the combination of the density functional method, B3LYP with the 1997 basis set provides reasonably accurate heats of reaction. Due to the lower computational cost of B3LYP compared with the QCISD method, B3LYP was also considered for further rate constant calculations in conjunction with the highly accurate 1992 and 1997 basis sets.

Table 3-11 shows a comparison of experimental geometries and frequencies to the theoretical predictions regarding reaction (3.17). Again, the 1992 and 1997 basis sets, regardless of the method used in conjunction with each, outperform the built-in LANL2DZ Gaussian basis set. The SDD basis set was not considered for the kinetic predictions since the previous errors were so great for the thermodynamic analysis. Recall, the focus of these calculations is to test the accuracy of the low level B3LYP method to see how it measures up in accuracy to the more computationally demanding QCISD method. Table 3-12 lists the theoretically predicted activation energies and rate constants for various basis set and method combinations for reaction (3.17).

Unfortunately, there are currently no reported experimental rate constant predictions for this reaction so validation of this data is based upon the previous geometry, frequency and heat of reaction agreement discussed above. Examination of Table 3-12 shows that activation energies for 1992/QCISD and 1997/B3LYP differ by less than 1.43 kcal/mol in the forward direction and by less than 2.39 kcal/mol in the reverse direction. In fact, at

298 K, their rate constants are within one order of magnitude of each other in the forward direction. The close agreement of the 1997/B3LYP combination to the higher level QCISD method suggests that the lower level method may indeed be sufficiently accurate for use in a combustion model.

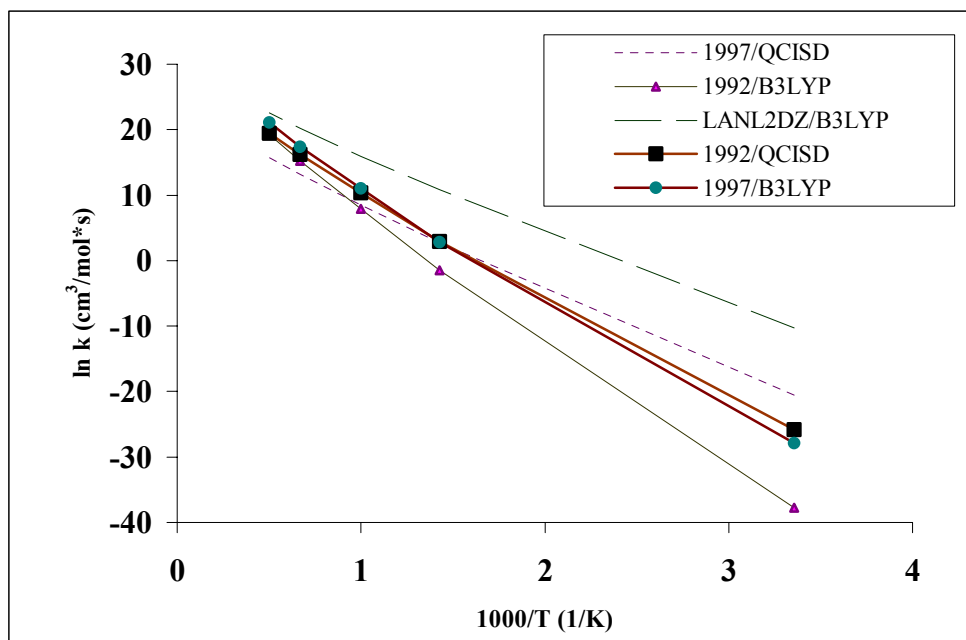


Figure 3-18. Rate Comparison of B3LYP with QCISD, $\text{HgCl} + \text{HCl} \rightarrow \text{HgCl}_2 + \text{H}$

Transition state theory was used to calculate the theoretical rate constant data for reaction (3.17) in Figure 3.19. Using this figure, the rate expressions calculated via density functional theory for the oxidation of mercury chloride via hydrogen chloride are:

$$k^{\text{TST}} [\text{cm}^3/\text{mol*s}] = 1.61 \times 10^{12} e^{-19772/T}, \text{ using B3LYP/1992}$$

$$k^{\text{TST}} [\text{cm}^3/\text{mol*s}] = 2.22 \times 10^{12} e^{-16931/T}, \text{ using B3LYP/1997}$$

in the temperature range of 298 - 2000 K.

Recall Table 3-3 strongly suggests that the incorporation of the diffuse and polarization functions in the 1992 basis set in order to gain more balanced basis sets for each of the atoms within a given reaction will lead to improved energetics. In future work, these extensions should be pursued for their validation with other mercury speciation reactions involving HgCl_2 . Overall, the present kinetic results suggest that the 1992 Stevens et al. basis set used in conjunction with the QCISD calculational method should be used to accurately predict both thermodynamic and kinetic data for mercury oxidation reactions involving chlorine. However, if the computational expense is a factor, the density functional method, B3LYP in combination with the Stuttgart 1997 basis set provides reasonable accurate results also.

3.4. Discrepancies with other Theoretical Results Published in the Literature

This section discusses comments on an article entitled, “A study on the reaction mechanism and kinetic of mercury oxidation by chlorine species” that was published in the Journal of Molecular Structure (Theochem) in 2003. Within the previous work by Lai-Cai Li, et al., the complexity of some of these mercury oxidation reactions was drastically underestimated and therefore this current section will attempt to correct some of these simplifications.

The following reactions were discussed in the previous work and will be referred to often throughout this section.



Barrierless Reactions: Examining reactions (3.18) and (3.19) with the QCISD method and high quality pseudopotentials for mercury (Küchle et al., 1991; Häussermann et al.,

1993; Dolg et al., 1991; Stevens et al., 1992) shows that they take place on the $S = 0$ potential energy surface, resulting in each reaction being barrierless. Lai-Cai Li, et al. reported a distinct saddle point on the singlet potential energy surface of each of these reactions at the lower geometry optimization level. Intrinsic reaction coordinate calculations done based on their structure showed that there was indeed a transition state leading to the correct products and reactants with the SDD basis set, but higher level calculations do not confirm the existence of this structure. One method of calculating a rate constant for a barrierless reaction would involve the use of a variational method such as variational transition state theory (VTST) developed by Truhlar. (Truhlar and Gordon, 1990)

Multichannel Reactions and Transition State Theory: The use of transition state theory for reactions (3.22) and (3.23) would also be more difficult than implied in Lai-Cai Li, et al's previous work. Each of these reactions has two transition states linking the products and reactants. One would need to use an aggregated form of multi-channel transition state theory to correctly estimate the reaction rate of these reactions and cannot simply use the activation energy they report in their work. Correcting this error with high level calculations would be extremely time intensive and is outside the scope of this comment.

Unimolecular Reactions and Transition State Theory: Lai-Cai Li, et al. used traditional transition state theory to calculate a rate constant for reaction (3.24), which is a unimolecular reaction in the reverse direction. Traditional transition state theory can be

used to estimate reaction rates for unimolecular reactions at the high pressure limit, but the reactions here are at high temperatures and low pressures, placing them in the fall-off regime where RRKM theory or a Master Equation approach must be employed for the rate constant estimation. (Holbrook et al., 1996)

Accuracy of Theoretical Results Compared to Experimental Data: In general, the quantum mechanical method and basis set used for the transition structure optimizations should be examined carefully in terms of their accuracy relative to experimental data. Due to the lack of experimental rate constant data available for mercury oxidation reactions, validation of the method and basis set combination must be pursued through the comparison of theoretical geometries and heats of reaction to experiment.

The following relativistic effective core potentials were recently developed in the literature for mercury and are the ones compared in the current work: Stuttgart 1997 and Stevens *et al.* 1992, and will be referred to as the 1997 and 1992 basis sets respectively. The basis sets used for all other atoms such as chlorine, oxygen and hydrogen are standard Pople basis sets including both diffuse and polarization functions; 6-311++G(3df, 3pd). All pseudopotentials were used in Gaussian 98 for the geometry optimizations and energy calculations. Table 3-1 provides a list of optimized bond lengths for all basis set and method combinations, showing the QCISD/1992 combination to be the most accurate with an average absolute error of 0.03 Angstroms. The 1992 and 1997 basis sets give low errors for all computational methods that have been examined.

In contrast, the research performed by Lai-Cai Li, et al. was based upon the SDD basis set and yielded an overall average error of 0.119 angstroms with the QCISD(T) method and 0.103 angstroms with the MP2 method. Inaccuracies in molecular geometries leads to incorrect vibrational analyses, shifting the partition functions to give an incorrect reaction rate. Determining how much their results are in error is again outside the scope of this comment because it would be time intensive to redo their calculations to obtain the theoretical data they did not report in their paper.

Again, Table 3-2 shows a summary of energy predictions for heats of reactions from theory compared to high quality experimental data from the National Institute of Standards and Technology database. (Ref. 61) All geometries were fully optimized at the indicated level of theory and basis set. Vibrational frequency calculations were performed to obtain thermal corrections including zero point energies to the electronic energies reported by Gaussian 98. The QCISD method with the 1992 basis set for mercury and the standard 6-311++G(3df,3pd) basis set for other atoms gives the best agreement with an average absolute error of 4.42 kcal/mol compared to experiment. On the other hand, the MP2 and QCISD results with the SDD basis sets lead to average errors that are between 16 and 15 kcal/mol.

We have calculated the activation energy for reaction (3.20) at the QCISD level of theory with both the 1992 and 1997 basis sets. We found that the activation energies are 30.27 and 27.10 kcal/mol for the 1992 and the 1997 basis sets respectively. Lai-Cai Li, et al.

calculated an activation energy of 13.64 kcal/mol using the SDD basis set at the QCISD(T) level of theory. Examination of Tables 3-1 and 3-2 reveals that this combination of method and basis set has greater error in both geometry and heats of reactions calculations when compared to the method and basis set combinations used in this work. Recall that errors in activation energies of only a few kcal/mol lead to reaction rates that are orders of magnitude different from experimental values. (Weston and Schwartz, 1972)

Referencing of Experimental Data: Some of the experimental values cited by Lai-Cai Li, et al. are estimates from previous kinetic models or from reactions that do not specifically involve mercury. The experimental data for reaction (3.19) was extracted from data by Widmer, et al. in conference proceedings that predate their publication. (Widmer et al., 2000) The publication, though, clearly shows that reaction (3.19) was not investigated as a fundamental reaction. Instead, they globally modeled the kinetics for the nonelementary reaction, $\text{Hg} + 2\text{HCl} \rightarrow \text{HgCl}_2 + \text{H}_2$.

In their research, Lai-Cai Li, et al. also referred to experimental data for reaction (3.21) by comparing the reaction to one where lithium replaced mercury. The authors failed to give justification of why the oxidation of lithium chloride via HCl would resemble the oxidation of mercuric chloride via HCl. Mercury and lithium are elements from different groups in the periodic table with substantially different electronic configurations. There has been no experimental rate constant data published on reaction (3.21) thus far and

theoretically this reaction has been studied by only two groups. (Sliger et al., 2000; Wilcox et al., 2003) The following rate expressions were calculated for reaction (3.21):

$$k^{\text{TST}} [\text{cm}^3/\text{mol*s}] = 3.11 \times 10^{11} e^{-15713/T} \text{ using QCISD/1992}$$

$$k^{\text{TST}} [\text{cm}^3/\text{mol*s}] = 1.95 \times 10^9 e^{-12586/T} \text{ using QCISD/1997}$$

in the temperature range of 298 – 2000 K. As Lai-Cai Li, et al. did not specify units on their reported rate constant, this data cannot be compared directly with theirs.

While the rate constants calculated by Lai-Cai Li, et al. agree very well with the lithium reaction data they use for comparison, the lithium data should not be used to replace unmeasured mercury data. To demonstrate why this should not be done, one only needs to consider similar literature from two homologous reactions. This work uses data for two reactions that are much more similar and still show large deviations from each other:



In this case, the activation energy for the sodium reaction is 9.99 kcal/mol (Plane et al., 1987) while the one for lithium is 1.75 kcal/mol (Plane et al., 1989). This leads to a difference of about two orders in magnitude in the rate constant around 800 K. Even in this instance where lithium and sodium are in the same group in the periodic table, the rate constant values are not within an order of magnitude of each other. This example

validates the necessity to estimate rate constants on a case by case basis instead of using data from homologous reactions.

Theoretically Calculated Results from Previous Work: The energy calculations from the work of Lai-Cai Li, et al. are also problematic for two reasons. First, their energy results were at the QCISD(T)/SDD//MP2/SDD level while their vibrational analysis were done at the MP2/SDD level. However, they do not use the reported zero point energies. Neglecting thermal and zero point energy corrections changes their heats of reaction by as much as 3.5 kcal/mol for some of the reactions, and possibly more for their activation energies at 973K where they do not report thermal corrections at that temperature. Secondly, much of the data for heats of reaction that are extracted from Table I and reported in Table II of their work are incorrectly computed from their own numbers.

CHAPTER 4. EXPERIMENTAL RESULTS

4.1. Experimental Objectives

The experimental results discussed in this work have been exploratory only, since the major contributions from the current research were on the theoretical side. The main objective for the experimental portion of this current research was to determine which mercury species could be measured quantitatively through quadrupole mass spectrometry. In addition, a large aspect of this experimental work dealt with the development of the experimental technique. Therefore, since this was only a preliminary study, the focus was on room temperature reactions only. The reactions discussed here are most likely taking place heterogeneously on the Pyrex surface, if the given reaction is taking place at all. The following two reactions have been studied experimentally due to the difficulty of purchasing HgCl directly. Mercuric chloride (HgCl) exists in the solid phase at room temperature and the company that supplies the permeation tubes, VICI Metronics, does not sell the compound due to the messy nature of its sublimation into the gas phase. Therefore, the overall oxidation process studied will be only those involving elemental mercury.



The reactions take place in a laminar flow reactor, which is modeled as axial dispersed plug flow. Both a coated and uncoated reactor were studied in this work, each made of

Pyrex. The reactions took place at ambient conditions, specifically with a slightly warm lab temperature of 305 K. The coating used for the coated reactor was a Halocarbon wax coating that was used in previous research where similar reactions were considered. (Ariya et al., 2002) Studying reactions (4.1) and (4.2) within each of the reactors, allowed for the determination of whether mercury oxidation occurs heterogeneously or strictly homogeneously. As reported previously in the background section of this work, there has been much research which supports the hypothesis that mercury oxidation at ambient conditions happens to some extent heterogeneously. (P'yankov, 1949; Medhekar et al., 1979; Hall et al., 1991; Ariya et al., 2002) Hence, the results of this research do not just address the mercury oxidation process in the flue gases of coal combustion, but also questions current sampling methods which may be affected by the heterogeneous oxidation of mercury.

The product species of each reaction are sampled through a series of orifices and are directly measured using a quadrupole mass spectrometer. This research is unique in that the mercury speciation is measured directly rather than by difference, which has been the traditional method of analyzing mercury speciation. (Laudal et al., 1997; Linak et al., 2001; Stratton et al., 2001) The mass spectrometer allows for the separation of the product species by their mass to charge ratio. Due to the limited sensitivity of the quadrupole mass spectrometer used in this work, the mercury concentrations will be measured in the ppm range and will have to be extrapolated for their comparison to the

ppb concentrations present in the flue gases. Table 4-1 lists the concentrations of mercury and chlorine species that are considered in this work.

Table 4-1. Mercury Concentrations Studied with Mass Spectrometry

Compound	Concentration in the flue gases	Modified concentration for current research
Hg ⁰	ppb range	5 ppm
HCl	1 –100 ppm	300 ppm
Cl ₂	Low ppm	5 ppm

For performing many of the calculations that are presented in the following sections and in developing the experimental apparatus, it was necessary to have many of the constants which are shown in Table 4-2 close at hand. (Hall, 1990)

Table 4-2. Physical Properties of Mercury

atomic number	80
atomic weight	200.59 amu
melting point	-38.87 °C
boiling point	356.57 °C
electronic configuration	(Xe)4f ¹⁴ 5d ¹⁰ 6s ²
density	13.546 g/cm ³ (20 °C)
solubility	6*10 ⁻⁶ g/100 g water (25 °C)
metallic radius	1.57 Å
covalent radius	1.49 Å
vapor pressure	1.85*10 ⁻⁴ Torr 1.201*10 ⁻³ Torr 2.729 * 10 ⁻¹ Torr
Electronic excited states Ultraviolet – visual spectrum	6s ¹ S ₀ → 6pP ₁ 184.957 nm 6s ¹ S ₀ → 6p ³ P ₁ 253.652 nm 6p ³ P ₁ → 7s ³ S ₁ 435.835 nm

In essence, the major aspect of this experimental work was the design and construction of an apparatus that can accurately and directly measure mercury speciation. Within the experimental set-up, there are aspects that require modification to further increase the reliability of the experimental results. These modifications will be addressed individually as they arise in the following sections of the experimental discussion. The experimental results obtained for reactions (4.1) and (4.2) are compared to the theoretical predictions from the earlier sections of this work, and conclusions are drawn on the potential for the heterogeneous oxidation of mercury in the reactor.

4.2. Experimental Background

The quadrupole mass spectrometer allows for the direct measurement of mercury speciation in a given flue gas environment. In fact, there exists only one other set of experimentally based calculations involving the direct measurement of mercury speciation. (Ariya et al., 2002) This limited amount of mercury speciation data highlights the uniqueness and importance of the current work. A major contribution of the current experimental work was to determine which mercury species could be measured quantitatively through quadrupole mass spectrometry. Traditionally, one uses difference techniques to analyze mercury speciation. In fact, many of the methods used for measuring mercury speciation combine the two different oxidized forms, Hg^+ and Hg^{2+} , and are unable to accurately distinguish between the two. Several of these traditional difference techniques are highlighted here.

Typically the analysis of mercury speciation in the combustion flue gases is performed through sampling trains where the sample is passed through a series of aqueous solutions to separate the elemental mercury, Hg^0 , from the oxidized forms, Hg^+ and Hg^{2+} . The Ontario Hydro method (OH) and the Alkaline Mercury Speciation (AMS) method are often used to measure mercury speciation. (Linak et al., 2001) However, research has shown for both the OH and AMS methods, that as little as 1 ppm of Cl_2 in the simulated flue gases can lead to a bias of 10 – 20 % of elemental mercury, Hg^0 , being misreported as oxidized mercury, Hg^{2+} . In addition, at a chlorine concentration of 100 ppm, the OH

method led to a similar bias. However, the AMS method showed an increased bias of 30 – 60 %. Linak et al. concluded in their research that with SO₂ present, the bias does not exist. Therefore, when using these measuring methods, it is important to consider the sulfur content of the source for the flue gases being analyzed.

The EPA Method 29 is very similar to the OH method, and is also an impinger based method. Research has shown that EPA Method 29 impinger solutions are not suitable for measuring mercury speciation in flue gases which are high in sulfur. (Laudal et al., 1997) It was found that the oxidized form of mercury, Hg²⁺, was not effectively captured in the acidified permanganate solution. They further conclude in their research that modifying the method by using KCl or trisbuffer solutions may provide more precise mercury speciation measurements. Laudal et al. also examined the Mercury Speciation Adsorption (MESA) method, which uses solid sorbents to selectively capture the oxidized mercury species. Also, Laudal et al. found that at concentrations of 1500 ppm of SO₂ and 600 ppm of NO_x, the MESA method did not speciate mercury correctly.

Lastly, a method that has been used to measure mercury speciation in the atmosphere is the Mist Chamber (MC) method. (Stratton et al., 2001) The downfall of this method is its inability to distinguish among the different forms of oxidized mercury; HgO, HgCl₂, HgBr₂, Hg(OH)₂ and Hg(NO₃)₂·H₂O. In addition, there are components of the mist chamber that are made of Teflon. Stratton et al. found that the oxidized form of mercury is highly reactive with Teflon and that the contamination is time consuming to clean.

Having considered several of the current methods that are being used to analyze mercury speciation both in the atmosphere and in the flue gases of coal combustion, it becomes evident that using direct mass spectrometry sampling is a novel approach that avoids many of the experimental difficulties involved with the traditional difference techniques.

4.3. Experimental Approach

4.3.1. Reactor and Plumbing

A tubular reactor as shown in Figure 4-1 has been employed throughout the experiments. The reactor is a laminar flow reactor with a typical Reynolds number of about 344, calculated from the following equation,

$$N_{Re} = \frac{D\bar{u}\rho}{\mu} \quad (4.3)$$

such that D is the reactor diameter, \bar{u} is the average gas velocity, ρ is the gas density and μ is the gas viscosity. Both the gas density and viscosity were calculated from derivations involving the kinetic theory of gases with the gas density of N₂ being 1.145 kg/m³ and the gas viscosity being 16.7*10⁻⁶ kg/ms.

The laminar flow reactor is modeled by axial-dispersed plug-flow. To model the flow as plug, the Peclet number must tend to infinity, while a Peclet number tending to zero exhibits a flow that is perfectly mixed, which would correspond to a continuously stirred tank reactor. The Peclet number is defined as,

$$N_{Pe} = \frac{R\bar{u}}{K} \quad (4.4)$$

such that, R is the reactor radius, \bar{u} is the average gas velocity, and K is the effective axial dispersion coefficient.

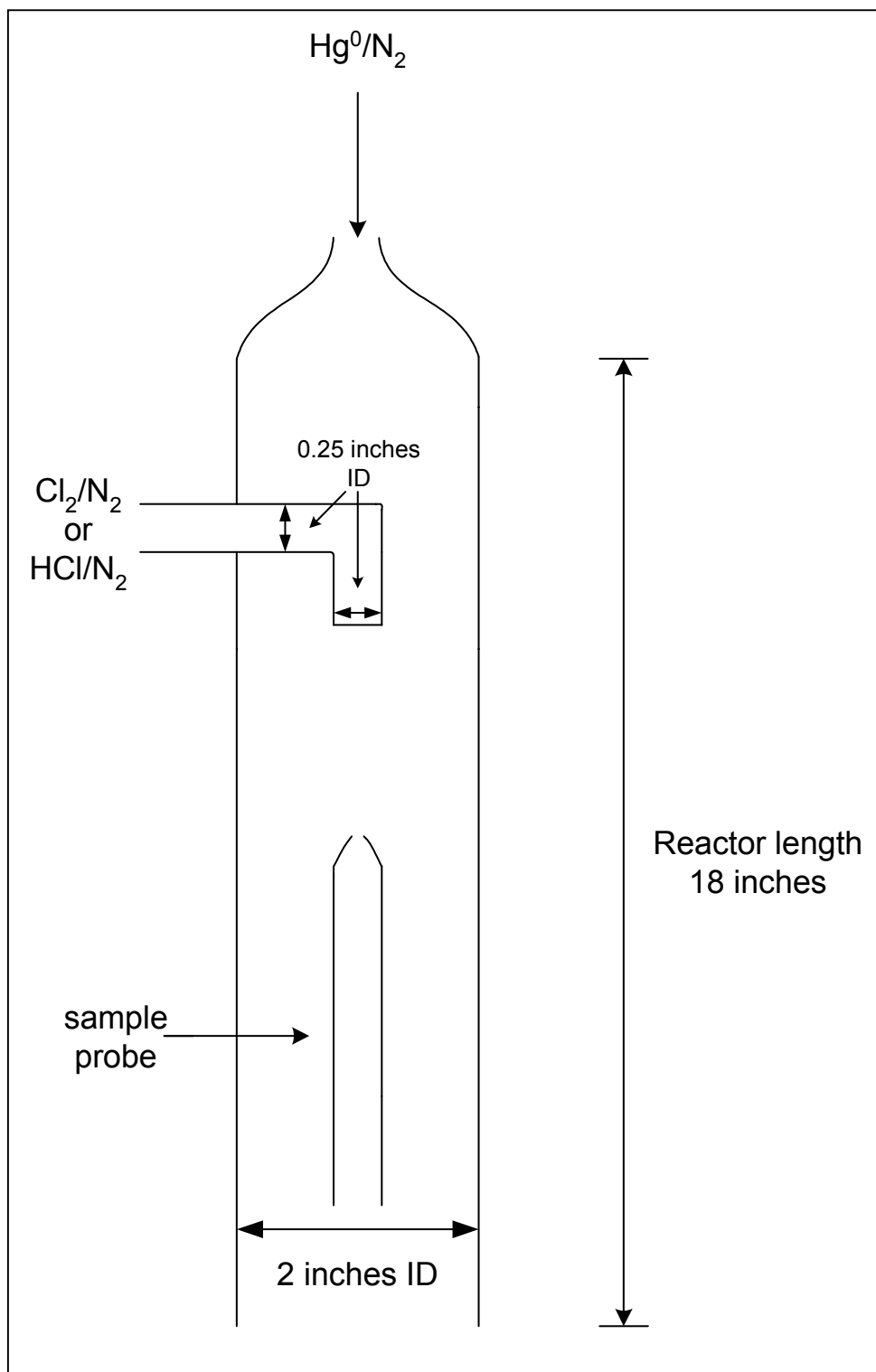


Figure 4-1. Schematic of the Reactor

The effective axial dispersion coefficient, K, is equal to the sum of the molecular diffusivity and molecular dispersion, which is given by,

$$K = D + \frac{R^2 \bar{u}^2}{48D} \quad (4.5)$$

such that D is the molecular diffusivity, R is the reactor radius, and \bar{u} is the average gas velocity. Using the following equation for self-diffusion of nitrogen from the kinetic theory of gases,

$$D = \lambda \bar{u} \quad (4.6)$$

yields a diffusion coefficient of about $0.105 \text{ cm}^2/\text{s}$. In equation (4.6), the diffusion coefficient is the product of the mean free path, λ , and the average gas molecule velocity, \bar{u} . From derivations using the kinetic theory of gases, a mean free path for N_2 of 6.3×10^{-8} meters and an average velocity of 500 m/s were used for the diffusivity calculation. The assumption is to use the self-diffusion of N_2 since chlorine and mercury are only available in the ppm concentration range. Also, since our reactions are taking place at ambient conditions, a lab temperature of 305 K and a pressure of 760 Torr are used for approximate conditions. In this case, the effective dispersion coefficient is approximately $87 \text{ cm}^2/\text{s}$. Substituting this value into equation (4.4) yields a Peclet number of about 0.576, which is lower than what was anticipated. As stated previously, a Peclet number which tends to infinity is desired for the application of the plug flow model. Since the effective dispersion coefficient is proportional to the square of the reactor diameter, a reduction in the reactor diameter would decrease the effective dispersion coefficient and

effectively increase the Peclet number. In future work this should be done so that potential dispersion effects can be neglected. It is important to note that the current reactor is based upon these preliminary calculations and that the reactor size should be reduced for future work.

The reactor is designed such that the sample probes can be exchanged out. Three different length sample probes were created in order to sample at different points along the reactor volume to obtain three distinct residence times. Table 4-3 below lists the possible residence times while considering various gas flow rates. The sampling points along the reactor are at ~ 23 cm, 30 cm, 45 cm providing three different residence times at flow rates ranging between 0.5 and 15 L/min.

Table 4-3. Reactor Residence Times

Volumetric Flow Rate (L/min)	Gas Velocity (cm/min)	Residence Time (s)	Distance Along Sample Probe (cm)
.5	24.68	SP1: 56 SP2: 73 SP3: 109	SP1: 23 SP2: 30 SP3: 45
1	49.36	SP1: 28 SP2: 36 SP3: 55	SP1: 23 SP2: 30 SP3: 45
5	246.8	SP1: 5.6 SP2: 7.3 SP3: 11	SP1: 23 SP2: 30 SP3: 45
10	493.6	SP1: 2.8 SP2: 3.6 SP3: 5.5	SP1: 23 SP2: 30 SP3: 45
15	740.4	SP1: 1.9 SP2: 2.4 SP3: 3.6	SP1: 23 SP2: 30 SP3: 45

To obtain optimum mixing between mercury and chlorine, the chlorine/nitrogen combination flow rate was required to be about 15 L/min. This flow rate requirement will be discussed in more detail in the next section, which discusses the mixing calculations. Using this value throughout the experiments yields residence times of ~ 1.9, 2.4, and 3.6 seconds.

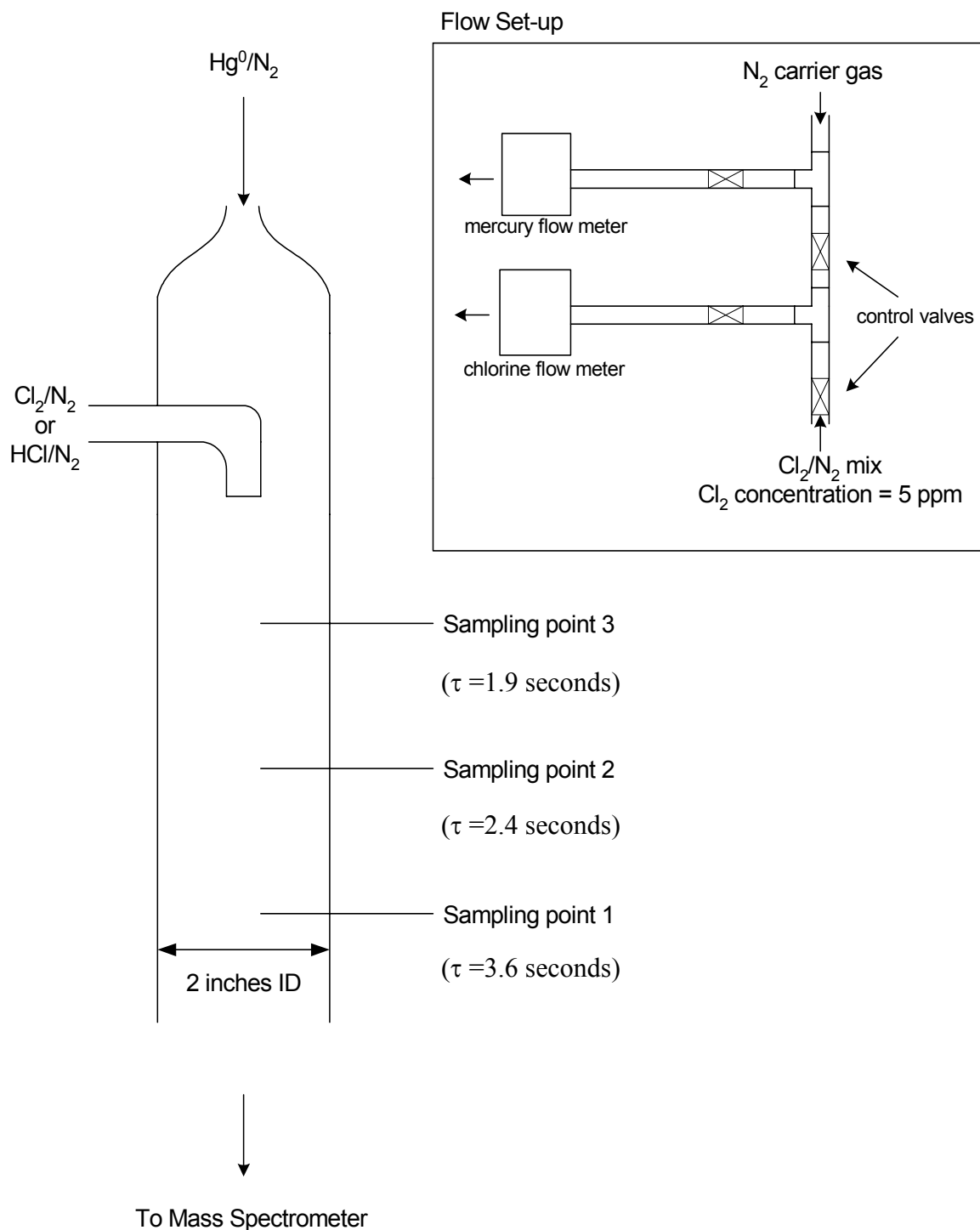


Figure 4-2. Schematic of the Mercury and Chlorine Flow System

Calculations to Obtain Optimum Mixing between Mercury and Chlorine:

The rapid effective mixing between chlorine and mercury in the reactor is crucial. To obtain this optimum mixing, the glass shop fixed a probe inside the reactor for the flow of the chlorine/nitrogen combination stream. The idea is to have this stream ‘spray’ radially into an existing mercury/nitrogen combination stream. Figure 4-3 below illustrates the set-up and provides an idea of the velocity profile of the gas steam through small holes in the probe.

The number and diameter of the holes can be determined using the following relationship:

$$Q = n \left(\frac{\pi}{4} \right) d_n^2 U \quad \text{or} \quad \frac{Q}{U} = n \left(\frac{\pi}{4} \right) d_n^2 \quad (4.7)$$

such that, Q = flow rate of the nitrogen/chlorine stream, n = number of holes, d_n = diameter of each hole, and U = discharge velocity of the nitrogen/chlorine stream(s). The nitrogen/chlorine stream flowing into the probe can be controlled by a valve and flowmeter as shown below in Figure 4-3. The discharge velocity can be calculated

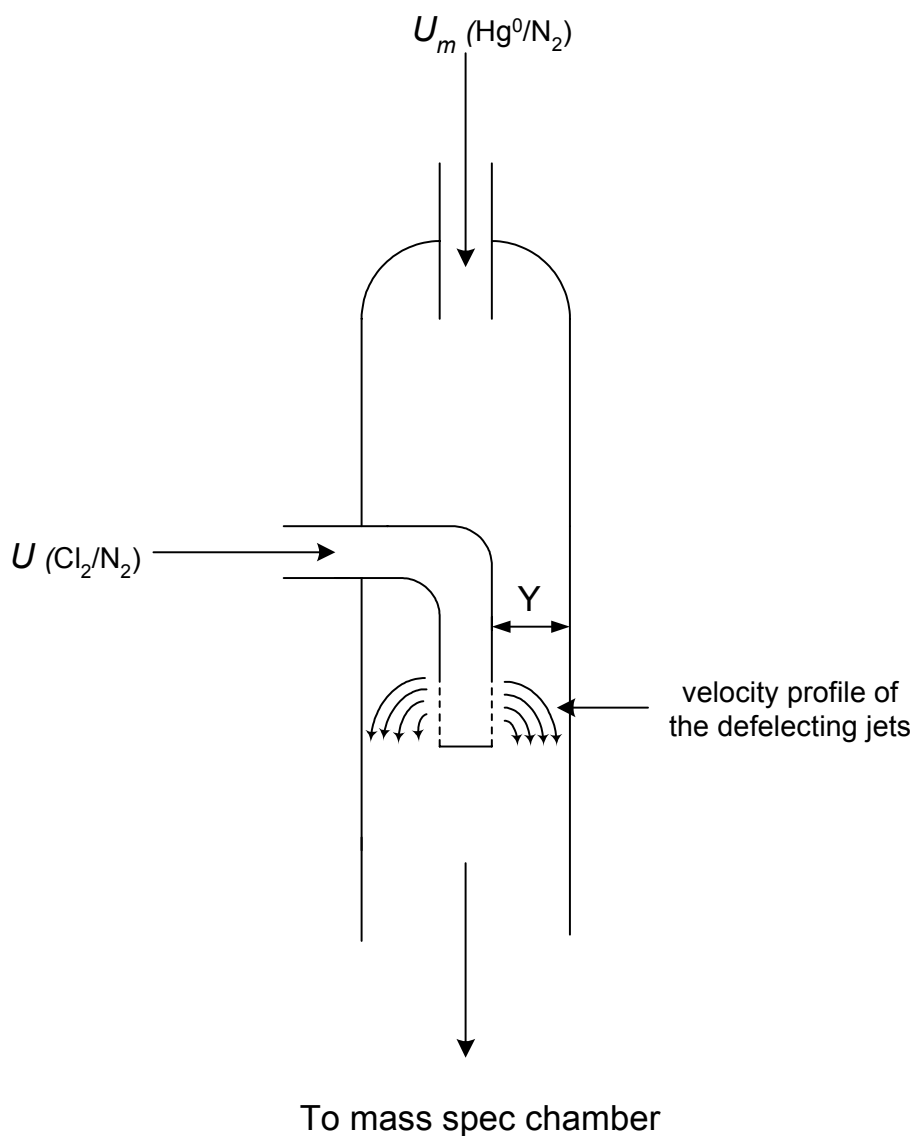


Figure 4-3. Flow Through Deflected Jets to Obtain Optimum Mixing

theoretically through the following equation (Cheremisinoff and Gupta, 1983):

$$\left(\frac{Y}{d_n}\right)_{\max} = 1.224 \left(\frac{\rho U^2}{\rho_m U_m^2}\right)^{\frac{1}{2}} \quad (4.8)$$

such that U is the desired discharge velocity required in equation (4.7), Y is the distance from the probe to the wall of the reactor, d_n is the hole diameter, $\rho = \rho_m$ since the chlorine and mercury are present in the ppm range, and U_m is the crossflow velocity of the mercury/nitrogen stream. It is important to note that equation (4.8) results in the upper limit of the depth penetration. Therefore, these calculations should ensure that the chlorine velocity stream will not penetrate the walls of the reactor. Substitution of equation (4.7) into (4.8) yields the following relationship:

$$\left(\frac{\text{flow rate of } Cl_2 / N_2}{\text{flow rate of } Hg^0 / N_2}\right)(0.0702) = nd_n. \quad (4.9)$$

However, the glass shop could only make holes in the Pyrex as small as 1mm in diameter. A total of 10 holes, each 1mm in diameter were drilled into the base of the sample probe, requiring a ratio of ~140:1 of the Cl_2/N_2 and Hg^0/N_2 flow rates. In the experimental set-up, a flow rate for the mercury/nitrogen stream was set to ~ 0.1 L/min and the flow rate for the chlorine/nitrogen stream was set to ~ 14 L/min.

Control Panel Calculations:

A schematic of the control panel can be seen in Figure 4-4 below. The following two basic equations were used for all the calculations involving the control panel:

$$P = I \cdot V, V = I \cdot R \quad (4.10)$$

such that, P = power (watts), I = current (amps), V = voltage and R = resistance (ohms).

The control panel contains three toggle switches; one for each of the two mechanical pumps and one for the diffusion pump. Each pump draws anywhere between 10 and 15 amps of current so that three 20 amp relays were purchased, one for each pump. The control panel also has two rocker switches, one for each solenoid, which in turn control the opening and closing of the gate valves. The gate valves require compressed air to push an internal piston that opens the valve. The gate valves have the option of being operated manually or through use of a solenoid. Currently only one of the solenoids is being used, but the control panel is set up to allow both solenoids to function. The function of the solenoid is that of a switch, simply opening or closing the inlet of the compressed air so that the user does not have to disconnect and reconnect the compressed air connections. The solenoids draw very little current so that two 2 amp relays were purchased for the solenoid wiring.

Each of the switches has an LED wired to it so that the user is always aware of the instruments that are running or the valves that are open. In terms of the total power demand, the LEDs pull so little current that their value was nearly irrelevant. However, a 12 VDC power supply was purchased for the panel so that all the components purchased for the panel had to correspond to the 12 VDC power supply.

There was one complexity concerning the control panel. In the event of an unexpected power failure in the lab, the control panel should remain turned off when the power comes back on. One wants to avoid pumps automatically turning back on when the power resumes. In order to bring power back to the control panel, a reset button needs to be depressed. In terms of the wiring, the current should only be allowed to flow in one direction. To force current only in one direction, a diode had to be wired next to the reset button switch.

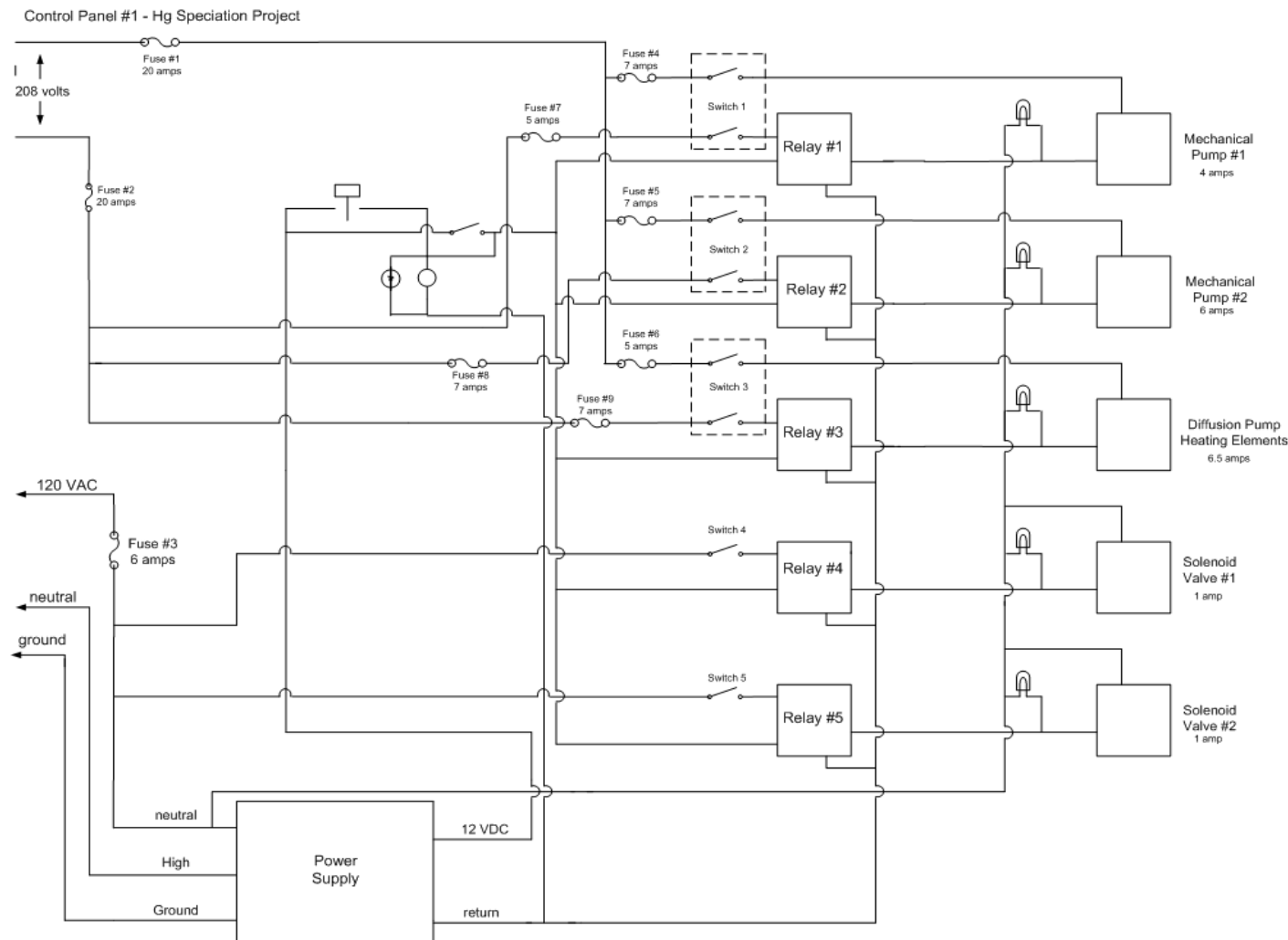


Figure 4-4. Schematic of Control Panel Wiring

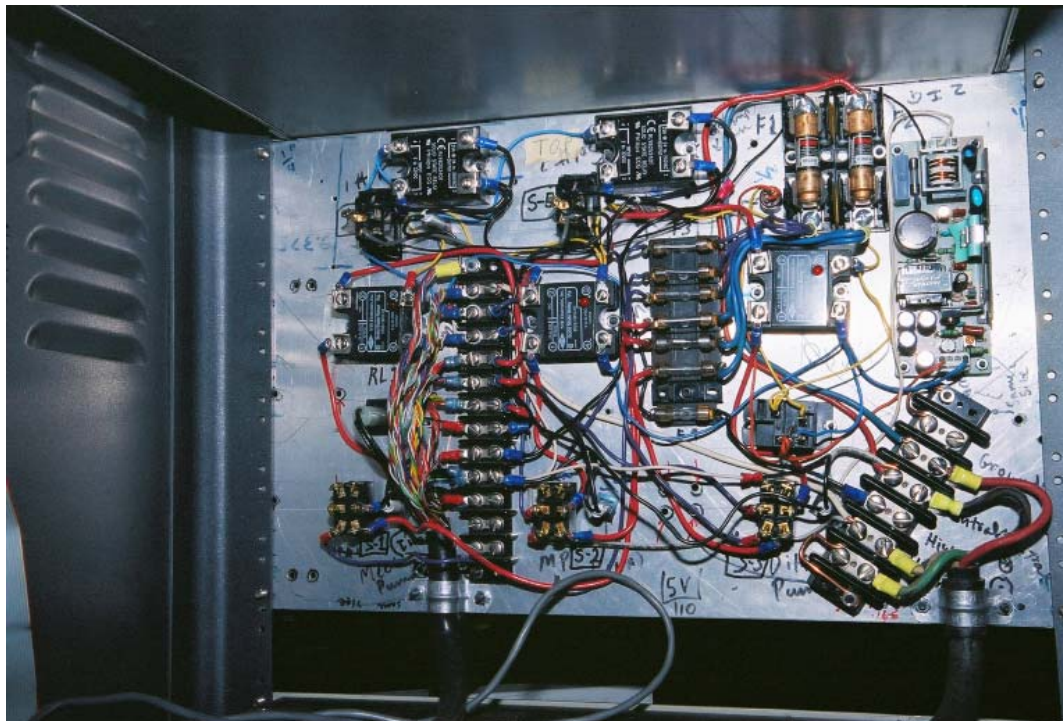


Figure 4-5. Photograph of Control Panel

4.3.2. Sample Probe Calculations

Orifice Diameter Calculations:

Two different sized orifices were required for the experimental set-up. The first orifice is at the tip of the sampling probe. The orifice was required to obtain a pressure gradient from atmospheric pressure to a lower pressure inside the sampling probe. Figure 4-6 below shows the sampling probe located in the reactor and the orifice parameters. This first stage of low pressure was required to minimize further gas collisions inside the sampling probe. The idea was to have the reactions all take place inside the reactor. The purpose of the sampling probe is to sample the gas at different points along the reactor, thus providing multiple residence times.

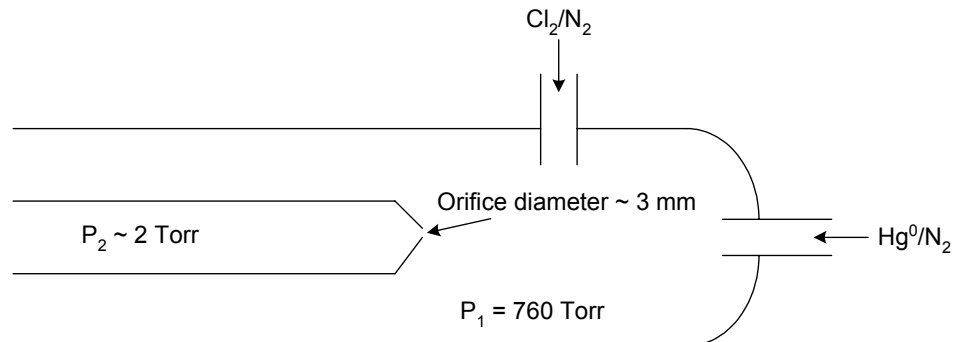


Figure 4-6. Parameters for the Sample Probe Orifice in the Reactor

To calculate the flow through an orifice, the following equation can be used (O'Hanlon, 1980):

$$\frac{Q}{A} = P_1 (.85) \left(\frac{kT}{m} \frac{2\gamma}{\gamma + 1} \right)^{\frac{1}{2}} \left(\frac{2}{\gamma + 1} \right)^{\frac{1}{(\gamma - 1)}} \quad (4.11)$$

Using N₂ as a carrier gas,

$$\gamma = C_p/C_v = 1.4$$

$$P_1 = 760 \text{ Torr}$$

$$T = 298 \text{ K}$$

$$M_{N2} = 28 \text{ amu} = 4.65 * 10^{-26} \text{ kg}$$

$$K = \text{Boltzmann's constant} = 1.38 * 10^{-23} \text{ J/K}$$

Orifice #1:

$$\text{yielding, } \frac{Q}{A} = 1.30 * 10^5 \frac{\text{Torr} * m}{s} \quad \text{or} \quad Q = A \left(1.30 * 10^5 \frac{\text{Torr} * m}{s} \right)$$

The mechanical pump has a pumping speed of 40 m³/h, and with the first stage of pressure between 1 and 20 Torr, to reduce further collisions in the sample probe results in a range of orifice diameters between 2.56 mm to 11.4 mm. The glass shop can draw holes as small as 0.5 mm. The current lab sample probes have inner diameters of ~ 3 mm yielding a base pressure inside the sample probe of about 2 Torr.

Within these orifice calculations, the Knudsen number becomes important. The Knudsen number for this situation is defined as the ratio of the mean free path to the diameter of the orifice. Using the following equation for the mean free path,

$$\lambda(mm) = \frac{1}{\sqrt{2\pi}d_0^2 n} \quad (4.12)$$

such that d_0 is the diameter of N₂ and n = P/kT. This yields a mean free path of N₂ at 298 K of $\sim 2.7 \times 10^{-6}$ mm. Recall the calculated orifice diameter was at most 11.4 mm, producing a Knudsen number of $\sim 2.4 \times 10^{-7}$. In this case, since the mean free path is much smaller than the diameter of the orifice, there will be continuous flow through the orifice and the equation is valid. Notice, if the mean free path (distance between collisions) was greater than the diameter of the orifice, the molecules would never get through and these calculations would not be valid.

Orifice #2:

Again using equation (4.11), with P₂ = 2 Torr.

yields, $\frac{Q}{A} = 3.43 \times 10^2 \frac{\text{Torr} * m}{s}$ or $Q = A \left(3.43 \times 10^2 \frac{\text{Torr} * m}{s} \right)$

The diffusion pump has a pumping speed of 760 L/s. To run the mass spectrometer properly with minimum interference, the operating pressure should not go above 1×10^{-5} Torr range. It is important to note here that the base pressure of the mass spectrometer will be in the low minus six Torr region (i.e. $\sim 3.5 \times 10^{-6}$ Torr) and this upper stage of high six or low five Torr region will only occur when a sample is being introduced into the vacuum chamber. Ideally, the highest pressure desired is $\sim 8 \times 10^{-6}$ Torr. Too high of a pressure at this point can damage the electron multiplier and also destroy the filaments. Replacement of the filament is very time consuming, but monetarily negligible. A new multiplier, however, is $\sim \$2000$. At this point, the gauge controller and mass spec electronics are not interfaced so the pressure requires close monitoring when the filament and multiplier are turned on.

With a 760 L/s diffusion pump, in order to obtain a base pressure of $\sim 3.5 \times 10^{-6}$ Torr, the orifice diameter must be ~ 0.1 mm in diameter. This size diameter is too small for the department machine shop to drill. A company named Bird Precision laser drilled a 0.1 mm diameter hole in a sapphire which was then carefully, yet securely set into a blank copper gasket.

Again, the Knudsen number can be checked to be sure the flow is continuous. A calculated Knudsen number of 2.7×10^{-5} concludes that the flow is continuous and the equation above is valid.

Once the reaction occurs, the molecules are sampled through the probe, which is at about 2 Torr, restricting the collisions to within the reactor volume. Once sampled, the molecules travel through to the second orifice where they enter the vacuum chamber to reach a reduced pressure in the 10^{-6} Torr range. Figures 4-7 and 4-8 display the entire vacuum assembly.

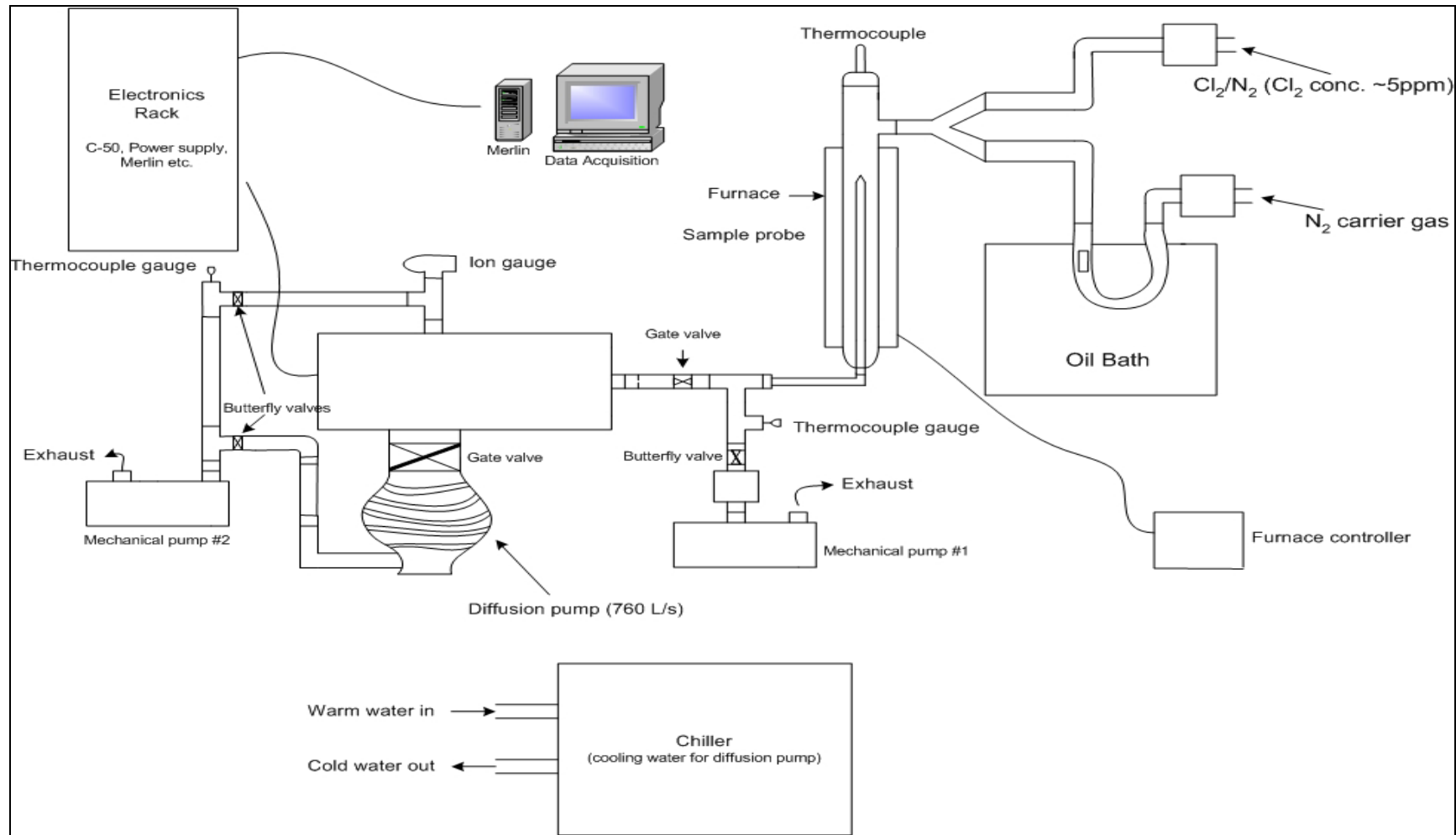


Figure 4-7. Schematic of the Experimental Set-up

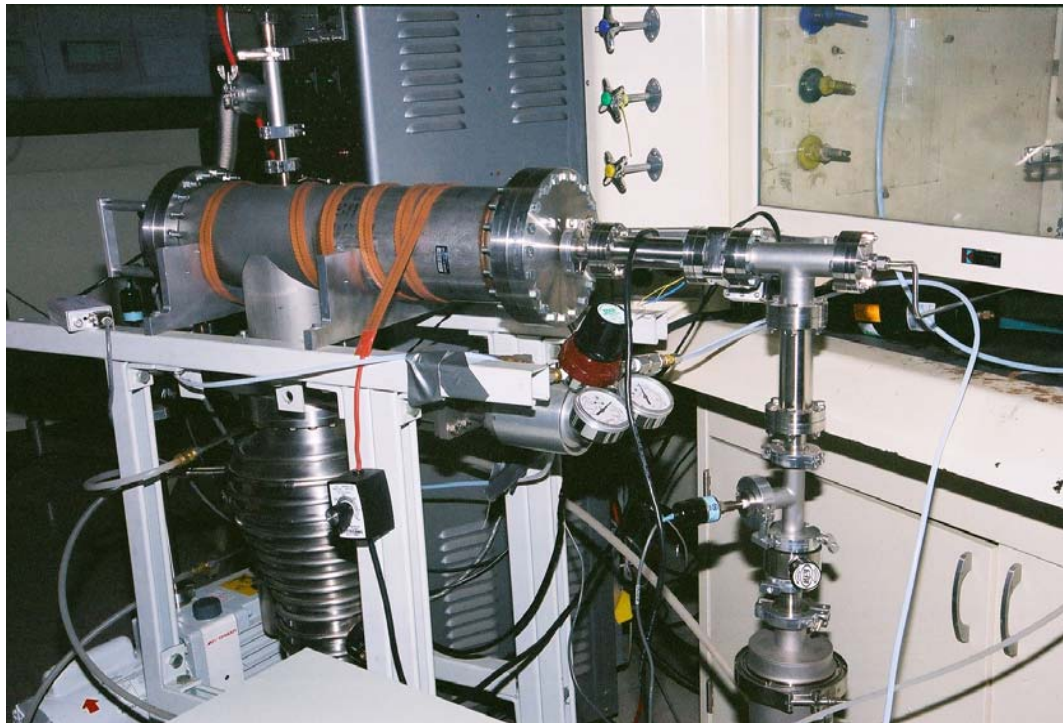


Figure 4-8. Photograph of Vacuum Assembly

4.3.3. Quadrupole Mass Spectrometry

Prior to addressing the results of the mass spectrometry research, it is necessary to briefly discuss the basic principles of how a mass spectrometer works. When molecules enter the vacuum chamber, they are first ionized and then directed through a mass separator before they are detected. Different types of mass spectrometers can be distinguished from one another by the way in which they accomplish each of these three processes. The ionization source for the current work is an electron ionization source. The mass separator is of the quadrupole type and lastly, the ions are detected via an electron multiplier.

For the ionization step, the electrons from the filament are drawn toward an anode and, while crossing the area to the anode, the electrons collide with the molecules that are approaching from the orifice of the vacuum chamber. When the electrons bombard the gas molecules, they strip off one or more of their electrons, thus creating positive ions. Table 4-6 lists various ionization potentials for a series of compounds that are of interest in the current work. Currently, 70eV are applied to the filament in the ion source, which is typical for these systems. (O'Hanlon, 1980)

For the mass separation process, an RF quadrupole developed by Paul (Paul et al., 1953) is used. In essence, the quadrupole mass filter consists of four rods, hyperbolically spaced. One rod pair has a positive DC potential, while the other rod pair has a negative

DC potential. The addition of an RF field with magnitude greater than each of the DC fields, creates a scenario in which the positive ions are on a potential hill for the positively charged rod pair and exist on a potential valley for the negatively charged rod pair. The positive rod pair acts as a high-pass mass filter where the heavy ions are retained and the light ions are lost. The negative rod pair acts as a low-pass mass filter where the light ions are retained and the heavy ions are lost. Together, the filters form a band that allows ions of particular mass ranges to go through and ultimately get detected. Whether an ion is lost or retained depends on whether or not its trajectory is stable. These details will be omitted here, however there are many reference texts available for the reader. (March and Hughes, 1989; Dawson, 1995; McDowell, 1963)

The current mass spectrometer is equipped with an electron multiplier detector. The ion detector current is directly proportional to the pressure by the following equation (O'Hanlon, 1980):

$$i_n = S_n * P_n \quad (4.12)$$

Such that i_n is the ion current, S_n is the sensitivity of the ionizer and the filter, and P_n is the partial pressure of the nth gas. The Merlin data acquisition software records the mass to charge ratio against the ion intensity. The multiplier acts as an amplifier so that the ion current can be accurately recorded.

Overall, the assembly of the mass spectrometry set-up was a very involved process.

When work commenced on the project, the mass spectrometry housing was still in boxes and the vacuum assembly components still needed to be ordered. In fact, one of the major roadblocks of the project was the fact that the internal wiring for the lenses and filaments was completely missing. New wiring and insulating beads had to be ordered and the entire ion source rewired. In addition, both of the tungsten filaments had to be replaced.

Due to the original state of the mass spectrometer, it became imperative to run controls through the mass spectrometer to ensure that it was functioning properly. The original plan was to run hydrogen chloride, chlorine, nitrogen and mercury each through the mass spectrometer individually and to compare their isotopic abundances to experimental values from the NIST webbook. (Afeefy et al., 2003) However, due to contamination of oil in the vacuum chamber, the only “clean” spectra that was obtained was that of hydrogen chloride. This was because the mass range of hydrogen chloride did not coincide with the mass range of the oil species. The contamination was a result of two combined incidences. First, the original oils that was being used in the diffusion pumps and mechanical pumps were not low back streaming oils. Since switching to newer oils, the back streaming has decreased substantially, but it is predicted that the mass spectrometer housing has been contaminated and requires ultrasonic cleaning. This will have to be performed by the company that manufactures these spectrometers, ABB/Extrel. The second incidence was the use of the lab’s compressed air, which

contains oil. The compressed air was used to open a pneumatic gate valve, and oil from the compressed air may have also contributed to the total oil contamination in the vacuum chamber. Due to this contamination, it was not possible to obtain “clean” spectra for the mercury chlorine species of interest. In addition, when analyzing the results, a blank run of nitrogen had to be subtracted from all of the intensities obtained at each of the mass ranges of interest.

The molecular stream is bombarded by a stream of electrons that are ‘boiled off’ an electron ionization source. The source is a tungsten filament with an energy distribution of about 70 electron volts. This number does not necessarily need to be this high since the ionization potentials of the species of interest are of the same order of magnitude as the dissociation energies as reported below in Table 4-4. However, one should not apply less than 30 eV since the probability of an electron hitting a molecule in this region is ~ 1 in 100,000 due to the reduced pressure.

Table 4-4. Dissociation Energies and Ionization Potentials of Mercury Species

Compound	Dissociation Energy (eV)	First Ionization Potential (eV)
HgCl	1.02	---
HCl	4.43	12.749
Cl ₂	2.49	11.48
HHg	0.409	---
Hg ₂	0.0822	9.10
HgCl ₂	3.567	11.38
Hg	---	10.43
Cl	---	12.96

The filament is controlled through the ABB/Extrel C-50 unit on the electronics rack. In addition, the multiplier, dynode and lenses are controlled on this C-50 unit. Once the molecule is bombarded with more than enough energy (ionization energy) to remove its outermost electron, two things happen. First, after losing the electron, the species is now positively charged and, second, provided it has enough excess energy, it can fragment. Many species have been studied through mass spectrometry and many fragment ‘fingerprints’ have been recorded. After fragmenting, the positively charged species are focused through a series of lenses and through the mass range of the quadrupoles until it reaches the electron multiplier, which amplifies the signal. The preamp converts this signal so that the intensity of a species can be obtained through the data acquisition software. The software used in this case is Merlin Data Acquisition, which was developed through ABB/Extrel. The intensities are graphed versus the mass to charge ratio and concentrations of the product species are directly proportional to the relative intensities. In this way, the concentration of the product species are determined given three differing residence times in the reactor.

In order for a mass spectrometer to account for concentrations in the ppb range, the sensitivity becomes crucial. In the wiring of the current mass spec, an analog preamp controls the signal from the mass spec. To account for increased sensitivity, a counting preamp must be employed. Also, to use a counting preamp, the multiplier must be compatible and be a counting multiplier. The current system is too outdated to be compatible with a counting preamp. Hence, due to the inability of the current mass

spectrometer to measure accurately in the ppb range, the mercury concentrations will be in the ppm range and the results will have to be extrapolated to account for the lower concentrations that exist in the flue gases.

4.4. Experimental Results

4.4.1. Preliminary Results

Mass spectrometry is a very sensitive technique and becomes even more sensitive when the focus is on detecting concentrations in the ppm range. To observe mercury and chlorine components in the ppm range, the backstreaming from both the diffusion pump and mechanical pumps must be minimal. Figure 4-8 below is a mass spectrum of the 180 to 220 mass to charge ratio (m/z) range. Hg^+ should be detected in this range with its major isotopes existing at 200 and 202 m/z ratio. However, at this time, Dow Corning 704 was being used for the diffusion pump oil and Inland TW was being used for the mechanical pump oil. What Figure 4-8 clearly exhibits is the requirement of an oil with very minimal backstreaming. The oils that were being used were not the best choices for mass spectrometry work. For mass spectrometry, the diffusion pump oil of choice is Santovac 5 and the mechanical pump oil of choice is Inland 45. Both of these oils have minimal backstreaming due to their low vapor pressures as shown below in Table 4-5. (O'Hanlon, 1980)

Table 4-5. Vapor Pressure of Common Pump Oils

Oil	Pump type	Vapor Pressure (Torr at 25°C)
Dow Corning 704	diffusion	2.3×10^{-8}
Santovac 5	diffusion	4.5×10^{-10}
Inland TW	mechanical	1.0×10^{-6}
Inland 45	mechanical	1.0×10^{-7}

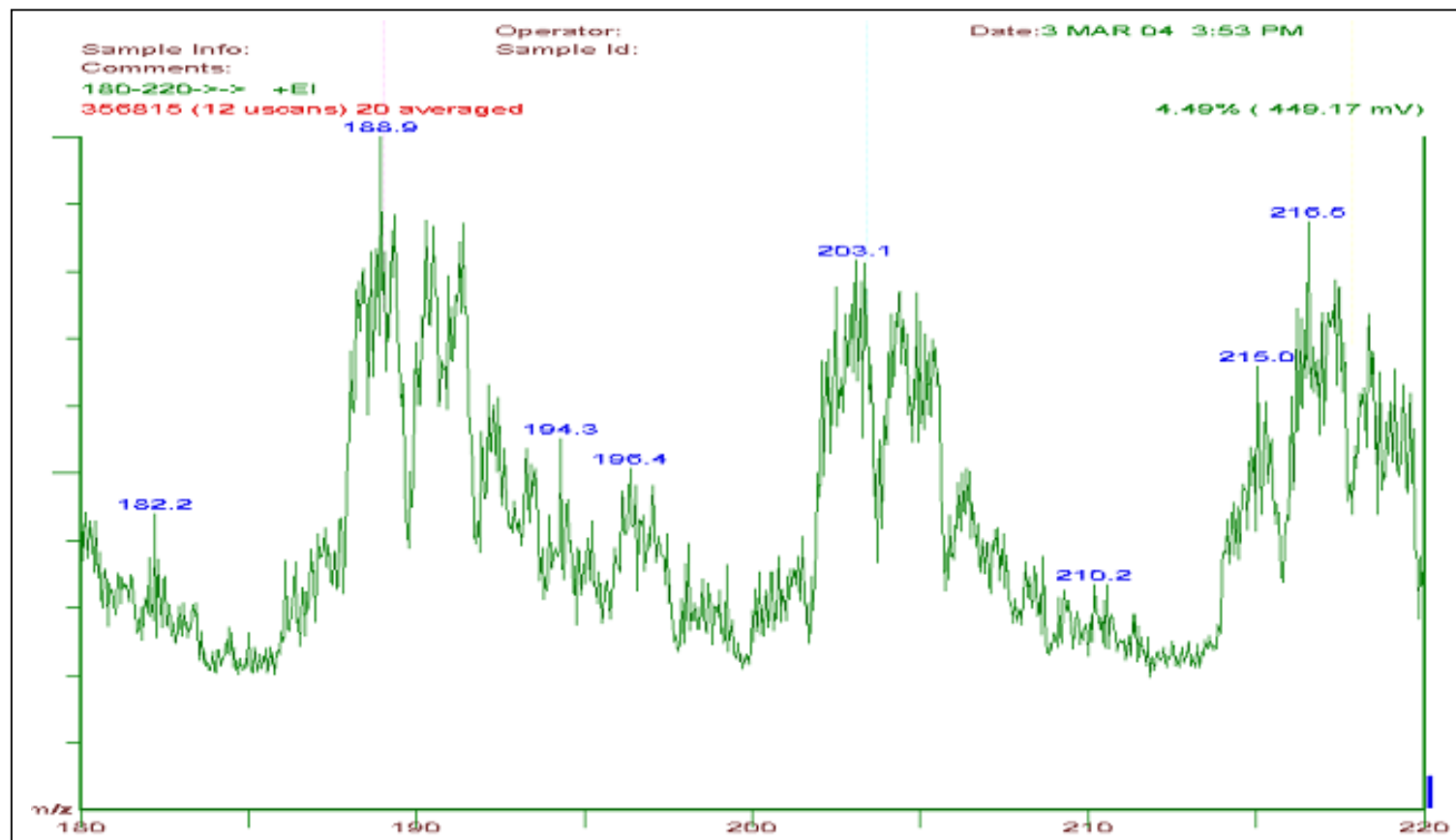


Figure 4-9. Mass Spectrum of Oil Backstreaming from DC 704

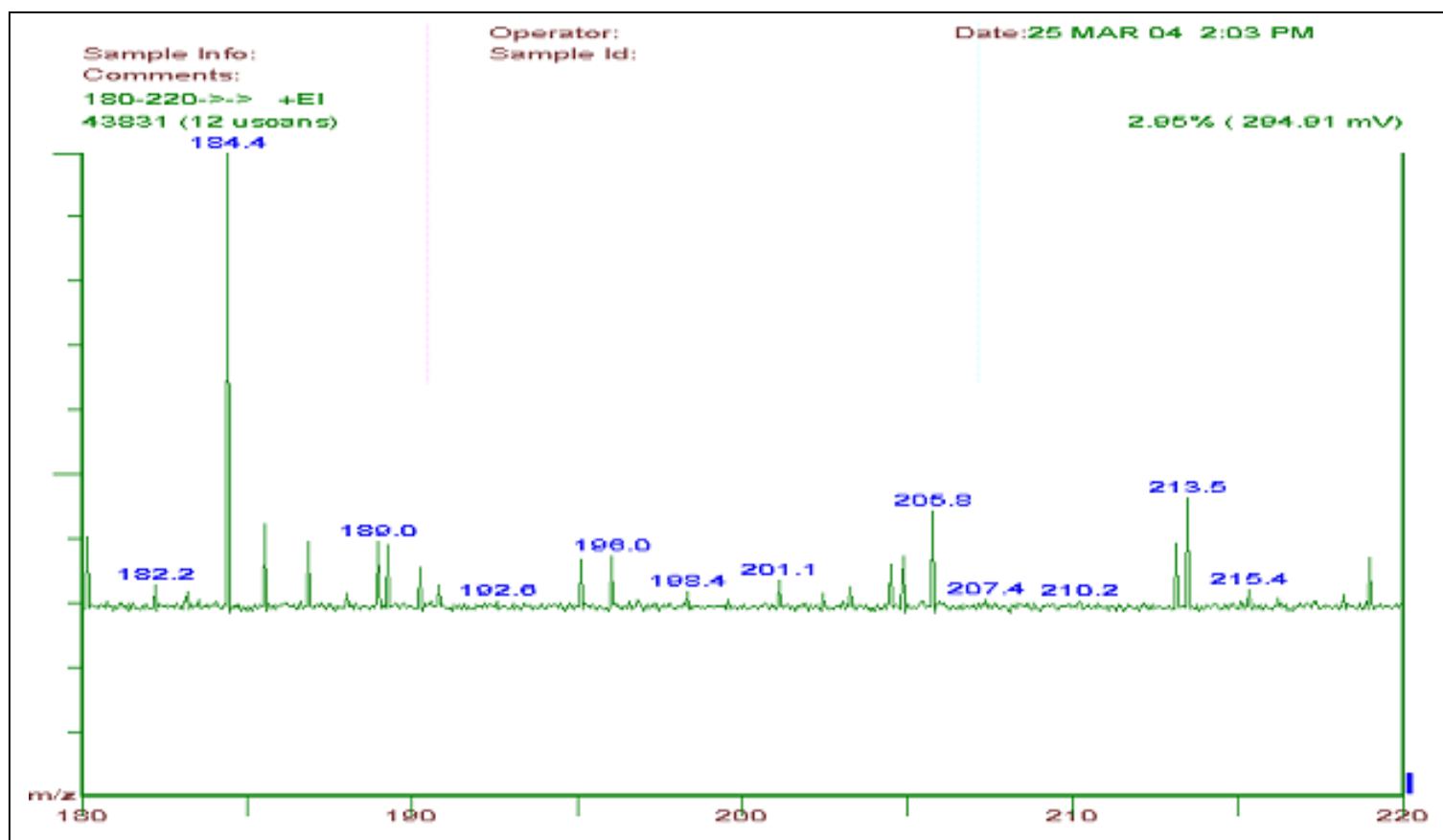


Figure 4-10. Mass Spectrum of Oil Backstreaming from Santovac 5

Figure 4-10 above is the mass spectrum of the same vacuum chamber, but with the two high vapor pressure oils replaced with Santovac 5 and Inland 45. The system was also baked out for four days to ensure the most effective removal of the oil contamination. From the spectrum of Figure 4-8, the signature peaks of elemental mercury at 200 and 202 m/z should be obtained.

Table 4-8 lists the major isotopes of the species of interest in the current work. The mercury and hydrogen chloride vapor is created from permeation tubes purchased from VICI Metronics. The mercury flow rate from the permeation tube is 536 ng/min, with a concentration of 5 ppm. The hydrogen chloride flow rate is 964 ng/min, with a concentration of 300 ppm. The chlorine gas is from a cylinder which contains Cl₂ at 325 ppm with the balance being nitrogen. Figure 4-11 is the mass spectrum of HCl. When HCl gets bombarded with electrons, the resulting HCl ion still has energy which allows it to fragment. The two stable isotopes of chlorine are ³⁵Cl and ³⁷Cl so that, as the molecule fragments, these isotopes appear as can be seen in Figure 4-11 at the 35 and 37 m/z. The most prominent peak is at approximately 36 m/z, which corresponds to HCl⁺, agreeing with other experimental data for the HCl spectrum. (NIST) In addition, there is a second HCl⁺ peak at the approximate 38 m/z, which corresponds to the less abundant chlorine isotope, ³⁷Cl.

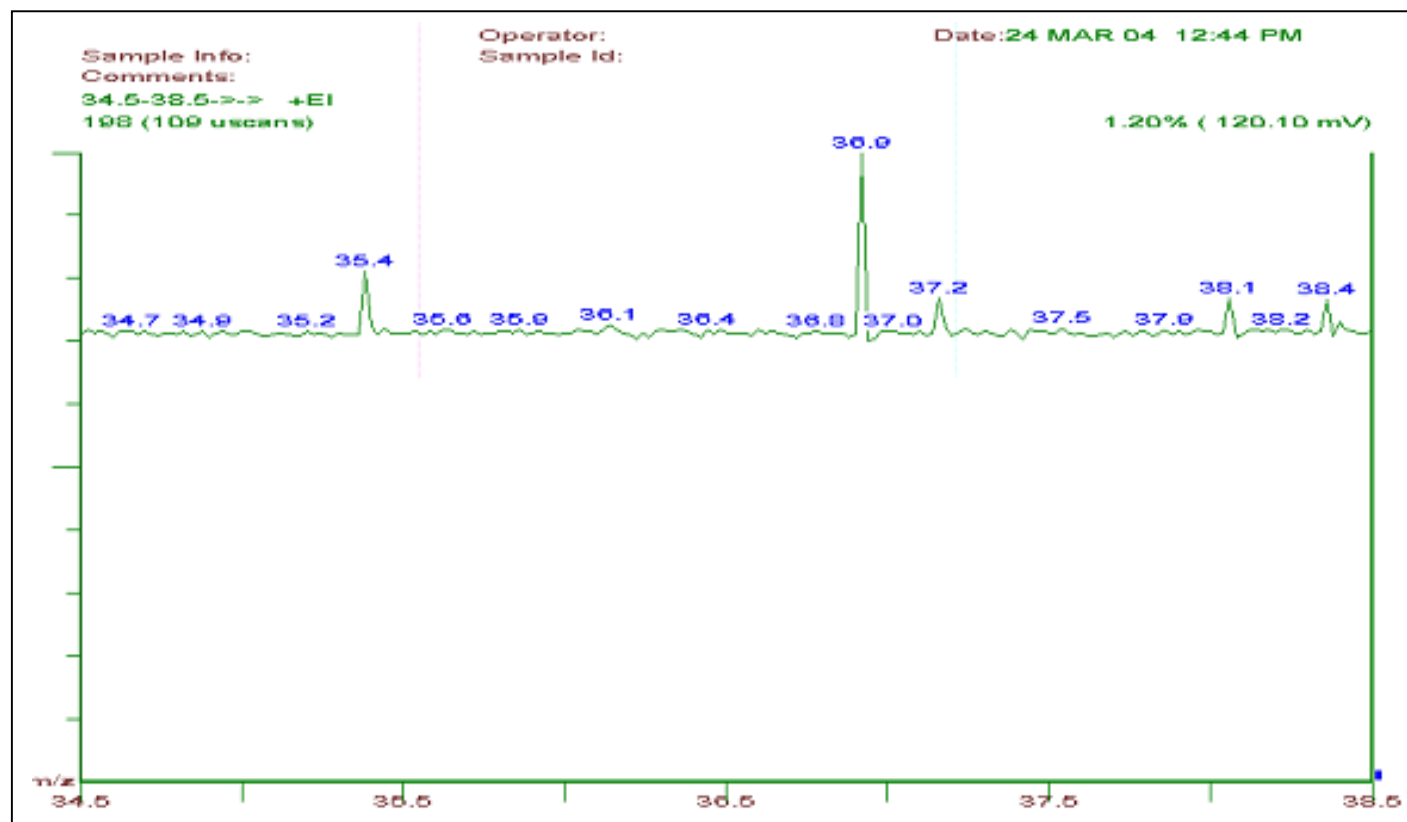


Figure 4-11. Mass Spectrum of HCl, 300 ppm

Table 4-6. Mass Ranges for Mercury and Chlorine Species

Species	Mass:Charge
Cl^+	*35, 37
Cl^{2+}	17.5, 18.5
Cl_2^+	*70, 72, 74
Cl_2^{2+}	*35, 36, 37
HCl^+	*36, 38
Hg^+	204, *202, 201, *200, *199, 198
Hg^{2+}	102, *101, *100, 99
HgCl^+	241, 239, 238, *237, 236, *235, *234, 233,
HgCl^{2+}	120.5, 119.5, 119, *118.5, 118, *117.5, *117, 116.5
HgCl_2^+	276, 274, 273, *272, 271, *270, *269, 268
HgCl_2^{2+}	138, 137, 136.5, *136, 135.5, *135, *134.5, 134
Hg_2Cl_2^+	*474, *470, *468
$\text{Hg}_2\text{Cl}_2^{2+}$	*237, *235, *234

*represents the isotope combination with the highest abundances

Table 4-6 above, lists the mass ranges of interest for the species studied in the current work and Table 4-7 below lists the six stable isotopes of mercury and their relative abundances. This characteristic isotope pattern allows for easy identification using mass spectrometry. The concentration of mercury was 5 ppm, which made it difficult to detect. Although high quality, low backstreaming oil is being used in the pumps of the vacuum assembly, the oil will still backstream to a certain degree. Unfortunately, the isotopes of mercury exist at the same mass to charge ratios as cracking patterns of the pump oils. To accurately measure elemental mercury using the mass spectrometer, the intensities of a blank run involving only nitrogen was subtracted from the run including

the mercury and nitrogen carrier gas combination. To obtain data with increased accuracy, the mass spectrometry housing should be sent to the manufacturer, ABB/Extrel, for ultrasonic cleaning. Other errors in the experimental data could be due to the inaccuracy of the lab's gauge controller. The gauge controller is an 880 RS Varian Controller, which was manufactured in 1978. The ion gauge LED indicator on the gauge controller tends to flicker on and off when the temperature of the room gets above 30 degrees Celsius. Unfortunately, the lab is not connected to the central air conditioning so that the temperature gets very high during the spring and summer months. In addition, the chiller and two mechanical pumps produce a great amount of heat, increasing the temperature of the room further. In total, the equipment would work better in a room that was properly air-conditioned. Due to the inability to accurately measure the pressure inside the chamber when a sample is being introduced further increases the possible inaccuracies of the current experimental errors.

Table 4-7. Stable Mercury Isotopes and their Relative Abundances

Mercury Isotope	Relative Abundance
^{196}Hg	0.15
^{198}Hg	9.97
^{199}Hg	16.87
^{200}Hg	23.1
^{201}Hg	13.18
^{202}Hg	29.86
^{204}Hg	6.87

Table 4-8 lists mercury intensity data obtained from the difference between a blank run with nitrogen and a run with the nitrogen and mercury combination. To maximize the probability of seeing mercury, the permeation tube was exposed to 100 degrees Celsius for 20 minutes before the nitrogen gas was allowed to flow through. After this 20 minute period, the nitrogen flowed through at approximately 5 liters per minute. The original pressure in the chamber was 5×10^{-7} Torr and the final pressure, after the sample was introduced was 4×10^{-6} Torr.

Table 4-8. Stable Mercury Isotopes and their Relative Abundances

Mercury Isotopes	Intensity (mV)	Abundances in this work	Actual Abundances
^{199}Hg	44.25	11%	17%
^{200}Hg , ^{201}Hg	156.87	41%	23%, 13%
^{202}Hg	183.55	48%	30%

It is important to note that all the abundances listed above are not including the mercury isotopes with 198 and 204 atomic mass units. If the mass spectrometer was more sensitive it may be possible to identify these minor isotopes and possibly decrease the error in the relative abundances observed in Table 4-8. The ability of the mass spectrometer to measure these differences implies that the current sensitivity of the measuring device is at least 5 ppm, which is the concentration of mercury within these experimental runs.

4.4.2. Final Results

Two different experiments were performed with the mass spectrometer. The first experiment involved the reaction between molecular chlorine and elemental mercury in the gas phase at ambient conditions. The second experiment involved the reaction between hydrogen chloride and elemental mercury also in the gas phase at ambient conditions. During these experiments, the room temperature was 305 degrees Kelvin, which is considerably higher than typical ambient conditions, and could possibly make a difference when comparing the experimental results with those obtained from theory. The reactor used in the experiments was a laminar flow reactor that is being modeled as an axially dispersed plug-flow model. In both cases, the flow rate of the chlorine/nitrogen stream was approximately 10 liters per minute at a concentration of 325 ppm chlorine with the balance being nitrogen. The flow rate of the mercury/nitrogen stream was approximately 2 liters per minute with a concentration of 5 ppm of mercury with the balance being nitrogen. Again, the flow rates were the same for both sets of reactions. It is important to note that since the flow rate of the mercury/nitrogen stream is one-fifth that of the chlorine/nitrogen stream, the mercury concentration is reduced further to 1 ppm. In addition, both an uncoated reactor and a coated reactor were examined in order to test the reactivity of the Pyrex for heterogeneous mercury-chlorine species. It is also important to note that spectra of the oxidized mercury species are not shown in these results. Due to the backstreaming of the oil and the oil contamination built-up on the mass spectrometry housing, blank runs with nitrogen had to be subtracted

from each of the experimental reaction runs. The intensity units have an order of magnitude between 10^6 and 10^7 , so that the difference between the oil background peaks from the reaction run peaks is difficult to see visually. Instead of providing these spectra, tables of the raw data were created and these detailed quantitative results are available in Appendix H.

Table 4-9 lists the mercury speciation measurements using direct sampling via the quadrupole mass spectrometer.

Table 4-9. Mercury Speciation of Hg + Cl₂ For the Uncoated Reactor

	$\tau = 2.2$ seconds	$\tau = 4.2$ seconds
Hg ⁺	negligible	negligible
HgCl ⁺	82%	36%
HgCl ₂ ⁺	negligible	10%
Hg ₂ Cl ₂ ⁺	18%	54%

The most obvious conclusion from these preliminary experiments is that 100% of mercury oxidation was achieved in under 2.2 seconds. In fact, this experimental observation agrees with other mercury speciation measurements. (Lee et al., 1998) Lee et al. also obtained 100% mercury oxidation at 40 degrees Celsius with a mercury concentration of .04 ppm of mercury and 50 ppm of Cl₂. This corresponds to a Cl₂ to Hg⁰ ratio of 1250, where the ratio of the current work is 325. Hall et al., on the other hand, obtained only 70% mercury oxidation, but both the mercury and chlorine concentrations were much lower than the current work and the research of Lee et al. More specifically, .12 ppm of mercury and only up to 10 ppm of Cl₂, were used in an experiment performed

at 20 degrees Celsius. (Hall et al., 1991) This corresponds to a Cl_2 to Hg^0 ratio of only 83.

At a residence time of 4.2 seconds, the major product formed, at 54%, was Hg_2Cl_2 , which is known as calomel or mercurous chloride. The second major product formed was HgCl , at 36%. At a residence time of 2.2 seconds, the major product containing mercury was HgCl at 82% and Hg_2Cl_2 at 18%. From Figure 4-12, it is clear that HgCl is not a kinetically favored product for this reaction and that this reaction proceeds very slowly at 305 K, with a rate constant of $8.57 \times 10^{-4} \text{ cm}^3/\text{mol} \cdot \text{s}$. However, the reaction is thermodynamically favorable at room temperature with an equilibrium constant of 4.61×10^{13} . This implies that the reaction pathway to form HgCl is feasible as long as the concentration of Cl_2 is high. Since the concentration for chlorine is 325 ppm, it seems that this pathway is thermodynamically favored at low temperatures, but kinetically limited. It is also possible that this product is formed through fragmentation within the mass spectrometer. The fragments could come from both HgCl_2 and Hg_2Cl_2 product species. Recall from Table 4-6, that the dissociation energies of many of the mercury chlorine species are on the order of 4 electron volts or less. Since the filament of the mass spectrometer is applying 70 electron volts to the sample, it is most likely that the fragments such as HgCl^+ and Cl^+ are not products of the reaction, but are products of the fragmentation of HgCl_2 and Hg_2Cl_2 . When Hg_2Cl_2 decomposes or dissociates, it breaks down into Hg and HgCl , further accounting for the high percentage of HgCl observed. Other research suggests that oxidation via Cl_2 cannot occur at ambient conditions in a

strictly homogeneous fashion, but rather occurs heterogeneously with the Pyrex surface acting as a catalyst. (Hall et al., 1991; Medhekar et al., 1979; Ariya et al., 2002; Menke and Wallis, 1980; Skare and Johansson, 1992)

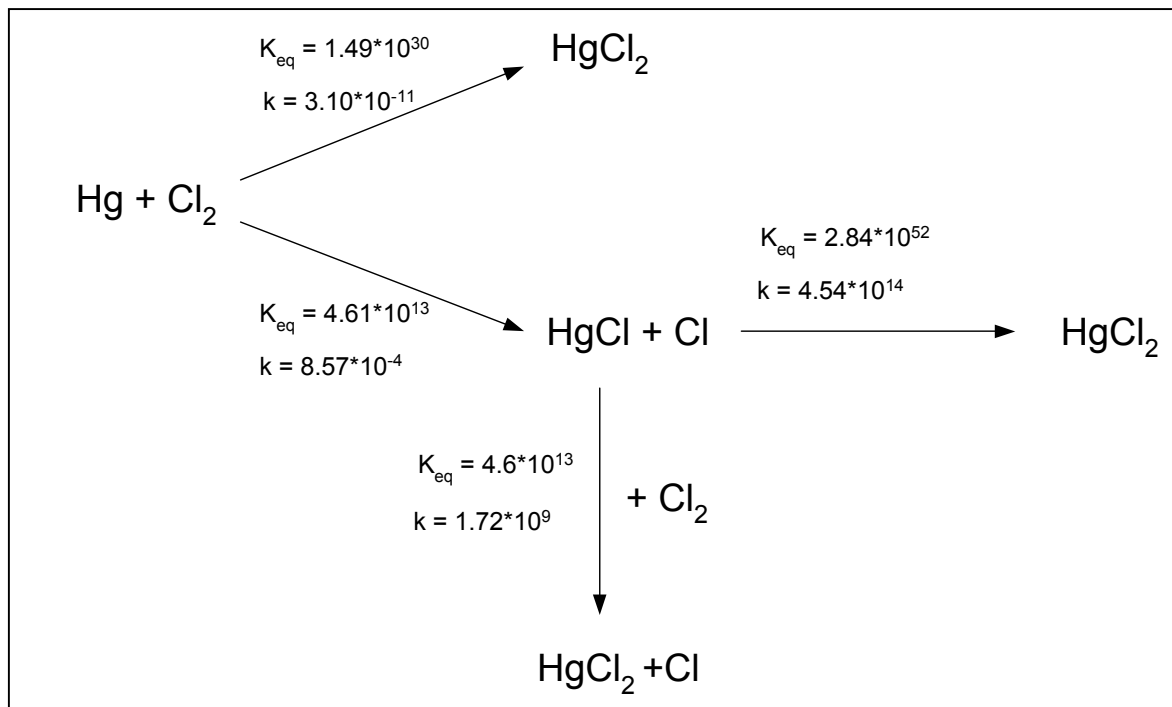
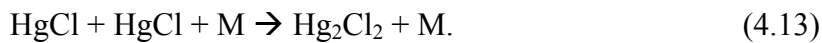


Figure 4-12. Possible Homogeneous Reaction Pathways, $\text{Hg} + \text{Cl}_2$
Note: k has units of $\text{cm}^3/\text{mol} \cdot \text{s}$ and $T = 305\text{K}$

At a residence time of 4.2 seconds, both HgCl_2 and Hg_2Cl_2 were detected in the mass spectrometer. This is consistent with other experimental observations found in the literature. (Hall et al., 1991; Horne et al., 1968; Schroeder et al., 1991; P'yankov, 1949) In all of these experiments, the presence of both HgCl_2 and Hg_2Cl_2 as product species was observed. Specifically, in the work of Horne et al. and P'yankov it was assumed that

the principal formation from the reaction of mercury with chlorine is mercurous mercury, Hg_2Cl_2 . Much of the current research, which involves the elucidation of determining the proper mechanism by which mercury is oxidized in the flue gases, has neglected this form of mercury since it is not stable in the flue gases under atmospheric conditions. (Galbreath and Zygarlicke, 1996) In fact, the decomposition temperature of Hg_2Cl_2 is 382 degrees Celsius and reactions occurring above this temperature would never see this form of mercurous chloride, but would instead see the decomposition products, Hg and HgCl . (Sliger et al., 1998) Much of the research from the literature, however, reports HgCl_2 to be the major product species above 400 degrees Celsius. This could be explained via HgCl readily scavenging chlorine atoms that become available from either homogeneous reactions involving other chemical species in the flue gases or through a reactive surface such as quartz or Pyrex. Since this mercurous form of mercury is presumed to be unimportant in the flue gases of coal combustion, theoretical rate constants were not predicted for this mercury compound in the current work. However, the major pathway of formation that has been predicted in the literature (Horne et al., 1968) is through the following association reaction,



This pathway of formation of mercurous chloride is in agreement with the current findings due to the high abundance of HgCl possibly being formed in the reactor.

In order to further examine the heterogeneous reactivity of the Pyrex, additional experiments have been performed with a coated reactor. In previous research where similar experiments were tested, the coated reactor proved to be successful in eliminating the surface side reactions. (Ariya et al., 2002) Ariya et al. examined reactions involving mercury with chlorine molecules and atoms and found a significant difference in the amount of oxidized product formed with the uncoated reactor. The coating they used was a Halocarbon wax coating. In order to eliminate the possibility of these surface reactions in the current work, the wax coating was purchased and applied to one of the lab reactors. The Halocarbon wax coating had to be mixed with acetone and then applied to the Pyrex reactor and be allowed to cure for a week. Unfortunately, the Halocarbon wax coating was not as successful as anticipated. The wax coating did not seem to decrease the amount of product formed. In fact, the mercury speciation with the coated reactor was nearly identical to the speciation observed with the uncoated reactor, as is demonstrated by the results shown in Table 4-10.

Table 4-10. Mercury Speciation of Hg + Cl₂ For the Coated Reactor

	$\tau = 4.2$ seconds
Hg ⁺	2%
HgCl ⁺	31%
HgCl ₂ ⁺	negligible
Hg ₂ Cl ₂ ⁺	67%

The results obtained from the coated reactor are suspect. If the results are to be trusted, this would imply that the oxidation of Hg⁰ via Cl₂ occurs homogeneously at 305 degrees

Celsius. This disagrees with the current theoretical predictions and other experimental research. (Ariya et al., 2002) Even if this reaction does take place homogeneously at ambient conditions, there should still be a more noticeable decrease in the amount of mercury oxidized than the current result of 2% as shown in Figure 4-12. It is presumed that the coating in this case has additionally acted as a reactive surface, which could explain the current results observed. In addition, it was found that the wax coating became severely contaminated with both Hg_2Cl_2 and HgCl components. This made further experiments within this work difficult to perform with this coated reactor.

Recall, the second reaction examined experimentally was the gas phase addition reaction of mercury with hydrogen chloride. Both the coated and uncoated reactors were vented overnight and flushed with nitrogen in an attempt to remove possible product residue from the previous reaction with molecular chloride. Figure 4-13 clearly exhibits the fact that the reaction of mercury and hydrogen chloride should not proceed at room temperature. The reaction is both kinetically and thermodynamically limited at ambient conditions. The uncoated reactor was tested at a residence time of 4.4 seconds and it was found that the only products detected were mercury, chlorine and hydrogen chloride. There were no appreciable oxidized mercury compounds, which validates the theoretical prediction that this reaction does not proceed at room temperature.

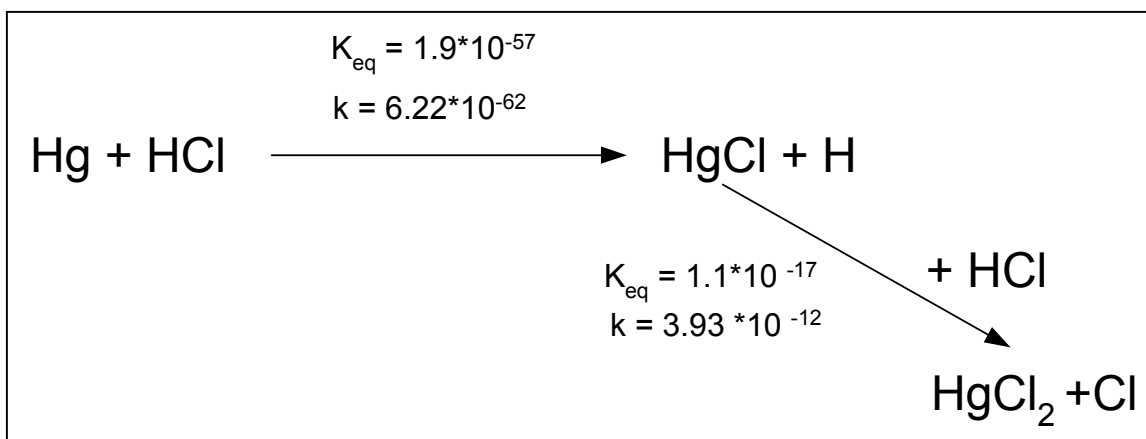


Figure 4-13. Possible Homogeneous Reaction Pathways, $Hg + HCl$

Note: k has units of $\text{cm}^3/\text{mol} \cdot \text{s}$ and $T = 305\text{K}$

In addition, the coated reactor was tested and oxidized mercury products were detected.

The mass spectrometer detected Cl_2 , HgCl and Hg_2Cl_2 . It appears that the halocarbon wax surface allows for with the build up of the product species from the first reaction and then subsequent release, or the wax is functioning as a catalyst. Since this reaction did not proceed in the uncoated reactor at room temperature, and Cl_2 was not even a participant in the current reaction, these results were taken lightly. In general, the coated reactor is not recommended for future mercury chlorine research due to the ability of the mercury components to impregnate the wax to contaminate the reaction environment. It may also be that the Halocarbon wax coating was not given ample time to cure. This is still in question, but for future work, only reactions involving the uncoated reactor will be considered.

4.5. Modeling Results

A very detailed thermodynamic and kinetic analysis was performed for the seven mercury oxidation reactions of focus. Based on this investigation, the oxidation of mercury is highly dependent upon both the concentration of the oxidizing species and temperature. Within this examination kinetic and thermodynamic limitations for the reactions are examined in detail. In essence, these theoretical predictions are the basis for Figures 4-12 and 4-13 in Chapter 4.4.2.

In addition, a global model was developed that not only takes into account more than just mercury and chlorine species, but also includes other complex reaction mechanisms involving hydrocarbons and NO_x mechanisms that may exist in the coal combustion flue gas environment. However, some of the theoretical rate constants that were used in this model have since been proven to be improbable due to being above the bimolecular collision limit for the particular reactions.

4.5.1. Thermodynamic and Kinetic Analysis

Due to the many questions that remain regarding the mechanisms by which mercury is oxidized in the flue gases of coal combustion, a small-scale “model” involving the results of rate constant calculations for the series of mercury oxidation reactions of interest will allow for the prediction of mercury speciation in a less complex environment. The best methodology to understanding the entire picture is to examine each complexity in isolation, one at a time. Examining the rate constants for mercury reactions involving solely chlorine species will allow for the understanding of chlorine’s role in the mercury oxidation process. As mentioned previously in the background section, there is some controversy involving the speciation of mercury at low temperatures.

The experimental results of the current work is in agreement with the experimental results of Hall et al. and conclude that mercury reacts readily with Cl_2 at room temperature. However, it is important to note that the amount of mercury oxidized is dependent upon the reaction vessel. As was exhibited in the final experimental results, the Pyrex surface is highly reactive to mercury-chlorine species and it has been concluded from this experimental work that the oxidation of mercury via Cl_2 at ambient conditions must occur, to a certain extent, heterogeneously. Results of Mamani-Paco et al. are very different and claim that, at low temperatures, mercury oxidation via Cl_2 is not favored. However, the reactor materials of construction are not addressed in their work. A study was performed by Medhekar et al. determining that mercury-chlorine species are

reactive on the surfaces of Inconel, quartz, stainless steel and Teflon-coated stainless steel.

In addition, there has been a great deal of mercury speciation research involving mercury with the addition of HCl. Again, at approximately 500 degrees Celsius, Hall et al. obtain high levels of mercury oxidation. On the other hand, work by Sliger et al. and Mamani-Paco et al. indicate that the mercury oxidation via HCl is not favored even at elevated temperatures. The current experimental research concludes that mercury does not react with hydrogen chloride at room temperature.

Examination of the possible reaction mechanisms that result in the combination of mercury with each of the chlorine species will allow for the elucidation of the speciation of mercury that may exist in the coal combustion flue gases. Table 4-13 lists both the theoretically predicted rate constant and the experimentally derived equilibrium constants for a series of mercury oxidation reactions that may take place in the flue gases. The collision number is defined as the number of bimolecular collisions per unit time per unit volume. (Moore and Pearson, 1981) In general, the collision number can be used as the upper limit for the rate. The collision limit for hard spheres is given by,

$$k_{coll} = (\pi d_{AB}^2) \left(\frac{8kT}{\pi \mu} \right)^{\frac{1}{2}} \quad (4.14)$$

such that d_{AB} is the diameter of the combined species A and B, k is Boltzmann's constant, T is temperature in degrees Kelvin, and μ is the reduced mass of species A and B. Table

4-11 lists the hard sphere collision model parameters and predictions for different bimolecular reactant combinations and Table 4-12 lists the collision model expressions as a function of temperature.

Table 4-11. Hard Sphere Collision Model Predictions

	mass	d_{ab}		Reduced Mass	$\langle v \rangle$	k_{coll}	k_{coll}
	(g/mol)	(m)		(g/mol)	(m/s)	(cm ³ /mol*s)	(M*s) ⁻¹
HgCl	236.04	5.27*10 ⁻¹⁰					
Cl ₂	70.9	3.97*10 ⁻¹⁰	HgCl + Cl ₂	54.5	340.1949	5.49*10 ¹⁴	5.49*10 ¹¹
HgCl ₂	271.49	10.04*10 ⁻¹⁰	Hg + Cl ₂	52.38	347.0111	1.98*10 ¹⁴	1.98*10 ¹¹
Cl	35.45	1.98*10 ⁻¹⁰	Hg + Cl	30.13	457.5373	1.06*10 ¹⁴	1.06*10 ¹¹
Hg	200.59	1.52*10 ⁻⁹	HgCl + Cl	30.82	452.3866	4.50*10 ¹⁴	4.50*10 ¹¹

Table 4-12. Hard Sphere Collision Model Rate Expressions

	k_{coll} (cm ³ /mol*s)	k_{coll} (M*s) ⁻¹
HgCl + Cl ₂	3.18*10 ¹³ * T ^{1/2}	3.18*10 ¹⁰ * T ^{1/2}
Hg + Cl ₂	1.15*10 ¹³ * T ^{1/2}	1.15*10 ¹⁰ * T ^{1/2}
Hg + Cl	6.14*10 ¹² * T ^{1/2}	6.14*10 ⁹ * T ^{1/2}
HgCl + Cl	2.60*10 ¹³ * T ^{1/2}	2.60*10 ¹⁰ * T ^{1/2}

Examining Table 4-13, one will notice that reactions (4.1) and (4.7) both have negative activation energies. A negative activation energy seems counterintuitive, implying that the reaction decreases with increasing temperature. This is also known as a negative temperature dependence and is quite common given these association reactions. These

reactions do not follow the familiar Arrhenius form. A more accurate expression would include a T^{-n} term in the rate expression. The details of this negative temperature dependence are omitted here, but can be found elsewhere. (Wayne, 1993)

Many conclusions can be drawn from Table 4-13. The focus of the conclusions, which are discussed in detail in chapter 5, will be based upon a prediction of a reaction pathway in which mercury is oxidized by chlorine species that may be present in the flue gases of coal combustion.

Table 4-13. Comparison of Rate and Equilibrium Constants at Various Temperatures

Reaction	Temperature (K)	Rate Constant (M⁻¹s⁻¹)	Equilibrium Constant	Activation Energy (kcal/mol)	Basis Set/Method
(4.1) $\text{Hg} + \text{Cl} + \text{M} \rightarrow \text{HgCl} + \text{M}$	298	1.57×10^{12}	1.2×10^{14}	-9.138	1992/QCISD
	600	1.74×10^9	6.7×10^4		
	1000	9.53×10^7	1.2×10^1		
	1200	2.76×10^6	8.3×10^{-2}		
(4.2) $\text{Hg} + \text{Cl}_2 \rightarrow \text{HgCl} + \text{Cl}$	298	3.68×10^{-7}	1.21×10^{-1}	88.95	1997/B3LYP
	600	4.11×10^1	7.38×10^2		
	1000	6.17×10^4	5.00×10^{-4}		
	1200	3.84×10^5	1.43×10^{-5}		
(4.3) $\text{Hg} + \text{HCl} \rightarrow \text{HgCl} + \text{H}$	298	6.22×10^{-65}	1.9×10^{-57}	98.29	1992/QCISD
	600	1.20×10^{-28}	1.1×10^{-28}		
	1000	2.52×10^{-14}	2.7×10^{-17}		
	1200	9.59×10^{-11}	2.0×10^{-14}		
(4.4) $\text{Hg} + \text{Cl}_2 + \text{M} \rightarrow \text{HgCl}_2 + \text{M}$	298	2.26×10^{-16}	9.7×10^{30}	34.46	1997/B3LYP
	600	8.32×10^{-2}	5.2×10^{12}		
	1000	5.11×10^4	3.5×10^5		
	1200	1.50×10^6	5.9×10^3		

Reaction	Temperature (K)	Rate Constant (M⁻¹s⁻¹)	Equilibrium Constant	Activation Energy (kcal/mol)	Basis Set/Method
(4.5) HgCl + HCl → HgCl ₂ + H	298	3.93*10 ⁻¹⁵	1.1*10 ⁻¹⁷	31.22	1992/QCISD
	600	1.32*10 ⁻³	3.3*10 ⁻¹⁰		
	1000	4.67*10 ¹	4.2*10 ⁻⁷		
	1200	6.40*10 ²	2.6*10 ⁻⁶		
(4.6) HgCl + Cl ₂ → HgCl ₂ + Cl	298	1.48*10 ⁶	1.21*10 ¹⁴	4.01	1997/B3LYP
	600	4.47*10 ⁷	7.47*10 ¹		
	1000	1.71*10 ⁸	4.04*10 ⁻⁶		
	1200	2.40*10 ⁸	4.16*10 ⁻⁸		
(4.7) HgCl + Cl + M → HgCl ₂ + M	298	2.02*10 ¹⁴	7.04*10 ⁵³	-1.28	1997/B3LYP
	600	8.04*10 ⁹	2.19*10 ²²		
	1000	3.17*10 ⁴	1.73*10 ⁶		
	1200	1.11*10 ³	1.29*10 ²		

4.5.2. Global model

The global model developed in this work is based upon theoretical predictions of activation energies and rate constants as listed below in Table 4-14. The parameters listed below correspond to the following Arrhenius expression:

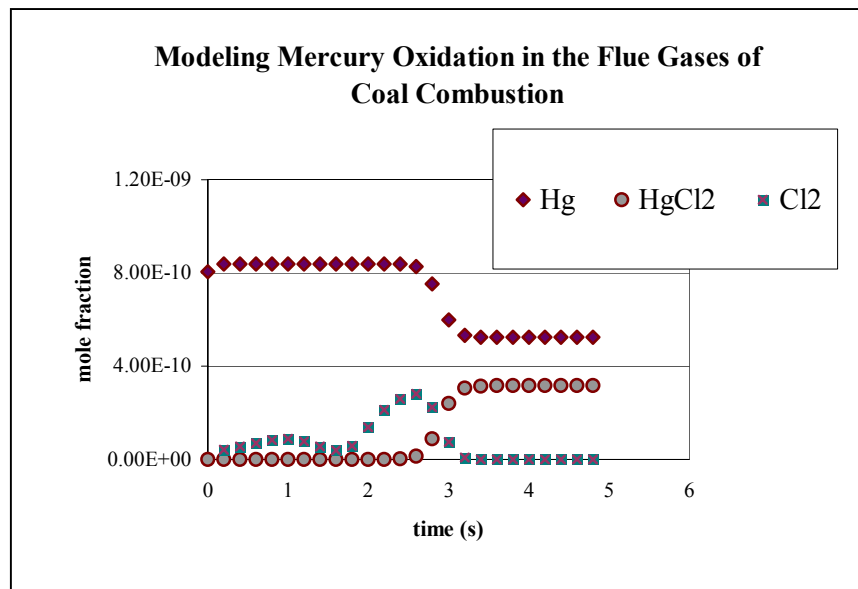
$$k = A \exp[-E_a/RT] \quad (4.15)$$

such that E_a is the activation energy, T is the temperature and A is the preexponential factor. The model is valid in the range of 298 to 2000 K. The reactions for the rest of the model were essentially taken from an existing combustion model. However, the original combustion model did not have any information about mercury oxidation reactions.

In essence, this model is a prediction of how mercury speciates in the chaotic flue gas environment and involves many complicated hydrocarbon, nitrogen and chlorine side reactions. The theoretically derived kinetic parameters from this work, which are based upon high-level quantum mechanical calculations, served as the foundation of the mercury speciation model predictions.

Table 4-14. Theoretical Combustion Model parameters

	Reaction	Basis Set/Method	A (cm³/mol s)	E_a (kcal/mol)
1	$\text{HgCl} + \text{M} \rightarrow \text{Hg} + \text{Cl} + \text{M}$	1992/QCISD	4.25E+13	16.13
2	$\text{HgCl}_2 + \text{M} \rightarrow \text{Hg} + \text{Cl}_2 + \text{M}$	1997/B3LYP	4.04E+21	44.76
3	$\text{Hg} + \text{Cl}_2 \rightarrow \text{HgCl} + \text{Cl}$	1992/QCISD	1.394E+26	27.76
4	$\text{Hg} + \text{HCl} \rightarrow \text{HgCl} + \text{H}$	1997/QCISD	1.394E+26	87.52
5	$\text{HgCl} + \text{HCl} \rightarrow \text{HgCl}_2 + \text{H}$	1992/QCISD	4.5E+13	30.27

**Figure 4-14. Graphical Results of the Large-Scale Modeling of Mercury**

The conclusions of this preliminary model predict that HgCl_2 is the dominant form of oxidized mercury in the flue gases of coal combustion. HgO was examined using a preexponential factor and rate constant obtained from Hall et al. (Hall, 1995), but its mole fraction remained constant throughout the process implying that it was not participating as an oxidized product species. In addition, the model predicted that Cl and Cl_2 are the major oxidizing agents of Hg^0 . HCl was considered, but its mole fraction remained nearly constant throughout the process, implying that it did not take part greatly in mercury's oxidation. From Figure 4-14 it is clear that the predictions mentioned in the background of this work are in general agreement with this preliminary model. The major pathways of mercury's oxidation involve both Cl_2 and Cl radical.

It is important to note that this model and Figure 4-14 was preliminary and some of the rate constant approximations listed in Table 4-14 have changed slightly. In general, these global model results agree with the results of the current models available in the literature. (Widmer et al., 2000; Senior et al., 2000; Niksa et al., 2002) Due to the unrealistic nature of the high frequency factors of equations (3) and (4) in Table 4-14, the global model agreement implies that these reactions may not play a key role in the mercury oxidation process. Table 4-15 is a list of the updated theoretically calculated rate constants.

Table 4-15. Complete List of Theoretical Combustion Model parameters

	A	units on A	Ea (kcal/mol)	beta c	Method/Basis set
(1) HgCl + M ---> Hg + Cl + M	4.25×10^{10}	$(M^*s)^{-1}$	17.06	0.2	QCISD/1992
(2) HgCl ₂ + M --> Hg + Cl ₂ + M	4.05×10^{18}	$(M^*s)^{-1}$	88.95	0.1	B3LYP/1997
(3) Hg + HCl --> HgCl + H	7.66×10^7	$(M^*s)^{-1}$	98.3		QCISD/1992
(4) Hg + Cl ₂ --> HgCl + Cl	3.59×10^9	$(M^*s)^{-1}$	21.81		QCISD/1997
(5) HgCl ₂ + M --> HgCl + Cl + M	2.04×10^{14}	$(M^*s)^{-1}$	73.42	0.1	B3LYP/1997
(6) HgCl + HCl --> HgCl ₂ + H	3.11×10^8	$(M^*s)^{-1}$	31.22		QCISD/1992
(7) HgCl + Cl ₂ --> HgCl ₂ + Cl	1.29×10^9	$(M^*s)^{-1}$	4.01		B3LYP/1997
(8) Cl ₂ + M --> Cl + Cl + M	1.203×10^{11}	$(M^*s)^{-1}$	20.03	0.1	QCISD/6-311++(3df,3pd)

The rates for the mercury oxidation reactions can be extracted from Table 4-15 at a given temperature through the Arrhenius expression (4.15). One interesting point to note is the unrealistic nature of the preliminary rate constants for reactions (3) and (4) of Table 4-14. Although these values are clearly above the collision limit, the global model still managed to produce realistic results of mercury speciation in the flue gas environment. This suggests that reactions (3) and (4) may not play key roles in the mercury oxidation process. More specifically, the direct oxidation of Hg⁰ via HCl and Cl₂ may not occur homogeneously in flue gases. However, as suggested from the experimental results in this work, the oxidation of mercury via Cl₂ can take place heterogeneously, which is not taken into consideration in the global model. In reality, fly ash exists in the flue gas environment, and much research has been done on the catalytic effect of the fly ash with

respect to mercury oxidation. (Lee et al., 1998; Bool L.E. et al, 1995; Gullett B.K. et al., 1990; Niksa et al., 2002; Miller et al., 1998; Norton et al., 2000)

CHAPTER 5. CONCLUSIONS

The purpose of the thermodynamic and kinetic data presented previously in Table 4-13 is to predict the speciation of mercury amongst HCl and Cl₂ in an attempt to elucidate the mechanism by which mercury is oxidized. This prediction will answer the question of whether mercury can be oxidized by one, both or neither of these species at ambient conditions.

Recall that the flue gases from coal combustion processes tend to contain higher concentrations of HCl than Cl₂. (Hall et al., 1991) For this reason, possible oxidation of mercury via hydrogen chloride will be considered first. From the data in Table 4-13, from both a thermodynamic and kinetic viewpoint, it would be impossible for mercury's first stage of oxidation to take place via HCl. From reaction (4.5) in Table 4-13, mercury's second stage of oxidation via HCl to the water-soluble form, HgCl₂ is neither thermodynamically nor kinetically favorable at low temperatures. However, at very high HCl concentrations and at temperatures above 1000 degrees Kelvin, this second stage of oxidation is possible. In general, the elemental form of mercury is dominant at high temperatures such as those present during the combustion process, and the oxidized forms of mercury are dominant at the lower temperatures such as those of the flue gases during the post combustion processes. The flue gases are cooled prior to entering the pollution control devices so that both stages of mercury's oxidation play key roles within

the possible oxidation mechanism. Since this reaction (4.5) is only favorable at high temperatures, it will not be considered as a dominant reaction in the present mechanism prediction for mercury's oxidation. However, due to the high concentration of HCl in the flue gases of coal combustion, its participation should not be neglected completely. Recall the work of Sliger et al. where it was proposed that chlorine atoms were formed via the following bimolecular reaction,



A theoretical rate expression calculated from transition state theory (Steckler et al., 1997) is given by,

$$k(\text{cm}^3 / \text{molecule} * \text{s}) = 2.36 * 10^{-13} \left(\frac{T}{298K} \right)^{1.66} e^{\frac{-2777(J/mole)}{RT}} \quad (5.2)$$

from 138 to 1060 K. The question is whether reaction (5.1) is favored as the flue gases are quenched. Recalling from Table 2-4, reaction (5.1) is thermodynamically favored from 298 to 1200 degrees Kelvin. This reaction is also kinetically favored from 298 to 1200 degrees Kelvin. Using equation (5.2), the reaction rate at 298K is $4.35 * 10^{11}$ $\text{cm}^3/\text{mol*s}$ and is $1.89 * 10^{12}$ $\text{cm}^3/\text{mol*s}$ at 1200K. Since HCl is present in the flue gases at much higher temperatures than Cl_2 it is likely that the reaction which produces chlorine atoms involves HCl.

However, there are other reactions which may result in the formation of chlorine atoms that should also be considered. Chlorine atoms can be produced from the decomposition

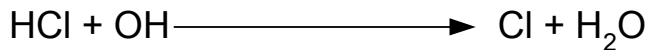
reactions of HgCl and Cl₂. With a quick glance back at Table 2-4, one can easily see that the formation of chlorine atoms via the decomposition of Cl₂ is not thermodynamically favored up to 1200K. In addition, the decomposition of Cl₂ at ambient conditions occurs slowly with a rate constant of 0.245 cm³/mol*s as predicted from the theoretical expressions in Table 4-15. At higher temperatures, on the other hand, this decomposition is not as kinetically limited, with a rate constant of 2.11*10⁵ cm³/mol*s at 500 K. Therefore, depending on the final temperatures the flue gases are cooled to, this pathway of chlorine atom formation may be important.

The decomposition of HgCl to form chlorine atoms should also be considered. At 298 K, this decomposition reaction is both thermodynamically and kinetically limited, with a equilibrium constant of 8.25*10⁻¹⁵ and a corresponding rate constant of 13.05 cm³/mol*s. At a higher temperature of 500 K, the reaction is not as slow and proceeds with a rate constant of 1.4*10⁶ cm³/mol*s. However, even at high temperatures, this reaction is thermodynamically limited with an equilibrium constant of 2.16*10⁻⁷ at 500 K.

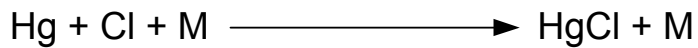
When comparing these three distinct pathways for the formation of chlorine atoms, it appears that reaction (5.1) is the most kinetically and thermodynamically favorable in the temperature range of which the flue gases are quenched. Therefore, as quenching takes place, the most likely pathway of producing chlorine radicals is via HCl with the addition of OH. It appears at this point that the formation of chlorine atoms plays an important role in the mercury oxidation process.

Further examination of Table 4-13 is required to determine if Cl_2 or Cl atoms plays the major role in the oxidation of mercury. Reaction (4.2) is neither thermodynamically nor kinetically favorable from 298 to 1200K and will not be considered further. Reaction (4.6) is thermodynamically favorable at low temperatures and also thermodynamically favorable at temperatures above 600K, given high concentrations of Cl_2 . Due to the low concentration of Cl_2 in the flue gas relative to the HCl concentrations, this reaction may be a secondary pathway, but certainly not a dominating one for mercury's oxidation. Given these arguments, a possible mechanism for mercury's oxidation in the flue gases is proposed in Figure 5-1.

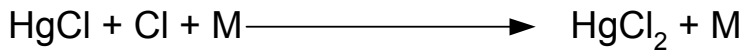
Major pathway for the production of Cl atoms:



Major pathway for the 1st stage of mercury oxidation:



Major pathway for the 2nd stage of mercury oxidation:



Possible competing pathway for the 2nd stage of mercury oxidation:

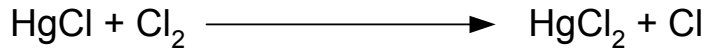


Figure 5-1. Proposed Mercury Oxidation Model via Chlorine Species

In total, a mechanism by which mercury oxidation takes place in the flue gases is proposed. Consideration should be taken into the initial step of the mechanism involving the formation of chlorine atoms. Much work has been done, as previously addressed, on the heterogeneous oxidation of mercury involving fly ash particles in the flue gas environment. (Lee et al., 1998; Bool L.E. et al, 1995; Gullett B.K. et al., 1990) Due to the high concentration of HCl in the flue gases, relative to that of Cl₂, another possible pathway of creating chlorine atoms could involve the heterogeneous reaction, in which HCl reacts with the fly ash to create chlorine atoms, which are then scavenged to create both the mercurous (HgCl) and mercuric (HgCl₂) forms of oxidized mercury. This heterogeneous pathway should be examined both theoretically and experimentally in future work involving mercury speciation measurements.

CHAPTER 6. FUTURE WORK

6.1. On the Theoretical Front

A unique aspect of the current theoretical research is that it is the first time such an in-depth quantum mechanically based kinetic analysis has been performed on mercury oxidation reactions involving chlorine-containing species. When considering future theoretical work involving these mercury oxidation reaction, the following question arises, "How can the accuracy of these current quantum mechanical theoretical calculations be improved?" The use of a more complex quantum mechanical method for solving the approximate Schrödinger's Wave Equation (SWE) can sometimes increase the accuracy of the energetics calculations. Due to the computational expense of the QCISD method it was not used for all of the calculations in this work. The validity of the B3LYP calculational method used with these mercury oxidation reactions should be pursued further. The QCISD calculational method should be used in addition to B3LYP to test the reproducibility of the theoretical energy predictions.

In addition to using the higher-level method, another way to increase the accuracy of the energetics calculations is to include spin-orbit interactions in the Hamiltonian operator. Recall that spin-orbit effects become increasingly important as the atomic number of the species of interest increases. With mercury having 80 electrons, the inclusion of spin-orbit coupling may improve the heats of reaction predictions and also the activation energy predictions. This direction involving the study of spin-orbit coupling can also be

applied to the potential nonadiabatic nature of the following two reactions studied within this work.



When studying these reactions in this work, the probability of surface hopping was neglected and the potential energy surface generated in each case existed on the lowest lying singlet surface. Future work could involve the study of the potential energy surfaces of excited states and also the interaction energies of the various calculated surfaces.

Aside from improving the theoretical energetics predictions, another direction of future research is to consider species other than chlorine to simulate a more realistic flue gas environment. Consideration of the inhibitory or promoting effects of SO_x and NO_x species on mercury oxidation would allow for a more complete global combustion model involving mercury speciation. Much experimental work has been performed with simulated flue gases involving these chemical species, and the theoretical study would allow for a direct comparison.

Recall from the experimental results of the current work that the product species, calomel (Hg_2Cl_2), plays a major role in the mercury speciation outcome at temperatures less than about 500 degrees Celsius. A theoretical study on the possible dissociation and formation

pathways of this oxidized form would help in understanding how mercury speciates among chlorine species at lower temperatures that exist after the flue gases are quenched. The current experimental results also indicate that heterogeneous reactions are involved in the oxidation of elemental mercury via molecular chlorine. Although ab initio techniques are still in their beginning stages for predicting energetics involving surface catalyzed reactions, this discussion of “future work” would not be complete without mentioning the prospect of pursuing this avenue of research. Although it appears that there is much theoretical research still to be performed on elucidating the mercury oxidation process in the flue gases of coal combustion, the current research has made substantial advances in narrowing the focus of this study.

6.2. On the Experimental Front

It is important to note that the current experimental work is preliminary and the results have been qualitative. Future work will be quantitative, and complement the preliminary qualitative experimental results reported here. A major aspect of the experimental approach that has been described has been the design and construction of the experimental apparatus used in this research. Specifically, there are some improvements that should be made in the near future in order to further increase the accuracy of the experimental device. Due to the oil contamination of the vacuum chamber, the mass spectrometer housing should be sent to ABB/Extrel for ultrasonic cleaning. This will reduce the background oil peaks that currently exist in the spectra. Reducing these background peaks will allow for an increase in sensitivity of the device and, in turn, lead to more accurate measurements.

In addition, recall that a laminar flow reactor is being used and is modeled by axial dispersed plug flow. However, with the current dimensions of the reactor, the calculated Peclet number is not ideal for the plug flow assumption. To assume the reactor to be plug flow, the Peclet number must tend to infinity. The Peclet number calculated in this work is 0.576, which results in an approximation closer to a continuously stirred tank reactor. This implies that the dispersion effects for the current reactor should not be neglected and, in fact, there will exist some substantial dispersion. The Peclet number is inversely proportional to the dispersion coefficient and the dispersion coefficient is directly

proportional to the square of the reactor radius. Hence, if the radius of the reactor was reduced from 2.54 cm to 1.27 cm, this would increase the Peclet number by a factor of 4, which would be more suitable for the plug flow approximation. Therefore, for future research, the reactor diameter should be reduced by at least a factor of one-half.

It is important to emphasize that this experimental work was exploratory only, since the main contributions from the research were on the theoretical side. Recall, from the experimental results that within 2.2 seconds, 100% mercury oxidation was achieved. Examining the speciation of mercury with reduced chlorine concentrations would help to validate this result. To these ends, a useful study that would ensure the accuracy of the instrument would be to obtain a plot of the mercury speciation versus chlorine concentration and compare these experimental findings to similar studies available in the literature. Also, recalling that surface reactions became important for the reactions involving elemental mercury and molecular chlorine, one could change the surface area inside the reactor and observe how the rate of mercury oxidation changes with a change in surface area to account for heterogeneous reactions. This would allow for the calculation of branching ratios, enabling one to compare relative rates of heterogeneous versus homogeneous reactions. In addition, future work should include a focused study on homogeneous mercury oxidation reactions, which take into account the prior knowledge of heterogeneous reactions.

From the conclusions of this work that the predicted oxidation mechanism was highly dependent upon reactions involving chlorine radicals, future work should involve the study of elemental mercury reacting with chlorine radicals. There has been previous research performed that describes methods of creating chlorine radicals. (Horne et al., 1968; Ariya et al., 2002) In particular, Horne et al., create chlorine radicals through photolysis. The experimental study of mercury speciation via chlorine atoms will help to elucidate the mechanism of mercury oxidation further since this is a major component in the pathway of oxidation.

In future work these experiments need to take place at higher temperatures in order to simulate a more realistic flue gas environment. There has been much research on the study of NO_x , SO_2 , CO_2 , H_2O , and fly ash effects on the oxidation of mercury since all of these species can also exist in realistic flue gases. These species can act as inhibitors or promoters of mercury oxidation, and an accurate pathway would not be complete without the consideration of these effects. In previous studies, difference techniques were used to measure the mercury speciation. It would be interesting to see how the results of the previous measurements compare to results from direct mercury speciation measurements at similar conditions. Just as was the case with the discussion on future theoretical work, there are also many directions of further experimental work to pursue. In total, the experimental aspect of this research was successful in creating an apparatus that can directly measure the speciation of mercury in a simulated flue gas environment.

APPENDIX A. BASIS SETS

A.1. Mercury: Stuttgart, Stevens and Krauss, LANL2DZ, and SDD

Hg Basis Set Including Relativistic Pseudopotential Stuttgart RSC 1997 ECP

HG 0
S 3 1.00
20.4111810 -0.449360000E-01
8.00219000 1.30917600
6.06154600 -1.84510200
S 1 1.00
1.14870700 1.00000000
S 1 1.00
0.537926000 1.00000000
S 1 1.00
0.120312000 1.00000000
S 1 1.00
0.435100000E-01 1.00000000
S 1 1.00
0.150000000E-01 1.00000000
P 2 1.00
9.28385800 0.188894000
6.52194500 -0.425977000
P 2 1.00
1.68634500 0.502374000
0.879019000 0.515570000
P 1 1.00
0.393181000 1.00000000
P 1 1.00
0.112522000 1.00000000
P 1 1.00
0.375950000E-01 1.00000000
P 1 1.00
0.120000000E-01 1.00000000
D 4 1.00
5.01956200 -0.102136000
2.71380100 0.189480000
1.25783800 0.444149000
0.553544000 0.427615000
D 1 1.00
0.212165000 1.00000000
D 1 1.00
0.700000000E-01 1.00000000
D 1 1.00
0.200000000E-01 1.00000000

Effective Core Potentials		

HG 0		
HG-ECP 5 60		
H POTENTIAL		
1		
2	1.00000000	0.00000000
S-H POTENTIAL		
2		
2	12.98154900	274.53216900
2	6.49077400	49.18219200
P-H POTENTIAL		
2		
2	10.53809600	237.39577000
2	5.26904800	28.12158400
D-H POTENTIAL		
2		
2	8.10172100	114.25203400
2	4.05086000	18.49563800
F-H POTENTIAL		
1		
2	3.88579100	30.36499600
G-H POTENTIAL		
1		
2	6.24100000	-29.47311800

Hg Basis Set Including Relativistic Pseudopotential

Stevens and Krauss 1992

"SBKJC VDZ ECP"

HG 0		
SP 5 1.00		
25.5400000	-0.220410000E-01	-0.606800000E-02
8.45800000	0.309845000	0.630000000E-01
4.49300000	-1.08098400	-0.314502000
1.75100000	1.09360000	0.746398000
0.675300000	0.519202000	0.487253000
SP 1 1.00		
0.152000000	1.00000000	1.00000000
SP 1 1.00		
0.478000000E-01	1.00000000	1.00000000
SP 1 1.00		
1.58600000	1.00000000	1.00000000
D 3 1.00		
4.20400000	-0.558490000E-01	
1.87100000	0.478221000	
0.821500000	0.622006000	
D 1 1.00		
0.370000000	1.00000000	
D 1 1.00		
0.167400000	1.00000000	

Effective Core Potentials

HG 0		
HG-ECP 4 60		
g potential		
1		
1	4.85764000	-11.51618000
s-g potential		
3		
0	1.17357000	4.09547000
2	3.70966000	-310.08898000
2	4.18793000	394.68735000
p-g potential		
3		
0	0.95913000	3.61202000
2	2.99268000	-148.42850000
2	3.58353000	211.83161000
d-g potential		
2		
0	35.54665000	8.27074000
2	5.29318000	92.85678000
f-g potential		
1		
0	1.80978000	6.28302000

Hg Basis Set Including Relativistic Pseudopotential
LANL2DZ

```
S 2 1.00
 0.5275000000D+00 -0.1729258900D+01
 0.2334000000D+00  0.2127942000D+01
S 1 1.00
 0.6861000000D-01  0.1000000000D+01
P 2 1.00
 0.6503000000D+00 -0.1436715000D+00
 0.1368000000D+00  0.1064070300D+01
P 1 1.00
 0.4256000000D-01  0.1000000000D+01
D 2 1.00
 0.1484000000D+01  0.5630223000D+00
 0.5605000000D+00  0.5667893000D+00
D 1 1.00
 0.1923000000D+00  0.1000000000D+01
```

Hg Basis Set Including Relativistic Pseudopotential
SDD

S	3	1.00
	0.2684204900D+02	-0.2824770000D-01
	0.1032090900D+02	0.8202914000D+00
	0.6344923000D+01	-0.1740677000D+01
S	1	1.00
	0.1450305000D+01	0.1000000000D+01
S	1	1.00
	0.7082150000D+00	0.1000000000D+01
S	1	1.00
	0.1676060000D+00	0.1000000000D+01
S	1	1.00
	0.5906600000D-01	0.1000000000D+01
S	1	1.00
	0.2000000000D-01	0.1000000000D+01
P	2	1.00
	0.9772990000D+01	0.8855369000D+00
	0.7169095000D+01	-0.1836456400D+01
P	2	1.00
	0.1868009000D+01	0.4904267000D+00
	0.9733010000D+00	0.5415630000D+00
P	1	1.00
	0.4219970000D+00	0.1000000000D+01
P	1	1.00
	0.1252130000D+00	0.1000000000D+01
P	1	1.00
	0.4019000000D-01	0.1000000000D+01
D	4	1.00
	0.4911447000D+01	-0.1428567000D+00
	0.3049550000D+01	0.1988172000D+00
	0.1344501000D+01	0.4885401000D+00
	0.5766180000D+00	0.5143447000D+00
D	1	1.00
	0.2102450000D+00	0.1000000000D+01
D	1	1.00
	0.7000000000D-01	0.1000000000D+01

A.2. Chlorine: Pople, Dunning, LANL2DZ, and SDD

C1 Basis Set
Pople, 6-311++G(3pd,3df)

S	6	1.00
	0.1058190000D+06	0.7380000000D-03
	0.1587200000D+05	0.5718000000D-02
	0.3619650000D+04	0.2949500000D-01
	0.1030800000D+04	0.1172860000D+00
	0.3399080000D+03	0.3629490000D+00
	0.1245380000D+03	0.5841490000D+00
S	3	1.00
	0.1245380000D+03	0.1341770000D+00
	0.4951350000D+02	0.6242500000D+00
	0.2080560000D+02	0.2917560000D+00
S	1	1.00
	0.6583460000D+01	0.1000000000D+01
S	1	1.00
	0.2564680000D+01	0.1000000000D+01
S	1	1.00
	0.5597630000D+00	0.1000000000D+01
S	1	1.00
	0.1832730000D+00	0.1000000000D+01
P	5	1.00
	0.5897760000D+03	0.2391000000D-02
	0.1398490000D+03	0.1850400000D-01
	0.4514130000D+02	0.8137700000D-01
	0.1687330000D+02	0.2215520000D+00
	0.6741100000D+01	0.7725690000D+00
P	2	1.00
	0.6741100000D+01	-0.1572244000D+01
	0.2771520000D+01	0.9923890000D+00
P	1	1.00
	0.1023870000D+01	0.1000000000D+01
P	1	1.00
	0.3813680000D+00	0.1000000000D+01
P	1	1.00
	0.1094370000D+00	0.1000000000D+01
SP	1	1.00
	0.4830000000D-01	0.1000000000D+01
	0.1000000000D+01	
D	1	1.00
	0.3000000000D+01	0.1000000000D+01
D	1	1.00
	0.7500000000D+00	0.1000000000D+01
D	1	1.00
	0.1875000000D+00	0.1000000000D+01
F	1	1.00
	0.7000000000D+00	0.1000000000D+01

Cl Basis Set
Dunning, cc-PVTZ

S 11 1.00
0.4561000000D+06 0.4929936879D-04
0.6833000000D+05 0.3830247743D-03
0.1555000000D+05 0.2008517522D-02
0.4405000000D+04 0.8385490629D-02
0.1439000000D+04 0.2947030000D-01
0.5204000000D+03 0.8783398558D-01
0.2031000000D+03 0.2114886081D+00
0.8396000000D+02 0.3654367733D+00
0.3620000000D+02 0.3410832165D+00
0.1583000000D+02 0.1021137314D+00
0.6334000000D+01 0.2141475264D-02
S 11 1.00
0.4561000000D+06 0.3206141768D-06
0.6833000000D+05 0.2660724314D-05
0.1555000000D+05 0.1143104196D-04
0.4405000000D+04 0.4555161721D-04
0.5204000000D+03 -0.7534412750D-03
0.2031000000D+03 -0.7937035919D-02
0.8396000000D+02 -0.3700357367D-01
0.3620000000D+02 -0.1014582129D+00
0.1583000000D+02 0.9753640224D-02
0.6334000000D+01 0.5001875821D+00
0.2694000000D+01 0.5615467972D+00
S 11 1.00
0.4561000000D+06 0.3091797881D-08
0.6833000000D+05 -0.3253720654D-07
0.1555000000D+05 -0.1566444833D-07
0.4405000000D+04 -0.9878317834D-06
0.5204000000D+03 -0.1767777100D-04
0.2031000000D+03 0.6125948219D-05
0.3620000000D+02 0.1466855781D-02
0.1583000000D+02 0.4008479975D-03
0.6334000000D+01 -0.3899022244D-01
0.2694000000D+01 -0.2169385091D+00
0.4313000000D+00 0.7228638071D+00
S 1 1.00
0.9768000000D+00 0.1000000000D+01
S 1 1.00
0.1625000000D+00 0.1000000000D+01

P 6 1.00
0.6633000000D+03 0.2404632070D-02
0.1568000000D+03 0.1921615391D-01
0.4998000000D+02 0.8850970000D-01
0.1842000000D+02 0.2560087036D+00
0.7240000000D+01 0.4368283046D+00
0.2922000000D+01 0.3503581452D+00
P 6 1.00
0.6633000000D+03 0.1868888234D-04
0.1568000000D+03 0.1663909953D-03
0.1842000000D+02 -0.1388295249D-02
0.7240000000D+01 -0.1212937269D-01
0.2922000000D+01 0.2967377807D-02
0.3818000000D+00 0.5633880209D+00
P 1 1.00
0.1022000000D+01 0.1000000000D+01
P 1 1.00
0.1301000000D+00 0.1000000000D+01
D 1 1.00
0.1046000000D+01 0.1000000000D+01
D 1 1.00
0.3440000000D+00 0.1000000000D+01
F 1 1.00
0.7060000000D+00 0.1000000000D+01

C1 Basis Set
LANL2DZ

S 2 1.00
0.2231000000D+01 -0.4900589000D+00
0.4720000000D+00 0.1254268400D+01
S 1 1.00
0.1631000000D+00 0.1000000000D+01
P 2 1.00
0.6296000000D+01 -0.6356410000D-01
0.6333000000D+00 0.1014135500D+01
P 1 1.00
0.1819000000D+00 0.1000000000D+01

C1 Basis Set
SDD

S 5 1.00
0.4085000000D+05 0.2532000000D-02
0.6179000000D+04 0.1920700000D-01
0.1425000000D+04 0.9525700000D-01
0.4092000000D+03 0.3455890000D+00
0.1355000000D+03 0.6364010000D+00
S 3 1.00
0.1355000000D+03 0.1209560000D+00
0.5013000000D+02 0.6485110000D+00
0.2021000000D+02 0.2754870000D+00
S 1 1.00
0.6283000000D+01 0.1000000000D+01
S 1 1.00
0.2460000000D+01 0.1000000000D+01
S 1 1.00
0.5271000000D+00 0.1000000000D+01
S 1 1.00
0.1884000000D+00 0.1000000000D+01
P 4 1.00
0.2408000000D+03 0.1459500000D-01
0.5656000000D+02 0.9904700000D-01
0.1785000000D+02 0.3305620000D+00
0.6350000000D+01 0.6828740000D+00
P 2 1.00
0.6350000000D+01 -0.5617850000D+00
0.2403000000D+01 0.1351901000D+01
P 1 1.00
0.6410000000D+00 0.1000000000D+01
P 1 1.00
0.1838000000D+00 0.1000000000D+01

A.3. Hydrogen: Pople, Dunning, LANL2DZ, and SDD

H Basis Set

Pople, 6-311++G(3df,3pd)

S	3	1.00
	0.3386500000D+02	0.2549380000D-01
	0.5094790000D+01	0.1903730000D+00
	0.1158790000D+01	0.8521610000D+00
S	1	1.00
	0.3258400000D+00	0.1000000000D+01
S	1	1.00
	0.1027410000D+00	0.1000000000D+01
S	1	1.00
	0.3600000000D-01	0.1000000000D+01
P	1	1.00
	0.3000000000D+01	0.1000000000D+01
P	1	1.00
	0.7500000000D+00	0.1000000000D+01
P	1	1.00
	0.1875000000D+00	0.1000000000D+01
D	1	1.00
	0.1000000000D+01	0.1000000000D+01

H Basis Set

Dunning, cc-PVTZ

S	3	1.00
	0.3387000000D+02	0.6068000000D-02
	0.5095000000D+01	0.4530800000D-01
	0.1159000000D+01	0.2028220000D+00
S	1	1.00
	0.3258000000D+00	0.1000000000D+01
S	1	1.00
	0.1027000000D+00	0.1000000000D+01
P	1	1.00
	0.1407000000D+01	0.1000000000D+01
P	1	1.00
	0.3880000000D+00	0.1000000000D+01
D	1	1.00
	0.1057000000D+01	0.1000000000D+01

H Basis Set
LANL2DZ

```
S 3 1.00
0.1924060000D+02 0.3282800000D-01
0.2899200000D+01 0.2312080000D+00
0.6534000000D+00 0.8172380000D+00
S 1 1.00
0.1776000000D+00 0.1000000000D+01
```

H Basis Set
SDD

```
S 3 1.00
0.1924060000D+02 0.3282800000D-01
0.2899200000D+01 0.2312080000D+00
0.6534000000D+00 0.8172380000D+00
S 1 1.00
0.1776000000D+00 0.1000000000D+01
```

A.4. Oxygen: Pople, Dunning, LANL2DZ, and SDD

O Basis Set
 Pople, 6-311++G(3df,3pd)

S	6	1.00
	0.8588500000D+04	0.1895150000D-02
	0.1297230000D+04	0.1438590000D-01
	0.2992960000D+03	0.7073200000D-01
	0.8737710000D+02	0.2400010000D+00
	0.2567890000D+02	0.5947970000D+00
	0.3740040000D+01	0.2808020000D+00
SP	3	1.00
	0.4211750000D+02	0.1138890000D+00
	0.9628370000D+01	0.9208110000D+00
	0.2853320000D+01	-0.3274470000D-02
	0.8197020000D+00	
SP	1	1.00
	0.9056610000D+00	0.1000000000D+01
	0.1000000000D+01	0.1000000000D+01
SP	1	1.00
	0.2556110000D+00	0.1000000000D+01
	0.1000000000D+01	0.1000000000D+01
SP	1	1.00
	0.8450000000D-01	0.1000000000D+01
	0.1000000000D+01	0.1000000000D+01
D	1	1.00
	0.5168000000D+01	0.1000000000D+01
D	1	1.00
	0.1292000000D+01	0.1000000000D+01
D	1	1.00
	0.3230000000D+00	0.1000000000D+01
F	1	1.00
	0.1400000000D+01	0.1000000000D+01

O Basis Set
 Dunning, cc-PVTZ

S	7	1.00
	0.1533000000D+05	0.5080695061D-03
	0.2299000000D+04	0.3929462191D-02
	0.5224000000D+03	0.2024504538D-01
	0.1473000000D+03	0.7918100000D-01
	0.4755000000D+02	0.2306339643D+00
	0.1676000000D+02	0.4326564987D+00
	0.6207000000D+01	0.3490004302D+00
S	7	1.00
	0.1533000000D+05	0.5127202233D-05
	0.2299000000D+04	0.3409405034D-04
	0.5224000000D+03	0.1508798323D-03
	0.4755000000D+02	-0.3912244288D-02
	0.1676000000D+02	-0.3404320949D-01
	0.6207000000D+01	-0.9291371289D-01
	0.6882000000D+00	0.6014898165D+00
S	1	1.00
	0.1752000000D+01	0.1000000000D+01
S	1	1.00
	0.2384000000D+00	0.1000000000D+01
P	3	1.00
	0.3446000000D+02	0.1592800000D-01
	0.7749000000D+01	0.9974000000D-01
	0.2280000000D+01	0.3104920000D+00
P	1	1.00
	0.7156000000D+00	0.1000000000D+01
P	1	1.00
	0.2140000000D+00	0.1000000000D+01
D	1	1.00
	0.2314000000D+01	0.1000000000D+01
D	1	1.00
	0.6450000000D+00	0.1000000000D+01
F	1	1.00
	0.1428000000D+01	0.1000000000D+01

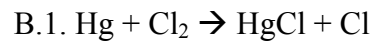
O Basis Set
LANL2DZ

S	7	1.00
0.7817000000D+04	0.1176000000D-02	
0.1176000000D+04	0.8968000000D-02	
0.2732000000D+03	0.4286800000D-01	
0.8117000000D+02	0.1439300000D+00	
0.2718000000D+02	0.3556300000D+00	
0.9532000000D+01	0.4612480000D+00	
0.3414000000D+01	0.1402060000D+00	
S	2	1.00
0.9532000000D+01	-0.1541530000D+00	
0.9398000000D+00	0.1056914000D+01	
S	1	1.00
0.2846000000D+00	0.1000000000D+01	
P	4	1.00
0.3518000000D+02	0.1958000000D-01	
0.7904000000D+01	0.1242000000D+00	
0.2305000000D+01	0.3947140000D+00	
0.7171000000D+00	0.6273760000D+00	
P	1	1.00
0.2137000000D+00	0.1000000000D+01	

O Basis Set
SDD

S	6	1.00
0.7816540000D+04	0.2031000000D-02	
0.1175820000D+04	0.1543600000D-01	
0.2731880000D+03	0.7377100000D-01	
0.8116960000D+02	0.2476060000D+00	
0.2718360000D+02	0.6118320000D+00	
0.3413600000D+01	0.2412050000D+00	
S	1	1.00
0.9532200000D+01	0.1000000000D+01	
S	1	1.00
0.9398000000D+00	0.1000000000D+01	
S	1	1.00
0.2846000000D+00	0.1000000000D+01	
P	4	1.00
0.3518320000D+02	0.1958000000D-01	
0.7904000000D+01	0.1241890000D+00	
0.2305100000D+01	0.3947270000D+00	
0.7171000000D+00	0.6273750000D+00	
P	1	1.00
0.2137000000D+00	0.1000000000D+01	

APPENDIX B. PES DATA



1997/QCISD

R Cl-Cl	R Cl-Hg	Singlet	Triplet	R Cl-Cl	R Cl-Hg	Singlet	Triplet
1.25	2.35	-613.2569	-613.092	2.25	2.5	-613.187	-613.09
1.25	2.4	-613.26454	-613.098	2.3	2.4	-613.183	-613.08
1.25	2.45	-613.27113	-613.103	2.3	2.45	-613.184	-613.09
1.25	2.5	-613.27681	-613.107	2.3	2.5	-613.184	-613.09
1.3	2.35	-613.25922	-613.101	2.3	2.4	-613.181	-613.08
1.3	2.4	-613.26668	-613.106	2.35	2.45	-613.181	-613.09
1.3	2.45	-613.2731	-613.111	2.35	2.5	-613.182	-613.09
1.3	2.5	-613.27862	-613.114	3	2.3	-613.165	-613.18
1.35	2.35	-613.25902	-613.108	3	2.4	-613.167	-613.18
1.35	2.5	-613.27787	-613.118	3	2.5	-613.166	-613.1
1.4	2.35	-613.25695	-613.114	3	2.7	-613.158	-613.12
1.4	2.4	-613.26399	-613.117	3.5	2.3	-613.162	-613.18
1.4	2.45	-613.27002	-613.12	3.5	2.4	-613.164	-613.18
1.4	2.5	-613.2752	-613.122	3.5	2.5	-613.162	-613.18
2	2.35	-613.19839	-613.163	3.5	2.7	-613.153	-613.12
2	2.4	-613.20184	-613.164	1	2.3	-613.158	-612.97
2	2.45	-613.20455	-613.164	1	2.4	-613.176	-612.99
2	2.5	-613.20666	-613.083	1	2.5	-613.19	-613.01
2.5	2.35	-613.17427	-613.179	1	2.7	-613.208	-613.03
2.5	2.4	-613.17552	-613.083	1.4	2.7	-613.29	-613.04
2.5	2.45	-613.17595	-613.09	1.7	2.7	-613.252	-613.14
2.5	2.5	-613.17575	-613.096	1.7	3	-613.258	-613.09
1.9	2.35	-613.20694	-613.157	1.9	3	-613.228	-613.11
1.9	2.4	-613.2	-613.158	1	2	-613.059	-612.94
1.9	2.45	-613.21435	-613.158	1.4	2	-613.16	-613.04
1.9	2.5	-613.21706	-613.157	1.4	2.3	-613.249	-613.11
2.1	2.35	-613.19123	-613.168	1.7	2	-613.145	-613.08
2.1	2.4	-613.19409	-613.169	1.7	2.3	-613.221	-613.14
2.1	2.45	-613.19621	-613.081	3.5	2	-613.109	-613.13
2.1	2.5	-613.19775	-613.087	3.5	3	-613.135	-613.13
1.9	3	-613.22763	-613.109	3	2	-613.112	-613.13
2	3	-613.21354	-613.114	3	3	-613.143	-613.13
2.1	3	-613.20073	-613.119	2.6	2	-613.116	-613.12
2.5	3	-613.16376	-613.129	2.6	2.3	-613.17	-613.18
1.9	2	-613.13397	-613.101	2.6	2.7	-613.167	-613.12

1992/QCISD

R	Cl	Cl	R	Hg	Cl	Singlet	Triplet	R	Cl	Cl	R	Hg	Cl	Singlet	Triplet
2.7		2.25		-1072.3639		-1072.3377		2.3		2.1		-1072.3353		-1072.3173	
2.7		2.35		-1072.3563		-1072.3459		2.3		2.25		-1072.3369		-1072.3395	
2.7		2.45		-1072.3493		-1072.3511		2.3		2.35		-1072.3363		-1072.3483	
2.7		2.55		-1072.3426		-1072.3541		2.3		2.55		-1072.3351		-1072.3576	
2.6		2.25		-1072.3592		-1072.3413		2.3		1.9		-1072.3238		-1072.2618	
2.6		2.35		-1072.3535		-1072.3497		2.4		1.9		-1072.3411		-1072.2662	
2.6		2.45		-1072.3478		-1072.355		2.1		1.8		-1072.2497		-1072.1906	
2.6		2.55		-1072.3423		-1072.3582		2.1		1.9		-1072.271		-1072.2336	
2.8		2.25		-1072.368		-1072.3335		2.1		2.1		-1072.2936		-1072.2896	
2.8		2.35		-1072.359		-1072.3414		2.1		2.25		-1072.3015		-1072.3122	
2.8		2.45		-1072.3504		-1072.3464		2.1		2.35		-1072.3053		-1072.3213	
2.8		2.55		-1072.3426		-1072.3493		2.1		2.45		-1072.3083		-1072.3273	
2.5		2.25		-1072.3538		-1072.3435		2.1		2.55		-1072.3107		-1072.3311	
2.5		2.35		-1072.3498		-1072.3521		2.1		2.9		-1072.3162		-1072.3359	
2.5		2.55		-1072.3415		-1072.3608		2.3		2.9		-1072.3341		-1072.3616	
2.5		2.1		-1072.3589		-1072.3218		2.4		2.9		-1072.3349		-1072.3646	
2.6		2.1		-1072.3673		-1072.3199		2.5		2.9		-1072.3331		-1072.364	
2.7		2.1		-1072.374		-1072.3167		2.6		2.9		-1072.3298		-1072.361	
2.8		2.1		-1072.3793		-1072.3131		2.8		2.9		-1072.3221		-1072.3517	
2.5		1.8		-1072.3375		-1072.2263		2.1		3.3		-1072.3118		-1072.336	
2.6		1.8		-1072.3479		-1072.2262		2.3		3.3		-1072.3327		-1072.3611	
2.7		1.8		-1072.3557		-1072.2252		2.4		3.3		-1072.3321		-1072.3639	
2.8		1.8		-1072.3616		-1072.2238		2.5		3.3		-1072.3287		-1072.363	
2.5		1.9		-1072.3543		-1072.2671		2.6		3.3		-1072.3251		-1072.3598	
2.6		1.9		-1072.3643		-1072.2657		2.8		3.3		-1072.3119		-1072.3503	
2.7		1.9		-1072.372		-1072.2563		2.35		2.35		-1072.3408		-1072.3508	
2.8		1.9		-1072.3778		-1072.2605		2.55		1.8		-1072.3431		-1072.2264	
2.4		1.8		-1072.3239		-1072.2245		2.55		1.9		-1072.3597		-1072.2666	
2.4		2.1		-1072.3484		-1072.3213		2.55		2.1		-1072.3633		-1072.321	
2.4		2.25		-1072.3468		-1072.3433		2.55		2.25		-1072.3566		-1072.3426	
2.4		2.35		-1072.3444		-1072.3521		2.55		2.35		-1072.3518		-1072.3511	
2.4		2.55		-1072.3395		-1072.3611		2.65		2.35		-1072.3549		-1072.348	
2.3		1.8		-1072.3058		-1072.2195		2.65		2.45		-1072.3486		-1072.3532	
2.625		2.4		-1072.3512		-1072.3518		2.65		2.55		-1072.3425		-1072.3563	
2.625		2.35		-1072.3542		-1072.3489		2.55		2.45		-1072.3467		-1072.3565	

B.2. $\text{Hg} + \text{HCl} \rightarrow \text{HgCl} + \text{H}$

1992/B3LYP

	Energy
HCl	-460.831
HgCl	-614.025
H	-0.48392
Hg	-153.82

R H-Cl	R Hg-Cl	Singlet Energy	Triplet Energy
2	2.3	-614.5345321	-614.4905679
2	2.4	-614.5438214	-614.494831
2	2.5	-614.5496308	-614.4953408
2	2.6	-614.5530898	-614.4361149
2.2	2.3	-614.5164542	-614.4978948
2.2	2.4	-614.5244582	-614.5022227
2.2	2.5	-614.5290736	-614.5029387
2.2	2.6	-614.5314313	-614.5013469
2.4	2.3	-614.5012041	-614.5023402
2.4	2.4	-614.5082117	-614.5067218
2.4	2.5	-614.5118941	-614.5075517
2.4	2.6	-614.5134196	-614.5061327
2.6	2.3	-614.4885156	-614.5048491
2.6	2.4	-614.4947691	-614.5092764
2.6	2.5	-614.4978108	-614.5101843

R H-Cl	R Hg-Cl	Singlet Energy	Triplet Energy
3.1	2	-614.4057221	-614.4476742
3.1	2.3	-614.4651545	-614.5066519
3.1	2.5	-614.4725409	-614.5120832
3.1	2.8	-614.4684186	-614.5052614
2.8	2.6	-614.4863685	-614.510238
1.8	2	-614.479482	-614.4195754
1.8	2.3	-614.5551966	-614.479371
1.8	2.5	-614.573335	-614.4843103
1.8	2.8	-614.5832101	-614.4396705
2	2	-614.4639249	-614.4314087
2	2.8	-614.5559303	-614.4488734
2.2	2	-614.4497176	-614.4388406
2.2	2.8	-614.5323816	-614.4539347
2.4	2	-614.4372877	-614.4432764
2.4	2.8	-614.512829	-614.4565555
2.6	2	-614.4265993	-614.4458008
2.6	2.8	-614.4968935	-614.5030131
2.8	2	-614.4173929	-614.447105
2.8	2.8	-614.4839389	-614.5045354

B3LYP/1997	
	Energy
HCl	-460.831
HgCl	-613.302
H	-0.48392
Hg	-153.085

R H-Cl	R Hg-Cl	Singlet Energy	Triplet Energy
2	2.3	-613.8054771	-613.7708969
2	2.4	-613.8140582	-613.774752
2	2.5	-613.8193211	-613.7749649
2.2	2.3	-613.7886958	-613.7774646
2.2	2.4	-613.7960073	-613.7812602
2.2	2.5	-613.8000686	-613.7814575
2.2	2.6	-613.8019505	-613.7793173
2.4	2.3	-613.7745732	-613.7814228
2.4	2.4	-613.7809652	-613.785221
2.4	2.5	-613.7840979	-613.7854714
2.4	2.6	-613.7850759	-613.7833872
2.6	2.3	-613.7627941	-613.7836292
2.6	2.4	-613.7685291	-613.7874409
2.6	2.6	-613.7713111	-613.7857406
2.8	2.3	-613.7530129	-613.7847145
2.8	2.5	-613.7601223	-613.7888163
2.8	2.6	-613.7600401	-613.7868834

R H-Cl	R Hg-Cl	Singlet Energy	Triplet Energy
1.8	2	-613.7520853	-613.7019608
1.8	2.5	-613.8417023	-613.7655421
1.8	2.8	-613.8506145	-613.7555929
2	2	-613.7377328	-613.7131389
2	2.8	-613.8244585	-613.7645431
2.2	2	-613.7245994	-613.7201037
2.2	2.8	-613.8020611	-613.7715122
2.4	2	-613.7130256	-613.7242123
2.4	2.8	-613.7835714	-613.775952
2.6	2	-613.703072	-613.726482
2.6	2.8	-613.7685872	-613.7785013
2.8	2	-613.6927118	-613.7276045
2.8	2.8	-613.7563986	-613.7797376
3.1	2	-613.6833659	-613.7280114
3.1	2.3	-613.7410466	-613.7850725
3.1	2.5	-613.7473542	-613.7892016
3.1	2.8	-613.7421046	-303.7545525

QCISD/1992	
	Energy
HCl	-460.305
HgCl	-612.703
H	-0.47896
Hg	-153.004

R H-Cl	R Hg-Cl	Singlet Energy	Triplet Energy	R H-Cl	R Hg-Cl	Singlet Energy	Triplet Energy
1.25	2.35	-613.257	-613.092	2.1	2.4	-613.194	-613.169
1.25	2.4	-613.265	-613.098	2.1	2.45	-613.196	-613.081
1.25	2.45	-613.271	-613.103	2.1	2.5	-613.198	-613.087
1.25	2.5	-613.277	-613.107	1.9	3	-613.228	-613.109
1.3	2.35	-613.259	-613.101	2	3	-613.214	-613.114
1.3	2.4	-613.267	-613.106	2.1	3	-613.201	-613.119
1.3	2.45	-613.273	-613.111	2.5	3	-613.164	-613.129
1.3	2.5	-613.279	-613.114	1.9	2	-613.134	-613.101
1.35	2.35	-613.259	-613.108	2	2	-613.13	-613.108
1.35	2.5	-613.278	-613.118	2.1	2	-613.126	-613.112
1.4	2.35	-613.257	-613.114	2.5	2	-613.117	-613.123
1.4	2.4	-613.264	-613.117	2.6	2.4	-613.173	-613.084
1.4	2.45	-613.27	-613.12	2.6	2.45	-613.173	-613.091
1.4	2.5	-613.275	-613.122	2.6	2.5	-613.173	-613.097
2	2.35	-613.198	-613.163	2.6	2.55	-613.172	-613.103
2	2.4	-613.202	-613.164	2.25	2.4	-613.185	-613.078
2	2.45	-613.205	-613.164	2.25	2.45	-613.186	-613.085
2	2.5	-613.207	-613.083	2.25	2.5	-613.187	-613.092
2.5	2.35	-613.174	-613.179	2.3	2.4	-613.183	-613.08
2.5	2.4	-613.176	-613.083	2.3	2.45	-613.184	-613.087
2.5	2.45	-613.176	-613.09	2.3	2.5	-613.184	-613.093
2.5	2.5	-613.176	-613.096	2.3	2.4	-613.181	-613.081
1.9	2.35	-613.207	-613.157	2.35	2.45	-613.181	-613.088
1.9	2.4	-613.211	-613.158	2.35	2.5	-613.182	-613.094
1.9	2.45	-613.214	-613.158	3	2.3	-613.165	-613.181
1.9	2.5	-613.217	-613.157	3	2.4	-613.167	-613.183
2.1	2.35	-613.191	-613.168	3	2.5	-613.166	-613.099

QCISD/1992			
R H-Cl	R Hg-Cl	Singlet Energy	Triplet Energy
3	2	-613.112	-613.127
3	3	-613.143	-613.132
2.6	2	-613.116	-613.125
2.6	2.3	-613.17	-613.178
2.6	2.7	-613.167	-613.116
2.6	3	-613.158	-613.13
2.25	2.43	-613.186	-613.083
2.25	2.44	-613.186	-613.084
2.25	2.46	-613.187	-613.087
2.25	2.47	-613.187	-613.088
2.26	2.43	-612.402	-612.396
2.26	2.44	-613.186	-613.084
2.26	2.45	-613.186	-613.086
2.26	2.46	-613.186	-613.087
2.26	2.47	-613.186	-613.088
2.27	2.43	-613.185	-613.083
2.27	2.44	-613.185	-613.085
2.27	2.45	-613.185	-613.086
2.27	2.46	-613.185	-613.087
2.27	2.47	-613.186	-613.089
2.28	2.43	-613.184	-613.083
2.28	2.44	-613.185	-613.085
2.28	2.45	-613.185	-613.086

R H-Cl	R Hg-Cl	Singlet Energy	Triplet Energy
2.28	2.46	-613.185	-613.087
2.28	2.47	-613.185	-613.089
3	2.7	-613.158	-613.118
3.5	2.3	-613.162	-613.181
3.5	2.4	-613.164	-613.183
3.5	2.5	-613.162	-613.182
3.5	2.7	-613.153	-613.118
1	2.3	-613.158	-612.974
1	2.4	-613.176	-612.992
1	2.5	-613.19	-613.006
1	2.7	-613.208	-613.026
1.4	2.7	-613.29	-613.039
1.7	2.7	-613.252	-613.136
1.7	3	-613.258	-613.093
1.9	3	-613.228	-613.109
1	2	-613.059	-612.936
1.4	2	-613.16	-613.044
1.4	2.3	-613.249	-613.11
1.7	2	-613.145	-613.084
1.7	2.3	-613.221	-613.14
3.5	2	-613.109	-613.127
3.5	3	-613.135	-613.132

QCISD/1997	
	Energy
HCl	-460.305
HgCl	-611.924
H	-0.47896
Hg	-152.214

R H-Cl	R Hg-Cl	Singlet Energy	Triplet Energy	R H-Cl	R Hg-Cl	Singlet Energy	Triplet Energy
1.25	2.35	-612.339	-612.467	2.6	2.5	-612.401	-612.392
1.25	2.4	-612.345	-612.475	2.6	2.55	-612.399	-612.391
1.25	2.45	-612.35	-612.481	2.25	2.4	-612.396	-612.402
1.25	2.5	-612.354	-612.487	2.25	2.45	-612.396	-612.403
1.3	2.35	-612.341	-612.469	2.25	2.5	-612.395	-612.403
1.3	2.4	-612.347	-612.477	2.3	2.45	-612.397	-612.4
1.3	2.45	-612.351	-612.483	2.3	2.5	-612.396	-612.401
1.3	2.5	-612.355	-612.488	2.35	2.45	-612.398	-612.399
1.35	2.35	-612.339	-612.469	2.35	2.5	-612.397	-612.399
1.35	2.4	-612.345	-612.476	3	2.3	-612.402	-612.387
1.35	2.45	-612.343	-612.482	3	2.4	-612.405	-612.389
1.35	2.5	-612.346	-612.488	3	2.5	-612.403	-612.388
1.4	2.35	-612.34	-612.467	3	2.7	-612.394	-612.378
1.4	2.4	-612.344	-612.474	2.1	2.35	-612.391	-612.406
1.4	2.45	-612.347	-612.48	2.1	2.4	-612.391	-612.409
1.4	2.5	-612.349	-612.485	2.1	2.45	-612.391	-612.411
2	2.35	-612.386	-612.412	2.1	2.5	-612.39	-612.412
2	2.4	-612.387	-612.415	1.9	3	-612.352	-612.438
2	2.45	-612.387	-612.418	2	3	-612.357	-612.424
2	2.5	-612.386	-612.42	2.1	3	-612.361	-612.412
2.5	2.35	-612.401	-612.394	2.5	3	-612.372	-612.377
2.5	2.4	-612.401	-612.395	1.9	2	-612.324	-612.349
2.5	2.45	-612.401	-612.395	2	2	-612.33	-612.346
2.5	2.5	-612.4	-612.394	1.9	2.4	-612.382	-612.424
1.9	2.35	-612.381	-612.42	1.9	2.45	-612.382	-612.427

QCISD/1997			
R H-Cl	R Hg-Cl	Singlet Energy	Triplet Energy
3.5	2.3	-612.402	-612.385
3.5	2.4	-612.405	-612.387
3.5	2.7	-612.394	-612.374
1	2.3	-612.248	-612.369
1	2.4	-612.261	-612.387
1	2.5	-612.27	-612.4
1	2.7	-612.282	-612.418
1	3	-612.29	-612.431
1.4	2.7	-612.356	-612.499
1.7	2.7	-612.362	-612.462
1.7	3	-612.348	-612.468
1.9	2.7	-612.372	-612.438
1.4	2	-612.268	-612.372
1.4	2.3	-612.336	-612.459
1.7	2	-612.308	-612.358
1.7	2.3	-612.365	-612.433
3.5	2	-612.348	-612.332
3.5	3	-612.377	-612.354
3	2	-612.348	-612.334
3	3	-612.377	-612.36
2.6	2	-612.346	-612.337
2.6	2.3	-612.4	-612.39
2.6	2.7	-612.392	-612.385
2.6	3	-612.374	-612.372
2.6	2.4	-612.402	-612.393
2.6	2.45	-612.402	-612.393
2.1	2	-612.335	-612.343
2.5	2	-612.345	-612.337
1.9	2.5	-612.381	-612.429

B.3. $\text{HgCl} + \text{Cl}_2 \rightarrow \text{HgCl}_2 + \text{Cl}$

1992/B3LYP					R1	R2	Energy	TC	Total Energy
		E(Hartrees)	T.C.	Total Energy	2.2	2.2	-1534.46	0.0078	-1534.4476
Cl2		-920.4247	0.003788	-920.420884	2.2	2.25	-1534.46	0.0077	-1534.45216
HgCl		-614.0247	0.003412	-614.021326	2.2	2.3	-1534.46	0.0076	-1534.45524
HgCl2		-1074.311	0.006592	-1074.30397	2.2	2.6	-1534.47	0.0064	-1534.45947
Cl		-460.1684	0.001416	-460.16699	2.2	2.8	-1534.46	0.0064	-1534.4514
					2.2	3.5	-1534.45	0.0083	-1534.43711
					2.2	4	-1534.44	0.0084	-1534.43343
					2.3	2.1	-1534.45	0.0079	-1534.44037
					2.3	2.15	-1534.46	0.0078	-1534.4488
					2.3	2.2	-1534.46	0.0077	-1534.4548
					2.3	2.25	-1534.47	0.0076	-1534.45886
					2.3	2.3	-1534.47	0.0076	-1534.4614
					2.3	2.7	-1534.46	0.0064	-1534.4555
					2.3	3.1	-1534.45	0.0082	-1534.43896
					2.3	3.5	-1534.44	0.0083	-1534.43025
					2.3	3.7	-1534.44	0.0083	-1534.42759
					2.5	2.1	-1534.46	0.0079	-1534.44966
					2.5	2.15	-1534.47	0.0078	-1534.45762
					2.5	2.2	-1534.47	0.0077	-1534.46309
					2.5	2.25	-1534.47	0.0076	-1534.46657
					2.5	2.3	-1534.48	0.0076	-1534.46847
					2.5	2.4	-1534.48	0.0075	-1534.46871
					2.5	2.55	-1534.47	0.0073	-1534.46327
					2.5	2.75	-1534.46	0.0064	-1534.45219
					2.5	3	-1534.44	0.0082	-1534.43518
					2.5	3.1	-1534.44	0.0082	-1534.43002
					2.6	3.6	-1534.41	0.0073	-1534.40676
					2.75	2.3	-1534.48	0.0076	-1534.47183
					2.75	2.4	-1534.48	0.0075	-1534.47129
					2.75	2.45	-1534.48	0.0074	-1534.46962
					2.75	2.55	-1534.47	0.0074	-1534.46438
					2.75	2.75	-1534.46	0.0064	-1534.4508
					2.75	3	-1534.44	0.0082	-1534.4296
					2.75	3.1	-1534.43	0.0073	-1534.42351
					2.8	2.4	-1534.48	0.0075	-1534.47147
					2.9	2.3	-1534.48	0.0075	-1534.4724
					2.9	2.4	-1534.48	0.0075	-1534.47163
					2.9	2.45	-1534.48	0.0074	-1534.46984

R1	R2	Energy	TC	Total Energy	R1	R2	Energy	TC	Total Energy
2.1	3	-1534.455	0.008374	-1534.44674	2.9	3	-1534.44	0.0075	-1534.47021
2.1	3.1	-1534.454	0.008392	-1534.44554	2.9	3.1	-1534.43	0.0093	-1534.46533
2.1	3.3	-1534.452	0.008421	-1534.44348	3	2.3	-1534.48	0.0083	-1534.44763
2.1	3.4	-1534.451	0.008433	-1534.44263	3	2.44	-1534.48	0.0073	-1534.4275
2.1	3.5	-1534.45	0.008443	-1534.44188	3	2.5	-1534.47	0.0075	-1534.47248
2.1	3.6	-1534.45	0.008452	-1534.44124	3	2.75	-1534.46	0.0093	-1534.46819
2.1	3.8	-1534.449	0.008466	-1534.44024	3	3	-1534.43	0.0093	-1534.46514
2.15	2.1	-1534.435	0.007969	-1534.42703					
2.2	2.1	-1534.44	0.007954	-1534.43229					
2.2	2.15	-1534.449	0.007852	-1534.44114					

1992/B3LYP				
RXN - Cl2 + HgCl --> HgCl2 + Cl				
R1	R2	Energy	TC	Total Energy
3.2	2.3	-1534.48	0.007544	-1534.47239
3.2	2.44	-1534.477	0.009344	-1534.46801
3.2	2.5	-1534.474	0.008367	-1534.46587
3.3	2.3	-1534.48	0.007544	-1534.47227
3.3	2.44	-1534.477	0.008403	-1534.46877
3.3	2.75	-1534.455	0.008273	-1534.44636
3.3	3	-1534.433	0.007305	-1534.4254
3.3	3.1	-1534.424	0.007299	-1534.41703
3.4	2.3	-1534.48	0.006601	-1534.4731
3.4	2.44	-1534.477	0.008405	-1534.4686
3.4	2.5	-1534.474	0.008373	-1534.46545

1997/B3LYP

R1	R2	Energy	TC	Total Energy	R1	R2	Energy	TC	Total Energy
1.8	2.7	-1533.701	0.00822	-1533.6926	2.5	2.4	-1533.76	0.00749	-1533.7561
1.8	3.1	-1533.706	0.00826	-1533.6975	2.5	2.55	-1533.76	0.00737	-1533.7505
1.9	3.1	-1533.725	0.00789	-1533.7167	2.5	2.75	-1533.75	0.00636	-1533.7388
2	3.5	-1533.73	0.00672	-1533.7235	2.5	3	-1533.73	0.00823	-1533.7205
2	4	-1533.728	0.00675	-1533.7216	2.5	3.1	-1533.72	0.00823	-1533.7147
2.2	3.5	-1533.726	0.00834	-1533.7172	2.6	3.6	-1533.7	0.00728	-1533.6896
2.2	4	-1533.721	0.00837	-1533.7124	2.75	2.3	-1533.77	0.00755	-1533.7595
2	2.2	-1533.539	0.00806	-1533.5308	2.75	2.4	-1533.77	0.00748	-1533.759
2	2.4	-1533.559	0.00789	-1533.5508	2.75	2.45	-1533.76	0.00745	-1533.7573
2	2.6	-1533.735	0.00758	-1533.7277	2.75	2.55	-1533.76	0.00739	-1533.7521
2	2.8	-1533.735	0.00663	-1533.7283	2.75	2.75	-1533.74	0.00637	-1533.7382
2	3	-1533.734	0.00666	-1533.7269	2.75	3	-1533.72	0.00824	-1533.7162
2	3.1	-1533.733	0.00667	-1533.7261	2.75	3.1	-1533.72	0.00729	-1533.7097
2.1	2.4	-1533.743	0.00755	-1533.7357	2.8	2.4	-1533.77	0.00748	-1533.7592
2.1	2.6	-1533.744	0.00648	-1533.7371	2.9	2.3	-1533.77	0.00754	-1533.7601
2.1	2.8	-1533.74	0.00647	-1533.7337	2.9	2.4	-1533.77	0.00747	-1533.7594
2.1	3.1	-1533.735	0.00839	-1533.7263	2.9	2.45	-1533.77	0.00744	-1533.7576
2.1	3.7	-1533.728	0.00846	-1533.7198	2.9	2.55	-1533.76	0.00739	-1533.7521
2.15	2.1	-1533.721	0.008	-1533.7133	2.9	2.75	-1533.74	0.00826	-1533.7357
2.15	2.15	-1533.721	0.008	-1533.7133	2.9	3	-1533.72	0.00824	-1533.7145
2.15	2.2	-1533.721	0.008	-1533.7133	2.9	3.1	-1533.71	0.00729	-1533.7074
2.15	2.25	-1533.721	0.008	-1533.7133	3	2.5	-1533.76	0.00931	-1533.7531
2.15	2.3	-1533.721	0.008	-1533.7133	3	2.75	-1533.74	0.00827	-1533.7352
2.15	2.7	-1533.739	0.00831	-1533.7305	3	3	-1533.72	0.0073	-1533.7145
2.15	3.1	-1533.734	0.00834	-1533.7259	3.2	2.5	-1533.76	0.00931	-1533.7527
2.2	2.1	-1533.727	0.00798	-1533.7188	3.3	3	-1533.72	0.00731	-1533.7124
2.2	2.15	-1533.735	0.00788	-1533.7276	3.3	3.1	-1533.71	0.0073	-1533.7038
2.2	2.2	-1533.742	0.00778	-1533.734	3.4	2.5	-1533.76	0.00837	-1533.7531
2.2	2.25	-1533.746	0.0077	-1533.7384					
2.2	2.3	-1533.749	0.00763	-1533.7414					
2.3	2.1	-1533.735	0.00794	-1533.7273					
2.3	2.15	-1533.744	0.00785	-1533.7357					
2.3	2.2	-1533.749	0.00775	-1533.7417					
2.3	2.25	-1533.753	0.00767	-1533.7457					
2.3	2.3	-1533.756	0.00761	-1533.7482					
2.3	2.5	-1533.755	0.00741	-1533.748					
2.3	2.7	-1533.747	0.00638	-1533.7409					
2.3	3	-1533.734	0.00825	-1533.7255					

Cl	-460.168	0.00142	-460.16699
Cl2	-920.425	0.00379	-920.42088
HgCl	-613.302	0.00343	-613.29842
HgCl2	-1073.6	0.00659	-1073.5911
react	-1533.7		
prod	-1533.8		

APPENDIX C. TRANSITION STATE THEORY RATE CONSTANT DATA



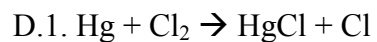
1992 – QCISD – 700 K

HgCl		HCl		HgCl2		H		TS	
Freq	Qv	Freq	Qv	Freq	Qv	Freq	Qv	Freq	Qv
290.5631	2.223	2947.1	1.00331	97.7492	5.491	None	None	508.42	1.094
				97.7492	5.792			508.42	1.094
				340.798	2.068			300.91	1.305
				394.047	1.872			250.32	1.425
								81.865	3.061
								81.865	3.061
								-1648	-3E-04
Qvtot =			1.00331		123.1		1		20.85
Qe =	2.223		1		1		2		2
Qt =			7.2E+07		1E+09		335889		2E+08
Qt(corr. m^-3)	2		7.5E+32		2E+34		4E+30		4E+33
Qr =	1E+09		46.5599		5340		1		4979
Qtot (m^-3)	1E+34		3.5E+34		1E+40		7E+30		9E+38
	5005								
Qtot (cm^-3)	3E+38		3.5E+28		1E+34		7E+24		9E+32
Qts =	2E-26							2E-24	cm^3
ko =	1E+11	for					ko=	2E+13	rev
Tunnel:									
k(T) =	1.479								
k w/tunnel	2E+11	for		k w/tunnel	3E+13	rev			
		k = ko*exp[-Ea/RT]							
	E	TC	E(Har)	E(kcal/mol)	E(kJ/mol)	Ea/RT			
HgCl	-612.7	0.0078	-612.69	-384472	-2E+06				
HCl	-460.3	0.0123	-460.29						
HgCl2	-1072	0.0146	-1072.5						
H	-0.479	0.0033	-0.4756						
TS	-1073	0.0194	-1072.9						
forward	Ea=	0.0513		32.1755	134.6				
							k=	18.851	
reverse	Ea=	0.01		6.30026	26.36				
							k=	3E+11	

1992/QCISD					
	Rate (cm ³ /mol*s)		Act En (kcal/mol)		
Temp (K)	forward	reverse	forward	reverse	
298	5.929*10 ⁻¹²	2.012*10 ⁻⁹	30.54	6.12	
700	18.85	3.099*10 ¹¹	32.18	6.3	
1000	3.05*10 ⁴	1.88*10 ¹²	33.48	6.54	
1500	1.11*10 ⁷	6.75*10 ¹²	35.49	6.99	
2000	2.87*10 ⁸	1.46*10 ¹³	37.32	7.47	
1997/QCISD					
	Rate (cm ³ /mol*s)		Act En (kcal/mol)		
Temp (K)	forward	reverse	forward	reverse	
298	1.18*10 ⁻⁹	4.46*10 ⁸	27.43	6.93	
700	14.91	2.139*10 ¹¹	28.95	6.99	
1000	4.77*10 ³	1.00*10 ¹²	30.28	7.26	
1500	5.35*10 ⁵	4.08*10 ¹²	32.3	7.72	
2000	6.52*10 ⁶	9.42*10 ¹²	34.14	8.21	

1992/B3LYP					
	Rate (cm ³ /mol*s)		Act En (kcal/mol)		
Temp (K)	forward	reverse	forward	reverse	
298	4.08*10 ⁻¹⁷	5.929*10 ⁻¹²	37.29	8.12	
700	2.26*10 ⁻¹	1.12*10 ¹¹	39.13	8.5	
1000	2.73*10 ³	1.78*10 ⁶	40.45	8.79	
1500	4.06*10 ⁶	1.12*10 ¹³	42.53	9.28	
2000	2.23*10 ⁸	3.23*10 ¹³	44.38	9.78	
1997/B3LYP					
	Rate (cm ³ /mol*s)		Act En (kcal/mol)		
Temp (K)	forward	reverse	forward	reverse	
298	7.99*10 ⁻¹³	1.66*10 ⁷	31.57	8.68	
700	1.71*10 ¹	1.04*10 ¹¹	33.41	9.05	
1000	5.99*10 ⁴	1.89*10 ¹²	34.76	9.34	
1500	3.47*10 ⁷	1.33*10 ¹³	36.81	9.84	
2000	1.48*10 ⁹	4.02*10 ¹³	41.77	0.35	

APPENDIX D. VARIATIONAL TST RATE CONSTANT DATA



1997-QCISD
298K
Transition Structure: Cl-Cl 2.8Å, Cl-Hg 2.5Å

Hg		Cl2		HgCl		Cl		TS	
Freq	Qv	Freq	Qv	Freq	Qv	Freq	Qv	Freq	Qv
None	None	562.21	1.0708	261.03	1.39534	None	None	-145.1	-0.984
								110.6	2.416
								110.61	2.416
Qvtot =	1		1.0708		1.39534		1		5.835
Qe =	1		1		2		2		1
Qt =	1.13E+08		2.3E+07		1.4E+08		8E+06		2E+08
Qt(corr. m^-3) =	2.78E+33		5.7E+32		3.5E+33		2E+32		4E+33
Qr =	1		428.538		2224.76		1		11398
Qtot (m^-3)=	2.78E+33		2.6E+35		2.2E+37		4E+32		3E+38
Qtot (cm^-3) =	2.78E+27		2.6E+29		2.2E+31		4E+26		3E+32
Qts =		4E-25	cm^3		Qts =			3E-26	cm^3
ko =	1.5E+12						ko=	1E+11	

Tunnel:							
k(T) =	1.020475						
k w/tunnel	1.53E+12	for		k w/tunnel	1.2E+11	rev	
	E	TC	E(Har)	E(kcal/mol)	E(kJ/mol)	Ea/RT	
HgCl	-152.214	0.0014	-152.21	-95514.7	-399627		
HCl	-919.392	0.0038	-919.39				
HgCl ₂	-611.924	0.0034	-611.92				
H	-459.657	0.0014	-459.66				
TS	-1071.57	0.0053	-1071.6				
forward	Ea=	0.0339		21.2431	88.8795	35.874	
						k= 0.0004	
reverse	Ea=	0.0093		5.8337	24.4078	9.8515	
						k= 7E+06	

1997/QCISD					
	Rate (cm³/mol*s)		Act En (kcal/mol)		
Temp (K)	forward	reverse	forward	reverse	
298	4.03*10 ⁻⁴	6.58*10 ⁶	21.24	5.83	
700	4.45*10 ⁵	2.18*10 ⁹	21.78	6.24	
1000	5.67*10 ⁷	8.66*10 ⁹	22.11	6.54	
2000	1.78*10 ¹⁰	4.99*10 ¹⁰	23.15	7.53	



1992-QCISD

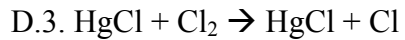
298K

Transition Structure: Cl-Cl 2.8Å, Cl-Hg 2.4Å

Hg		HCl		HgCl		H		TS	
Freq	Qv	Freq	Qv	Freq	Qv	Freq	Qv	Freq	Qv
None	None	3025.6	1	290.563	1.32565	None	None	-472.8	-0.113
								242.57	1.449
								290.86	1.325
Qvtot =	1		1		1.32565		1		1.92
Qe =	1		1		2		2		1
Qt =	1.13E+08		8481880		1.4E+08		39768		1E+08
Qt(m^-3) =	2.78E+33		2.1E+32		3.5E+33		1E+30		4E+33
Qr =	1		19.5425		2132.24		1		7.185
Qtot (m^-3)=	2.78E+33		4.1E+33		2E+37		2E+30		5E+34
Qtot (cm^-3) =	2.78E+27		4.1E+27		2E+31		2E+24		5E+28
Qts =		4E-27	cm^3		Qts =			1E-27	cm^3
ko =	1.62E+10						ko=	5E+09	

Tunnel:							
k(T) =	1.217414						
k w/tunnel	1.97E+10	for		k w/tunnel	5.7E+09	rev	
	E	TC	E(Har)	E(kcal/mol)	E(kJ/mol)	Ea/RT	
HgCl	-153.004	0.0014	-153	-96010.5	-401701		
HCl	-460.323	0.0093	-460.31				
HgCl2	-612.703	0.0035	-612.7				
H	-0.49982	0.0014	-0.4984				
TS	-613.17	0.005	-613.16				
forward	Ea=	0.1513		94.9537	397.279	160.4	
						k=	5E-60
reverse	Ea=	0.0329		20.6641	86.4572	34.9	
						k=	4E-06

1992/QCISD				
	Rate (cm ³ /mol*s)		Act En (kcal/mol)	
Temp (K)	forward	reverse	forward	reverse
298	4.51*10 ⁻⁶⁰	3.99*10 ⁻⁶	94.95	20.66
700	6.79*10 ⁻²⁰	3.11*10 ³	95.64	20.63
1000	2.00*10 ⁻¹¹	3.06*10 ⁴	96.12	20.62
1500	1.29*10 ⁻³	1.56*10 ⁷	96.71	20.61
2000	6.09	1.14*10 ⁸	97.09	20.61



1992-B3LYP-298 K

Transition Structure: HgCl – 3.3 Cl₂ – 2.3

HgCl		Cl2		HgCl ₂		Cl		TS	
Freq	Qv	Freq	Qv	Freq	Qv	Freq	Qv	Freq	Qv
244.4004	1.4431	540.501	1.0793	92.67	2.77068	None	None	292.1	1.3224
				92.67	2.77068			117.7	2.306
				318.5	1.27323			98.49	2.641
				374.5	1.19585			98.41	2.6427
								50.05	4.6553
								50.04	4.656
								-208.5	-0.5753
Qvtot =	1.4431		1.0793		11.6885		1		461.32
Qe =	2		1		1		2		2
Qt =	1E+08		2E+07		1.8E+08		8E+06		2E+08
Qt(corr. m^-3)	4E+33		6E+32		4.3E+33		2E+32		5E+33
Qr =	2271.1		434.41		2312.65		1		17332
Qtot (m^-3)	2E+37		3E+35		1.2E+38		4E+32		8E+40
Qtot (cm^-3)	2E+31		3E+29		1.2E+32		4E+26		8E+34
Qts	1E-26	cm^3			Qts =	2E-24	cm^3		
ko =	5E+10	for			ko=	7E+12	rev		
Tunnel									
k(T) =	1.0423								
ko (w/tunn)	5E+10	for			(w/tunn)	7E+12	rev		
	E	TC	E(Har)		kcal/mol	kJ/mol			
HgCl	-614	0.00341	-614		-385304	-2E+06			
Cl2	-920.4	0.00379	-920.4						
HgCl2	-1074	0.00659	-1074						
Cl	-460.2	0.00142	-460.2						
TS	-1534	0.00825	-1534						
		Ea=	0.0032		2.03853	8.529			
					k=	2E+09	for		
		Ea=	0.032		20.0803	84.014			
					k=	0.0129	rev		

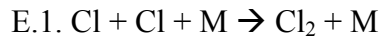
1992-B3LYP**Transition Structure: HgCl – 3.3 Cl₂ – 2.3**

1992/B3LYP				
	Rate (cm ³ /mol*s)		Act En (kcal/mol)	
Temp (K)	forward	reverse	forward	reverse
298	1.69*10 ⁹	1.29*10 ⁻²	2.03	20.08
700	2.08*10 ¹¹	5.98*10 ⁷	0.413	17.62
1000	3.38*10 ¹¹	3.92*10 ⁹	1.37	17.97
1500	6.85*10 ¹¹	1.23*10 ¹¹	2.88	18.47

1997-B3LYP**Transition Structure: HgCl – 3.3 Cl₂ – 2.3**

1997/B3LYP				
	Rate (cm ³ /mol*s)		Act En (kcal/mol)	
Temp (K)	forward	reverse	forward	reverse
298	1.32*10 ⁹	2.03*10 ⁻⁷	2.28	26.59
700	1*10 ¹¹	2.7*10 ⁵	2.04	25.52
1000	1.2*10 ¹¹	4.57*10 ⁷	4.53	27.39
1500	4.28*10 ¹¹	7.19*10 ⁹	6.042	27.9

APPENDIX E. VARIATIONAL RRKM THEORY RATE CONSTANT DATA



$\beta_c = 0.1$

Pople 6-311++G(3df, 3pd)/QCISD

T	ZLJ[M]	Area (P=230 torr)	Q2=1
1500	69285191.46	0.0056	$\text{Q1}^+/\text{Q1}=1$
2000	56892741.57	6.20E-03	
2500	48919689.39	6.60E-03	
3000	43290306.44	6.90E-03	
<hr/>			
T	exp(-Ea/RT)	k predicted (1/s)	k (cm ³ /molec*s)
1500	1.13489E-06	1.91E+02	3.89E-17
2000	3.47708E-05	6.46E+03	1.76E-15
2500	0.000271001	5.36E+04	1.83E-14
3000	0.00106531	2.20E+05	9.01E-14
Planck's constant	3.34E-11	(s/cm)	

$\beta_c = 0.2$

Pople 6-311++G(3df, 3pd)/QCISD

T	ZLJ[M]	Area (P=230 torr)	Q2=1
1500	138570382.9	0.0113	$\text{Q1}^+/\text{Q1}=1$
2000	113785483.1	1.23E-02	
2500	97839378.79	1.32E-02	
3000	86580612.89	1.39E-02	
<hr/>			
T	exp(-Ea/RT)	k predicted (1/s)	k (cm ³ /molec*s)
1500	1.13489E-06	3.85E+02	7.86E-17
2000	3.47708E-05	1.28E+04	3.49E-15
2500	0.000271001	1.07E+05	3.65E-14
3000	0.00106531	4.44E+05	1.81E-13
Planck's constant	3.34E-11	(s/cm)	

$\beta_c = 0.4$

Pople 6-311++G(3df, 3pd)/QCISD

T	ZLJ[M]	Area (P=230 torr)	Q2=1
1500	277140765.8	0.0226	Q1 ⁺ /Q1=1
2000	227570966.3	2.46E-02	
2500	195678757.6	2.64E-02	
3000	173161225.8	2.78E-02	
<hr/>			
T	exp(-Ea/RT)	k predicted (1/s)	k (cm ³ /molec*s)
1500	1.13489E-06	7.69E+02	1.57E-16
2000	3.47708E-05	2.56E+04	6.99E-15
2500	0.000271001	2.15E+05	7.31E-14
3000	0.00106531	8.88E+05	3.63E-13
Planck's constant	3.34E-11	(s/cm)	

$\beta_c = 0.7$

Pople 6-311++G(3df, 3pd)/QCISD

T	ZLJ[M]	Area (P=230 torr)	Q2=1
1500	484996340.2	0.0395	Q1 ⁺ /Q1=1
2000	398249191	0.0431	
2500	342437825.8	0.0461	
3000	303032145.1	0.0486	
<hr/>			
T	exp(-Ea/RT)	k predicted (1/s)	k (cm ³ /molec*s)
1500	1.13489E-06	1.34E+03	2.75E-16
2000	3.47708E-05	4.49E+04	1.22E-14
2500	0.000271001	3.75E+05	1.28E-13
3000	0.00106531	1.55E+06	6.35E-13
Planck's constant	3.34E-11	(s/cm)	



1992/MP4SDQ
T = 393 K

Bond dist = 3.12A	Act En															
Energy(react)	-612.7018471	Hartrees	kcal/mol	cm^-1	kJ/mol											
TH Corr	0.004472	0.0272736	17.1144431	5984.071	71.6056											
Tot E(react)	-612.6973751	Q2	exp(-Ea/RT)													
Energy (TS) =	-612.6732125	1	3.0322E-10													
TH Corr	0.003111	k(tunnel)	1.04778381													
Tot E(TS)	-612.6701015															
<hr/>																
Beta C	LJ	Area	k(1/s)	k(1/M s)	k(VTST)											
1	1948264328	0.0666	0.60462687	20.31142	21.282											
0.8	1558611462	0.0533	0.48388307	16.25524	17.032											
0.6	1168958597	0.04	0.36313926	12.19905	12.782											
0.4	779305731.2	0.0266	0.24148761	8.112369	8.50001											
0.2	389652865.6	0.0133	0.12074381	4.056184	4.25											
<hr/>																
<table border="1" style="margin-left: auto; margin-right: auto;"> <tr> <td>Planck's const</td> <td>(s/cm)</td> <td>(J/s)</td> </tr> <tr> <td></td> <td>3.34E-11</td> <td>6.63E-34</td> </tr> <tr> <td>speed light - c</td> <td>30000000000</td> <td></td> </tr> <tr> <td>k (boltz)</td> <td>1.38E-23</td> <td></td> </tr> </table>					Planck's const	(s/cm)	(J/s)		3.34E-11	6.63E-34	speed light - c	30000000000		k (boltz)	1.38E-23	
Planck's const	(s/cm)	(J/s)														
	3.34E-11	6.63E-34														
speed light - c	30000000000															
k (boltz)	1.38E-23															

1992/MP4SDQ
T = 700 K

Bond dist = 3.12A	Act En				
Energy(react)	-612.7018471	Hartrees	kcal/mol	cm^-1	kJ/mol
TH Corr	0.007825	0.0263516	16.5358793	5781.776	69.1849
Tot E(react)	-612.6940221	Q2	exp(-Ea/RT)		
Energy (TS) =	-612.6732125	1	6.8681E-06		
TH Corr	0.005542	k(tunnel)	1.01506155		
Tot E(TS)	-612.6676705				
<hr/>					
Beta C	LJ	Area	k(1/s)	k(1/M s)	k(VTST)
1	1257188571	0.0628	12913.7331	433815.1	440349
0.8	1005750857	0.0502	10322.7612	346775.7	351999
0.6	754313142.6	0.0377	7752.35251	260427.2	264350
0.4	502875428.4	0.0251	5161.38058	173387.9	175999
0.2	201150171.4	0.0101	2076.89019	69769.62	70820.5

1992/MP4SDQ

T = 1000 K

Bond dist = 3.12A		Act En			
Energy(react)	-612.7018471	Hartrees	kcal/mol	cm^-1	kJ/mol
TH Corr	0.01113	0.0254216	15.9522955	5577.726	66.7432
Tot E(react)	-612.6907171	Q2	exp(-Ea/RT)		
Energy (TS) =	-612.6732125	1	0.00032609		
TH Corr	0.007917	k(tunnel)	1.00738016		
Tot E(TS)	-612.6652955				
Beta C		LJ	Area	k(1/s)	k(1/M s)
1	749858000	0.0639	6.24E+05	2.10E+07	2.11E+07
0.8	599886400	0.0511	4.99E+05	1.68E+07	1.69E+07
0.6	449914800	0.0384	3.75E+05	1.26E+07	1.27E+07
0.4	299943200	0.0256	2.50E+05	8.40E+06	8.46E+06
0.2	149971600	0.0128	1.25E+05	4.20E+06	4.23E+06

1992/MP4SDQ

T = 1500 K

Bond dist = 3.12A		Act En			
Energy(react)	-612.7018471	Hartrees	kcal/mol	cm^-1	kJ/mol
TH Corr	0.016657	0.0238536	14.9683606	5233.693	62.6265
Tot E(react)	-612.6851901	Q2	exp(-Ea/RT)		
Energy (TS) =	-612.6732125	1	0.00659069		
TH Corr	0.011876	k(tunnel)	1.00328007		
Tot E(TS)	-612.6613365				
Beta C		LJ	Area	k(1/s)	k(1/M s)
1	691344081	0.081	1.60E+07	5.37E+08	5.39E+08
0.8	553075264.8	0.0648	1.28E+07	4.30E+08	4.31E+08
0.6	414806448.6	0.0486	9.59E+06	3.22E+08	3.23E+08
0.4	276537632.4	0.0324	6.39E+06	2.15E+08	2.15E+08
0.2	138268816.2	0.0162	3.20E+06	1.07E+08	1.08E+08

1997/MP4SDQ
T=393 K

Bond dist	3.12A	Act En			
Energy(react)	-611.8881292	Hartrees	kcal/mol	kJ/mol	cm-1
TH Corr	0.00311	0.0331429	20.79748461	87.015123	7271.848
Tot E(react)	-611.8850192	Q2	exp(-Ea/RT)		
Energy (TS) =	-611.9226411	1	2.71286E-12		
TH Corr	0.004479	k(tunnel)	1.050437966		
Tot E(TS)	-611.9181621				
<hr/>					
Beta C	LJ	Area	k(1/s)	k(1/M s)	k(VTST)
1	1948264328	0.065	5.29E-03	1.78E-01	1.87E-01
0.8	1558611462	0.052	4.23E-03	1.42E-01	1.49E-01
0.6	1168958597	0.039	3.17E-03	1.07E-01	1.12E-01
0.4	779305731.2	0.026	2.11E-03	7.10E-02	7.46E-02
0.2	311722292.5	0.0104	8.46E-04	2.84E-02	2.99E-02

1997/MP4SDQ
T=700 K

Bond dist	3.12A	Act En			
Energy(react)	-611.8881292	Hartrees	kcal/mol	kJ/mol	cm-1
TH Corr	0.005542	0.0322249	20.22143089	84.604957	7070.43
Tot E(react)	-611.8825872	Q2	exp(-Ea/RT)		
Energy (TS) =	-611.9226411	1	4.85358E-07		
TH Corr	0.007829	k(tunnel)	1.01589815		
Tot E(TS)	-611.9148121				
<hr/>					
Beta C	LJ	Area	k(1/s)	k(1/M s)	k(VTST)
1	1257188571	0.0817	1.19E+03	3.99E+04	4.06E+04
0.8	1005750857	0.0654	9.52E+02	3.20E+04	3.25E+04
0.6	754313142.6	0.049	7.13E+02	2.40E+04	2.43E+04
0.4	502875428.4	0.0327	4.76E+02	1.60E+04	1.62E+04
0.2	201150171.4	0.0131	1.91E+02	6.40E+03	6.51E+03

1997/MP4SDQ**T=1000 K**

Bond dist	3.12A	Act En			
Energy(react)	-611.8881292	Hartrees	kcal/mol	kJ/mol	cm ⁻¹
TH Corr	0.007917	0.0312959	19.63847456	82.1659	6866.6
Tot E(react)	-611.8802122	Q2	exp(-Ea/RT)		
Energy (TS) =	-611.9226411	1	5.10105E-05		
TH Corr	0.011133	k(tunnel)	1.007790093		
Tot E(TS)	-611.9115081				
<hr/>					
Beta C	LJ	Area	k(1/s)	k(1/M s)	k(VTST)
1	749858000	0.0594	9.09E+04	3.05E+06	3.08E+06
0.8	599886400	0.0475	7.26E+04	2.44E+06	2.46E+06
0.6	449914800	0.0356	5.44E+04	1.83E+06	1.84E+06
0.4	299943200	0.0238	3.64E+04	1.22E+06	1.23E+06
0.2	119977280	0.0095	1.45E+04	4.88E+05	4.92E+05

1997/MP4SDQ**T=1500 K**

Bond dist = 3.12A	Act En				
Energy(react)	-611.8881292	Hartrees	kcal/mol	cm ⁻¹	kJ/mol
TH Corr	0.011876	0.0297289	18.6551672	78.05183	6522.79
Tot E(react)	-611.8762532	Q2	exp(-Ea/RT)		
Energy (TS) =	-611.9226411	1	0.00191302		
TH Corr	0.016659	k(tunnel)	1.00346226		
Tot E(TS)	-611.9059821				
<hr/>					
Beta C	LJ	Area	k(1/s)	k(1/M s)	k(VTST)
1	691344081	0.0785	4.50E+06	1.51E+08	1.52E+08
0.8	553075264.8	0.0628	3.60E+06	1.21E+08	1.21E+08
0.6	414806448.6	0.0471	2.70E+06	9.08E+07	9.11E+07
0.4	276537632.4	0.0314	1.80E+06	6.05E+07	6.07E+07
0.2	110615053	0.0126	7.23E+05	2.43E+07	2.44E+07

1992/QCISD
T=393 K

Bond dist	3.12A	Act En			
Energy(react)	-612.7026425	Hartrees	kcal/mol	kJ/mol	cm-1
TH Corr	0.004471	0.0257184	16.13854032	67.5224	5642.85
Tot E(react)	-612.6981715	Q2	exp(-Ea/RT)		
Energy (TS) =	-612.6755641	1	1.05806E-09		
TH Corr	0.003111	k(tunnel)	1.047131477		
Tot E(TS)	-612.6724531				
<hr/>					
Beta C	LJ	Area	k(1/s)	k(1/M s)	k(VTST)
1	1948264328	0.0655	2.08E+00	6.98E+01	7.31E+01
0.8	1558611462	0.0524	1.66E+00	5.58E+01	5.85E+01
0.6	1168958597	0.0393	1.25E+00	4.19E+01	4.39E+01
0.4	779305731.2	0.0262	8.31E-01	2.79E+01	2.92E+01
0.2	389652865.6	0.0131	4.16E-01	1.40E+01	1.46E+01

1992/QCISD
T=700 K

Bond dist	3.12A	Act En			
Energy(react)	-612.7026425	Hartrees	kcal/mol	kJ/mol	cm-1
TH Corr	0.007824	0.0247964	15.55997657	65.1018	5440.55
Tot E(react)	-612.6948185	Q2	exp(-Ea/RT)		
Energy (TS) =	-612.6755641	1	1.38533E-05		
TH Corr	0.005542	k(tunnel)	1.014855938		
Tot E(TS)	-612.6700221				
<hr/>					
Beta C	LJ	Area	k(1/s)	k(1/M s)	k(VTST)
1	1257188571	0.0827	3.44E+04	1.15E+06	1.17E+06
0.8	1005750857	0.0661	2.75E+04	9.22E+05	9.36E+05
0.6	754313142.6	0.0496	2.06E+04	6.92E+05	7.02E+05
0.4	502875428.4	0.0331	1.37E+04	4.62E+05	4.69E+05
0.2	201150171.4	0.0132	5.48E+03	1.84E+05	1.87E+05

1992/QCISD
T=1000 K

Bond dist	3.12A	Act En			
Energy(react)	-612.7026425	Hartrees	kcal/mol	kJ/mol	cm-1
TH Corr	0.01113	0.0238654	14.97576522	62.6575	5236.28
Tot E(react)	-612.6915125	Q2	exp(-Ea/RT)		
Energy (TS) =	-612.6755641	1	0.000533062		
TH Corr	0.007917	k(tunnel)	1.007279409		
Tot E(TS)	-612.6676471				
<hr/>					
Beta C	LJ	Area	k(1/s)	k(1/M s)	k(VTST)
1	749858000	0.0603	9.64E+05	3.24E+07	3.26E+07
0.8	599886400	0.0482	7.70E+05	2.59E+07	2.61E+07
0.6	449914800	0.0362	5.79E+05	1.94E+07	1.96E+07
0.4	299943200	0.0241	3.85E+05	1.29E+07	1.30E+07
0.2	149971600	0.0121	1.93E+05	6.50E+06	6.54E+06

1992/QCISD
T=1500 K

Bond dist	3.12A	Act En			
Energy(react)	-612.7026425	Hartrees	kcal/mol	kJ/mol	cm-1
TH Corr	0.016657	0.0222974	13.99183033	58.5408	4892.25
Tot E(react)	-612.6859855	Q2	exp(-Ea/RT)		
Energy (TS) =	-612.6755641	1	0.009145828		
TH Corr	0.011876	k(tunnel)	1.003235293		
Tot E(TS)	-612.6636881				
<hr/>					
Beta C	LJ	Area	k(1/s)	k(1/M s)	k(VTST)
1	691344081	0.0915	2.51E+07	8.43E+08	8.46E+08
0.8	553075264.8	0.0732	2.01E+07	6.74E+08	6.77E+08
0.6	414806448.6	0.0549	1.51E+07	5.06E+08	5.07E+08
0.4	276537632.4	0.0366	1.00E+07	3.37E+08	3.38E+08
0.2	138268816.2	0.0183	5.02E+06	1.69E+08	1.69E+08

1997/QCISD
T=393 K

Bond dist	3.12A	Act En			
Energy(react)	-611.92393	Hartrees	kcal/mol	kJ/mol	cm-1
TH Corr	0.004477	0.0321241	20.158178	7048.314	84.340312
Tot E(react)	-611.91946	Q2	exp(-Ea/RT)		
Energy (TS) =	-611.89044	1	6.151E-12		
TH Corr	0.003111	k(tunnel)	1.0497677		
Tot E(TS)	-611.88733				
<hr/>					
Beta C	LJ	Area	k(1/s)	k(1/M s)	k(VTST)
1	1.948E+09	0.0471	8.67E-03	2.91E-01	3.06E-01
0.8	1.559E+09	0.0377	6.94E-03	2.33E-01	2.45E-01
0.6	1.169E+09	0.0283	5.21E-03	1.75E-01	1.84E-01
0.4	779305731	0.0188	3.46E-03	1.16E-01	1.22E-01
0.2	389652866	0.0094	1.73E-03	5.82E-02	6.11E-02

1997/QCISD
T=700 K

Bond dist	3.12A	Act En			
Energy(react)	-611.92393	Hartrees	kcal/mol	kJ/mol	cm-1
TH Corr	0.007829	0.0312031	19.580242	6846.2383	81.92227
Tot E(react)	-611.9161	Q2	exp(-Ea/RT)		
Energy (TS) =	-611.89044	1	7.696E-07		
TH Corr	0.005542	k(tunnel)	1.0156869		
Tot E(TS)	-611.8849				
<hr/>					
Beta C	LJ	Area	k(1/s)	k(1/M s)	k(VTST)
1	1.257E+09	0.075	1.73E+03	5.81E+04	5.90E+04
0.8	1.006E+09	0.06	1.38E+03	4.64E+04	4.72E+04
0.6	754313143	0.045	1.04E+03	3.48E+04	3.54E+04
0.4	502875428	0.03	6.91E+02	2.32E+04	2.36E+04
0.2	251437714	0.015	3.46E+02	1.16E+04	1.18E+04

1997/QCISD
T=1000 K

Bond dist	3.12A	Act En			
Energy(react)	-611.92393	Hartrees	kcal/mol	kJ/mol	cm-1
TH Corr	0.011133	0.0302741	18.997285	6642.4075	79.483224
Tot E(react)	-611.9128	Q2	exp(-Ea/RT)		
Energy (TS) =	-611.89044	1	7.044E-05		
TH Corr	0.007917	k(tunnel)	1.0076866		
Tot E(TS)	-611.88253				
<hr/>					
Beta C	LJ	Area	k(1/s)	k(1/M s)	k(VTST)
1	749858000	0.0689	1.45E+05	4.88E+06	4.92E+06
0.8	599886400	0.0552	1.16E+05	3.91E+06	3.94E+06
0.6	449914800	0.0414	8.73E+04	2.93E+06	2.96E+06
0.4	299943200	0.0276	5.82E+04	1.96E+06	1.97E+06
0.2	149971600	0.0138	2.91E+04	9.78E+05	9.85E+05

1997/QCISD
T=1500 K

Bond dist	3.12A	Act En			
Energy(react)	-611.92393	Hartrees	kcal/mol	kJ/mol	cm-1
TH Corr	0.016659	0.0287071	18.013978	6298.5937	75.369139
Tot E(react)	-611.90727	Q2	exp(-Ea/RT)		
Energy (TS) =	-611.89044	1	0.0023722		
TH Corr	0.011876	k(tunnel)	1.0034163		
Tot E(TS)	-611.87857				
<hr/>					
Beta C	LJ	Area	k(1/s)	k(1/M s)	k(VTST)
1	691344081	0.0873	6.20E+06	2.08E+08	2.09E+08
0.8	553075265	0.0699	4.96E+06	1.67E+08	1.67E+08
0.6	414806449	0.0524	3.72E+06	1.25E+08	1.25E+08
0.4	276537632	0.0349	2.48E+06	8.33E+07	8.36E+07
0.2	138268816	0.0175	1.24E+06	4.18E+07	4.19E+07



1997/B3LYP

$\beta_c=0.1$

Freq(react)	Qvib	Freq (TS)	Qvib	Act En	wavenumbers	kcal/mol
84.3248	2.98839515	-237.3599		0.1353787	29703.29383	84.95142035
84.3248	2.98839515	96.6409	2.68049576			kJ/mol
319.3017	1.27195247	227.4371	1.49982589			355.4304019
373.0301	1.19749695					
E(react)	E (TS)		Q(react)	Q (TS)		
-1073.5977	-1073.4605	trans	176236000	176236000		
0.006585	0.004831	rot	2315.81	303403		
-1073.5911	-1073.4557					
T	ZLJ[M]		Area (P=760 torr)	exp(-Ea/RT)	k predicted	(1/s)
298	308484674		820.1128	4.9253E-63	1.16648E-48	

Freq(react)	Qvib	Freq (TS)	Qvib	Act En	wavenumbers	kcal/mol
84.3248	6.28013932	-237.3599		0.1336567	29325.47167	83.87084899
84.3248	6.28013932	96.6409	5.54745574			
319.3017	2.07700844	227.4371	2.6765354			
373.0301	1.86667464					
E(react)	E (TS)		Q(react)	Q (TS)		
-1073.5977	-1073.4605	trans	1488510000	1488510000		
0.014607	0.011131	rot	5437.09	1091480		
-1073.583	-1073.4494					
T	ZLJ[M]	Area (P=760 torr)	exp(-Ea/RT)	k predicted	(1/s)	
700	148529809	3916.8858	6.4889E-27	7.3399E-12		

Freq(react)	Qvib	Freq (TS)	Qvib	Act En	wavenumbers	kcal/mol
84.3248	8.74681948	-237.3599		0.1322767	29022.68737	83.00488588
84.3248	8.74681948	96.6409	7.69859461			
319.3017	2.71341766	227.4371	3.58108794			
373.0301	2.40647937					
E(react)	E (TS)		Q(react)	Q (TS)		
-1073.5977	-1073.4605	trans	3630840000	3630840000		
0.020723	0.015867	rot	7767.27	1863660		
-1073.5769	-1073.4447					
T	ZLJ[M]	Area (P=760 torr)	exp(-Ea/RT)	k predicted	(1/s)	
1000	114546405	6624.9978	7.2077E-19	0.00137897		
<hr/>						
Freq(react)	Qvib	Freq (TS)	Qvib	Act En	wavenumbers	kcal/mol
84.3248	12.8618011	-237.3599		0.1299367	28509.27051	81.53651365
84.3248	12.8618011	96.6409	11.2882339			
319.3017	3.78836307	227.4371	5.09895046			
373.0301	3.32267916					
E(react)	E (TS)		Q(react)	Q (TS)		
-1073.5977	-1073.4605	trans	1.0005E+10	1.0005E+10		
0.030969	0.023773	rot	11650.9	3423770		
-1073.5667	-1073.4367					
T	ZLJ[M]	Area (P=760 torr)	exp(-Ea/RT)	k predicted	(1/s)	
1500	85887860.2	10706.7638	1.3157E-12	4068.08235		
<hr/>						
Freq(react)	Qvib	Freq (TS)	Qvib	Act En	wavenumbers	kcal/mol
84.3248	16.9784676	-237.3599		0.1275797	27992.12369	80.05747376
84.3248	16.9784676	96.6409	14.8798037			
319.3017	4.86962213	227.4371	6.62133512			
373.0301	4.24622489					
E(react)	E (TS)		Q(react)	Q (TS)		
-1073.5977	-1073.4605	trans	2.0539E+10	2.0539E+10		
0.041238	0.031685	rot	15534.5	5271230		
-1073.5564	-1073.4288					
T	ZLJ[M]	Area (P=760 torr)	exp(-Ea/RT)	k predicted	(1/s)	
2000	70306788.6	13985.7579	1.7824E-09	7198865.63		

1997/B3LYP

 $\beta_c=0.3$

Freq(react)	Qvib	Freq (TS)	Qvib	Act En	cm ⁻¹	kcal/mol
84.3248	2.9883952	-237.3599		0.1353787	29703.2938	84.95142
84.3248	2.9883952	96.6409	2.6804958			kJ/mol
319.3017	1.2719525	227.4371	1.4998259			355.4304
373.0301	1.197497					
E(react)	E (TS)		Q(react)	Q (TS)		
-1073.5977	-1073.4605	trans	176236000	176236000		
0.006585	0.004831	rot	2315.81	303403		
-1073.5911	-1073.4557					
T	ZLJ[M]		Area	exp(-Ea/RT)	k predicted	(1/s)
298	925454023		893.9113	4.97E-63	1.28E-48	
<hr/>						
Freq(react)	Qvib	Freq (TS)	Qvib	Act En	cm ⁻¹	kcal/mol
84.3248	6.2801393	-237.3599		0.1336567	29325.4717	83.870849
84.3248	6.2801393	96.6409	5.5474557			kJ/mol
319.3017	2.0770084	227.4371	2.6765354			350.90937
373.0301	1.8666746					
E(react)	E (TS)		Q(react)	Q (TS)		
-1073.5977	-1073.4605	trans	1.489E+09	1.489E+09		
0.014607	0.011131	rot	5437.09	1091480		
-1073.583	-1073.4494					
T	ZLJ[M]	Area	exp(-Ea/RT)	k predicted	(1/s)	
700	445589428	5629.167	6.51E-27	1.06E-11		

Freq(react)	Qvib	Freq (TS)	Qvib	Act En	cm ⁻¹	kcal/mol
84.3248	8.7468195	-237.3599		0.1322767	29022.6874	83.004886
84.3248	8.7468195	96.6409	7.6985946			kJ/mol
319.3017	2.7134177	227.4371	3.5810879			347.286
373.0301	2.4064794					
E(react)	E (TS)		Q(react)	Q (TS)		
-1073.5977	-1073.4605	trans	3.631E+09	3.631E+09		
0.020723	0.015867	rot	7767.27	1863660		
-1073.5769	-1073.4447					
T	ZLJ[M]	Area	exp(-Ea/RT)	k predicted	(1/s)	
1000	343639216	11093.5265	7.23E-19	0.0023154		
<hr/>						
Freq(react)	Qvib	Freq (TS)	Qvib	Act En	cm ⁻¹	kcal/mol
84.3248	12.861801	-237.3599		0.1299367	28509.2705	81.536514
84.3248	12.861801	96.6409	11.288234			kJ/mol
319.3017	3.7883631	227.4371	5.0989505			341.143
373.0301	3.3226792					
E(react)	E (TS)		Q(react)	Q (TS)		
-1073.5977	-1073.4605	trans	1.00E+10	1.00E+10		
0.030969	0.023773	rot	11650.9	3423770		
-1073.5667	-1073.4367					
T	ZLJ[M]	Area	exp(-Ea/RT)	k predicted	(1/s)	
1500	257663581	21183.2252	1.32E-12	8062.9824		
<hr/>						
Freq(react)	Qvib	Freq (TS)	Qvib	Act En	cm ⁻¹	kcal/mol
84.3248	16.978468	-237.3599		0.1275797	27992.1237	80.057474
84.3248	16.978468	96.6409	14.879804			kJ/mol
319.3017	4.8696221	227.4371	6.6213351			334.954
373.0301	4.2462249					
E(react)	E (TS)		Q(react)	Q (TS)		
-1073.5977	-1073.4605	trans	2.05E+10	2.05E+10		
0.041238	0.031685	rot	15534.5	5271230		
-1073.5564	-1073.4288					
T	ZLJ[M]	Area	exp(-Ea/RT)	k predicted	(1/s)	
2000	210920366	30655.535	1.78E-09	15799944		

1997/B3LYP **$\beta_c=0.7$**

Freq(react)	Qvib	Freq (TS)	Qvib	Act En	cm ⁻¹	kcal/mol
84.3248	2.9883952	-237.3599		0.1353787	29703.2938	84.95142
84.3248	2.9883952	96.6409	2.6804958			kJ/mol
319.3017	1.2719525	227.4371	1.4998259			355.4304
373.0301	1.197497					
E(react)	E (TS)		Q(react)	Q (TS)		
-1073.5977	-1073.4605	trans	176236000	176236000		
0.006585	0.004831	rot	2315.81	303403		
-1073.5911	-1073.4557					
T	ZLJ[M]		Area	exp(-Ea/RT)	k predicted	(1/s)
298	2.159E+09		920.2995	4.97E-63	1.32E-48	
<hr/>						
Freq(react)	Qvib	Freq (TS)	Qvib	Act En	cm ⁻¹	kcal/mol
84.3248	6.2801393	-237.3599		0.1336567	29325.4717	83.870849
84.3248	6.2801393	96.6409	5.5474557			kJ/mol
319.3017	2.0770084	227.4371	2.6765354			350.90937
373.0301	1.8666746					
E(react)	E (TS)		Q(react)	Q (TS)		
-1073.5977	-1073.4605	trans	1.489E+09	1488510000		
0.014607	0.011131	rot	5437.09	1091480		
-1073.583	-1073.4494					
T	ZLJ[M]	Area	exp(-Ea/RT)	k predicted	(1/s)	
700	1.04E+09	6.68E+03	6.51E-27	1.2576E-11		

Freq(react)	Qvib	Freq (TS)	Qvib	Act En	cm ⁻¹	kcal/mol
84.3248	8.7468195	-237.3599		0.1322767	29022.6874	83.004886
84.3248	8.7468195	96.6409	7.6985946			KJ/mol
319.3017	2.7134177	227.4371	3.5810879			347.28625
373.0301	2.4064794					
E(react)	E (TS)		Q(react)	Q (TS)		
-1073.5977	-1073.4605	trans	3.631E+09	3630840000		
0.020723	0.015867	rot	7767.27	1863660		
-1073.5769	-1073.4447					
T	ZLJ[M]	Area	exp(-Ea/RT)	k predicted	(1/s)	
1000	801824838	1.47E+04	7.227E-19	0.00305796		
<hr/>						
Freq(react)	Qvib	Freq (TS)	Qvib	Act En	cm ⁻¹	kcal/mol
84.3248	12.861801	-237.3599		0.1299367	28509.2705	81.536514
84.3248	12.861801	96.6409	11.288234			KJ/mol
319.3017	3.7883631	227.4371	5.0989505			341.14269
373.0301	3.3226792					
E(react)	E (TS)		Q(react)	Q (TS)		
-1073.5977	-1.07E+03	trans	1.001E+10	1.0005E+10		
0.030969	0.023773	rot	11650.9	3423770		
-1073.5667	-1073.4367					
T	ZLJ[M]	Area	exp(-Ea/RT)	k predicted	(1/s)	
1500	601215021	3.20E+04	1.318E-12	12196.3794		
<hr/>						
Freq(react)	Qvib	Freq (TS)	Qvib	Act En	cm ⁻¹	kcal/mol
84.3248	16.978468	-237.3599		0.1275797	27992.1237	80.057474
84.3248	16.978468	96.6409	14.879804			KJ/mol
319.3017	4.8696221	227.4371	6.6213351			334.95449
373.0301	4.2462249					
E(react)	E (TS)		Q(react)	Q (TS)		
-1073.5977	-1.07E+03	trans	2.054E+10	2.0539E+10		
0.041238	0.031685	rot	15534.5	5271230		
-1073.5564	-1073.4288					
T	ZLJ[M]	Area	exp(-Ea/RT)	k predicted	(1/s)	
2000	492147520	5.09E+04	1.785E-09	26217599		

1997/B3LYP **$\beta_c=1.0$**

Freq(react)	Qvib	Freq (TS)	Qvib	Act En	cm ⁻¹	kcal/mol
84.3248	2.9883952	-237.3599		0.1353787	29703.2938	84.95142
84.3248	2.9883952	96.6409	2.6804958			kJ/mol
319.3017	1.2719525	227.4371	1.4998259			355.4304
373.0301	1.197497					
E(react)	E (TS)		Q(react)	Q (TS)		
-1073.5977	-1073.4605	trans	176236000	176236000		
0.006585	0.004831	rot	2315.81	303403		
-1073.5911	-1073.4557					
T	ZLJ[M]		Area	exp(-Ea/RT)	k predicted	(1/s)
298	3.085E+09		926.6999	4.97E-63	1.33E-48	
<hr/>						
Freq(react)	Qvib	Freq (TS)	Qvib	Act En	cm ⁻¹	kcal/mol
84.3248	6.2801393	-237.3599		0.1336567	29325.4717	83.870849
84.3248	6.2801393	96.6409	5.5474557			kJ/mol
319.3017	2.0770084	227.4371	2.6765354			350.90937
373.0301	1.8666746					
E(react)	E (TS)		Q(react)	Q (TS)		
-1073.5977	-1073.4605	trans	1.489E+09	1488510000		
0.014607	0.011131	rot	5437.09	1091480		
-1073.583	-1073.4494					
T	ZLJ[M]	Area	exp(-Ea/RT)	k predicted	(1/s)	
700	1.485E+09		7.02E+03	6.5144E-27	1.321E-11	

Freq(react)	Qvib	Freq (TS)	Qvib	Act En	cm⁻¹	kcal/mol
84.3248	8.7468195	-237.3599		0.1322767	29022.6874	83.004886
84.3248	8.7468195	96.6409	7.6985946			KJ/mol
319.3017	2.7134177	227.4371	3.5810879			347.28625
373.0301	2.4064794					
E(react)	E (TS)		Q(react)	Q (TS)		
-1073.5977	-1073.4605	trans	3.631E+09	3630840000		
0.020723	0.015867	rot	7767.27	1863660		
-1073.5769	-1073.4447					
T	ZLJ[M]	Area	exp(-Ea/RT)	k predicted	(1/s)	
1000	1.145E+09		15988.715	7.2272E-19	0.00333705	
<hr/>						
Freq(react)	Qvib	Freq (TS)	Qvib	Act En	cm⁻¹	kcal/mol
84.3248	12.861801	-237.3599		0.1299367	28509.2705	81.536514
84.3248	12.861801	96.6409	11.288234			KJ/mol
319.3017	3.7883631	227.4371	5.0989505			341.14269
373.0301	3.3226792					
E(react)	E (TS)		Q(react)	Q (TS)		
-1073.5977	-1073.4605	trans	1.001E+10	1.0005E+10		
0.030969	0.023773	rot	11650.9	3423770		
-1073.5667	-1073.4367					
T	ZLJ[M]	Area	exp(-Ea/RT)	k predicted	(1/s)	
1500	858878602		36936.168	1.318E-12	14059.0335	
<hr/>						
Freq(react)	Qvib	Freq (TS)	Qvib	Act En	cm⁻¹	kcal/mol
84.3248	16.978468	-237.3599		0.1275797	27992.1237	80.057474
84.3248	16.978468	96.6409	14.879804			KJ/mol
319.3017	4.8696221	227.4371	6.6213351			334.95449
373.0301	4.2462249					
E(react)	E (TS)		Q(react)	Q (TS)		
-1073.5977	-1073.4605	trans	2.054E+10	2.0539E+10		
0.041238	0.031685	rot	15534.5	5271230		
-1073.5564	-1073.4288					
T	ZLJ[M]	Area	exp(-Ea/RT)	k predicted	(1/s)	
2000	703067886		61066.579	1.7847E-09	31473876.2	

1992/B3LYP **$\beta_c=0.1$**

Freq(react)	Qvib	Freq (TS)	Qvib	Act En	cm ⁻¹	kcal/mol
92.6702	2.7706816	-247.4352		0.1276792	28013.9549	80.119911
92.6702	2.7706816	105.3072	2.5076895			KJ/mol
318.5398	1.2732294	222.0807	1.5197403			335.21573
374.4751	1.1958538					
E(react)	E (TS)		Q(react)	Q (TS)		
-1074.3106	-1074.1811	trans	176236000	176236000		
0.006592	0.00483	rot	2312.65	303224		
-1074.304	-1074.1763				k predicted	
T	ZLJ[M]		Area	exp(-Ea/RT)	(1/s)	k(1/Ms)
298	308484674		751.5	1.72E-59	4.35E-45	1.065E-43

Freq(react)	Qvib	Freq (TS)	Qvib	Act En	cm ⁻¹	kcal/mol
92.6702	5.7623388	-247.4352		0.1259632	27637.4492	79.043105
92.6702	5.7623388	105.3072	5.1349177			KJ/mol
318.5398	2.0805226	222.0807	2.7271864			330.71045
374.4751	1.8618859					
E(react)	E (TS)		Q(react)	Q (TS)		
-1074.3106	-1074.1811	trans	1.489E+09	1488510000		
0.014609	0.011131	rot	5429.68	1090830		
-1074.296	-1074.17				k predicted	
T	ZLJ[M]		Area	exp(-Ea/RT)	(1/s)	k(1/Ms)
700	148529809		3.23E+03	2.095E-25	2.28E-10	1.307E-08

Freq(react)	Qvib	Freq (TS)	Qvib	Act En	cm⁻¹	kcal/mol
92.6702	8.0060648	-247.4352		0.1245832	27334.6649	78.177142
92.6702	8.0060648	105.3072	7.1081759			kJ/mol
318.5398	2.7185301	222.0807	3.6541049			327.08732
374.4751	2.3994655					
E(react)	E (TS)		Q(react)	Q (TS)		
-1074.3106	-1074.1811	trans	3.631E+09	3630840000		
0.020725	0.015867	rot	7756.68	1862570		
-1074.2898	-1074.1653				k predicted	
T	ZLJ[M]		Area	exp(-Ea/RT)	(1/s)	k(1/Ms)
1000	114546405		5241.8	8.2053E-18	1.45E-02	1.1870871
<hr/>						
Freq(react)	Qvib	Freq (TS)	Qvib	Act En	cm⁻¹	kcal/mol
92.6702	11.749836	-247.4352		0.1222432	26821.248	76.708769
92.6702	11.749836	105.3072	10.401741			kJ/mol
318.5398	3.7961067	222.0807	5.2090074			320.94377
374.4751	3.3120169					
E(react)	E (TS)		Q(react)	Q (TS)		
-1074.3106	-1074.1811	trans	1.001E+10	1.0005E+10		
0.030971	0.023773	rot	11635	3421750		
-1074.2796	-1074.1573				k predicted	
T	ZLJ[M]		Area	exp(-Ea/RT)	(1/s)	k(1/Ms)
1500	85887860		8138.4	6.658E-12	1.82E+04	2243261.1
<hr/>						
Freq(react)	Qvib	Freq (TS)	Qvib	Act En	cm⁻¹	kcal/mol
92.6702	15.495458	-247.4352		0.1198872	26304.3206	75.230357
92.6702	15.495458	105.3072	13.697409			kJ/mol
318.5398	4.8799823	222.0807	6.7683267			314.7582
374.4751	4.2319418					
E(react)	E (TS)		Q(react)	Q (TS)		
-1074.3106	-1074.1811	trans	2.054E+10	2.0539E+10		
0.041239	0.031685	rot	15513.4	5268130		
-1074.2693	-1074.1494				k predicted	
T	ZLJ[M]		Area	exp(-Ea/RT)	(1/s)	k(1/Ms)
2000	70306789		10384.4	6.0126E-09	2.10E+07	3.447E+09

1992/B3LYP

$\beta_c=0.3$

Freq(react)	Qvib	Freq (TS)	Qvib	Act En	cm ⁻¹	kcal/mol
92.6702	2.7706816	-247.4352		0.1276792	28013.9549	80.119911
92.6702	2.7706816	105.3072	2.5076895			kJ/mol
318.5398	1.2732294	222.0807	1.5197403			335.21573
374.4751	1.1958538					
E(react)	E (TS)		Q(react)	Q (TS)		
-1074.3106	-1074.1811	trans	176236000	176236000		
0.006592	0.00483	rot	2312.65	303224		
-1074.304	-1074.1763					
T	ZLJ[M]		Area	exp(-Ea/RT)	k predicted	(1/s)
298	925454023		834	1.72E-59	4.83E-45	
<hr/>						
Freq(react)	Qvib	Freq (TS)	Qvib	Act En	cm ⁻¹	kcal/mol
92.6702	5.7623388	-247.4352		0.1259632	27637.4492	79.043105
92.6702	5.7623388	105.3072	5.1349177			kJ/mol
318.5398	2.0805226	222.0807	2.7271864			330.71045
374.4751	1.8618859					
E(react)	E (TS)		Q(react)	Q (TS)		
-1074.3106			-1074.1811	trans	1488510000	1.489E+09
0.014609			0.011131	rot	5429.68	1090830
-1074.296			-1074.17			
T	ZLJ[M]		Area	exp(-Ea/RT)	k predicted	(1/s)
700	445589428		4.84E+03	2.0873E-25	3.39E-10	

Freq(react)	Qvib	Freq (TS)	Qvib	Act En	cm ⁻¹	kcal/mol
92.6702	8.0060648	-247.4352		0.1245832	27334.6649	78.177142
92.6702	8.0060648	105.3072	7.1081759			kJ/mol
318.5398	2.7185301	222.0807	3.6541049			327.08732
374.4751	2.3994655					
E(react)	E (TS)		Q(react)	Q (TS)		
-1074.3106	-1074.1811	trans	3.631E+09	3630840000		
0.020725	0.015867	rot	7756.68	1862570		
-1074.2898	-1074.1653					
T	ZLJ[M]		Area	exp(-Ea/RT)	k predicted	(1/s)
1000	343639216		9158.4	8.1843E-18	2.52E-02	
<hr/>						
Freq(react)	Qvib	Freq (TS)	Qvib	Act En	cm ⁻¹	kcal/mol
92.6702	11.749836	-247.4352		0.1222432	26821.248	76.708769
92.6702	11.749836	105.3072	10.401741			kJ/mol
318.5398	3.7961067	222.0807	5.2090074			320.94377
374.4751	3.3120169					
E(react)	E (TS)		Q(react)	Q (TS)		
-1074.3106	-1074.1811	trans	1.001E+10	1.0005E+10		
0.030971	0.023773	rot	11635	3421750		
-1074.2796	-1074.1573					
T	ZLJ[M]		Area	exp(-Ea/RT)	k predicted	(1/s)
1500	257663581		16720.9	6.6468E-12	3.74E+04	
<hr/>						
Freq(react)	Qvib	Freq (TS)	Qvib	Act En	cm ⁻¹	kcal/mol
92.6702	15.495458	-247.4352		0.1198872	26304.3206	75.230357
92.6702	15.495458	105.3072	13.697409			kJ/mol
318.5398	4.8799823	222.0807	6.7683267			314.7582
374.4751	4.2319418					
E(react)	E (TS)		Q(react)	Q (TS)		
-1074.3106	-1074.1811	trans	2.054E+10	2.0539E+10		
0.041239	0.031685	rot	15513.4	5268130		
-1074.2693	-1074.1494					
T	ZLJ[M]		Area	exp(-Ea/RT)	k predicted	(1/s)
2000	210920366		23508.3	6.0052E-09	4.75E+07	

1992/B3LYP **$\beta_c=0.7$**

Freq(react)	Qvib	Freq (TS)	Qvib	Act En	cm ⁻¹	kcal/mol
92.6702	2.7706816	-247.4352		0.1276792	28013.9549	80.119911
92.6702	2.7706816	105.3072	2.5076895			kJ/mol
318.5398	1.2732294	222.0807	1.5197403			335.21573
374.4751	1.1958538					
E(react)	E (TS)		Q(react)	Q (TS)		
-1074.3106	-1074.1811	trans	176236000	176236000		
0.006592	0.00483	rot	2312.65	303224		
-1074.304	-1074.1763					
T	ZLJ[M]		Area	exp(-Ea/RT)	k predicted	(1/s)
298	2.159E+09		864.7	1.72E-59	5.01E-45	
<hr/>						
Freq(react)	Qvib	Freq (TS)	Qvib	Act En	cm ⁻¹	kcal/mol
92.6702	5.7623388	-247.4352		0.1259632	27637.4492	79.043105
92.6702	5.7623388	105.3072	5.1349177			kJ/mol
318.5398	2.0805226	222.0807	2.7271864			330.71045
374.4751	1.8618859					
E(react)	E (TS)		Q(react)	Q (TS)		
-1074.3106	-1074.1811	trans	1.489E+09	1488510000		
0.014609	0.011131	rot	5429.68	1090830		
-1074.296	-1074.17					
T	ZLJ[M]		Area	exp(-Ea/RT)	k predicted	(1/s)
700	1.04E+09		5.91E+03	2.0873E-25	4.15E-10	

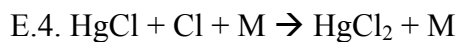
Freq(react)	Qvib	Freq (TS)	Qvib	Act En	cm⁻¹	kcal/mol
92.6702	8.0060648	-247.4352		0.1245832	27334.6649	78.177142
92.6702	8.0060648	105.3072	7.1081759			KJ/mol
318.5398	2.7185301	222.0807	3.6541049			327.08732
374.4751	2.3994655					
E(react)	E (TS)		Q(react)	Q (TS)		
-1074.3106	-1074.1811	trans	3.631E+09	3630840000		
0.020725	0.015867	rot	7756.68	1862570		
-1074.2898	-1074.1653					
T	ZLJ[M]		Area	exp(-Ea/RT)	k predicted	(1/s)
1000	801824838		12523.9	8.1843E-18	3.45E-02	
<hr/>						
Freq(react)	Qvib	Freq (TS)	Qvib	Act En	cm⁻¹	kcal/mol
92.6702	11.749836	-247.4352		0.1222432	26821.248	76.708769
92.6702	11.749836	105.3072	10.401741			KJ/mol
318.5398	3.7961067	222.0807	5.2090074			320.94377
374.4751	3.3120169					
E(react)	E (TS)		Q(react)	Q (TS)		
-1074.3106			-1074.1811	trans	1.0005E+10	1.001E+10
0.030971			0.023773	rot	11635	3421750
-1074.2796			-1074.1573			
T	ZLJ[M]		Area	exp(-Ea/RT)	k predicted	(1/s)
1500	601215021		26209.6	6.6468E-12	58593.8477	
<hr/>						
Freq(react)	Qvib	Freq (TS)	Qvib	Act En	cm⁻¹	kcal/mol
92.6702	15.495458	-247.4352		0.1198872	26304.3206	75.230357
92.6702	15.495458	105.3072	13.697409			KJ/mol
318.5398	4.8799823	222.0807	6.7683267			314.7582
374.4751	4.2319418					
E(react)	E (TS)		Q(react)	Q (TS)		
-1074.3106	-1074.1811	trans	2.054E+10	2.0539E+10		
0.041239	0.031685	rot	15513.4	5268130		
-1074.2693	-1074.1494					
T	ZLJ[M]		Area	exp(-Ea/RT)	k predicted	(1/s)
2000	492147520		40313	6.0052E-09	81423487.1	

1992/B3LYP

 $\beta_c=1.0$

Freq(react)	Qvib	Freq (TS)	Qvib	Act En	cm ⁻¹	kcal/mol
92.6702	2.7706816	-247.4352		0.1276792	28013.9549	80.119911
92.6702	2.7706816	105.3072	2.5076895			kJ/mol
318.5398	1.2732294	222.0807	1.5197403			335.21573
374.4751	1.1958538					
E(react)	E (TS)		Q(react)	Q (TS)		
-1074.3106	-1074.1811	trans	176236000	176236000		
0.006592	0.00483	rot	2312.65	303224		
-1074.304	-1074.1763					
T	ZLJ[M]		Area	exp(-Ea/RT)	k predicted	(1/s)
298	3.085E+09		872.3	1.72E-59	5.05E-45	
<hr/>						
Freq(react)	Qvib	Freq (TS)	Qvib	Act En	cm ⁻¹	kcal/mol
92.6702	5.7623388	-247.4352		0.1259632	27637.4492	79.043105
92.6702	5.7623388	105.3072	5.1349177			kJ/mol
318.5398	2.0805226	222.0807	2.7271864			330.71045
374.4751	1.8618859					
E(react)	E (TS)		Q(react)	Q (TS)		
-1074.3106	-1074.1811	trans	1.489E+09	1488510000		
0.014609	0.011131	rot	5429.68	1090830		
-1074.296	-1074.17					
T	ZLJ[M]		Area	exp(-Ea/RT)	k predicted	(1/s)
700	1.485E+09		6.27E+03	2.0873E-25	4.40E-10	

Freq(react)	Qvib	Freq (TS)	Qvib	Act En	cm⁻¹	kcal/mol
92.6702	8.0060648	-247.4352		0.1245832	27334.6649	78.177142
92.6702	8.0060648	105.3072	7.1081759			kJ/mol
318.5398	2.7185301	222.0807	3.6541049			327.08732
374.4751	2.3994655					
E(react)	E (TS)		Q(react)	Q (TS)		
-1074.3106	-1074.1811	trans	3.631E+09	3630840000		
0.020725	0.015867	rot	7756.68	1862570		
-1074.2898	-1074.1653					
T	ZLJ[M]		Area	exp(-Ea/RT)	k predicted	(1/s)
1000	1.145E+09		13857.3	8.1843E-18	3.81E-02	
<hr/>						
Freq(react)	Qvib	Freq (TS)	Qvib	Act En	cm⁻¹	kcal/mol
92.6702	11.749836	-247.4352		0.1222432	26821.248	76.708769
92.6702	11.749836	105.3072	10.401741			kJ/mol
318.5398	3.7961067	222.0807	5.2090074			320.94377
374.4751	3.3120169					
E(react)	E (TS)		Q(react)	Q (TS)		
-1074.3106	-1074.1811	trans	1.001E+10	1.0005E+10		
0.030971	0.023773	rot	11635	3421750		
-1074.2796	-1074.1573					
T	ZLJ[M]		Area	exp(-Ea/RT)	k predicted	(1/s)
1500	858878602		30695.2	6.6468E-12	68621.7979	
<hr/>						
Freq(react)	Qvib	Freq (TS)	Qvib	Act En	cm⁻¹	kcal/mol
92.6702	15.495458	-247.4352		0.1198872	26304.3206	75.230357
92.6702	15.495458	105.3072	13.697409			kJ/mol
318.5398	4.8799823	222.0807	6.7683267			314.7582
374.4751	4.2319418					
E(react)	E (TS)		Q(react)	Q (TS)		
-1074.3106	-1074.1811	trans	2.054E+10	2.0539E+10		
0.041239	0.031685	rot	15513.4	5268130		
-1074.2693	-1074.1494					
T	ZLJ[M]		Area	exp(-Ea/RT)	k predicted	(1/s)
2000	703067886		49156.6	6.0052E-09	99285634.5	



Transition Structure: Hg-Cl 2.35Å, Cl-Cl 4.2 Å
1997/B3LYP
 $\beta_c=0.1$

Freq(react)	Qvib	Freq (TS)	Qvib	Act En	cm ⁻¹	kcal/mol
84.3248	2.9883952	-91.3067		0.1236215	27123.6593	77.573666
84.3248	2.9883952	27.1245	8.1415994			kJ/mol
319.3017	1.2719525	27.1834	8.1250892			324.56243
373.0301	1.197497	320.1569	1.2705278			
E(react)	E (TS)		Q(react)	Q (TS)		
-1073.5977	-1073.4728	trans	176236000	176236000		
0.006585	0.005376	rot	9767.47	303403		
-1073.5911	-1073.4674				k(tunnel)	1.0081259
T	ZLJ[M]		Area	exp(-Ea/RT)	k predicted	(1/s)
298	260435556		3922.9	1.27E-57	3.41E-43	

Freq(react)	Qvib	Freq (TS)	Qvib	Act En	cm ⁻¹	kcal/mol
84.3248	6.2801393	-91.3067		0.1224965	26876.8243	76.867717
84.3248	6.2801393	27.1245	18.429069			kJ/mol
319.3017	2.0770084	27.1834	18.390241			321.60879
373.0301	1.8666746	320.1569	2.0730846			
E(react)	E (TS)		Q(react)	Q (TS)		
-1073.5977	-1073.4728	trans	1.489E+09	176236000		
0.014607	0.012273	rot	22932.2	303403		
-1073.583	-1073.4606				k(tunnel)	1.0014727
T	ZLJ[M]		Area	exp(-Ea/RT)	k predicted	(1/s)
700	129116664		8.22E+03	9.9731E-25	2.13E-11	

Freq(react)	Qvib	Freq (TS)	Qvib	Act En	cm ⁻¹	kcal/mol
84.3248	8.7468195	-91.3067		0.1215815	26676.0651	76.293546
84.3248	8.7468195	27.1245	26.109569			kJ/mol
319.3017	2.7134177	27.1834	26.054093			319.2065
373.0301	2.4064794	320.1569	2.7077087			
E(react)	E (TS)		Q(react)	Q (TS)		
-1073.5977	-1073.4728	trans	3.631E+09	176236000		
0.020723	0.017474	rot	32760.2	303403		
-1073.5769	-1073.4554				k(tunnel)	1.0007216
T	ZLJ[M]		Area	exp(-Ea/RT)	k predicted	(1/s)
1000	94928520		9808.2	2.1119E-17	1.15E-04	
Freq(react)	Qvib	Freq (TS)	Qvib	Act En	cm ⁻¹	kcal/mol
84.3248	12.861801	-91.3067		0.1155015	25342.0589	72.478289
84.3248	12.861801	27.1245	38.911641			kJ/mol
319.3017	3.7883631	27.1834	38.828421			303.24375
373.0301	3.3226792	320.1569	3.7797154			
E(react)	E (TS)		Q(react)	Q (TS)		
-1073.5977	-1073.4728	trans	1.001E+10	176236000		
0.030969	0.02164	rot	49140.4	303403		
-1073.5667	-1073.4512				k(tunnel)	1.0003207
T	ZLJ[M]		Area	exp(-Ea/RT)	k predicted	(1/s)
1500	71002906		10865	2.7482E-11	26.5457464	
Freq(react)	Qvib	Freq (TS)	Qvib	Act En	cm ⁻¹	kcal/mol
84.3248	16.978468	-91.3067		0.1184565	25990.4123	74.332579
84.3248	16.978468	27.1245	51.714256			kJ/mol
319.3017	4.8696221	27.1834	51.603294			311.00196
373.0301	4.2462249	320.1569	4.8580523			
E(react)	E (TS)		Q(react)	Q (TS)		
-1073.5977	-1073.4728	trans	2.054E+10	176236000		
0.041238	0.034864	rot	65520.5	303403		
-1073.5564	-1073.438				k(tunnel)	1.0001804
T	ZLJ[M]		Area	exp(-Ea/RT)	k predicted	(1/s)
2000	58034116		13641	7.5273E-09	2391.74733	

Transition Structure: Hg-Cl 2.35 Å, Cl-Cl 4.2 Å

1997/B3LYP

$\beta_c=0.3$

Freq(react)	Qvib	Freq (TS)	Qvib	Act En	cm ⁻¹	kcal/mol
84.3248	2.9883952	-91.3067		0.1236215	27123.6593	77.573666
84.3248	2.9883952	27.1245	8.1415994			kJ/mol
319.3017	1.2719525	27.1834	8.1250892			324.56243
373.0301	1.197497	320.1569	1.2705278			
E(react)	E (TS)		Q(react)	Q (TS)		
-1073.5977	-1073.4728	trans	176236000	176236000		
0.006585	0.005376	rot	9767.47	303403		
-1073.5911	-1073.4674				k(tunnel)	1.0081259
T	ZLJ[M]		Area	exp(-Ea/RT)	k predicted	(1/s)
298	781306667		7172	1.27E-57	6.23E-43	

Freq(react)	Qvib	Freq (TS)	Qvib	Act En	cm ⁻¹	kcal/mol
84.3248	6.2801393	-91.3067		0.1224965	26876.8243	76.867717
84.3248	6.2801393	27.1245	18.429069			kJ/mol
319.3017	2.0770084	27.1834	18.390241			321.60879
373.0301	1.8666746	320.1569	2.0730846			
E(react)	E (TS)		Q(react)	Q (TS)		
-1073.5977	-1073.4728	trans	1.489E+09	176236000		
0.014607	0.012273	rot	22932.2	303403		
-1073.583	-1073.4606				k(tunnel)	1.0014727
T	ZLJ[M]		Area	exp(-Ea/RT)	k predicted	(1/s)
700	387349992		2.45E+04	3.8763E-27	2.46E-13	

Freq(react)	Qvib	Freq (TS)	Qvib	Act En	cm⁻¹	kcal/mol
84.3248	8.7468195	-91.3067		0.1215815	26676.0651	76.293546
84.3248	8.7468195	27.1245	26.109569			kJ/mol
319.3017	2.7134177	27.1834	26.054093			319.2065
373.0301	2.4064794	320.1569	2.7077087			
E(react)	E (TS)		Q(react)	Q (TS)		
-1073.5977	-1073.4728	trans	3.631E+09	176236000		
0.020723	0.017474	rot	32760.2	303403		
-1073.5769	-1073.4554				k(tunnel)	1.0007216
T	ZLJ[M]		Area	exp(-Ea/RT)	k predicted	(1/s)
1000	284785560		32224	4.339E-19	7.77E-06	
<hr/>						
Freq(react)	Qvib	Freq (TS)	Qvib	Act En	cm⁻¹	kcal/mol
84.3248	12.861801	-91.3067		0.1155015	25342.0589	72.478289
84.3248	12.861801	27.1245	38.911641			kJ/mol
319.3017	3.7883631	27.1834	38.828421			303.24375
373.0301	3.3226792	320.1569	3.7797154			
E(react)	E (TS)		Q(react)	Q (TS)		
-1073.5977	-1073.4728	trans	1.001E+10	176236000		
0.030969	0.02164	rot	49140.4	303403		
-1073.5667	-1073.4512				k(tunnel)	1.0003207
T	ZLJ[M]		Area	exp(-Ea/RT)	k predicted	(1/s)
1500	213008717		38940	2.0615E-12	7.1367696	
<hr/>						
Freq(react)	Qvib	Freq (TS)	Qvib	Act En	cm⁻¹	kcal/mol
84.3248	16.978468	-91.3067		0.1184565	25990.4123	74.332579
84.3248	16.978468	27.1245	51.714256			kJ/mol
319.3017	4.8696221	27.1834	51.603294			311.00196
373.0301	4.2462249	320.1569	4.8580523			
E(react)	E (TS)		Q(react)	Q (TS)		
-1073.5977	-1073.4728	trans	2.054E+10	176236000		
0.041238	0.034864	rot	65520.5	303403		
-1073.5564	-1073.438				k(tunnel)	1.0001804
T	ZLJ[M]		Area	exp(-Ea/RT)	k predicted	(1/s)
2000	174102347		49944	1.0789E-09	1255.18517	

Transition Structure: Hg-Cl 2.35Å, Cl-Cl 4.2 Å

1997/B3LYP

$\beta_c=0.7$

Freq(react)	Qvib	Freq (TS)	Qvib	Act En	cm ⁻¹	kcal/mol
84.3248	2.9883952	-91.3067		0.1236215	27123.6593	77.573666
84.3248	2.9883952	27.1245	8.1415994			kJ/mol
319.3017	1.2719525	27.1834	8.1250892			324.56243
373.0301	1.197497	320.1569	1.2705278			
E(react)	E (TS)		Q(react)	Q (TS)		
-1073.5977	-1073.4728	trans	176236000	176236000		
0.006585	0.005376	rot	9767.47	303403		
-1073.5911	-1073.4674				k(tunnel)	1.0081259
T	ZLJ[M]		Area	exp(-Ea/RT)	k predicted	(1/s)
298	1.823E+09		10303	1.27E-57	8.96E-43	
<hr/>						
Freq(react)	Qvib	Freq (TS)	Qvib	Act En	cm ⁻¹	kcal/mol
84.3248	6.2801393	-91.3067		0.1224965	26876.8243	76.867717
84.3248	6.2801393	27.1245	18.429069			kJ/mol
319.3017	2.0770084	27.1834	18.390241			321.60879
373.0301	1.8666746	320.1569	2.0730846			
E(react)	E (TS)		Q(react)	Q (TS)		
-1073.5977	-1073.4728	trans	1.489E+09	176236000		
0.014607	0.012273	rot	22932.2	303403		
-1073.583	-1073.4606				k(tunnel)	1.0014727
T	ZLJ[M]		Area	exp(-Ea/RT)	k predicted	(1/s)
700	903816648		4.47E+04	3.8763E-27	4.49E-13	

Freq(react)	Qvib	Freq (TS)	Qvib	Act En	cm⁻¹	kcal/mol
84.3248	8.7468195	-91.3067		0.1215815	26676.0651	76.293546
84.3248	8.7468195	27.1245	26.109569			kJ/mol
319.3017	2.7134177	27.1834	26.054093			319.2065
373.0301	2.4064794	320.1569	2.7077087			
E(react)	E (TS)		Q(react)	Q (TS)		
-1073.5977	-1073.4728	trans	3.631E+09	176236000		
0.020723	0.017474	rot	32760.2	303403		
-1073.5769	-1073.4554				k(tunnel)	1.0007216
T	ZLJ[M]		Area	exp(-Ea/RT)	k predicted	(1/s)
1000	664499639		63612	4.339E-19	1.53E-05	
<hr/>						
Freq(react)	Qvib	Freq (TS)	Qvib	Act En	cm⁻¹	kcal/mol
84.3248	12.861801	-91.3067		0.1155015	25342.0589	72.478289
84.3248	12.861801	27.1245	38.911641			kJ/mol
319.3017	3.7883631	27.1834	38.828421			303.24375
373.0301	3.3226792	320.1569	3.7797154			
E(react)	E (TS)		Q(react)	Q (TS)		
-1073.5977	-1073.4728	trans	1.001E+10	176236000		
0.030969	0.02164	rot	49140.4	303403		
-1073.5667	-1073.4512				k(tunnel)	1.0003207
T	ZLJ[M]		Area	exp(-Ea/RT)	k predicted	(1/s)
1500	497020340		82170	2.0615E-12	15.0597935	
<hr/>						
Freq(react)	Qvib	Freq (TS)	Qvib	Act En	cm⁻¹	kcal/mol
84.3248	16.978468	-91.3067		0.1184565	25990.4123	74.332579
84.3248	16.978468	27.1245	51.714256			kJ/mol
319.3017	4.8696221	27.1834	51.603294			311.00196
373.0301	4.2462249	320.1569	4.8580523			
E(react)	E (TS)		Q(react)	Q (TS)		
-1073.5977	-1073.4728	trans	2.054E+10	176236000		
0.041238	0.034864	rot	65520.5	303403		
-1073.5564	-1073.438				k(tunnel)	1.0001804
T	ZLJ[M]		Area	exp(-Ea/RT)	k predicted	(1/s)
2000	406238810		108360	1.0789E-09	2723.28738	

Transition Structure: Hg-Cl 2.35Å, Cl-Cl 4.2 Å
1997/B3LYP

$\beta_c=1.0$

Freq(react)	Qvib	Freq (TS)	Qvib	Act En	cm ⁻¹	kcal/mol
84.3248	2.9883952	-91.3067		0.1236215	27123.6593	77.573666
84.3248	2.9883952	27.1245	8.1415994			kJ/mol
319.3017	1.2719525	27.1834	8.1250892			324.56243
373.0301	1.197497	320.1569	1.2705278			
E(react)	E (TS)		Q(react)	Q (TS)		
-1073.5977	-1073.4728	trans	176236000	176236000		
0.006585	0.005376	rot	9767.47	303403		
-1073.5911	-1073.4674				k(tunnel)	1.0081259
T	ZLJ[M]		Area	exp(-Ea/RT)	k predicted	(1/s)
298	2.604E+09		11685	1.27E-57	1.02E-42	

Freq(react)	Qvib	Freq (TS)	Qvib	Act En	cm ⁻¹	kcal/mol
84.3248	6.2801393	-91.3067		0.1224965	26876.8243	76.867717
84.3248	6.2801393	27.1245	18.429069			kJ/mol
319.3017	2.0770084	27.1834	18.390241			321.60879
373.0301	1.8666746	320.1569	2.0730846			
E(react)	E (TS)		Q(react)	Q (TS)		
-1073.5977	-1073.4728	trans	1.489E+09	176236000		
0.014607	0.012273	rot	22932.2	303403		
-1073.583	-1073.4606				k(tunnel)	1.0014727
T	ZLJ[M]		Area	exp(-Ea/RT)	k predicted	(1/s)
700	1.291E+09		5.65E+04	3.8763E-27	5.68E-13	

Freq(react)	Qvib	Freq (TS)	Qvib	Act En	cm⁻¹	kcal/mol
84.3248	8.7468195	-91.3067		0.1215815	26676.0651	76.293546
84.3248	8.7468195	27.1245	26.109569			KJ/mol
319.3017	2.7134177	27.1834	26.054093			319.2065
373.0301	2.4064794	320.1569	2.7077087			
E(react)	E (TS)		Q(react)	Q (TS)		
-1073.5977	-1073.4728	trans	3.631E+09	176236000		
0.020723	0.017474	rot	32760.2	303403		
-1073.5769	-1073.4554				k(tunnel)	1.0007216
T	ZLJ[M]		Area	exp(-Ea/RT)	k predicted	(1/s)
1000	94928520		9808.2	2.1119E-17	1.15E-04	
<hr/>						
Freq(react)	Qvib	Freq (TS)	Qvib	Act En	cm⁻¹	kcal/mol
84.3248	12.861801	-91.3067		0.1155015	25342.0589	72.478289
84.3248	12.861801	27.1245	38.911641			KJ/mol
319.3017	3.7883631	27.1834	38.828421			303.24375
373.0301	3.3226792	320.1569	3.7797154			
E(react)	E (TS)		Q(react)	Q (TS)		
-1073.5977	-1073.4728	trans	1.001E+10	176236000		
0.030969	0.02164	rot	49140.4	303403		
-1073.5667	-1073.4512				k(tunnel)	1.0003207
T	ZLJ[M]		Area	exp(-Ea/RT)	k predicted	(1/s)
1500	71002906		10865	2.7482E-11	26.5457464	
<hr/>						
Freq(react)	Qvib	Freq (TS)	Qvib	Act En	cm⁻¹	kcal/mol
84.3248	16.978468	-91.3067		0.1184565	25990.4123	74.332579
84.3248	16.978468	27.1245	51.714256			KJ/mol
319.3017	4.8696221	27.1834	51.603294			311.00196
373.0301	4.2462249	320.1569	4.8580523			
E(react)	E (TS)		Q(react)	Q (TS)		
-1073.5977	-1073.4728	trans	2.054E+10	176236000		
0.041238	0.034864	rot	65520.5	303403		
-1073.5564	-1073.438				k(tunnel)	1.0001804
T	ZLJ[M]		Area	exp(-Ea/RT)	k predicted	(1/s)
1500	58034116		13641	7.5273E-09	2391.74733	

Transition Structure: Hg-Cl 2.38Å, Cl-Cl 4.2 Å

1992/B3LYP

$\beta_c=0.1$

Freq(react)	Qvib	Freq (TS)	Qvib	Act En	cm ⁻¹	kcal/mol
92.6702	2.7706816	-90.705		0.120209	26374.9264	75.432289
92.6702	2.7706816	46.7396	4.9471334			kJ/mol
318.5398	1.2732294	46.755	4.945681			315.60307
374.4751	1.1958538	303.0781	1.3007965			
E(react)	E (TS)		Q(react)	Q (TS)		
-1074.3106	-1074.1891	trans	176236000	1.76E+08		
0.006592	0.005364	rot	2312.65	9834.55		
-1074.304	-1074.1838				k(tunnel)	1.0080192
T	ZLJ[M]		Area	exp(-Ea/RT)	k predicted	(1/s)
298	260435556		2148.6	4.72E-56	1.11E-42	
Freq(react)	Qvib	Freq (TS)	Qvib	Act En	cm ⁻¹	kcal/mol
92.6702	5.7623388	-90.705		0.119095	26130.5049	74.733244
92.6702	5.7623388	46.7396	10.91013			kJ/mol
318.5398	2.0805226	46.755	10.906706			312.67831
374.4751	1.8618859	303.0781	2.1557914			
E(react)	E (TS)		Q(react)	Q (TS)		
-1074.3106	-1074.1891	trans	1.489E+09	1488510000		
0.014609	0.012267	rot	5.43E+03	23089.7		
-1074.296	-1074.1769				k(tunnel)	1.0014533
T	ZLJ[M]		Area	exp(-Ea/RT)	k predicted	(1/s)
700	129116664		5.36E+03	4.627E-24	2.46E-11	

Freq(react)	Qvib	Freq (TS)	Qvib	Act En	cm⁻¹	kcal/mol
92.6702	8.0060648	-90.705		0.118184	25930.6233	74.161583
92.6702	8.0060648	46.7396	15.365779			kJ/mol
318.5398	2.7185301	46.755	15.360886			310.28653
374.4751	2.3994655	303.0781	2.82793			
E(react)	E (TS)		Q(react)	Q (TS)		
-1074.3106	-1074.1891	trans	3.631E+09	3630840000		
0.020725	0.017472	rot	7756.68	32985.2		
-1074.2898	-1074.1717				k(tunnel)	1.0007121
T	ZLJ[M]		Area	exp(-Ea/RT)	k predicted	(1/s)
1000	94928520		6704.8	6.1753E-17	1.26E-04	
<hr/>						
Freq(react)	Qvib	Freq (TS)	Qvib	Act En	cm⁻¹	kcal/mol
92.6702	11.749836	-90.705		0.116627	25589.0037	73.18455
92.6702	11.749836	46.7396	22.793996			kJ/mol
318.5398	3.7961067	46.755	22.786655			306.1987
374.4751	3.3120169	303.0781	3.9617304			
E(react)	E (TS)		Q(react)	Q (TS)		
-1074.3106	-1074.1891	trans	1.001E+10	1.0005E+10		
0.030971	0.026161	rot	11635	49477.9		
-1074.2796	-1074.163				k(tunnel)	1.0003165
T	ZLJ[M]		Area	exp(-Ea/RT)	k predicted	(1/s)
1500	71002906		8512.7	2.1684E-11	13.5592121	
<hr/>						
Freq(react)	Qvib	Freq (TS)	Qvib	Act En	cm⁻¹	kcal/mol
92.6702	15.495458	-90.705		0.115059	25244.9705	72.200616
92.6702	15.495458	46.7396	30.223147			kJ/mol
318.5398	4.8799823	46.755	30.213359			302.08199
374.4751	4.2319418	303.0781	5.1015303			
E(react)	E (TS)		Q(react)	Q (TS)		
-1074.3106	-1074.1891	trans	2.054E+10	2.0539E+10		
0.041239	0.034861	rot	15513.4	65970.5		
-1074.2693	-1074.1543				k(tunnel)	1.000178
T	ZLJ[M]		Area	exp(-Ea/RT)	k predicted	(1/s)
2000	58034116		9813.6	1.2872E-08	3247.99582	

Transition Structure: Hg-Cl 2.38Å, Cl-Cl 4.2 Å

1992/B3LYP

$\beta_c=0.3$

Freq(react)	Qvib	Freq (TS)	Qvib	Act En	cm ⁻¹	kcal/mol
92.6702	2.7706816	-90.705		0.120209	26374.9264	75.432289
92.6702	2.7706816	46.7396	4.9471334			KJ/mol
318.5398	1.2732294	46.755	4.945681			315.60307
374.4751	1.1958538	303.0781	1.3007965			
E(react)	E (TS)		Q(react)	Q (TS)		
-1074.3106	-1074.1891	trans	176236000	1.76E+08		
0.006592	0.005364	rot	2312.65	9834.55		
-1074.304	-1074.1838				k(tunnel)	1.0080192
T	ZLJ[M]		Area	exp(-Ea/RT)	k predicted	(1/s)
298	781306667		3510.6	4.72E-56	1.81E-42	

Freq(react)	Qvib	Freq (TS)	Qvib	Act En	cm ⁻¹	kcal/mol
92.6702	5.7623388	-90.705		0.119095	26130.5049	74.733244
92.6702	5.7623388	46.7396	10.91013			KJ/mol
318.5398	2.0805226	46.755	10.906706			312.67831
374.4751	1.8618859	303.0781	2.1557914			
E(react)	E (TS)		Q(react)	Q (TS)		
-1074.3106	-1074.1891	trans	1.489E+09	1488510000		
0.014609	0.012267	rot	5.43E+03	23089.7		
-1074.296	-1074.1769				k(tunnel)	1.0014533
T	ZLJ[M]		Area	exp(-Ea/RT)	k predicted	(1/s)
700	387349992		1.22E+04	4.627E-24	5.58E-11	

Freq(react)	Qvib	Freq (TS)	Qvib	Act En	cm⁻¹	kcal/mol
92.6702	8.0060648	-90.705		0.118184	25930.6233	74.161583
92.6702	8.0060648	46.7396	15.365779			kJ/mol
318.5398	2.7185301	46.755	15.360886			310.28653
374.4751	2.3994655	303.0781	2.82793			
E(react)	E (TS)		Q(react)	Q (TS)		
-1074.3106	-1074.1891	trans	3.631E+09	3630840000		
0.020725	0.017472	rot	7756.68	32985.2		
-1074.2898	-1074.1717				k(tunnel)	1.0007121
T	ZLJ[M]		Area	exp(-Ea/RT)	k predicted	(1/s)
1000	284785560		16684	6.1753E-17	3.14E-04	
<hr/>						
Freq(react)	Qvib	Freq (TS)	Qvib	Act En	cm⁻¹	kcal/mol
92.6702	11.749836	-90.705		0.116627	25589.0037	73.18455
92.6702	11.749836	46.7396	22.793996			kJ/mol
318.5398	3.7961067	46.755	22.786655			306.1987
374.4751	3.3120169	303.0781	3.9617304			
E(react)	E (TS)		Q(react)	Q (TS)		
-1074.3106	-1074.1891	trans	1.001E+10	1.0005E+10		
0.030971	0.026161	rot	11635	49477.9		
-1074.2796	-1074.163				k(tunnel)	1.0003165
T	ZLJ[M]		Area	exp(-Ea/RT)	k predicted	(1/s)
1500	213008717		22764	2.1684E-11	36.2589899	
<hr/>						
Freq(react)	Qvib	Freq (TS)	Qvib	Act En	cm⁻¹	kcal/mol
92.6702	15.495458	-90.705		0.115059	25244.9705	72.200616
92.6702	15.495458	46.7396	30.223147			kJ/mol
318.5398	4.8799823	46.755	30.213359			302.08199
374.4751	4.2319418	303.0781	5.1015303			
E(react)	E (TS)		Q(react)	Q (TS)		
-1074.3106	-1074.1891	trans	2.054E+10	2.0539E+10		
0.041239	0.034861	rot	15513.4	65970.5		
-1074.2693	-1074.1543				k(tunnel)	1.000178
T	ZLJ[M]		Area	exp(-Ea/RT)	k predicted	(1/s)
2000	174102347		27203	1.2872E-08	9003.34539	

Transition Structure: Hg-Cl 2.38Å, Cl-Cl 4.2 Å

1992/B3LYP

$\beta_c=0.7$

Freq(react)	Qvib	Freq (TS)	Qvib	Act En	cm ⁻¹	kcal/mol
92.6702	2.7706816	-90.705		0.120209	26374.9264	75.432289
92.6702	2.7706816	46.7396	4.9471334			kJ/mol
318.5398	1.2732294	46.755	4.945681			315.60307
374.4751	1.1958538	303.0781	1.3007965			
E(react)	E (TS)		Q(react)	Q (TS)		
-1074.3106	-1074.1891	trans	176236000	1.76E+08	k(tunnel)	
0.006592	0.005364	rot	2312.65	9834.55		
-1074.304	-1074.1838					1.0080192
T	ZLJ[M]		Area	exp(-Ea/RT)	k predicted	(1/s)
298	1.823E+09		4650.8	4.72E-56	2.40E-42	
<hr/>						
Freq(react)	Qvib	Freq (TS)	Qvib	Act En	cm ⁻¹	kcal/mol
92.6702	5.7623388	-90.705		0.119095	26130.5049	74.733244
92.6702	5.7623388	46.7396	10.91013			kJ/mol
318.5398	2.0805226	46.755	10.906706			312.67831
374.4751	1.8618859	303.0781	2.1557914			
E(react)	E (TS)		Q(react)	Q (TS)		
-1074.3106	-1074.1891	trans	1.489E+09	1488510000		
0.014609	0.012267	rot	5.43E+03	23089.7		
-1074.296	-1074.1769				k(tunnel)	1.0014533
T	ZLJ[M]		Area	exp(-Ea/RT)	k predicted	(1/s)
700	903816648		2.14E+04	4.627E-24	9.81E-11	

Freq(react)	Qvib	Freq (TS)	Qvib	Act En	cm⁻¹	kcal/mol
92.6702	8.0060648	-90.705		0.118184	25930.6233	74.161583
92.6702	8.0060648	46.7396	15.365779			kJ/mol
318.5398	2.7185301	46.755	15.360886			310.28653
374.4751	2.3994655	303.0781	2.82793			
E(react)	E (TS)		Q(react)	Q (TS)		
-1074.3106	-1074.1891	trans	3.631E+09	3630840000		
0.020725	0.017472	rot	7756.68	32985.2		
-1074.2898	-1074.1717				k(tunnel)	1.0007121
T	ZLJ[M]		Area	exp(-Ea/RT)	k predicted	(1/s)
1000	664499639		32079	6.1753E-17	6.04E-04	
<hr/>						
Freq(react)	Qvib	Freq (TS)	Qvib	Act En	cm⁻¹	kcal/mol
92.6702	11.749836	-90.705		0.116627	25589.0037	73.18455
92.6702	11.749836	46.7396	22.793996			kJ/mol
318.5398	3.7961067	46.755	22.786655			306.1987
374.4751	3.3120169	303.0781	3.9617304			
E(react)	E (TS)		Q(react)	Q (TS)		
-1074.3106	-1074.1891	trans	1.001E+10	1.0005E+10		
0.030971	0.026161	rot	11635	49477.9		
-1074.2796	-1074.163				k(tunnel)	1.0003165
T	ZLJ[M]		Area	exp(-Ea/RT)	k predicted	(1/s)
1500	497020340		47013	2.1684E-11	74.8833198	
<hr/>						
Freq(react)	Qvib	Freq (TS)	Qvib	Act En	cm⁻¹	kcal/mol
92.6702	15.495458	-90.705		0.115059	25244.9705	72.200616
92.6702	15.495458	46.7396	30.223147			kJ/mol
318.5398	4.8799823	46.755	30.213359			302.08199
374.4751	4.2319418	303.0781	5.1015303			
E(react)	E (TS)		Q(react)	Q (TS)		
-1074.3106	-1074.1891	trans	2.054E+10	2.0539E+10		
0.041239	0.034861	rot	15513.4	65970.5		
-1074.2693	-1074.1543				k(tunnel)	1.000178
T	ZLJ[M]		Area	exp(-Ea/RT)	k predicted	(1/s)
2000	406238810		58276	1.2872E-08	19287.5402	

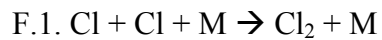
Transition Structure: Hg-Cl 2.38Å, Cl-Cl 4.2 Å
1992/B3LYP

β_c=1.0

Freq(react)	Qvib	Freq (TS)	Qvib	Act En	cm ⁻¹	kcal/mol
92.6702	2.7706816	-90.705		0.120209	26374.9264	75.432289
92.6702	2.7706816	46.7396	4.9471334			kJ/mol
318.5398	1.2732294	46.755	4.945681			315.60307
374.4751	1.1958538	303.0781	1.3007965			
E(react)	E (TS)		Q(react)	Q (TS)		
-1074.3106	-1074.1891	trans	176236000	1.76E+08		
0.006592	0.005364	rot	2312.65	9834.55		
-1074.304	-1074.1838				k(tunnel)	1.0080192
T	ZLJ[M]		Area	exp(-Ea/RT)	k predicted	(1/s)
298	2.604E+09		5108.2	4.72E-56	2.63E-42	
<hr/>						
Freq(react)	Qvib	Freq (TS)	Qvib	Act En	cm ⁻¹	kcal/mol
92.6702	5.7623388	-90.705		0.119095	26130.5049	74.733244
92.6702	5.7623388	46.7396	10.91013			kJ/mol
318.5398	2.0805226	46.755	10.906706			312.67831
374.4751	1.8618859	303.0781	2.1557914			
E(react)	E (TS)		Q(react)	Q (TS)		
-1074.3106	-1074.1891	trans	1.489E+09	1488510000		
0.014609	0.012267	rot	5.43E+03	23089.7		
-1074.296	-1074.1769				k(tunnel)	1.0014533
T	ZLJ[M]		Area	exp(-Ea/RT)	k predicted	(1/s)
700	1.291E+09		2.66E+04	4.627E-24	1.22E-10	

Freq(react)	Qvib	Freq (TS)	Qvib	Act En	cm⁻¹	kcal/mol
92.6702	8.0060648	-90.705		0.118184	25930.6233	74.161583
92.6702	8.0060648	46.7396	15.365779			kJ/mol
318.5398	2.7185301	46.755	15.360886			310.28653
374.4751	2.3994655	303.0781	2.82793			
E(react)	E (TS)		Q(react)	Q (TS)		
-1074.3106	-1074.1891	trans	3.631E+09	3630840000		
0.020725	0.017472	rot	7756.68	32985.2		
-1074.2898	-1074.1717				k(tunnel)	1.0007121
T	ZLJ[M]		Area	exp(-Ea/RT)	k predicted	(1/s)
1000	949285199		41609	6.1753E-17	7.84E-04	
<hr/>						
Freq(react)	Qvib	Freq (TS)	Qvib	Act En	cm⁻¹	kcal/mol
92.6702	11.749836	-90.705		0.116627	25589.0037	73.18455
92.6702	11.749836	46.7396	22.793996			kJ/mol
318.5398	3.7961067	46.755	22.786655			306.1987
374.4751	3.3120169	303.0781	3.9617304			
E(react)	E (TS)		Q(react)	Q (TS)		
-1074.3106	-1074.1891	trans	1.001E+10	1.0005E+10		
0.030971	0.026161	rot	11635	49477.9		
-1074.2796	-1074.163				k(tunnel)	1.0003165
T	ZLJ[M]		Area	exp(-Ea/RT)	k predicted	(1/s)
1500	710029057		63141	2.1684E-11	100.572346	
<hr/>						
Freq(react)	Qvib	Freq (TS)	Qvib	Act En	cm⁻¹	kcal/mol
92.6702	15.495458	-90.705		0.115059	25244.9705	72.200616
92.6702	15.495458	46.7396	30.223147			kJ/mol
318.5398	4.8799823	46.755	30.213359			302.08199
374.4751	4.2319418	303.0781	5.1015303			
E(react)	E (TS)		Q(react)	Q (TS)		
-1074.3106	-1074.1891	trans	2.054E+10	2.0539E+10		
0.041239	0.034861	rot	15513.4	65970.5		
-1074.2693	-1074.1543				k(tunnel)	1.000178
T	ZLJ[M]		Area	exp(-Ea/RT)	k predicted	(1/s)
2000	580341158		79699	1.2872E-08	26377.8857	

APPENDIX F. EQUILIBRIUM CONSTANT DATA



F.1.1. forward

From NIST webbook (Shomate Equation)

$$\begin{aligned} H^\circ - H^\circ_{298.15} &= A * T + B * T^2/2 + C * T^3/3 + D * T^4/4 - E/T + F - H \\ S^\circ &= A * \ln(T) + B * T + C * T^2/2 + D * T^3/3 - E/(2*T^2) + G \end{aligned}$$

Such that $T = \text{temperature}/1000$

	Cl (298-600)	Cl (600-6000)	Cl ₂ (298-1000)	Cl ₂ (1000-3000)
A	13.38298	23.26597	33.0506	42.6773
B	42.33999	-1.555939	12.2294	-5.00957
C	-64.74656	0.34691	-12.0651	1.904621
D	32.99532	-0.025961	4.38533	-0.165641
E	0.063319	0.153212	-0.159494	-2.09848
F	116.1491	114.6604	-10.8348	-17.2898
G	171.7038	193.8882	259.029	269.84
H	121.3021	121.3021	0	0

						298 K		
DH	(298-600)	(600-6000)	(298-1000)	(1000-3000)	DH _{rxn}	DH _{rxn}		J/mol
0.773	0.773	6.80321284	7.09524902	7.09524902	8.78013587	-6.51118	-242.6	-249.1
1	1	16.0067616	16.0908879	16.0908879	23.3107043	-16.0909	-242.6	-258.7
1.5	1.5	21.1528206	20.5045262	20.5045262	30.8120422	-10.197	-242.6	-252.8
2	2	65.5885294	37.8116583	37.8116583	61.2473712	-14.3759	-242.6	-257

						298 K	
DS	(298-600)	(600-6000)	(298-1000)	(1000-3000)	DSrxn	DSrxn	
0.773	15.726238	16.5077207	24.7878486	19.7013478	-6.66463	-107.3	-114
1	27.4587644	28.0106139	43.7061305	38.1990538	-12.3151	-107.3	-119.6
1.5	32.139063	32.0347417	50.5633316	45.0363516	-19.0331	-107.3	-126.3
2	58.9681139	43.0986603	70.9194371	64.4546398	-21.7427	-107.3	-129

DG	J/mol	Keq	
773	-180732.4	773	5.43E+15
1000	-139075.791	1000	18400780
1500	-101197.252	1500	25419.14
2000	1109.41597	2000	0.935457

F.1.2. reverse

	Cl	Cl	Cl ₂	Cl ₂
	(298-600)	(600-6000)	(298-1000)	(1000-3000)
A	13.38298	23.26597	33.0506	42.6773
B	42.33999	-1.555939	12.2294	-5.00957
C	-64.74656	0.34691	-12.0651	1.904621
D	32.99532	-0.025961	4.38533	-0.165641
E	0.063319	0.153212	-0.159494	-2.09848
F	116.1491	114.6604	-10.8348	-17.2898
G	171.7038	193.8882	259.029	269.84
H	121.3021	121.3021	0	0

						298 K		
DH	(298-600)	(600-6000)	(298-1000)	(1000-3000)	DHrxn	DHrxn		J/mol
0.773	6.80321284	7.09524902	7.09524902	8.780135873	6.5111767	242.6	249.11	249111.2
1	16.0067616	16.0908879	16.0908879	23.31070428	16.090888	242.6	258.69	258690.9
1.5	21.1528206	20.5045262	20.5045262	30.8120422	10.19701	242.6	252.8	252797
2	65.5885294	37.8116583	37.8116583	61.2473712	14.375945	242.6	256.98	256975.9

						298 K	
DS	(298-600)	(600-6000)	(298-1000)	(1000-3000)	DSrxn	DSrxn	
0.773	15.726238	16.5077207	24.7878486	19.70134779	6.6646273	107.3	113.96
1	27.4587644	28.0106139	43.7061305	38.19905383	12.315097	107.3	119.62
1.5	32.139063	32.0347417	50.5633316	45.03635157	19.033132	107.3	126.33
2	58.9681139	43.0986603	70.9194371	64.45463983	21.742681	107.3	129.04

DG	J/mol	Keq	
773	180732.4	773	1.842E-16
1000	139075.791	1000	5.435E-08
1500	101197.252	1500	3.934E-05
2000	-1109.41597	2000	1.0689958

F.2. $\text{HCl} + \text{OH} \rightarrow \text{Cl} + \text{H}_2\text{O}$

	HCl	OH	Cl	Cl	H_2O
	(298-1200K)	(298-1300)	(298-600)	(600-6000)	(500-1700)
A	32.12392	32.27768	13.38298	23.26597	30.092
B	-13.45805	-11.36291	42.33999	-1.555939	6.832514
C	19.86852	13.60545	-64.74656	0.34691	6.793435
D	-6.853936	-3.846486	32.99532	-0.025961	-2.53448
E	-0.049672	-0.001335	0.063319	0.153212	0.082139
F	-101.6206	29.75113	116.1491	114.6604	-250.881
G	228.6866	225.5783	171.7038	193.8882	223.3967
H	-92.31201	38.98706	121.3021	121.3021	-241.8264

							298 K		
DH	(298-1200K)	(298-1300)	(298-600)	(600-6000)	(500-1700)	DHrxn	DHrxn		J/mol
0.6	8.83935585	8.94735	8.94735	7.09524902	10.5050759	1.66572	-67.21	-65.54	-65544.28
1	21.0501233	20.939963	20.939963	16.0908879	26.0068879	0.107689	-67.21	-67.1	-67102.3105
1.2	27.4876887	27.164629	27.164629	20.5045262	34.5104166	0.362625	-67.21	-66.85	-66847.3746
2	53.6197523	53.494338	53.494338	37.8116583	72.7357767	3.433345	-67.21	-63.78	-63776.6553

							298 K	
DS	(298-1200K)	(298-1300)	(298-600)	(600-6000)	(500-1700)	DSrxn	DSrxn	
0.6	20.4675749	20.753682	15.726238	16.5077207	24.2323316	-1.26269	-16.58	-17.84
1	36.01666879	36.044126	27.458764	28.0106139	43.9216694	-0.12853	-16.58	-16.71
1.2	41.8822249	41.716042	32.139063	32.0347417	51.6666634	0.103138	-16.58	-16.48
2	58.6168782	58.48694	58.968114	43.0986603	75.9195363	1.914379	-16.58	-14.67

DG	J/mol	Keq	
773	-54838.667	773	59470.63
1000	-50393.779	1000	428.94
1500	-47075.14	1500	112.00
2000	-34445.413	2000	7.94



	Hg	Cl	Cl	HgCl
	(629-6000K)	(298-600)	(600-6000)	(298-6000)
A	20.67243	13.38298	23.26597	37.36504
B	0.179353	42.33999	-1.555939	0.85485
C	-0.08012	-64.74656	0.34691	-0.011692
D	0.010547	32.99532	-0.025961	0.001004
E	0.007013	0.063319	0.153212	-0.107381
F	55.23215	116.1491	114.6604	66.91178
G	199.9797	171.7038	193.8882	304.3622
H	61.38012	121.3021	121.3021	78.45

						298 K		
DH	(629-6000K)	(298-600)	(600-6000)	(298-6000)	DHrxn	DHrxn		J/mol
0.773	6.27449804	6.80321284	6.80321284	11.2180793	-1.859632	-104.23	-106.09	-106090
1	14.5868953	16.0067616	16.0067616	26.36322293	-4.230434	-104.23	-108.46	-108460
1.5	18.7453962	21.1528206	21.1528206	34.00383331	-5.894383	-104.23	-110.12	-110124
2	35.3844659	65.5885294	65.5885294	64.9333311	-36.03966	-104.23	-140.27	-140270

						298 K		
DS	(629-6000K)	(298-600)	(600-6000)	(298-6000)	DSrxn	DSrxn		
0.773	14.5410266	15.726238	16.5077207	25.95059392	-4.316671	-80.16	-84.477	
1	25.1561264	27.4587644	28.0106139	45.28062495	-7.886115	-80.16	-88.046	
1.5	28.9470311	32.139063	32.0347417	52.24531318	-8.73646	-80.16	-88.896	
2	39.5715755	58.9681139	43.0986603	71.97948387	-10.69075	-80.16	-90.851	

DG	J/mol	Keq	
773	-55403.6292	773	66602.201
1000	-20414.3186	1000	11.651265
1500	-3448.63189	1500	1.4129294
2000	41431.8396	2000	0.0827699

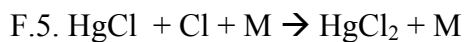


	Hg	Cl2	Cl2	HgCl2
	(629-6000K)	(298-1000)	(1000-3000)	(1500-6000)
A	4.94083	7.899283	10.2001	14.8335
B	0.042866	2.922897	-1.1973	0.060202
C	-0.019149	-2.883629	0.45522	-0.016325
D	0.002521	1.04812	-0.0396	0.001394
E	0.001676	-0.03812	-0.5015	-0.086559
F	13.2008	-2.58958	-4.1324	-39.6805
G	47.7963	61.90942	64.4933	87.90141
H	14.6702	0	0	-34.96511

	(629-6000K)	(298-1000)	(1000-3000)	(1500-6000)		298 K		
DH					DHrxn	DHrxn		cal/mol
0.77	2.35869447	4.08998274		6.88048943	0.4318122	-49.634	-49.2	-49202
1	3.48635168	6.11135422		10.2316856	0.6339797	-49.634	-49	-49000
1.5	5.97151736		10.65672359	17.6457006	1.0174597	-49.634	-48.62	-48617
2	8.45709143		15.57790505	25.0793449	1.0443484	-49.634	-48.59	-48590

	(629-6000K)	(298-1000)	(1000-3000)	(1500-6000)		298 K	
DS					DSrxn	DSrxn	
0.77	4.73341836	8.15376591		13.7487948	0.86161	-24.682	-23.82
1	6.0124584	10.4460159		17.5495479	1.09107	-24.682	-23.59
1.5	8.02771879		12.78077588	23.5609719	2.75248	-24.682	-21.93
2	9.45783411		15.40502792	27.8378542	2.97499	-24.682	-21.71

DG	cal/mol	Keq	
773	-30789.027	773	5.08E+08
1000	-25409.094	1000	357777.6
1500	-15722.256	1500	195.3983
2000	-5175.6359	2000	3.678019



	HgCl	Cl	Cl	HgCl ₂
	(298-6000)	(298-600)	(600-6000)	(1500-6000)
A	37.37	13.38	23.27	14.83
B	0.85	42.34	-1.20	0.06
C	-0.01	-64.75	-1.56	-0.02
D	0.00	33.00	-0.03	0.00
E	-0.11	0.06	0.15	-0.09
F	66.91	116.15	114.66	-39.68
G	304.36	171.70	193.89	87.90
H	78.45	121.30	121.30	-34.97

					298 K		
DH	(298-6000)	(600-6000)	(1500-6000)	DHrxn	DHrxn		cal/mol
0.298				0	-82.705	-82.71	-82705.00
0.6	11.22	6.80	4.34	-6.88	-82.705	-89.58	-89582.39
0.7	14.98	9.08	5.81	-18.26	-82.705	-100.96	-100961.67
1	26.36	16.01	10.23	-32.14	-82.705	-114.84	-114843.30
1.2	34.00	21.15	13.19	-41.96	-82.705	-124.67	-124668.04
1.5	45.54	31.44	17.65	-59.33	-82.705	-142.03	-142030.32
2	64.93	65.59	25.08	-105.44	-82.705	-188.15	-188147.52

DS	(298-6000)	(600-6000)	(1500-6000)	DSrxn	DSrxn	
0.298	0	0	0	0	-31.166	-31.17
0.6	25.95	16.36	10.03	-15.92	-31.166	-47.09
0.7	31.76	19.78	12.29	-19.47	-31.166	-50.63
1	45.28	27.40	17.55	-55.13	-31.166	-86.29
1.2	52.25	31.07	20.25	-63.07	-31.166	-94.23
1.5	60.82	35.28	23.56	-72.54	-31.166	-103.71
2	71.98	39.99	27.84	-84.13	-31.166	-115.30

DG	cal/mol	K _{eq}	
298	-73417.53	298	7.0477E+53
600	-61330.39	600	2.195E+22
700	-65519.28	700	2.869E+20
1000	-28550.79	1000	1738949.2
1200	-11586.76	1200	128.947422
1500	13529.90	1500	0.01067903
2000	42443.40	2000	2.2994E-05

F.6. $\text{Hg} + \text{HCl} \rightarrow \text{HgCl} + \text{H}$

	Hg	HCl	H	HgCl
	(629-6000K)	(298-1200)	(298-6000)	(298-6000)
A	20.67243	32.12392	20.78603	37.36504
B	0.179353	-13.45805	4.85E-10	0.85485
C	-0.08012	19.86852	-1.58E-10	-0.011692
D	0.010547	-6.853936	1.53E-11	0.001004
E	0.007013	-0.049672	3.2E-11	-0.107381
F	55.23215	-101.6206	211.802	66.91178
G	199.9797	228.6866	139.8711	304.3622
H	61.38012	-92.31201	217.9994	78.45

						298 K		
DH	(629-6000K)	(298-1200)	(298-6000)	(298-6000)	DHrxn	DHrxn		J/mol
0.3	0	0	0	0	0	327.38	327.38	327380
0.6	6.27449804	8.83935585	8.83935585	11.2180793	4.943581	327.38	332.32	332323.6
1	14.5868953	21.0501233	21.0501233	26.36322293	11.77633	327.38	339.16	339156.3
1.2	18.7453962	27.4876887	27.4876887	34.00383331	15.25844	327.38	342.64	342638.4
2	35.3844659	53.6197523	53.6197523	64.9333311	29.54887	327.38	356.93	356928.9

DS	(629-6000K)	(298-1200)	(298-6000)	(298-6000)	DSrxn	DSrxn	
0.298	0	0	0	0	0	12.85	12.85
0.6	14.5410266	20.467575	14.546816	25.9505939	5.4888	12.85	18.339
1	25.1561264	36.016688	25.164852	45.2806249	9.2727	12.85	22.123
1.2	28.9470311	41.882225	28.954594	52.2453132	10.371	12.85	23.221
2	39.5715755	58.616878	39.57263	71.9794839	13.364	12.85	26.214

DG	J/mol	K _{eq}	
298	323550.7	298	2E-57
600	321320.3	600	1E-28
1000	317033.7	1000	3E-17
1200	314773.7	1200	2E-14
2000	304501.5	2000	1E-08



	HgCl	HCl	H	HgCl2
	(298-6000K)	(298-1200)	(298-6000)	(1500-6000)
A	37.36504	32.12392	20.78603	62.06336
B	0.85485	-13.45805	4.851E-10	0.251886
C	-0.011692	19.86852	-1.583E-10	-0.068302
D	0.001004	-6.853936	1.525E-11	0.005831
E	-0.107381	-0.049672	3.196E-11	-0.362161
F	66.91178	-101.6206	211.802	-166.0232
G	304.3622	228.6866	139.8711	367.7795
H	78.45	-92.31201	217.9994	-146.294

						298 K		
DH	(298-6000K)	(298-1200)	(298-6000)	(1500-6000)	DHrxn	DHrxn		J/mol
0.773	11.2180793	8.83935585	8.83935585	18.1614484	6.9433691	85.57	92.513	92513
1	26.3632229	21.0501233	21.0501233	42.8093745	16.446152	85.57	102.02	1E+05
1.5	34.0038333	27.4876887	27.4876887	55.2020917	21.198258	85.57	106.77	1E+05
2	64.9333311	53.6197523	53.6197523	104.931978	39.998647	85.57	125.57	1E+05

						298 K	
DS	(298-6000K)	(298-1200)	(298-6000)	(1500-6000)	DSrxn	DSrxn	
0.773	25.9505939	20.4675749	14.5468156	41.9652589	10.093906	-37.4	-27.306
1	45.2806249	36.0166879	25.1648523	73.4273141	17.294854	-37.4	-20.105
1.5	52.2453132	41.8822249	28.9545937	84.7242382	19.551294	-37.4	-17.849
2	71.9794839	58.6168782	39.5726304	116.473585	25.449854	-37.4	-11.95

DG	J/mol	Keq	
773	108897.03	773	3.3E-10
1000	122121.3	1000	4.2E-07
1500	128186.71	1500	2.6E-06
2000	149468.94	2000	0.00012

APPENDIX G. MODELING PARAMETERS

G.1. Mechanism.dat File

Only mercury oxidation parameters listed here – many other reactions were considered, including hydrocarbon-chlorine submechanisms.

RXN:	A (cm³/mol s)	E₀ (cal/mol)
HGCL+M=HG+CL+M	4.25E+13	1.613E4
HGCL2+M=HG+CL2+M	4.04E+21	4.476E4
HG+CL2=HGCL+CL	1.394E+26	2.776E4
HG+HCL=HGCL+H	1.394E+26	8.752E4
HG+O+M=HGO+M	3.40E+9	0.
HG+HOCL=HGCL+OH	4.27E+13	1.9E4
HGCL+CL+M=HGCL2+M	1.95E+13	0.
HGCL+CL2=HGCL2+CL	1.39E+14	1.0E3
HGCL+HCL=HGCL2+H	4.5E+13	3.027E4
HGCL+HOCL=HGCL2+OH	4.27E+13	1.0E3

G.2. Thermo.dat File

Only mercury containing species are recorded here, although many other species were accounted for in the modeling work.

HG	113103HG_1	G_300	5000	1000	1
2.50E+00	0.00E+00	0.00E+00	0.00E+00	0.00E+00	2.00E+00
6.64E+03	6.80E+00	2.51E+00	-1.99E-05	1.39E-08	3.00E+00
-3.94E-12	3.91E-16	6.63E+03	6.75E+00		4.00E+00
HGCL	113103HG_1CL_1	G_300	5000	1000	1.00E+00
3.31E+00	7.05E-03	-1.60E-05	1.63E-08	-6.06E-12	2.00E+00
8.25E+03	1.02E+01	1.16E+01	-0.01954203E_00	1.97E-05	3.00E+00
-8.54E-09	1.36E-12	6.06E+03	-3.20E+01		4.00E+00
HGCL2	113103HG_1CL_2	G_300	5000	1000	1.00E+00
5.40E+00	9.07E-03	-1.60E-05	1.30E-08	-3.97E-12	2.00E+00
-1.95E+04	1.96E+00	7.57E+00	-5.35E-04	7.17E-07	3.00E+00
-3.62E-10	0.06368887E-12-	1.99E+04	-8.33E+00		4.00E+00
HGO	113103HG_1O_1	G_300	5000	1000	1.00E+00
2.88E+00	5.40E-03	7.22E-06	4.40E-09	-1.00E-12	2.00E+00
3.99E+03	1.10E+01	5.52E+00	-3.62E-03	4.26E-06	3.00E+00
-2.05E-09	3.54E-13	3.38E+03	-2.17E+00		4.00E+00

APPENDIX H. DATA FROM MASS SPECTROMETRY RESULTS



Residence time = 2.2 seconds

Cl⁺ 35,37		hgcl2.1g		hgcl2.2h		hgcl2.2f	
34.7	15187227	34.59	14763788	34.43	12481364	34.47	13314329
35.72	14551893	35.68	16764714	35.29	12416034	35.38	12261665
36.68	13555591	36.75	13983173	36.19	12878563	36.19	11103268
37.6	12812917	37.69	12758143	37.08	12514566	36.98	11520089
	56107628		58269818	37.92	11812223	37.83	12483876
			2162190		62102750		60683227
			0.193366502		5995122		4575599
					0.33355856		0.635374904
N ₂ alone							
Cl₂⁺, 70, 72							
69.77	12617851	69.63	12783671	69.53	12153639	70.13	12360328
70.65	12918692	70.57	14850396	70.4	12633128	71.04	13845322
71.54	12987250	71.48	12196359	71.27	12460249	71.94	12455759
72.43	12564776	72.37	12811458	72.13	12297170	72.78	11727634
73.31	12536812	73.28	13562354	73	12714758	73.58	11000826
	63625381		66204238		62258944		61389869
			2578857		-1366437		-2235512
			0.230629388		0		0
Hg⁺, 198	199,	200,	201,	202			
197.77	13862212	197.54	11157327	197.6	12329387	198.23	13494531
198.69	13178870	198.25	10276251	198.44	11821003	199.09	11087769
199.62	13682645	198.98	10603145	199.27	12117707	199.88	11934740
200.54	13226108	199.73	10656701	200.15	12464554	200.71	11933766
201.45	13282149	200.58	13403566	201.02	12966637	201.56	12870986
202.31	12526528	201.48	12278496	201.94	13554392	202.51	14148582
	79758512	202.26	10439302				
			78814788		75253680		75470374
			-943724		-4504832		-4288138
			0		0		0

Residence time = 2.2 seconds

HgCl⁺	234,	235,	237				
233.04	10631943	233.27	11754902	233.66	13021567	233.67	13260898
233.85	12219115	234.13	12330890	234.55	12453669	234.59	12759820
234.71	12718349	235	13246081	235.45	12705847	235.45	11544431
235.55	11847313	235.91	12470469	236.3	12182525	236.23	10828844
236.39	11695003	236.8	13117099	237.23	13838004	237	11828024
237.18	11484021	237.72	12939257	238.17	13359614	237.84	12063000
	70595744		75858698		77561226		72285017
			5262954		6965482		1689273
			0.47067048		0.38754776		0.234575117
HgCl₂⁺	269,	270,	272				
268.44	12463071	268.57	11816353	267.91	13137122	267.81	10238830
269.3	11991230	269.36	10892238	268.86	13574084	268.59	11728121
270.15	12756898	270.17	12740986	269.79	13330449	269.45	12605429
271.03	12679603	271.07	13058593	270.74	14104020	270.32	12087490
271.91	13369761	271.95	12529403	271.7	13345905	271.17	13026099
272.79	12720135	272.85	13550448	272.62	13501736	272.07	13128141
	75980698		74588021		80993316		72814110
			-1392677		5012618		-3166588
			0		0.27889368		0
Hg₂Cl₂⁺	468,	470,	474				
467.7	13811362	467.8	13098052	467.92	12008418	467.52	11049803
468.63	13202866	468.68	12890117	468.73	12010052	468.27	11434957
469.49	12938598	469.55	12553412	469.57	12463296	469.1	12840923
470.38	12898436	470.4	11707722	470.41	12011135	469.96	12610840
473.86	12367845	473.57	11788136	473.96	12701673	473.42	12716169
474.6	9636660	474.45	13996150	474.62	7914830	474.38	15139619
	74855767		76033589		69109404		75792311
			1177822		-5746363		936544
			0.105333629		0		0.130049979

Residence time = 3.0 seconds

N₂ alone							
Cl₂⁺, 70, 72		hgcl2.1d		hgcl2.2e		hgcl2.2f	
70.65	12918692	70.66	13201118	70.5	12569508	70.62	13291261
71.54	12987250	71.56	14024236	71.36	12413228	71.51	12544380
72.43	12564776	72.46	11967220	72.27	13550398	72.42	13250486
73.31	12536812	73.25	11527765	73.21	13389746	73.38	14517387
	51007530		50720339		51922880		53603514
Hg⁺, 198	199,	200,	201,	202			
197.77	13862212	197.16	15568869	197.45	13109854	197.3	11826036
198.69	13178870	198.16	14251125	198.34	12589688	198.11	10863882
199.62	13682645	199.09	13044059	199.2	11989729	198.88	11922314
200.54	13226108	199.99	12996117	200.05	12268080	199.71	11988608
201.45	13282149	200.87	12193931	200.92	12459285	200.61	12965354
202.31	12526528	201.75	13350291	201.81	12598666	201.52	13156654
	79758512	202.67	13376695	202.68	12338248	202.41	12606312
			79212218		87353550		73503124
HgCl⁺	234,	235,	237				
233.04	10631943	233.69	13434055	233.37	11386028	234.35	10657716
233.85	12219115	234.63	13659321	234.2	12371056	235.02	9983540
234.71	12718349	235.59	13506423	235.1	13358945	235.86	13236818
235.55	11847313	236.55	14000965	236.08	14369913	236.75	12380383
236.39	11695003	237.52	13714561	237.07	13967998	237.63	12591092
237.18	11484021		68315325		65453940		58849549
	70595744		1.37E+08		1.31E+08		1.18E+08
HgCl₂⁺	269,	270,	272				
268.44	12463071	268.09	12791961	268.39	12323110	268.51	13704036
269.3	11991230	269.05	14956833	269.24	12460668	269.4	11744828
270.15	12756898	270.1	15466133	270.13	12579501	270.21	12245924
271.03	12679603	271.09	12868021	271.02	13002246	271.08	12924630
271.91	13369761	271.98	13004500	271.94	13415628	271.98	13137857
272.79	12720135	272.89	14015418	272.82	12531949	272.86	11594595
	75980698		83102866		76313102		75351870
Hg₂Cl₂⁺	468,	470,	474				
467.7	13811362	467.74	16522430	468.02	13415328	467.86	13801928
468.63	13202866	468.79	16099443	468.93	13400101	468.81	13739896
469.49	12938598	469.76	13805647	469.87	13262754	469.82	15858064
470.38	12898436	470.72	15298928	470.76	12546647	470.82	13074495
473.86	12367845	474.02	11836695	473.45	12926580	473.53	13219406
474.6	9636660	474.64	7633951	474.38	14418617	474.46	13423790
	74855767		81197094		79970027		83117579

Residence time = 4.2 seconds

Cl+ 35,37		hgcl2.1b		hgcl2.2b		hgcl2.2	
34.7	15187227	34.25	13194428	34.26	12597536	34.13	12786078
35.72	14551893	35.13	12285920	35.14	12468972	35.02	12595835
36.68	13555591	35.99	11915904	36	12135966	35.9	12536883
37.6	12812917	36.84	12748686	36.87	13126980	36.79	13036043
	56107628	37.75	12886807	37.79	12840841	37.69	12954550
			63031745		63170295		63909389
			6924117		7062667		7801761
			0.346749848		0.3941078		0.27111885
N ₂ alone							
Cl ₂ ⁺ , 70, 72							
69.77	12617851	69.52	12200628	69.46	12807702	70.13	14204825
70.65	12918692	70.38	13359404	70.34	13054423	71.03	13199892
71.54	12987250	71.29	13171430	71.22	13289210	71.94	12782914
72.43	12564776	72.19	12847451	72.13	12823772	72.84	12965510
73.31	12536812	73.12	13825592	73.01	12566670	73.7	12045672
	63625381		65404505		64541777		65198813
			1779124		916396		1573432
			0.089095978		0.0511363		0.05467831
Hg ⁺ , 198	199,	200,	201,	202			
197.77	13862212	197.86	13960827	197.82	13434055	198.23	13494531
198.69	13178870	198.77	12495710	198.71	12705523	199.09	11087769
199.62	13682645	199.67	13044653	199.57	12243628	199.88	11934740
200.54	13226108	200.59	13395447	200.45	13235280	200.71	11933766
201.45	13282149	201.5	12800211	201.41	14177798	201.56	12870986
202.31	12526528	202.38	12497253	202.36	13313458	202.51	14148582
	79758512		78194101		79109742		75470374
			-1564411		-648770		-4288138
			0		0		0

Residence time = 4.2 seconds

HgCl⁺	234,	235,	237				
233.04	10631943	233.73	13078972	233.7	13090202	233.23	14013575
233.85	12219115	234.62	12294561	234.59	12511424	234.18	13346614
234.71	12718349	235.49	12725848	235.5	13477049	235.08	12891995
235.55	11847313	236.3	10728712	236.38	11585514	236.01	13723597
236.39	11695003	237.13	12812025	237.2	12072702	237	14537366
237.18	11484021	238.03	13053702	238.05	12388204	237.99	14009457
	70595744		74693820		75125095		82522604
			4098076		4529351		11926860
			0.205225768		0.2527448		0.41447009
HgCl₂⁺	269,	270,	272				
268.44	12463071	268.41	12362614	268.5	10335900	268.08	12298833
269.3	11991230	269.28	12690890	269.25	11580396	268.95	12415331
270.15	12756898	270.18	13310902	270.13	13400125	269.82	12835323
271.03	12679603	271.02	11422240	271.05	13195196	270.71	13396971
271.91	13369761	271.89	13158224	271.95	12717700	271.66	14625981
272.79	12720135	272.85	14192189	272.85	14069266	272.63	14774972
	75980698		77137059		75298583		80347411
			1156361		-682115		4366713
			0.0579089		0		0.15174756
Hg₂Cl₂⁺	468,	470,	474				
467.7	13811362	467.35	13601520	467.36	13431658	467.64	12910019
468.63	13202866	468.25	12926985	468.28	13472975	468.47	13546319
469.49	12938598	469.09	13442628	469.13	12941256	469.32	14342378
470.38	12898436	470	13825451	470	13136248	470.24	14442570
473.86	12367845	473.56	13867663	473.49	12942572	473.85	13444008
474.6	9636660	474.49	13202465	474.42	14343292	474.6	9277873
	74855767		80866712		80268001		77963167
			6010945		5412234		3107400
			0.301019504		0.3020111		0.1079852

Coated Reactor - Hg + Cl₂ → ...

Residence time = 4.2 seconds

Cl+ 35,37	nb.txt	chgcl2.e		chgcl1.e		chgcl2.a	
34.79	11944329	34.68	13177284	34.75	13341312	34.11	13702427
35.57	10582441	35.6	12901212	35.69	13541989	35.02	13027718
36.31	10710864	36.52	13186578	36.59	12291413	36	14557370
37.13	12490126	37.42	12716502	37.44	12337002	36.99	13755746
	45727760		51981576		51511716		55043261
			6253816		5783956		9315501
			0.2484637		0.229796		0.515474
Cl₂⁺, 70, 72							
69.9	12270693	69.28	13905114	69.37	13794056	69.81	12774668
70.75	12096249	70.27	15099126	70.34	14483652	70.7	12397460
71.63	12782391	71.3	14367965	71.32	13563651	71.55	12350546
72.52	12735539	72.26	13376630	72.27	13189314	72.43	12738083
73.41	12764483	73.17	12775886	73.16	12899936	73.18	12899936
74.3	12748830	74.05	12337558	74.04	12279010	73.95	11955914
	75398185		81862279		80209619		75116607
			6464094		4811434		-281578
			0.256818		0.191158		0
Hg⁺, 198	199,	200,	201,				
197.97	11451098	197.66	13175761	197.63	13511376	197.41	12003885
198.8	12271736	198.57	13497989	198.57	13702625	198.23	12070331
199.69	13079871	199.47	12578836	199.49	12750227	199.09	12456274
200.59	12664230	200.3	11026535	200.33	11167708	200.02	13609383
201.48	12596861	201.09	11477554	201.06	10185424	200.9	11880563
202.36	12484103	201.86	11280965	201.83	11866617	201.76	12590779
203.18	11409890	202.71	13060759	202.71	13316600	202.63	12430343
	85957789		86098399		86500577		87041558
			140610		542788		1083769
			0.0055864		0.021565		0.0599704

Coated Reactor - Hg + Cl₂ → ...

Residence time = 4.2 seconds

HgCl⁺	234,	235,	237				
233.07	12438859	232.72	12222654	232.69	12892058	233.24	12771427
233.94	12575673	233.61	13193732	233.61	13218146	234.13	12615263
234.82	12462636	234.5	12454087	234.52	12767392	234.91	12767392
235.69	12505948	235.38	12830906	235.42	13383477	235.67	12092566
236.54	11692634	236.27	12460575	236.32	12451966	236.54	12470785
237.37	12339359	237.15	12771007	237.22	13204651	237.43	13221767
238.22	11866479	238.08	13825728	238.14	13450898	238.36	13008007
	85881588		89758689		91368588		88947207
			3877101		5487000		3065619
			0.154037		0.217998		0.1696363
HgCl₂⁺	269,	270,	272				
268.32	13094456	268.2	12546154	268.17	12539917	268.29	12731788
269.23	12977780	269.05	12428797	269.02	11996760	269.14	11517890
270.13	12687769	269.95	13163179	269.89	13105318	269.98	12576253
271.02	13052673	270.85	12729299	270.8	13099835	270.84	12427372
271.98	14586179	271.74	12927111	271.73	13534225	271.74	13264031
272.95	13259969	272.63	13048759	272.63	12589958	272.64	12736729
	79658826		76843299		76866013		75254063
			-2815527		-2792813		-4404763
			0		0		0
Hg₂Cl₂⁺	468,	470,	474				
467.59	12862883	467.77	13653103	467.79	14981265	467.38	12499961
468.51	13136757	468.65	16256347	468.7	15454830	468.25	12713462
469.41	12430593	469.49	15237092	469.55	14890665	469.14	12776946
470.29	13187993	470.41	15608254	470.48	16091377	470	12499388
473.95	11598256	474.06	13889437	474.11	13860478	473.61	12849620
474.61	8777614	474.66	5784179	474.7	5319819	474.48	13261548
	71994096		80428412		80598434		76600925
			8434316		8604338		4606829
			0.3350948		0.34185		0.2549193



Residence time = 4.2 seconds

HCl^+/Cl^+	nb.txt	hcl.2		hcl.4		HCl^+/Cl^+	nb.txt
34.79	11944329	34.45	12511427	34.88	14026048	34.79	11944329
35.57	10582441	35.33	12196834	35.82	13119528	35.57	10582441
36.31	10710864	36.16	11812461	36.75	13027871	36.31	10710864
37.13	12490126	37.05	13407838	37.66	13015734	37.13	12490126
45727760		49928560		53189181		45727760	
		4200800		7461421			
		0.515242		0.60245205			
$\text{Hg}^+, 198$	199,	200,	201,	202		$\text{Hg}^+, 198$	199,
197.97	11451098	198.11	13370302	197.93	13921779	197.97	11451098
198.8	12271736	199.02	12647094	198.89	13183322	198.8	12271736
199.69	13079871	199.9	12710293	199.78	12959531	199.69	13079871
200.59	12664230	200.77	12277927	200.69	12815123	200.59	12664230
201.48	12596861	201.65	12949576	201.57	12494740	201.48	12596861
202.36	12484103	202.57	13109098	202.46	12467919	202.36	12484103
203.18	11409890	203.47	12845746	203.33	12424418	203.18	11409890
85957789		89910036		90266832		85957789	
		3952247		4309043			
		0.484757		0.3479219			
HgCl^+	234,	235,	237			HgCl^+	234,
233.07	12438859	233.44	11629590	233.04	11733633	233.07	12438859
233.94	12575673	234.29	12082645	233.83	11306083	233.94	12575673
234.82	12462636	235.14	12520867	234.66	12525325	234.82	12462636
235.69	12505948	235.99	11576087	235.55	12414896	235.69	12505948
236.54	11692634	236.74	10587214	236.4	12289092	236.54	11692634
237.37	12339359	237.54	11515951	237.27	12473030	237.37	12339359
238.22	11866479	238.29	10395908	238.11	12050498	238.22	11866479
85881588		80308262		84792557		85881588	
		-5573326		-1089031			
		0		0			
HgCl_2^+	269,	270,	272			HgCl_2^+	269,
268.32	13094456	268.56	11885642	268.5	12639633	268.32	13094456
269.23	12977780	269.36	11235781	269.37	12689914	269.23	12977780
270.13	12687769	270.18	12419458	270.32	14377292	270.13	12687769
271.02	13052673	271.08	12786340	271.31	13908910	271.02	13052673
271.98	14586179	271.98	13262302	272.25	13126949	271.98	14586179
272.95	13259969	272.91	13275786	273.14	12614885	272.95	13259969
79658826		74865309		79357583		79658826	
		-4793517		-301243			
		0		0			

Coated Reactor (contaminated) /Hg + HCl → ...

Residence time = 4.2 seconds

HgCl⁺	234,	235,	237		
233.07	12438859	232.76	12481315	232.73	12257067
233.94	12575673	233.63	12605404	233.61	12839912
234.82	12462636	234.51	12633116	234.5	12767521
235.69	12505948	235.43	13609135	235.43	13667925
236.54	11692634	236.36	13047541	236.38	13368704
237.37	12339359	237.29	13281894	237.29	12873914
238.22	11866479	238.19	12639461	238.19	12956232
	85881588		90297866		90731275
			4416278		4849687
			0.15295582		0.1679667
HgCl₂⁺	269,	270,	272		
268.32	13094456	268.56	9397948	268.67	8791184
269.23	12977780	269.25	10455890	269.29	9893414
270.13	12687769	270.08	13152588	270.06	11970943
271.02	13052673	271	13340288	270.95	13589545
271.98	14586179	271.85	11086975	271.82	11750630
272.95	13259969	272.63	11981670	272.61	11527959
	79658826		69415359		67523675
			-10243467		-12135151
			0		0
Hg₂Cl₂⁺	468,	470,	474		
470.29	13187993	470.19	18904389	470.18	18363346
471.2	12941974	471.07	15542194	471.05	15239385
472.12	13107143	472.02	14550627	472	14846749
473.06	13730714	472.94	13086645	472.96	13384189
473.95	11598256	473.85	13437254	473.86	13150500
	64566080		75521109		74984169
			10955029		10418089
			0.37942255		0.3608259

Coated Reactor (contaminated) /Hg + HCl → ...

Residence time = 4.2 seconds

HCl+/Cl+	nb.txt	chcl.c		chcl.d	
34.79	11944329	34.73	13791816	34.69	13751803
35.57	10582441	35.75	14976465	35.7	14850125
36.31	10710864	36.75	13754456	36.71	14057613
37.13	12490126	37.69	13139625	37.66	13272016
	45727760		55662362		55931557
			9934602		10203797
			0.34408052		0.353404
Cl₂⁺					
69.9	12270693	69.98	13606027	69.98	13943555
70.75	12096249	70.91	12665070	70.91	12686848
71.63	12782391	71.79	13256910	71.8	13216896
72.52	12735539	72.71	12896465	72.71	12927092
73.41	12764483	73.6	12640950	73.61	12809465
74.3	12748830	74.49	13103992	74.51	12749278
	75398185		78169414		78333134
			2771229		2934949
			0.09598028		0.1016507
Hg⁺, 198	199,	200,	201,		
197.97	11451098	198.07	13257325	198.03	14186402
198.8	12271736	198.96	12831536	198.96	13098769
199.69	13079871	199.89	13308934	199.87	13056527
200.59	12664230	200.71	10656090	200.72	11301411
201.48	12596861	201.46	10849463	201.51	11539914
202.36	12484103	202.3	13151019	202.37	12811993
203.18	11409890	203.2	12699183	203.24	12245733
	85957789		86753550		88240749
			795761		2282960
			0.02756083		0.0790693

APPENDIX I. CONTACT INFORMATION

Contact Information for the Experimental Apparatus:

I. Electronics (local)

- **Elliott Electronics Inc.**
1251 South Tyndall Ave.
Tucson, AZ 85713
Phone: (520)884-7394
- **Electronic City**
1300 South Park
Tucson, AZ 85713
Phone: (520) 622-1173
- **Crescent Electronic Supply Company**
523 E 10th Street
Tucson, AZ 85705
Phone: (520) 624-8241

II. Vacuum Assembly

For purchasing:

- **MDC**
23842 Cabot Blvd.
Hayward, CA 94545-1661
Phone: 800-443-8817
Fax: 510-887-0626
<http://www.mdc-vacuum.com/>
- **Kurt J Lesker**
1515 Worthington Ave
Clairton, Pa 15025
Phone: 800-245-1656
<http://www.lesker.com/newweb/index.cfm>

III. Mass Spectrometry

For purchasing and troubleshooting:

➤ ABB/Extrel

- **Brian Regel**
brian.regel@us.abb.com
- **Kevin Kuchta**
kevin.kuchta@us.abb.com

APPENDIX J. STEPS FOR PUMPING DOWN THE VACUUM ASSEMBLY

Steps on Pumping Down:

1. Close roughing line valve and open the backing line .
2. Connect and switch on the cooling water supply.
3. Turn on mechanical pump #2 and reduce the pressure in the backing line/diffusion pump to \leq 375 millitorr.
4. Turn on the electrical supply to the diffusion pump ($P = 1350$ Watts, $I \sim 6.5$ amps, $V = 208$ volts).
5. Allow the diffusion pump to warm up for 30 minutes.
6. Close the backing line and open the roughing line.
7. Let the pressure reduce to \leq 225 millitorr. (also, at this point before 225 millitorr is reached, mechanical pump #1 can be switched on)
8. Close the roughing line and open the backing line.
9. Slowly open the 8" gate valve 5 psig at a time. If the valve opens too quickly, the pump may stall.
10. If the pump stalls, (a) close 8" valve (b) turn off heater and (c) start over

Pump shut-down:

1. Close the 8" gate valve.
2. Switch off the heater and allow the pump to cool.
3. Close both backing and roughing lines.
4. Allow air into the pump 1 system and then shut off pump 1.
5. Allow air into the pump 2 system and then shut off pump 2.
6. Turn off cooling-water supply after diff pump has cooled sufficiently.

APPENDIX K. STEPS ON OBTAINING DATA FROM MERLIN

Steps to running samples and using Merlin Data Acquisition Software:

It is important to note that the electronics (i.e. filament, multiplier and dynode) of the mass spectrometer require a maximum pressure of $\sim 3 \times 10^{-5}$ Torr to run without being damaged. For instance, if the pressure becomes higher than this base, the multiplier can become contaminated. Dirty multipliers can be cleaned depending on the extent of contamination, but it is best to keep the chamber pressure below this 10^{-5} maximum. The current vacuum assembly has a base pressure of $\sim 4 \times 10^{-7}$ Torr and reaches a pressure of $\sim 4 \times 10^{-6}$ Torr when a sample is being introduced.

Before beginning an experiment, it needs to be decided which sample probe to place inside the reactor. Recall that the lab is equipped with three different sample probes of three lengths, each resulting in a unique residence time. To verify that the results of the experiment are reproducible, a run should be performed at least three times for a given residence time. When the data is plotted, error bars representing the deviation of the experimental runs should be plotted with the data. (Wilks, 1995)

Once the base pressure of the vacuum chamber is reached and verified through the 880 RS Varian gauge controller, a sample is ready to be examined. The following list of steps are designed for running a reaction for which both reactant species are originating from permeation tubes. These steps can be easily generalized for any reaction, although the steps are specifically designed for running $Hg^0 + HCl \rightarrow \dots$

1. While the system is pumping down, the oil bath should be turned on since it takes about 10 minutes for the bath to reach 100 degrees Celsius, which is the required temperature for vaporizing both Hg^0 and HCl, as specified by VICI Metronics.
2. The Hg^0 and HCl permeation tubes should sit in the U-tubes for at least 20 minutes before passing the nitrogen carrier gas through. The idea is to saturate the lines with Hg^0 vapor and HCl vapor before beginning a reaction.
3. The nitrogen should flow through the mercury permeation tube initially so that the cross flow velocity of mercury can be established in the reactor. After allowing the mercury to flow for about 3 - 5 minutes, the valve for the nitrogen line to the HCl permeation tube can be opened, to allow HCl to flow into the crossflow of mercury in the reactor. Note that the chlorine will flow into the reactor through a series of small holes. This flow through the jets allows for the proper mixing of HCl with Hg^0 .
4. After the nitrogen has been allowed to flow for about 5 minutes, the power supply to the mass spectrometer can be turned on. This is the second component from the bottom of the electronics rack. Once the power supply is on, the electronics of the mass spectrometer can be turned on. These consist of the dynode, multiplier and filament on the C-50 controller, which is the component placed at the top of

the electronics rack. In addition, the Merlin Data Acquisition software can be turned on along with the Merlin electronics box, which is placed at the bottom of the electronics rack.

5. When the Merlin Data Acquisition software is turned on, there should be a series of beeps, which correspond to the communication between the computer and the Merlin electronics box. At this point, most of the work will be through the Merlin software.
6. A profile view is the default setting of the Merlin software. When the sample is ready to be observed, the green light on the following interface should be clicked.
7. Data can be acquired in either the profile or centroid format. The centroid format is preferred since it allows one to save the data in a list format, which can be exported into Excel. However, the profile view is better for presenting the raw data. Lists of numbers are not appealing to an audience during a presentation, for instance.
8. This interface also has an edit button as shown below. Clicking this edit button allows one to choose the mass ranges of interest.

9. Once all the settings have been chosen, data can be acquired by clicking on the start box. Once data is being acquired, one can use the different Macro's available in the Merlin software to allow for the export of the raw data. The raw data from the centroid format is in terms of intensity versus a mass to charge ratio (m/z).

Below is a list of some Macros in the Merlin software package that may be helpful.

- cent_to_list : This macro converts the centroid data into a list form that can be exported directly into Excel.
- spec_to_list : The spec window is for post-acquisition use. The spec window should be used alongside the chromatogram. The chromatogram can be clicked and at any one of these times, the raw data is shown in the spec view. This macro allows the spec data to be converted to the list format for exporting into Excel.
- list_to_pic: This macro allows for the list data to be put into a picture format. This macro has not been proven to be too useful since the x-axis is not marked on the pic format, which forces the user to manually identify what each mass is with respect to its location.

10. Once the data is saved in the list format, it can be exported into Excel. Since there is still backstreaming present in the vacuum chamber, it is important for the background oil peaks to be subtracted from the new data obtained. The intensities of the background oil peaks have been run previously and are saved under the

Methods folder on the hard drive under the name, N2.txt. It is important that the runs be performed under the same conditions that the N₂ was run under. The N₂ “blank” sample was introduced to the mass spectrometer at a flow rate of ~ 5 L/min increasing the pressure from ~ 4×10^{-7} Torr to ~ 4×10^{-6} Torr.

11. Once these background peak intensities have been subtracted from the new run intensities, the data is ready to be plotted.

APPENDIX L. TROUBLESHOOTING ON THE EXPERIMENTAL FRONT

I. Control Panel:

The control panel is designed to control two solenoids which each control a pneumatic gate valve and 3 pumps. The upper rocker switch on the right controls the solenoid that opens and closes the two inch inner diameter gate valve that separates the reactor from the vacuum chamber. The second rocker switch to the left controls a second solenoid that opens and closes an eight inch inner diameter gate valve that isolates the diffusion pump chamber from the vacuum chamber. The control panel also has three push button switches that control two mechanical pumps and one diffusion pump. Starting at the bottom left of the control panel, this push button turns the heating elements of the diffusion pump on and off. To the right is the push button for the second mechanical pump, which acts as the roughing pump for the diffusion pump. The last switch to the right operates the first mechanical pump, which is responsible for the first stage of pressure. The mechanical pumps, when they are first turned on pull a great deal of current. It has been estimated that they pull between 8 and 10 amps of current when first turned on. For this reason there should always be fuses between 12 and 15 amps in the control panel for the wiring of these pumps. Fuses lower than 10 amps have been tried and have failed in the past. The department electrician, Sal, usually has these fuses on hand. Otherwise they can be picked up at one of the local electronics shops such as Elliot's or Electronics City, both which are listed in Appendix H. It is important to note that the fuses can be replaced when the control panel is turned on, however, a fuse extractor must be used to do this.

The last button on the control panel is an automatic reset button. Any time the control panel is unplugged or the power goes out unexpectedly, this button must be pushed in order to bring power back to the panel. Also, solenoid #1 is not being used and the 2 inch ID gate valve has been replaced with an easier to use butterfly valve.

II. Vacuum Assembly:

One of the difficulties with the vacuum assembly is maintaining a good vacuum and preventing leaks. There are different aspects of leak testing that can be employed. A common method for checking leaks that may be preventing the vacuum to reach the 10^{-6} Torr region can be checked with isopropyl alcohol (ISA). The alcohol can be sprayed around all the joints and, when it detects a leak, it will essentially freeze and conceal the leak. At this point a decrease in the pressure on the gauge controller will be present and when the alcohol melts, the pressure will return back to where it was. This narrows down the source of the leak. Sometimes the vacuum will get to the 10^{-6} region, but remain in the “high six” range rather than the desired low six range. When this is the case, the mass spectrometer can be used as a residual gas analyzer (RGA) to determine where the source of the leak is. Helium gas, which has an isotopic fingerprint region around a 4.0 mass to charge ratio, can be sprayed around all the joints while the mass spec is turned on. Recall, the components of the mass spec that will be destroyed under too high a pressure are the filament and multiplier components. However, both of these components will

work fine to detect helium in the low minus five Torr region. When helium is spotted on the spectrum, the leak has been detected.

At times the ion collector in the Bayerd Alpert ion gauge can be dirty and will need to be degassed. The degas switch is on the gauge controller and activating this switch will heat the collector to remove all the molecules that may have adsorbed onto its surface.

Sometimes it may take up to an hour or two to degas the ion gauge and typically this reduces the pressure slightly. For example, if the pressure is consistently at 3.4×10^{-6} Torr, degassing could reduce the pressure further to $\sim 2.5 \times 10^{-6}$ Torr. Degassing should always be performed after the instrument has been exposed to atmosphere in order to obtain the true base pressure of the vacuum system.

Baking out the system is another useful tool in reducing the pressure. Oftentimes if the system has been exposed to atmosphere, there may be water vapor adsorbed to the surfaces inside the vacuum chamber. Also, after a reaction is run, there could be product species that remain behind in the vacuum chamber, depending on the vapor pressures of the different components. The lab is equipped with two different sets of heat tape, each equipped with their own regulators so that the heat distribution can be monitored. The heat tape can be wrapped over the outside of the vacuum chamber and turned on to 100%, which allows the stainless steel to get to about 120 degrees Celsius. Baking out overnight should be sufficient for ridding the surface of most adsorbed components on the inside the vacuum chamber. Oil vapor, on the other hand, is very difficult to remove

from the chamber. If there is oil contamination and the mass spec or the housing becomes contaminated, the equipment can be sent out for very thorough cleaning at ABB/Extrel. This process costs about \$1000 and the contact information is in Appendix H.

Baking out the assembly is also important since materials such as o-rings and stainless steel are capable of outgassing. If all the gas that needed to be removed from the system to obtain the optimum base pressure existed just in the volume of the vacuum chamber, then the system would reach base pressure fast and easily. For instance, the vacuum chamber in the lab has a volume of approximately 80 liters. The gas pressure is given by the following equation (O'Hanlon, 1980):

$$P = P_0 e^{\frac{-St}{V}} \quad (\text{L.1})$$

such that P_0 is the initial pressure (2 Torr in this case), S is the pumping speed of the pump (the lab is equipped with a 760 L/s diffusion pump), t is the time it takes to reach a pressure, P , and V is the vacuum chamber volume. If the chamber is the only volume where gas need to be evacuated, equation (L.1) implies a base pressure of 1.3×10^{-6} Torr that would be reached in 1.5 seconds. Of course this is not the case and, rather, outgassing of the components such as the steel surfaces and the o-rings places an impedance on the rate in which the system takes to reach the assembly's base pressure. The outgassing rate has units of W/m^2 , which is the quantity of gas evolved per unit time per unit surface area. The vacuum chamber, typically made of stainless steel is prebaked

before use so that the outgassing rate is minimal, being on the order of 10^{-10} W/m². Typical gases that are released from stainless steel outgassing are H₂, H₂O, CO, Ar, and CO₂. (O'Hanlon, 1980) The o-rings used in the vacuum system are also capable of outgassing. The current vacuum assembly contains both Viton and Buna-N o-rings for the quick flange connections. When installing o-rings into the vacuum assembly, a small amount of vacuum grease should be applied in an attempt to prevent outgassing. If not done previously, the o-rings should be baked out. The Buna-N and Viton o-rings can be baked at 200 ° C, which will remove most of the adsorbed gases. Higher temperatures should be avoided since the o-ring material could decompose. Much research has been performed on unbaked o-rings and it was found that the major gas released was water vapor. (Perkins, 1973; Hait, 1967; Barton and Govier, 1968)

III. Changing the Oil in the Pumps

If the same type of oil is being placed in the pumps, then it is not necessary to clean or recharge the pumps. However, if a new pump oil different than what was originally in the pump is being introduced, the process is more involved.

Changing the oil in the mechanical pumps is fairly straightforward even if the fluid type is changed. First, the old oil needs to be drained from the pump and disposed of properly. It is best if the pump was running prior to draining and not stagnant since warm oil will drain more efficiently. It is best to get as much of the old oil out of the system as

possible so that the pump can run efficiently in the future. The pump will now have to be filled with the new oil and the view ports are located on the side of the pump to prevent overfilling. After the pump is filled with new oil it should be turned on, but the inlet to the pump should be capped. It should run like this for thirty minutes to ensure that the fluid has run through the internal components of the pump. At this point the pump is being “charged”. Following this charging stage, the fluid should be drained and then refilled in the same manner as explained above. At this point the pump should be turned back on and should pump on a limited volume for thirty minutes. Following this, the pump is ready to be used continuously on the desired volume.

The diffusion pump oil replacement is more involved. First, the oil needs to be drained. The drain is located as a sidearm on the pump and unscrews from the bottom. Due to the very viscous nature of the diffusion pump fluid, the draining process is very time consuming. It can take up to 5 hours to completely drain the diffusion pump. The diffusion pump is attached to the vacuum chamber via a conflate flange. Each bolt will have to be taken out and, when replacing the diffusion pump, a new copper gasket will have to be used for the knife-edge seal to prevent any potential leaks. Once the diffusion pump is detached, it will need to be taken apart and cleaned thoroughly. Everything inside the pump should be taken out and disassembled except for the jet assembly. The jet assembly is a very delicate aspect of the diffusion pump and should be left assembled.

Each component of the diffusion pump should be cleaned alternately with methanol and acetone. Methanol acts as a reasonable solvent for the old oil and the acetone acts as a solvent to cleanse the acetone. Each will show peaks on the mass spectrum and this should be minimized. The cracking pattern of methanol is such that it will show up on the mass spectrum at 29, 31 and 32 m/z. The cracking pattern of acetone is such that it will show up on the mass spectrum at 43 and 58 m/z. Once the diffusion pump has been cleaned with methanol and acetone, it is best to heat the components with a heat gun to maximize the removal of methanol and acetone once they are sealed in the vacuum assembly. At this point, the diffusion pump can be assembled and the flange can be bolted with the new gasket in place. It should be noted that filling the pump with oil is a time consuming process and can take about an hour due to the high viscosity of Santovac 5. The 760 L/s diffusion pump requires 250 mL of oil. Also, there is an o-ring for the cap of the oil plug. If this o-ring appears damaged, it should be replaced, since this could be a source of possible leaks.

IV. Mass Spectrometer

The filament can be controlled via the C-50 controller, which is the top unit on the electronics rack. The source of the mass spectrometer is an electron ionization source by which a voltage is applied to the tungsten filaments. The filament becomes hot and “boils” off electrons which bombard the molecules coming in, presumably from the reactor. The electrons will hit 1 in every 100,000 molecules that come through the laser

drilled ruby orifice. For this reason, up to 70 eV are applied to the filament. The filament should always be operated in the low voltage or low emission range on the C-50 controller. Applying the high emission will burn out the filament. If the red light comes on, the C-50 controller implies that there is a problem with the filament. To be sure the filament is still intact, the connection between the C and D pins on the 10 pin connector of the vacuum flange can be tested. This is done using a voltmeter with the setting on resistance. If the filament is intact, the meter should read infinite resistance. Figure L-1

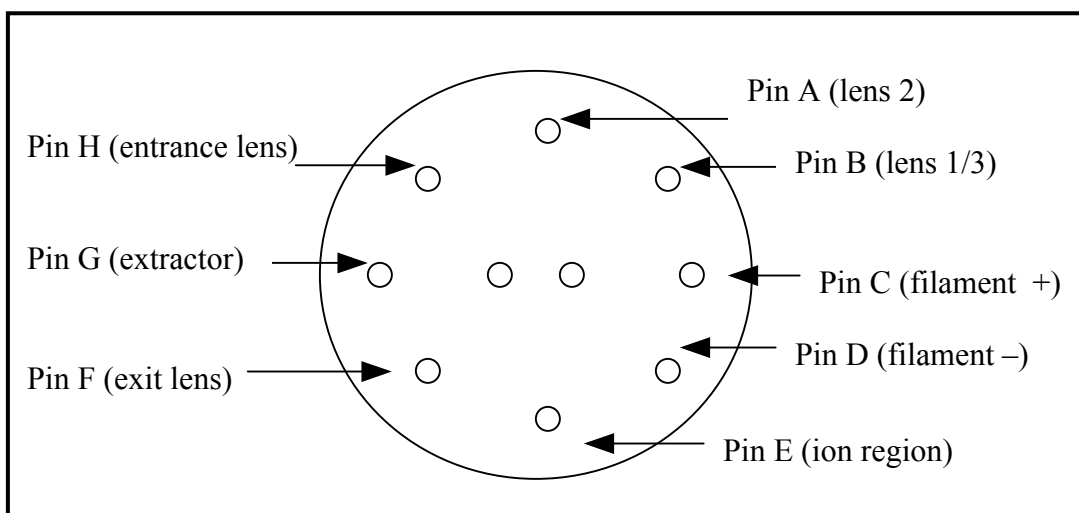


Figure L-1. Schematic of the 10-Pin Connector to Vacuum Flange

shows a schematic of the 10 pin connector that is attached to the vacuum flange. The voltages to the lenses of the mass spectrometer are also applied through this connector from the C-50 controller and are labeled below. The two center pins are labeled J and K and remain unconnected. The cable which connects to the vacuum flange at this 10-pin

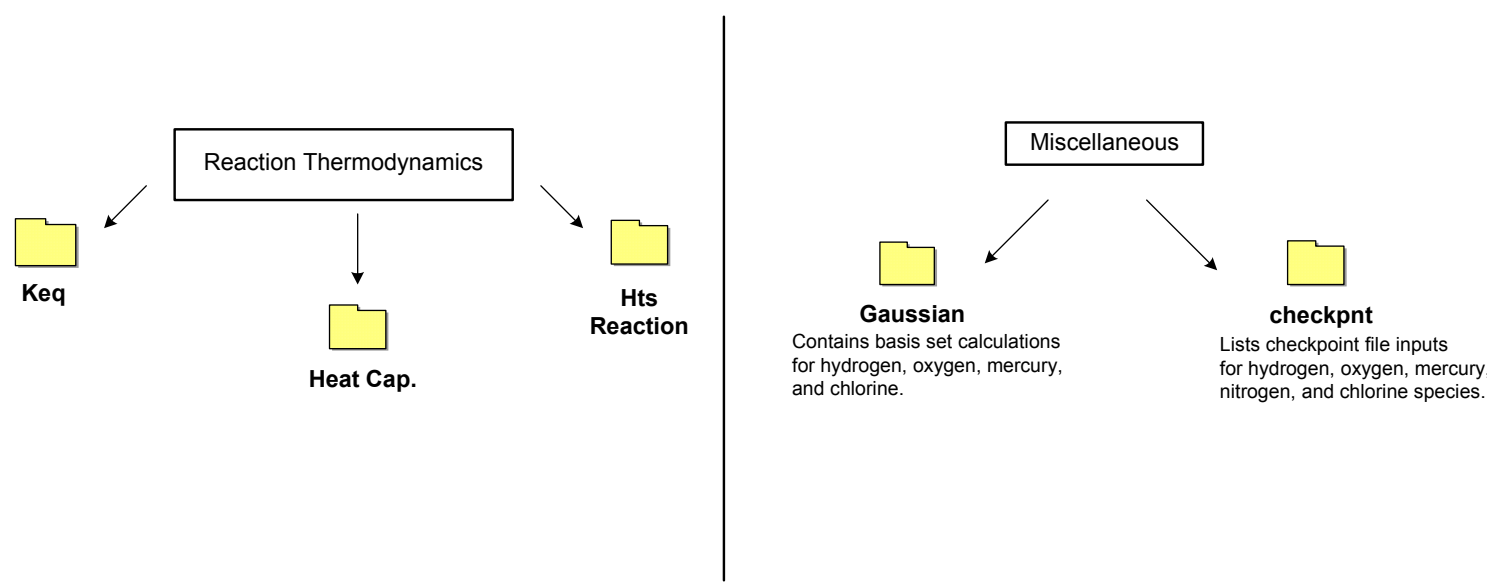
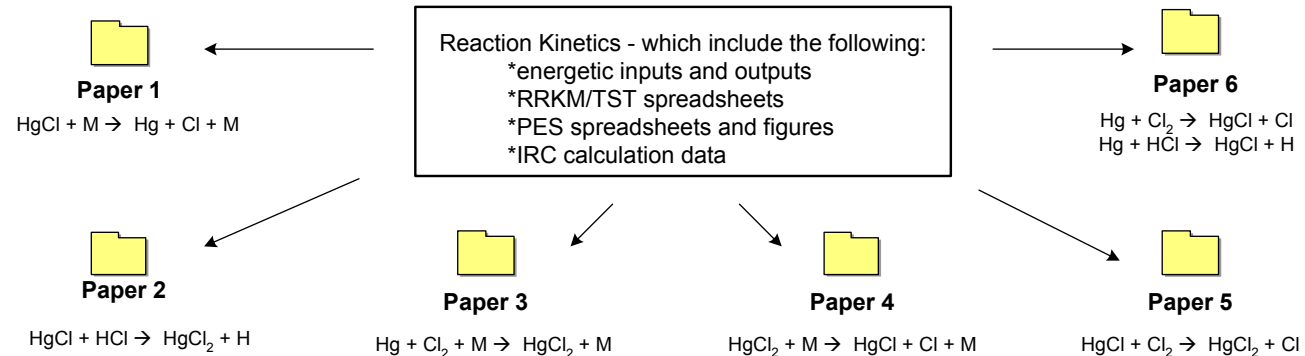
connection are attached to the back of the C-50 controller. The C-50 also controls the conversion dynode which is labeled CN on the vacuum flange. The mass spectrometer is set up to measure positive ions so that the multiplier connection needs to be connected to the mult (-) connection on the vacuum flange. The mult (+) connection has been purposely shorted out. The mult (+) connection would be used to measure negative ions. The RF connections on the outside of the flange connect to the power supply, which is the 3rd component down on the electronics rack. The RF connections supply power to the quadrupoles of the mass spectrometer. Lastly, the signal, which is labeled sig on the vacuum flange is controlled through the Merlin component, which is the 1st component at the base of the electronics rack. The signal cable is connected to Merlin via an analog preamp. In the future it may be beneficial to purchase a counting multiplier. The lab is already equipped with a counting preamp, but the current fifteen-year-old multiplier is not compatible with it. The counting preamp allows for increased sensitivity when measuring at low concentrations, such as the ppb range. The signal is the only component of the mass spectrometer that Merlin is controlling with the remainder of the components all being controlled through the C-50. The components of the C-50 are about 15 years old and may need to be replaced in the near future. The Merlin component consists of modules which can be installed if they are not working properly on the C-50 controller. This makes the process of replacing the old C-50 more affordable by purchasing just one component at a time. The contact information for troubleshooting and purchasing with the mass spectrometer is located in Appendix H.

If the filament is burned out, it can be replaced using the spare tungsten wires available in the lab. Each of the two filaments need to have between 5 and 6 turns in the tungsten wire. The tungsten wire in the lab has already been coiled. The filament replacement is time consuming due to the fact that the vacuum flange needs to be removed in order to get to the electron ionization source. The filament wire is dry soldered on the source. When putting the flange back on, the copper gasket will have to be replaced to ensure minimal leaks through the knife-edge seal.

APPENDIX M. DIRECTORY OF RESEARCH DATA

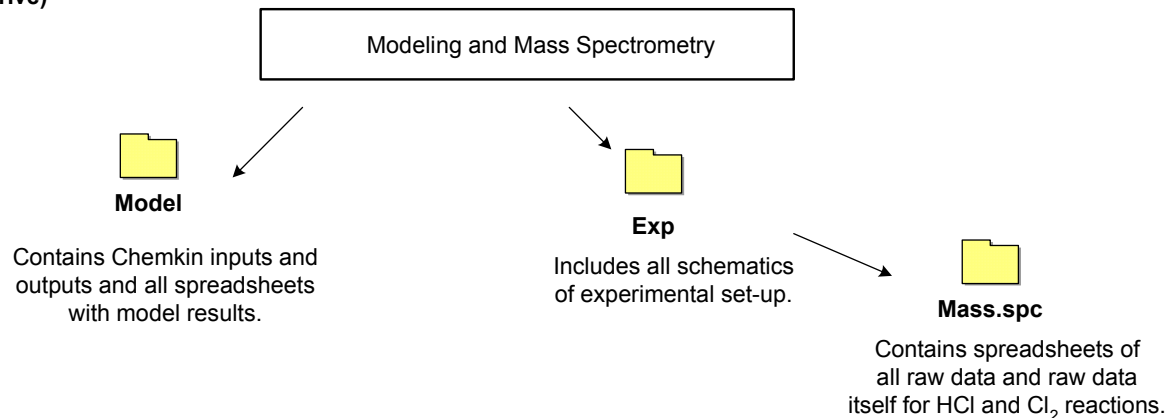
Theoretical Research:

(all data located in file name,
jwilcox on C drive)



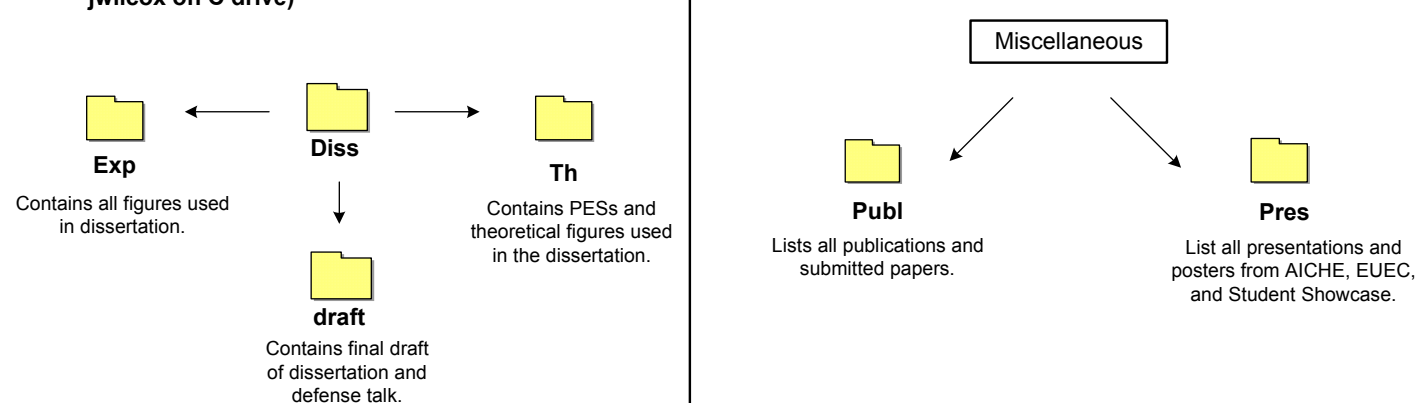
Experimental Research:

(all data located in file name,
jwilcox on C drive)



Miscellaneous:

(all data located in file name,
jwilcox on C drive)



APPENDIX N. CURRICULUM VITAE

2707 N. Orchard Ave
Tucson, AZ 85712
(520) 327-2043
jwilcox@email.arizona.edu

Jennifer Wilcox

website: www.u.arizona.edu/~jwilcox

EDUCATION:

- | | |
|--------------|--|
| 2000 – 2004 | University of Arizona , Tucson, AZ
Ph.D. in Chemical Engineering |
| 2002 -- 2004 | University of Arizona , Tucson, AZ
pursuing a M.A. in Physical Chemistry |
| 1994 – 98 | Wellesley College , Wellesley, MA
B.A. in Mathematics and Chemistry. |

WORK EXPERIENCE:

- Jan. 2000 – present **University of Arizona**, Tucson, AZ
Research Assistant, working on the development of mercury speciation from the flue gases of coal combustion processes. The research includes both experimental and theoretical methods of research.

Sept. 99 – present **Pima Community College**, Tucson, AZ
Adjunct Faculty/Mathematics/Chemistry, teaching intermediate algebra and introductory chemistry at the college level consisting of classes up to fifty students. Other responsibilities include creating a curriculum and exams for the course. On average, I taught 6 – 9 units per semester while in graduate school.

Aug. 02 - Dec. 2002 **University of Arizona**, Tucson, AZ
Teaching Assistant, developed solutions and held office hours for undergraduate chemical engineering kinetics course.

Jan. 99 – Dec. 1999 **Enviro Engineering, Inc.**, Tucson, AZ
Environmental Scientist, responsibilities included writing environmental site assessments and characterization reports, field investigations, and the installation and maintenance of monitoring wells.

Lab Technician, responsibilities included the analysis of environmental samples using gas chromatography; sample collection and tracking, preparation and analysis, lab maintenance, and client support.

Sept. – June 1998

Wellesley College, Wellesley, MA

Teaching Assistant, graded coursework in Calculus II and held weekly review sessions with up to thirty students.

AWARDS:

- 1st Place, “What Does Schrödiner’s Equation Have to do With Mercury in Our Fish?”, Student Showcase 2001, Engineering Division, University of Arizona, November 2001.
- 1st Place, “On the Path to Preventing Mercury Release from Coal Combustion”, Student Showcase 2002, Engineering Division, University of Arizona, November 2002.
- 1st Place, “On the Path to Elucidating the Speciation of Mercury in the Flue Gases of Coal Combustion”, Student Showcase 2003, Engineering Division, University of Arizona, November 2003.

PUBLICATIONS:

- 1) P. Blowers and J. Wilcox, “Integration of Communication Skills into the Introductory Material and Energy Balances Course in Chemical Engineering”, *Proceedings of the 2001 American Society for Engineering Education Annual Conference & Exposition, 2001*.
- 2) J. Wilcox, D.C.J. Marsden and P. Blowers, “Evaluation of Basis Sets and Theoretical Methods for Estimating Rate Constants of Mercury Oxidation Reactions Involving Chlorine”, *Fuel Processing Technology*, **2004**. (in press)
- 3) J. Wilcox, J. Robles, D.C.J. Marsden, and P. Blowers, “Theoretically predicted rate constants for mercury oxidation by hydrogen chloride in coal combustion flue gases”, *Environ. Sci. Technol.*, **37**(18) **2003**, 4199-4204.
- 4) J. Wilcox A. Bennett and P. Blowers, “Correction and Improvement of Mercury Speciation Kinetics Estimates from Quantum Chemical Calculations”, accepted to *Journal of Molecular Structure*.
- 5) J. Wilcox, D.C.J. Marsden and P. Blowers, “A Comparison of Quantum Mechanical Methods in Predicting Rate Constants for Mercury Oxidation Reactions Involving Chlorine-containing Species”, submitted to *Fuel Processing Technology*.
- 6) P. Blowers, X. Zheng and J. Wilcox, “An Accurate Heat of Formation Estimate for Mercuric Oxide Based on Quantum Chemical Calculations”, submitted to *Combustion and Flame*.
- 7) J. Wilcox and P. Blowers, “The Decomposition of Mercuric Chloride and its Application to Modeling Mercury in the Flue Gases of Coal Combustion”, submitted to *J. of Env. Chem.*
- 8) J. Wilcox and P. Blowers, “The Current Status of the Mercury Speciation in the Flue Gases of Coal Combustion: A Background on the Quantum Mechanics and Chemical Kinetics behind the Theoretical Calculations of Kinetic and Thermodynamic Data” (in progress).
- 9) J. Wilcox, J.O.L. Wendt and P. Blowers, “The Validation of a Theoretically Derived Model for Mercury Oxidation via Chlorine through Experimental Findings Using Quadrupole Mass Spectrometry” (in progress).
- 10) P. Blowers and J. Wilcox, “Estimation of Heat Capacities from Ab Initio Methods for Mercury-Containing Species: Further Justification of Accurate Basis Sets for Mercury Speciation Kinetics” (in progress).

PRESENTATIONS:

- 1) J. Wilcox (speaker), J.O.L. Wendt and P. Blowers, "On the Path to Elucidating the Speciation of Mercury in the Flue Gases of Coal Combustion", 7th Electrical Utilities Environmental Conference", Tucson, AZ, January 2004.
- 2) J. Wilcox (speaker), P. Blowers and J.O.L. Wendt, "Understanding the Kinetics of Mercury Oxidation in the Flue Gases of Coal Combustion: Experimental and Theoretical Results", AICHE Annual Meeting, San Francisco, CA, November 2003.
- 3) J. Wilcox (poster), P. Blowers and J.O.L. Wendt, "Modeling Mercury Oxidation in the Flue Gases of Coal Combustion", AICHE Annual Meeting, San Francisco, CA, November 2003.
- 4) J. Wilcox (speaker), P. Blowers and J.O.L. Wendt, "On the Path to Preventing Mercury Release into the Atmosphere", Chemical Engineering Departmental Seminar, University of Arizona, September 2003.
- 5) J. Wilcox (poster), "On the Path to Elucidating the Speciation of Mercury in the Flue Gases of Coal Combustion", Student Showcase 2003, University of Arizona, November 2003.
- 6) J. Wilcox (speaker), J. Robles, D. Marsden, P. Blowers, "An Ab Initio Investigation of Gas Phase Mercury Reactions Important in Coal Combustion", 6th Electrical Utilities Environmental Conference", Tucson, AZ, January 2003.
- 7) J. Wilcox (poster), "On the Path to Preventing Mercury Release from Coal Combustion", Student Showcase 2002, Board of Legislators, Phoenix, AZ, February 2003.
- 8) J. Wilcox (poster), "On the Path to Preventing Mercury Release from Coal Combustion", Student Showcase 2002, University of Arizona, November 2002.
- 9) J. Wilcox (speaker), J. Robles, D. Marsden, P. Blowers, "Mercury Speciation in Flue Gases: $HgCl_2 + H = HCl + HgCl$ ", AICHE Annual Meeting, Indianapolis, Indiana, November 2002.
- 10) J. Wilcox (poster), D. Marsden, P. Blowers, "Mercury Speciation in Flue Gases: $HgCl = Hg + Cl$ ", AICHE Annual Meeting, Indianapolis, Indiana, November 2002.
- 11) J. Wilcox (poster), "What Does Schrödiner's Equation Have to do With Mercury in Our Fish?", Student Showcase 2002, Board of Legislators, Phoenix, AZ, February 2002.
- 12) J. Wilcox (poster), "What Does Schrödiner's Equation have to do With Mercury in Our Fish?", Student Showcase 2001, University of Arizona, November 2001.
- 13) J. Wilcox (speaker), P. Blowers, "An Ab Initio Investigation of Gas Phase Mercury Reactions Important in Coal Combustion Vapor Emissions", AICHE Annual Meeting, Reno, Nevada, November 2001.
- 14) P. Blowers and J. Wilcox (speakers), "Integration of Communication Skills into the Introductory Material and Energy Balances Courses in Chemical Engineering", AICHE Annual Meeting, Reno, Nevada, November 2001.
- 15) J. Wilcox (invited speaker), P. Blowers, "An Ab Initio Investigation of Gas Phase Mercury Reactions Important in Coal Combustion Vapor Emissions", University of Arizona, Department of Mathematics Departmental Seminar, October 2001.
- 16) P. Blowers and J. Wilcox (speakers), "Integration of Communication Skills into the Introductory Material and Energy Balances Courses in Chemical Engineering", ASEE Annual Meeting, Albuquerque, NM, June 2001.
- 17) P. Blowers and J. Wilcox (speakers), "Integration of Communication & Teamwork Into Introductory Courses", Learning Technology Showcase 2000, Learning in the New Millennium: our Future Continues, University of Arizona, May 2001.

REFERENCES

1. Afeefy H.Y., Liebman J.F., and Stein S.E. (2003) "Neutral Thermochemical Data" in *NIST Chemistry WebBook, NIST Standard Reference Database 69*, Eds. P.J. Linstrom and W.G. Mallard, National Institute of Standards and Technology, Gaithersburg MD, 20899
2. Alcami M., Mo O., Yanez M. (2001) Computational Chemistry: A Useful (sometimes mandatory) Tool in Mass Spectrometry Studies. *Mass Spectrom. Rev.* **20**, 195-245.
3. Allen M.T., Yetter R.A., Dryer F.L. (1997) *Combust. Flame* **109**, 449-470.
4. Ariya P.A., Khalizov A., Gidas A. (2002) Reactions of Gaseous Mercury with Atomic and Molecular Halogens: Kinetics, Product Studies, and Atmospheric Implications. *J. Phys. Chem.* **106**, 7310-7320.
5. Aschner, M. (2001) Mercury Toxicity. *J. Pediat.* **138** (3), 450-451.
6. Balabanov N.B., Peterson K.A. (2003) Mercury and Reactive Halogens: The Thermochemistry of $\text{Hg} + \{\text{Cl}_2, \text{Br}_2, \text{BrCl}, \text{ClO}, \text{and BrO}\}$. *J. Phys. Chem. A* **107**, 7465-7470.
7. Bartlett R.J., Shavitt I. (1977) Comparison of high-order many-body perturbation theory and configuration interaction for H_2O . *Chem. Phys. Lett.* **50** (2), 190.
8. Barton R.S., Govier R.P. (1965) *J. Vac. Sci. Technol.* **2**, 113.
9. Berning A., Schweizer M., Werner H.J., Knowles P.J., Palmieri P. (2000) Spin-orbit Matrix Elements for Internally Contracted Multifrequency Configuration Interaction Wavefunctions. *Molecular Physics* **98** (21), 1823-1833.
10. Beyer T., Swinehart D.F. (1973) Algorithm 448. Number of Multiply-Restricted Partitions [A1]. *Commun. ACM* **16**, 379.
11. Billing G.D., Mikkelsen K.V. (1966) *Molecular Dynamics and Chemical Kinetics*, John Wiley & Sons, United States, Chapter 6.

12. Bird R.B., Stewart W.E., Lightfoot E.N. (2002) *Transport Phenomena*, John Wiley & Sons, Inc. U.S.
13. Boening D.W. (2000) Ecological effects, transport, and fate of mercury: a general review. *Chemosphere* **40**, 1335-1351.
14. Boole L.E., Helble J.J., Shah N., Shah A., Huffman G.P., Huggins F.E., Rao K.R.P.M., Sarofim A.F., Zeng T., Reschke R., Galline D., Peterson T.W. (1995) Fundamental Study of Ash Formation and Deposition; Effect of Reducing Stoichiometry. *DOE Report No. PSIT-1178/TR-1407*, Department of Energy, Pittsburgh Energy Technology Center.
15. Braune H., Knoke S. (1933) *Zeits. Physik. Chem.* **B23**, 163-170.
16. Brown T.D., Smith D.N., O'Dowd W.J., Hargis R.A. (2000) Control of Mercury Emissions from Coal-Fired Power Plants: A Preliminary Cost Assessment and the Next Steps for Accurately Assessing Control Costs. *Fuel Process. Technol.* **65-66**, 311-341.
17. Carabetta R.A., Palmer H.B. (1967) Rate of Dissociation of Chlorine in Shock Waves. *J Chem. Phys.* **16**, 1333.
18. Chase, M.W., Jr. (1998) NIST-JANAF Thermochemical Tables, Fourth Edition, *J. Phys. Chem. Ref. Data, Monograph 9*, 1-1951.
19. Cheremisinoff N.P., Gupta R. (1983) Handbook of Fluids in Motion. Butterworth Publishers, Stoneham, MA, p. 242.
20. Cizek J. (1966) *J. Chem. Phys.* **45**, 4256.
21. Cizek J., Paldus J. (1971) *Int. J. Quantum Chem.* **53**, 59.
22. Cosic et al., Fontijn A. (1999) *Paper 99F-007. Presented at the Fall 1999 Meeting of the Western States Section/The Combustion Institute*. University of California, Irvine, California, October 25-26.
23. Dawson P.H. (editor) (1976) *Quadrupole Mass Spectrometry and its Applications*. American Institute of Physics, Woodbury, New York.
24. Dicke R.H., Wittke J.P. (1960) *Introduction to Quantum Mechanics*. Addison-Wesley Publishing Company, Inc. U.S.

25. Dolg M., Küchle W., Stoll H., Preuss H., Schwerdtfeger P. (1991) *Ab initio* Pseudopotentials for Hg to Rn II. Molecular Calculations on the Hydrides of Hg to At and the Fluorides of Rn. *Molecular Physics*, **74** (6) 1265.
26. Dunning Jr. T.H., Hay P.J.(1976) *Modern Theoretical Chemistry*, Ed. H.F. Schaefer, Vol. III, Plenum, New York.
27. Dyall K.G. (2001) Formal Analysis of Effective Core Potential Methods. *J. Chem. Inf. Comput. Sci.* **41** (1), 30-37.
28. Edwards J.R., Srivastava R.K., Kilgroe J.D. (2001) A Study of Gas-Phase Mercury Speciation Using Detailed Chemical Kinetics. *J. Air & Waste Manage. Assoc.* **51**, 869-877.
29. EPA Method 101A, Determination of particulate and gaseous mercury emissions from sewage sludge incinerators, U.S. Federal Register, 1731-1754, date unknown.
30. EPA Method 29, Determination of metal emissions from stationary sources, U.S. Federal Register, 1461-1531, date unknown.
31. Eyring H.(1935) The Activated Complex in Chemical Reactions. *J. Chem. Phys.* **3**, 107.
32. Federal Register Notices for HAP (Title I, Sec. 112)-Preambles and Rules 1998.
33. Flagan R.C., Seinfeld J.H. (1988) Fundamentals of Air Pollution Engineering, Prentice-Hall, Englewood Cliffs, NJ, 217-219.
34. Fujiwara N., Fujita Y., Tomura K., Moritomi H., Tuji T., Takasu S., Niksa S. (2002) Mercury Transformations in the Exhausts From Lab-Scale Coal Flames. *Fuel* **81**, 2045-2052.
35. Galbreath K.C., Zygarlicke C.J. (1996) Mercury Speciation in Coal Combustion and Gasification Flue Gases. *Environ. Sci. Technol.* **30** (8), 2421-2426.
36. Galbreath K.C., Zygarlicke C.J., Toman D.L. (1998) Mercury Measurement and its Control: What We Know, Have Learned, and Need to Further Investigate. *Air & Waste Management Association's 91st Annual Meeting and Exhibition*, June 14 – 18, San Diego, California.

37. Gao J. L., Truhlar D. G. (2002) Quantum Chemical Methods For Enzyme Kinetics. *Ann. Rev. Phys. Chem.* **53**, 467-505.
38. Gaussian 98, Revision A.9. Frisch M. J., Trucks G. W., Schlegel H. B., Scuseria G. E., Robb M. A., Cheeseman J. R., Zakrzewski V. G., Montgomery J. A., Jr., Stratmann R. E., Burant J. C., Dapprich S., Millam J. M., Daniels A. D., Kudin K. N., Strain M. C., Farkas O., Tomasi J., Barone V., Cossi M., Cammi R., Mennucci B., Pomelli C., Adamo C., Clifford S., Ochterski J., Petersson G. A., Ayala P. Y., Cui Q., Morokuma K., Malick D.K., Rabuck A. D., Raghavachari K., Foresman J. B., Cioslowski J., Ortiz J. V., Baboul A. G., Stefanov B. B., Liu G., Liashenko A., Piskorz P., Komaromi I., Gomperts R., Martin R. L., Fox D. J., Keith T., Al-Laham M. A., Peng C. Y., Nanayakkara A., Challacombe M., Gill P. M. W., Johnson B., Chen W., Wong M. W., Andres J. L., Gonzalez C., Head-Gordon M., Replogle E. S., Pople J. A. (1998) Gaussian, Inc.: Pittsburgh, PA.
39. Ghorishi S.B., Sedman, C.B. (1998) Low Concentration Mercury Sorption Mechanisms and Control by Calcium-Based Sorbents: Application in Coal-Fired Processes. *J. Air & Waste Management* **48**, 1191-1198.
40. Glarborg P., Miller J.A., Kee R.J. *Combust. Flame* **65** (2), 177-202.
41. Gonzalez-Lafont A., Truong T.N., Truhlar D.G. (1991) Interpolated Variational Tranistion-state Theory: Practical Methods for Estimating Variational Tranistion-state Properties and Tunneling Contributions to Chemical Reaction Rates from Electronic Structure Calculations. *J. Chem. Phys.* **95**, 8875.
42. Gregg A.H., Hampson G.C., Jenkins G.I., Jones P.L.F., Sutton L.E. (1937) *Trans. Faraday Soc.* **33**, 852.
43. Gullet B.K., Bruce K.R., Beach L.O. (1990) The Effect of Metal Catalysts on the Formation of Polychlorinated Dibenzo-p-dioxin and Polychlorinated Dibenzofuran Precursors. *Chemosphere* **20** (10-12), 1945-1952.
44. Haeussermann U., Dolg M., Stoll H., Preuss H. (1993) Accuracy of Energy-adjusted Quasirelativistic *Ab Initio* Pseudopotentials All-electron and Pseudopotential Benchmark Calculations for Hg, HgH, and their Cations. *Mol. Phys.* **78**, 1211.
45. Hait P., (1967) *Vacuum* **17**, 547.

46. Hall B (1990) Reactions of Mercury with Flue Gas Components. *Report 00K 90:06*, ISSN 0283-8575.
47. Hall B. (1995) The Gas Phase Oxidation of Elemental Mercury By Ozone. *Water, Air, and Soil Pollut.* **80**, 301-315.
48. Hall B., Schager P., Lindqvist O. (1991) Chemical Reactions of Mercury in Combustion Flue Gases. *Water, Air and Soil Pollution* **56**, 3-14.
49. Hall B., Schager P., Weesmaa J. (1995) The Homogeneous Gas Phase Reaction of Mercury with Oxygen, and the Corresponding Heterogeneous Reactions in the Presence of Activated Carbon and Fly Ash. *Chemosphere* **30** (4), 611-627.
50. Häussermann U., Dolg M., Stoll H., Preuss H., Schwerdtfeger P., Pitzer R.M. (1993) Accuracy of Energy-adjusted Quasirelativistic *Ab Initio* Pseudopotentials All-electron and Pseudopotential Benchmark Calculations for Hg, HgH, and their Cations. *Molecular Physics* **78**(5) 1211.
51. Hay P.J., Wadt W.R. (1985) *Ab initio* Effective Core Potentials for Molecular Calculations. Potentials For the Transition Metal Atoms Sc to Hg. *J. Chem. Phys.* **82**, 270.
52. Hay P.J., Wadt W.R., Kahn L.R., Bobrowicz F.W. (1978) *Ab initio* Studies of AuH, AuCl, HgH and HgCl₂ Using Relativistic Effective Core Potentials. *J. Chem. Phys.* **69**(3), 984.
53. Hayes R.E. (2001) *Introduction to Chemical Reactor Analysis*, Gordon and Breach Science Publishers, Amsterdam, The Netherlands.
54. Hehre W.J., Radom L., Schleyer P.V., Pople J. (1986) *Ab Initio Molecular Orbital Theory*, Wiley, New York, 1986.
55. Hehre W.J., Stewart R.F., Pople J.A. (1969) Self-Consistent Molecular-Orbital Methods. I. Use of Gaussian Expansions of Slater-Type Atomic Orbitals. *J. Chem. Phys.* **51** (6), 2657.
56. Herzberg G. (1939) *Molecular Spectra and Molecular Structure I. Spectra of Diatomic Molecules*, Van Nostrand Reinhold, New York.

57. Herzberg G. (1966) *Molecular Spectra and Molecular Structure III. Electronic Spectra and Electronic Structure of Polyatomic Molecules*, Van Nostrand Reinhold, New York.
58. Holbrook K.A., Pilling M.J., Robertson S.H. (1996) *Unimolecular Reactions*, John Wiley & Sons, New York.
59. Horne D.G., Gosavi R., Strausz O.P. (1968) Reaction of Metal Atoms: The Combination of Mercury and Chlorine Atoms and the Dimerization of HgCl. *J. Chem. Phys.* **48**, 4758-4764.
60. Hranisavljevic J., Fontijn A. (1997) Kinetics of Ground-State Cd Reactions with Cl₂, O₂ and HCl Over Wide Temperature Ranges. *J. Phys. Chem. A* **101**, 2323-2326.
61. <http://www.emsl.pnl.gov:2080/forms/basisform.html>
62. <http://www.hbcpnetbase.com/>
63. <http://www.seas.ucla.edu/ma150c/senkin.pdf>
64. Karimi A., Moniri F., Nasihatkon A., Zarepoor M.J., Alborzi A. (1998) Mercury Exposure Among Residents of a Building Block in Shiraz, Iran. *Env. Res.* **88**, 41-43.
65. Keating M.H., Mahaffey K.R., Schoeny R., Rice G.E., Bullock O.R. (1997) *Mercury Study Report to Congress*, US Environmental Protection Agency: Research Triangle Park, NC.
66. Keck J., Carrier G. (1965) Diffusion Theory of Nonequilibrium Dissociation and Recombination. *J. Chem. Phys.* **43**, 2284.
67. Kiser R.W., Dillard J.G., Dugger D.L. (1966) Mass Spectrometry of Inorganic Halides. *Mass Spectrometry in Inorganic Chemistry*, American Chemical Society, p. 168.
68. Küchle, Dolg M., Stoll H., Preuss H. (1991) *Ab Initio* Pseudopotentials for Hg through Rn I. Parameter Sets and Atomic Calculations. *Molecular Physics* **74**(6) 1245.
69. Laidler K.J. (1969) *Theories of Chemical Reaction Rates*, McGraw-Hill, New York.

70. Landau L.D. (1932) *Phys. Z. Sow. Union* **2**, 46.
71. Laudal D.L., Brown T.D., Nott, B.R. (2000) Effects of Flue Gas Constituents on Mercury Speciation. *Fuel Proc. Tech.* **65-66**, 157-165.
72. Lee C.W., Kilgroe J.D., Ghorishi S.B. (1998) Mercury Control Research: Effects of Fly Ash and Flue Gas Parameters on Mercury Speciation. *Proceedings of the 6th Annual Waste-to-Energy Conference*, Miami, FL, 221-238.
73. Levine I.N. (1975) *Molecular Spectroscopy*, John Wiley & Sons, Inc. U.S.
74. Levine I.N. (2000) *Quantum Chemistry*, 5th Edition, Prentice-Hall, Inc. Upper Saddle River, New Jersey.
75. Li L.C., Deng P., Tian A.M., Xu M.H., Zheng C.G., Wong N.B. (2003) A Study on the Reaction Mechanism and Kinetic of Mercury Oxidation by Chlorine Species. *J. Mol. Struc. (Theochem)* **625**, 277-281.
76. Lide D. (editor) (2003-04) CRC Handbook of Chemistry and Physics, 84th Edition, CRC Press, LLC.
77. Linak W.P., Ryan J.V., Ghorishi B.S., Wendt J.O.L. (2001) Issues Related to Solution Chemistry in Mercury Sampling Impingers. *J. Air & Waste Manage. Assoc.* **51**, 688-698.
78. Lindqvist O., Rodhe H. (1985) Atmospheric Mercury – A Review. *Tellus* **37B**, 136-159.
79. Mamani-Paco R.M., Helble J.J. (2000) Bench-Scale Examination of Mercury Oxidation Under Non-Isothermal Conditions. *Proceedings of the A&WMA Annual Conference*, Salt Lake City; AWMA: Pittsburgh.
80. March R.E., Hughes R.J. (1989) *Quadrupole Storage Mass Spectrometry*, John Wiley & Sons, United States.
81. Martin J. M. L. (1999) Heat of Atomization of Sulfur Trioxide, SO₃: A Benchmark For Computational Thermochemistry. *Chem. Phys. Lett.* **310**, 271-276.
82. Maxwell L.R., Mosley V.M.(1940) Internuclear Distances in Se₂, Te₂, and HgCl by Electron Diffraction. *Phys. Rev.* **57**, 1-23.

83. Medhekar A.K., Rokni M., Trainor D.W., Jacob J.H. (1979) Surface Catalyzed Reaction of Hg + Cl₂. *Chem. Phys. Letters* **65**(3), 600-604.
84. Menke R., Wallis G. (1980) Detection of Mercury in Air in the Presence of Chlorine and Water Vapor. *Amer. Ind. Hyg. Assoc. J.* **41**, 120.
85. Miller S.J., Dunham G.E., Olsen E.S. (1998) Mercury Sorbent Development for Coal-Fired Boilers. In *Proceedings of the Conference on Air Quality: Mercury, Trace Elements, and Particulate Matter*, University of North Dakota Energy and Environmental Research Center: Grand Forks, ND.
86. Møller C., Plesset M.S. (1934) Note on Approximation Treatment of Many-Electron Systems. *Phys. Rev.* **46**, 618.
87. Moore J.W., Pearson R.G. (1981) *Kinetics and Mechanism*, John Wiley & Sons, Inc. U.S.
88. Mueller M.A., Yetter R.A., Dryer F.L. (1999a) Flow Reactor Studies and Kinetic Modeling of the H₂/O₂/NO_x and CO/H₂O/O₂/NO_x Reactions. *Int. J. Chem. Kinet.* **31**, 705-724.
89. Mueller M.A., Yetter R.A., Dryer F.L. (1999b) Flow Reactor Studies and Kinetic Modeling of the H₂/O₂ Reaction. *Int. J. Chem. Kinet.* **31**, 113-125.
90. Mueller M.A., Yetter R.A., Dryer F.L. (2000) Kinetic Modeling of the CO/H₂O/O₂/NO/SO₂ System: Implications For High-Pressure Fall-Off in the SO₂ + O(+M) = SO₃(+M) Reaction. *Int. J. Chem. Kinet.* **32**, 317-339.
91. Niksa S., Fujiwara N., Fujita Y., Tomura K., Moritomi H., Tuji T., Takasu S. (2002) A Mechanism for Mercury Oxidation in Coal-Derived Exhausts. *J. Air & Waste Manage. Assoc.* **52**, 894-901.
92. Niksa S., Helble J.J., Fujiwara N. (2001) Kinetic Modeling of Homogeneous Mercury Oxidation: The Importance of NO and H₂O in Predicting Oxidation in Coal-Derived Systems. *Environ. Sci. Technol.* **35**, 3701-3706.
93. Norton G.A., Yang H., Brown R.C., Laudal D.L., Dunham G.E., Okoh J.M. (2000) Effects of Fly Ash on Hg Oxidation in Simulated Flue Gas Environments. *Proceedings of the A&WMA Annual Conference*, Salt Lake City, UT; A&WMA: Pittsburgh, PA; Paper No. 00-167.
94. O'Hanlon J.F. (1980) A User's Guide to Vacuum Technology. John Wiley & Sons, Inc. U.S.

95. P'yankov V.A. (1949) Kinetics of the Reaction of Mercury Vapors with Ozone. *J. General Chem. (USSR)* **19**, 187-192.
96. Patra M., Sharma A. (2000) Mercury Toxicity in Plants. *Botanical Rev.* **66** (3), 379-422.
97. Paul W., Steinwedel H. (1953) *Naturforsch* **8A**, 448.
98. Perkins W.G. (1973) *J. Vac. Sci. Technol.* **10**, 543.
99. Pettersson L.G.M., Wahlgren U., Gropen O. (1983) Laser Induced Fluorescence of NH₂(A ²A₁) in the Supersonic Free Jet. *J. Chem. Phys.* **80**, 7.
100. Plane J.M.C., Rajasekhar B., Bartolotti L. (1989) An Experimental and Theoretical Study of the Reactions Na+HCl and Na+DCl. *J. Chem. Phys.* **91**, 6177-6186.
101. Plane J.M.C., Saltzman E.S. (1987) A Study of the Reaction Li+HCl By the Technique of Time-Resolved Laser-Induced Fluorescence Spectroscopy of Li (2 ²P_J-2 ²S_{1/2}, λ =670.7 nm) Between 700 and 1000 K. *J. Chem. Phys.* **87**, 4606.
102. Poirier R., Kari R., Csizmadia I.G. (1985) *Handbook of Gaussian Basis Sets*, Elsevier Science Publishers B.V., The Netherlands.
103. Polanyi J.C., Schreiber J.L. (1974) *The Dynamics of Bimolecular Reactions, Physical Chemistry, An Advanced Treatise* (Ed. W. Jost), Vol. VIA, Academic Press.
104. Pople J. A. (1999) Quantum Chemical Models. *Angew. Chem., Int. Ed.* **38**, 1894-1902.
105. Pople J.A., Scott A.P., Wong M.W., Radom L. (1993) *Isr. J. Chem.* **33**, 345.
106. Pople J.A., Seeger R., Krishnan R. (1977) *Int. J. Quantum Chem. Supp.* **11**, 149.
107. Prestbo E.M., Bloom N.S. (1995) Mercury Speciation Absorption Method (MESA) for Combustion Flue Gas: Methodology, Artifacts, Intercomparison, and Atmospheric Implications. *Water, Air, Soil Pollut.* **80**, 209-215.

108. Purvis G.D., Bartlett R.J. (1968) The Potential Energy Curve for the $X^1\Sigma^+$ State of Mg_2 Calculated with Many-Body Perturbation Theory. *J. Chem. Phys.* **68** (5), 2114.
109. Qian S.S., Warren-Hicks W., Keating J., Moore D.R.J., Teed R.S. (2001) A Predictive Model of Mercury Fish Tissue Concentrations for the Southeastern United States. *Env. Sci. & Tech.* **35**, 941-947.
110. Quack M, Troe J. (1981) Current Aspects of Unimolecular Reactions. *Int. Rev. Phys. Chem.* **1**, 97.
111. Rice O.K. (1967) *Statistical Mechanics Thermodynamics and Kinetics I*, W.H. Freeman and Company, U.S.
112. Ristori T., Bargigiani C. (1994) Chapter VIII.7, *Mercury Pollution: integration and synthesis, “Average mercury intake in an Italian diet”*, edited by Watras C.J.;Huckabee J.W.; Lewis Publishers, Boca Raton, FL.
113. Roesler J.F., Yetter R.A., Dryer F.L. (1992) *Combust. Sci. Technol.* **85**, 1-22.
114. Roesler J.F., Yetter R.A., Dryer F.L. (1995) *Combust. Flame* **100**, 495-504.
115. Schroeder W.H., Munthe J. (1998) Atmospheric Mercury – An Overview. *Atmospheric Environment* **32(5)**, 809-822.
116. Schroeder W.H., Yarwood G., Niki H. (1991) Transformation Processes Involving Mercury Species in the Atmosphere – Results From a Literature Survey. *Water, Air, and Soil Pollut.* **56**, 653-666.
117. Schwerdtfeger P., Dolg M., Schwarz W.H.E., Bowmaker G.A., Boyd P.D.W. (1989) The Baldet-Johnson ($B^2\Sigma^+ - A^2\Pi_i$) system of $^{13}C^{18}O^+$. *J. Chem. Phys.* **91**, 1762.
118. Seigneur C., Wrobel J., Constantinou E. (1994) A Chemical Kinetic Mechanism of Atmospheric Inorganic Mercury. *Environ. Sci. Tech.* **28**, 1589 – 2597.
119. Senior C.L., Sarofim A.F., Zeng T., Helble J.J., Mamani-Paco R. (2000) Gas-Phase Transformations of Mercury in Coal-Fired Power Plants. *Fuel Proc. Tech.* **63**, 197-213.

120. Shavitt I., Schaefer H.F.(1977) *Modern Theoretical Chemistry*, Vol.4, Plenum Press, New York.
121. Simons J. (2003) *An Introduction to Theoretical Chemistry*, Cambridge University Press, Cambridge, UK.
122. Simons J. (1991) An Experimental Chemist's Guide to Ab Initio Quantum Chemistry. *J. Phys. Chem.* **95**, 1017-1029.
123. Skare I., Johansson R. (1992) Reactions Between Mercury Vapor and Chlorine Gas at Occupational Exposure Levels. *Chemosphere* **24**(11), 1633-1644.
124. Slemr F., Schuster G., Seiler W. (1985) Distribution, Speciation, and Budget of Atmospheric Mercury. *Journal of Atmospheric Chemistry* **3**, 407-434.
125. Sliger R.N., Kramlich J.C., Marinov N.M. (2000) Towards the Development of a Chemical Kinetic Model for the Homogeneous Oxidation of Mercury by Chlorine Species. *Fuel Proc. Tech.* **65-66**, 423-438.
126. Steckler R., Thurman G.M., Watts J.D., Bartlett R.J. (1997) Ab Initio Direct Dynamics Study of OH + HCl → Cl + H₂O. *J. Chem. Phys.* **106**, 3926-3933.
127. Steinfeld J.I., Francisco J.S., Hase W.L. (1999) *Chemical Kinetics and Dynamics*, Prentice-Hall, New Jersey.
128. Stevens W.J., Krauss M., Basch H., Jasien P.G. (1992) Relativistic Compact Effective Potentials and Efficient, Shared-exponent Basis Sets for the Third-, Fourth-, and Fifth-row Atoms. *Can. J. Chem.* **70**, 612.
129. Stuckelberg E.C.G. (1932) *Helv. Phys. Acta* **5**, 369.
130. Szabo A., N.S. Ostlund N.S. (1989) *Modern Quantum Chemistry*, McGraw-Hill, Inc., New York.
131. Tardy D.C., Rabinovitch B.S. (1966) Collisional Energy Transfer. Thermal Unimolecular Systems in the Low-Pressure Region. *J. Chem. Phys.* **45**, 3720.
132. Toole-O'Neil B., Tewalt S.J., Finkleman R.B., Akers D.J. (1999) Mercury Concentration in Coal – Unraveling the Puzzle. *Fuel* **78**, 47-74.
133. Troe, J. (1983) Specific Rate Constants k(E,J) for Unimolecular Bond Fissions. *J. Phys. Chem.* **83** (114), 6017.

134. Troe J.(1977) Theory of Thermal Unimolecular Reactions at Low Pressures. II. Strong Collision Rate Constants. Applications. *J. Chem. Phys.* **66**,4758.
135. Truhlar D.G., Gordon M.S. (1990) *Science* **249**, 491.
136. Wayne R.P. (1993) *Chemistry of Atmospheres*, Oxford University Press, New York.
137. Wedig U., Dolg M., Stoll H., Preuss H. (1986) *Quantum Chemistry: The Challenge of Transition Metals and Coordination Chemistry*, Ed. A. Veillard, Reidel and Dordrecht, 79.
138. Wen C.Y., Fan L.T. (1975) *Models for Flow Systems and Chemical Reactors*, Marcel Dekker, Inc. New York.
139. Weston R.E., Schwarz H.A. (1972) *Chemical Kinetics*, Prentice-Hall, Inc. Englewood Cliffs, New Jersey.
140. Widmer N.C., Cole J.A., Seeker W.R., Gaspar J.A. (1998) Practical Limitation of Mercury Speciation in Simulated Municipal Waste Incinerator Flue Gas. *Combust. Sci. and Tech.* **134**, 315-326.
141. Widmer N.C., West J., Cole J.A. (2000) Thermochemical Study of Mercury Oxidation in Utility Boiler Flue Gases. *Proc. A&WMA Annual Conf.* Salt Lake City, AWMA: Pittsburgh.
142. Wilcox J., Blowers P., Marsden D.C.J. (2004) Evaluation of Basis Sets and Theoretical Methods for Estimating Rate Constants of Mercury Oxidation Reactions Involving Chlorine. *Fuel Proc. Tech.* **85**(5), 391-400.
143. Wilcox J., Robles J., Marsden D.C.J., Blowers P. (2003) Theoretically Predicted Rate Constants For Mercury by Hydrogen Chloride in the Flue Gases of Coal Combustion. *Environ. Sci. Technol.* **37**, 4199-4204.
144. Wilks D.S. (1995) Statistical Methods in Atmospheric Sciences: An Introduction. Academic Press, San Diego, California.
145. Xu M., Qiao Y., Zheng C., Li L., Liu J. (2003) Modeling of Homogeneous Mercury Speciation Using Detailed Chemical Kinetics. *Comb. and Flame* **132**, 208-218.
146. Zener C. (1932) *Proc. Roy. Soc. A* **137**, 696.